University of Cyprus
PV Technology

DEPARTMENT OF ELECTRICAL AND COMPUTER ENGINEERING

PV SYSTEM MODELS FOR ASSESSING THE VOLTAGE QUALITY BEHAVIOUR OF DISTRIBUTION GRIDS IN THE PRESENCE OF HIGH PV PENETRATION LEVELS

DOCTOR OF PHILOSOPHY DISSERTATION

MINAS PATSALIDES

2015

University of Cyprus
PV Technology

DEPARTMENT OF ELECTRICAL AND COMPUTER ENGINEERING

PV SYSTEM MODELS FOR ASSESSING THE VOLTAGE QUALITY BEHAVIOUR OF DISTRIBUTION GRIDS IN THE PRESENCE OF HIGH PV PENETRATION LEVELS

MINAS PATSALIDES

A Dissertation Submitted to the University of Cyprus in Partial Fulfilment of the Requirements for the Degree of Doctor of Philosophy

APRIL 2015

VALIDATION PAGE

Doctoral Candidate: Minas Patsalides

Doctoral Thesis Title: PV system models for assessing the voltage quality behaviour of distribution grids in the presence of high PV penetration levels

The present Doctoral Dissertation was submitted in partial fulfillment of the requirements for the Degree of Doctor of Philosophy at the Department of ***Electrical and Computer Engineering*** *and was approved on the* ***11/05/2015*** *by the members of the* ***Examination Committee.***

Examination Committee:

Research Supervisor: _____

George E. Georghiou, Associate Professor)

Committee Member (Chairman): _____

(Charalambos. A. Charalambous, Assistant Professor)

Committee Member: _____

(Elias Kyriakides, Associate Professor)

Committee Member: _____

(Teuvo Suntio, Professor)

Committee Member: _____

(Andreas Poullikkas, Associate Professor)

Committee Member: _____

(Andreas Stavrou, Senior Network Engineer)

DECLARATION OF DOCTORAL CANDIDATE

The present doctoral dissertation was submitted in partial fulfilment of the requirements for the degree of Doctor of Philosophy of the University of Cyprus. It is a product of original work of my own, unless otherwise mentioned through references, notes, or any other statements.

Minas Patsalides

……...…..

ΠΕΡΙΛΗΨΗ

Τα τελευταία χρόνια, η αυξανόμενη ανησυχία για τις κλιματικές αλλαγές και η φιλελευθεροποίηση της αγοράς ενέργειας έχουν δημιουργήσει τις κατάλληλες προϋποθέσεις για προώθηση των ανανεώσιμων πηγών ενέργειας. Ειδικότερα σε περιοχές με υψηλή ηλιακή ακτινοβολία, η διείσδυση φωτοβολταϊκών (ΦΒ) συστημάτων αναμένεται να είναι αρκετά μεγάλη στο εγγύς μέλλον, καθώς η τεχνολογία γίνεται όλο και πιο ανταγωνιστική. Η υψηλή διείσδυση φωτοβολταϊκών συστημάτων θα έχει σίγουρα σοβαρές συνέπειες για τη λειτουργία του δικτύου ηλεκτρικής ενέργειας και νέες προκλήσεις ενδέχεται να προκύψουν καθώς τα επίπεδα διείσδυσης αυξάνονται. Η ερευνητική αυτή εργασία αποτελεί αποτέλεσμα της ανάγκης για μελέτη της αυξανόμενης διείσδυσης των φωτοβολταϊκών συστημάτων με πρώτιστο στόχο την ανεύρεση των πιθανών προβλημάτων που ενδέχεται να παρουσιαστούν με την ανεξέλεγκτη διασύνδεση τους στο δίκτυο διανομής ηλεκτρικής ενέργειας. Συγκεκριμένα, η ερευνητική αυτή εργασία επικεντρώνεται στην ακριβή μοντελλοποίηση των ΦΒ συστημάτων προκειμένου να γινεί εφικτή η μελέτη της συμπεριφοράς του δικτύου διανομής υπό συνθήκες μεταβλητών συγκεντρώσεων ΦΒ συστημάτων. Αρχικά, δύο νέα μοντέλα ΦΒ συστημάτων έχουν δημιουργηθεί για μελέτες σταθερή κατάστασης. Τα μοντέλα αυτά (με επονομασία απλό και προηγμένο ΦΒ μοντέλο αντίστοιχα) έχουν χρησιμοποιηθεί για τη μελέτη της τάσης και των αρμονικών του δικτύων διανομής υπό συμμετρικές συνθήκες. Στην συνέχεια, ένα λεπτομερές μοντέλο ΦΒ συστήματος ρυθμίζεται και επαληθεύεται χρησιμοποιώντας μετρήσεις και ακολούθως αξιοποιείται σε μελέτες τάση, αρμονικών, ρύθμισης τάσης και σφαλμάτων. Επιπλέον, ένα γενικευμένο μοντέλο ΦΒ συστήματος έχει αναπτυχθεί για μελέτες στιγμιαίας απόκρισης και έχει την δυνατότητα να προσομοιώνει με ακρίβεια την δυναμική συμπεριφορά ενός φωτοβολταϊκού συστήματος σε συμμετρικές και ασύμμετρες συνθήκες τάσης. Το προτεινόμενο μοντέλο στιγμιαίας απόκρισης μπορεί να ρυθμιστεί με την βοήθεια μεθόδου καθορισμού παραμέτρων για να προσομοιώνει με επαρκή ακρίβεια την στιγμιαία απόκριση μετατροπέων με διαφορετική παραμετροποίηση. Επίσης, μπορεί να χρησιμοποιηθεί σε μελέτες, αρμονικών. Η ορθότητα της δυναμικής συμπεριφοράς του μοντέλο έχει επαληθευτεί με τη χρήση δεδομένων προσομοίωσης από το λεπτομερές μοντέλο ΦΒ συστήματος. Η σύγκριση μεταξύ του προτεινόμενου μοντέλου στιγμιαίας απόκρισης και του λεπτομερές μοντέλου ΦΒ συστήματος διεκπεραιώνεται υπό τις ίδιες διακυμάνσεις τάσης και υπό τις ίδιες μεταβολές ενεργού/άεργου ισχύος.

Η ανάδειξη τυχόν προβλημάτων ποιότητας ισχύος και η μελέτη της συμπεριφοράς του δικτύου διανομής στην παρουσία ΦΒ συστημάτων γίνεται με την βοήθεια ευρέως αναγνωρισμένων δεικτών ποιότητας ισχύος λαμβάνοντας υπόψη τα τρέχοντα διεθνή πρότυπα και πρακτικές. Επιπλέον, προέκταση της διατριβής αυτής αποτελεί η ακριβής μοντελλοποίηση του δικτύου διανομής, η οποία συνεισφέρει στην ορθή μελέτη των προβλημάτων ποιότητας ισχύος και συμβάλλει στην σύνθεση ενός ολοκληρωμένου εργαλείου προσομοίωσης για την μελέτη της συμπεριφοράς των ΦΒ συστημάτων.

Ο απώτερος στόχος της παρούσας διατριβής είναι η βελτίωση της δυνατότητας διασύνδεσης

υψηλών συγκεντρώσεων φωτοβολταϊκών συστημάτων στο δίκτυο διανομής, προτείνοντας ακριβής/απλουστευμένες μεθόδους μοντελλοποίησης για την μελέτη της ποιότητας ισχύος, των σφαλμάτων και της ασσυμετρίας φάσεων. Η ανάπτυξη κατάλληλων μοντέλων προσομοίωσης θέτει τις βάσεις για την ανεύρεση/κατανόηση των προβλημάτων ποιότητας ισχύος που σχετίζονται με την διεσπαρμένη παραγωγή για την περαιτέρω επίλυση τους.

ABSTRACT

In recent years, increasing concerns about climate change and the liberalisation of the energy market have provided the necessary impetus for alternative energy sources. Especially in regions with high solar irradiance, high penetration of photovoltaic (PV) systems is expected to arise in the near future as the technology becomes more competitive. High penetration of Photovoltaic (PV) systems will definitely have serious consequences on the operation of the electricity grid and further challenges will arise as penetration levels increase. The motivation of this work is the aforementioned expected increased penetration of PV and the potential problems associated with the uncontrolled deployment of PV technology. In more detail, the current research work focuses on the accurate modelling of PV systems for assessing the power quality behaviour of the distribution grid while varying the PV capacity. Initially, two PV system models are developed for steady-state studies. The aforementioned models, named simple and advanced PV system models, are used for the study of the voltage and harmonic behaviour of distribution grids under balanced conditions. In the next step, a detailed PV system model (DPVSM) is tuned and validated using measurements and further utilized in voltage, harmonic, voltage regulation and fault studies. Furthermore, a generic PV system model is developed for transient studies capable of representing the response of the PV system during balanced and unbalanced conditions. The proposed transient PV system model (TPVSM) is tuneable and via a parameter estimation method it can adapt to represent the transient response of various inverters found on the market. Also, it can be used for harmonic studies as well. The transient response of the proposed transient PV system model is validated by using simulation data from the detailed PV system model. The comparison is achieved by imposing both the DPVSM and the TPVSM under the same voltage fluctuations and active/reactive power changes.

The evaluation of power quality problems via the study of the distribution grid in the presence of PV systems is done with the help of widely accepted power quality indices and by taking into account the latest international standards and practices. Additionally, as an extension of the above work, accurate distribution grid modelling is undertaken which contributes in formulating a complete simulation tool for studying the behaviour of PV systems and enables the proper study of power quality problems.

The ultimate aim/goal of this PhD work is to improve the potential of installing high quantities of PV systems via the proposed accurate/reduced models of PV generation designed for use in power quality and fault/unbalanced studies. The development of appropriate models will improve the understanding of problems relative to distributed generation and will lead to the development of appropriate solutions.

ACKOWLEDGEMENT

First of all, I would like to express my immense gratitude to my supervisor Dr. George E. Georghiou, for his continuous support, guidance and encouragement throughout the period of my doctoral studies. Working with him has been an invaluable experience and very beneficial for my personal and professional development.

Especially, I would like to thank my friends and colleagues at the University of Cyprus and particularly those in the PV Technology group, for their help, fruitful discussions, encouragement and constructive collaboration at all times. Special thanks go to George Makrides, Despo Demetroude and Alexander Phinikarides who have generously offered their assistance and friendship.

I am also deeply grateful to Dr. Andreas Stavrou and Dr. Venizelos Efthymiou, for their expertise, vision, continuous support, suggestions and encouragement throughout the years.

I also gratefully acknowledge the staff of the Electricity Authority of Cyprus for their excellent collaboration and assistance. In addition to this, I would like to acknowledge the generous and continuous support of the Electricity Authority of Cyprus and express my thanks for giving me the opportunity to participate in activities which have contributed significantly in my PhD research study and to my professional development.

Finally, I would like to thank my wife and family that have been next to me with their love and patience, providing me with their support and encouragement throughout these years.

Contents

List of Figures

List of Tables

Abbreviations	
Acronym	**Definition**
APVSM	Advanced PV System Model
CAPF	Conventional Adaptive Power Factor
CDF	Cumulative Distribution Function
DFT	Discrete Fourier Transform
DG	Distributed Generation
DPVSM	Detailed PV System Model
DSO	Distribution System Operator
EDGM	Equivalent Distribution Grid Model
EN	European Standard
EU	European Union
GAPF	Generalized Adaptive Power Factor
HDGM	Harmonic Distribution Grid Model
HTEI	Harmonic Thevenin Equivalent Impedance
IEA	International Energy Agency
LV	Low Voltage
MPP	Maximum Power Point
MPPT	Maximum Power Point Tracking
MV	Medium Voltage
PCC	Point of Common Coupling
P	Active Power
PF	Power Factor
PI	Proportional-Integral
PLL	Phase Lock Loop
PMU	Phasor Measurement Unit
PQ	Power Quality
PR	Proportional-Resonant
PV	Photovoltaic
PWM	Pulse Width Modulation
Q	Reactive Power
RMS	Root Mean Square
SPVSM	Simple PV System Model
STC	Standard Test Conditions
TEC	Thevenin Equivalent Circuit
TEI	Thevenin Equivalent Impedance
TF	Transfer Function
THD	Total Harmonic Distortion
TPVSM	Transient PV System Model
VRC	Voltage Regulation Capability

Chapter 1
Introduction

1.1 Motivation

During the last years, a significant effort has been devoted to the definition of power quality and formulation of appropriate standards to guide utilities in revealing and mitigating power quality problems, in view of the upcoming technological advances and environmental challenges which started to impose an evolution in the structure and operation of electricity grids with both positive and negative consequences [1]–[3].

With the liberalization of the energy market, the power quality aspects are becoming a critical issue for distribution systems, as power quality can be transformed into a source of financial gain or an incentive for new electricity utilization strategies. For example, smart inverters and intelligent distribution transformers can be utilized in distribution grids to provide ancillary services on voltage regulation aiming in maximizing the allowable active power production from RES [4]. Consequently, the introduction of distributed energy sources into the electricity grid sets new requirements for utilities and power producers and creates a new market force that will inevitably change the structure of current distribution grids and move towards a more intelligent management of produced electrical energy. As a result, complete and revolutionary restructuring of the electricity network will have to take place in order to accommodate increased penetration of renewable energy sources (RES) and

distributed generation (DG) which is associated with electricity production from RES [5]–[10].

On the other hand, the daily activities of contemporary customers rely on electronic/electrical equipment requiring a reliable/good quality power supply to operate correctly and this imposes a burden on utilities to supply good quality electrical energy at all times. Although estimating the economic consequences of poor power quality in different sectors of daily life is quite difficult, a power quality survey conducted in the USA showed that the economic losses range roughly between 119 to 188 billion dollars a year. The main causes of the economic losses are supply outages and power quality related problems across all business sectors [5], [6]. Power quality costs in Europe are responsible for serious and avoidable reduction in industrial performance with an economic impact exceeding 150 billion Euros annually [7]. Recently, the Electric Power Research Institute (EPRI) has developed a detailed vision paper for power quality research for the next years. The target of the specific vision paper is not only to define the objectives of power quality research for the next 10-20 years and fill in critical gaps, but also to specify the role of power quality in enhancing the economic performance of modern electric suppliers and key organizations and companies [11].

The question arising from the power quality considerations relates to the steps required for effective and timely preconditioning of the distribution network to enable all the upcoming technological advances. One way to achieve the above is the establishment of reference standards for the design of the electrical devices and the proper development of a distribution network. This contribution is mainly concerned with one of EPRI's vision directions [11]: The improvement of power quality and reliability with network design in the presence of RES and in particular Photovoltaics (PV). Through the procedure adopted in this work, general conclusions about the impact of high connection densities of PV systems on the power quality response of the network were extracted through computer simulations. In particular, results showed that the levels of power quality of buses inside a distribution network can decrease by installing PV systems if proper planning is not undertaken. Therefore, this work aims to depict the need for appropriate standard and studies for the installation of PV systems inside the distribution grid.

More specifically, current trends and standards in PV system design were considered in order to construct PV system models for steady-state and transient analysis. The proposed PV system models are built and verified using experimental/simulation data, and further used to investigate the power quality behaviour of different PV penetration scenarios. Also the models are used to determine the effect of increased PV capacity on frequency and voltage

variations and to assess their response during faults. Modification of the models to incorporate reactive compensation algorithms proposed by standards gives the possibility to evaluate the distribution grid response during voltage regulation as well. Moreover, an accurate and simple distribution grid model is formulated to enhance the voltage regulation and power quality studies. In the final stage, an accurate and generic transient PV system model for power quality studies is developed. The proposed model is an important task as the implementation of an accurate transient PV system model gives the opportunity to analyse more aspects of power quality and voltage stability with higher accuracy.

1.2 Research objectives

This work aims to achieve the following objectives:

- Development of a Simple PV system model (SPVSM) - Three phase current source configured using measurements.
- Development of an Advanced PV system model (APVSM) - Three phase power sources configured via the help of regression fit equations - The voltage of fundamental frequency and voltage harmonics are used as an input to the model.
- Development of a Detailed PV system model (DPVSM) - Complete PV system model which includes DC/DC converter, AC/DC converter, MPPT , filter and Control Circuit - Validated and tuned using measurements.
- Power Quality Measurements in different PV installations – Investigation of power quality response of large PV Parks of 100 and 150 kW_p, in order to gather data for the validation of the new PV models to be developed.
- Development of an accurate PV system model to represent the transient behaviour of the detailed PV system – Validation of the proposed PV system model via simulations.
- Investigation of power quality behaviour of the electricity grid in the presence of different concentrations of PV systems, aiming at the development of guidelines for utilities.
- Reactive power management for assessing the benefits and the compensation level required.
- Investigation of the impact of PV generation on fault studies in electricity grids with different PV penetration levels.

1.3 Research Achievements

For the task of configuring the SPVSM, a unique measurement analysis method has been formulated with which the optimum number of simulation cases is selected. The

measurement data were analysed using the k-mean clustering algorithm and it was found that solar irradiance had a strong correlation with power quality indices. From the data analysis, three solar irradiance cases were extracted in order to render the simulations more tractable from a computational point of view.

A new PV system model (Advanced PV system model - APVSM) using regression fit equations, which is computationally efficient has also been developed. With this model both voltage levels and harmonic distortion of a proposed distribution grid is assessed.

Furthermore, a Detailed PV system model (DPVSM) is tuned and validated using measurements from a 150 kW_p PV system and it is then used in the simulation of different concentration scenarios. Its response is verified by utilizing measurements obtained before and after the installation of the 150 kW_p PV system. Moreover, the DPVSM is further used in the evaluation of different voltage regulation algorithms. Finally, the DPVSM is used in the study of fault response of the distribution grid.

In addition, a generic and accurate PV system model is developed for transient studies, the parameters of which can be tuned using transient data. The proposed model is a three phase representation capable of simulating with sufficient accuracy normal/unbalanced operating conditions and voltage regulation. Harmonics are also considered during the development of the aforementioned model.

Finally, a novel method for defining the distribution grid dynamics using power measurements has also been developed and used in improving the accuracy of power quality simulations. The method is critically essential in the evaluation of different PV penetration levels and voltage regulation methodologies.

1.4 Outline of the proposal

The PhD thesis is divided and organized into ten chapters. Specifically, chapter 1 is the introduction and includes the motivation, research objectives and achievements of the proposed thesis. A general overview for the different PV system modelling techniques and advances in PV technology and its usage are presented in chapter 2. Based on the literature findings, the aims and novelty of this work are presented. A description of power quality, current standards and PV inverter capabilities are given in chapter 3. In chapter 4, the Simple PV System model (SPVSM) formulated initially for the investigations is presented and evaluated and its weaknesses are identified. In the same chapter, a detailed overview of power quality measurements and data acquisition done in the framework of PV system modelling is provided as well as details for all the instrumentation associated with the investigations. Chapter 5 presents the Advanced PV system model (APVSM) developed by

considering both the weaknesses of the SPVSM and the gap in PV system modelling revealed by the literature findings. In chapter 6, the Detailed PV system model (DPVSM) is presented along with its tuning and validation procedure. Also, voltage regulation algorithms are incorporated into the DPVSM in order to assess their performance. Moreover, the simulation results for the power quality and fault investigations done for different PV concentration scenarios are presented. Chapter 7 describes and explains the development of an accurate and generic PV system model for transient power quality studies. The procedure followed for the formulation of the models is described thoroughly. Details for the distribution grid topologies/dynamics are presented in Chapter 8. In the same chapter the methodology followed for the development of an accurate equivalent distribution grid model is described. Furthermore, applications of the proposed equivalent distribution grid model are provided in Chapter 9. Finally, in the last chapter, chapter 10, the conclusions and future work are outlined.

Chapter 2
Literature Review

2.1 Introduction

The objective of this chapter is to present the need for assessing the effects of high PV penetrations and provide an overview of the existing PV system models. Based on the literature search findings, it has been found that the development of accurate and simplified PV system models is crucial in performing power quality studies in large power networks or in the context of the whole power network. Furthermore, it is evident from the literature that the distribution grid dynamics play a significant part in the simulation results.

The task of developing usable/practical models and simulation tools will enable the better understanding of the effects and impact of high PV penetration and will eventually allow solutions to be proposed. Until now, there is a lack of universal models or procedures for use in complete, accurate and computationally efficient power quality studies. This constitutes a major challenge for researchers which is discussed in detail in this chapter along with the novel contribution of this PhD work. Finally, the broad spectrum of PV inverter capabilities is highlighted to manifest the need for further studies using the appropriate simulation models which provide the required insight into how the future structure and efficient/reliable/optimum operation of electricity grid will be in the presence of distributed generation.

2.2 High PV penetration and Concerns about Uncontrolled Deployment: Problems and Possible Solutions

The large scale integration of photovoltaic systems and their effect on distribution networks is of great interest [12]–[14]. In recent years, research efforts have been initiated aiming to reveal the impact of uncontrolled deployment of photovoltaic systems. Three main concerns are arising when having a high PV penetration inside the electricity grid. The first one is the voltage rise beyond the limits proposed by international standards when the PV production is high and the load demand is low. The second concern is the extensive voltage distortion caused by distorted PV current or parallel and series resonance phenomena. The third main concern is actually the islanding operation of PV systems during the loss of utility supply after the occurrence of a fault. High PV penetrations have already materialised in different locations around the world and constitute invaluable sources of knowledge. Gunma village in Japan is one such example, where 553 houses have currently PV systems installed on their roofs [15]. In this specific case, the first preliminary results for approximately the first 200 installed residential PV systems indicated that both the PV production and reduced load increased the occurrence of over-voltages that were causing substantial yield reduction of the output power of PV systems [16]. No significant voltage distortion has been observed during the operation of the PV systems in Gunma village. It is reported that each PV system may cause different distortion levels depending on the inverter manufacturer [17].

Curtailment of PV produced power [18], voltage control strategies, reactive power control [19]–[22] and means of storage [15] are adopted to minimize the over-voltages observed and to improve the voltage profile during the variation of PV produced power in a proposed distribution grid with high PV penetration. The effect of weather conditions on voltage quality of a distribution grid is investigated in [23], [24] and the limits in installing high penetration of distributed generation (DG) in urban areas, using as a reference the ampacity of the cables, is considered in [25]. The electrical impact of PV plants in rural and urban networks is analysed in the framework of the EU project POLYCITY [26]. It has been demonstrated in [24] via Monte-Carlo simulations that the installation of PV-DGs may affect the power quality in the case when some background harmonics are present in a distribution system. The economical impact of poor power quality in rural and urban feeders due to PV system integration is also investigated by a group of researchers in [27]. The islanding behaviour of clustered PV systems is assessed using an experimental setup similar to a distribution feeder in [28] and by computer simulations using experimental data from one PV system in [29] and [30]. In [14], it is observed that clustered PV systems are not causing extensive voltage distortion if linear loads are connected in the distribution network. It is

also shown that the voltage distortion exceeds the limits proposed by the international standards if a certain number of nonlinear loads are used for the simulations.

Measurements done in Denmark on 29 houses each having 1 kW_p PV installed showed no detectable impact from the PV installations on the local voltage distortion. The highest voltage distortion was actually caused by external sources despite the fact that the installed capacity was reaching 30% of the feeding transformer's rated capacity [31]. A solar village located at the Sydney Olympic Site in Australia consists of up to 665 homes each having a 1 kW_p PV system. The results of the measurements from the Sydney Olympic Village showed that harmonic voltages were far below the IEEE 519-1992 limits even when all PV inverters were in operation on the same feeder [32]. In Bavaria (Germany), a real network is under development which will be used to conduct analysis and to perform field tests. The test region counts among those with the highest PV penetration in Germany. Currently, the ratio of installed PV capacity per household is as high as 3.9 kW_p (early 2010) in some low voltage networks and is expected to increase by 60 % in the coming years [33]. The simulations in [34] showed that it would take more than 80% saturation by the PV systems to cause the voltage distortion to exceed the IEEE recommended maximum of 5%. The capacitance at the interface of many DG units may cause harmonic resonances or shift resonant frequencies to lower values where the emission is higher. Resonance at frequencies below 1 kHz seems unlikely to happen and attention should be given to the potential resonances at higher frequencies [35]. Proper introduction of PV systems inside the electricity grid can eliminate the need for voltage regulators and phase balancers, reducing in that way the capital and maintenance costs as mentioned in [36].

Clearly, the impact of high penetration of PV systems is very important and appropriate modelling is required to reveal all the possible unwanted consequences of large deployment of PV systems as noted in the 2013 Annual Report of the International Energy Agency (IEA) [37]. The main goal of Task 14 of IEA is to promote the use of grid-connected PV systems as an important source in electricity grids at the higher penetration levels that may require additional efforts. The aim is to reduce the technical barriers to achieving high PV penetration levels and propose appropriate grid configurations to enhance this effort [9], [10].

2.3 Existing Photovoltaic System Models

Detailed modelling of PV systems has already been conducted by many researchers in an attempt to understand their behaviour, to develop new maximum power point tracking (MPPT) mechanisms for better utilization of solar energy [38] and to incorporate additional

functionalities like voltage regulation and reactive compensation [39]–[42]. In general, detailed models (MPV1) are very useful in testing new control algorithms and new circuit topologies such as for example the z-source inverter [43]. Additionally, detailed modelling is utilized in fault studies [44], [45], in testing multilevel inverters for their performance in terms of efficiency and power quality [46], in evaluating frequency/voltage support using PV systems with storage [47], [48], in active power curtailment studies for distribution grid feeders [18] and in the assessment of the behaviour of PV generation in microgrids [49], [50]. Even an embedded technique to determine the utility grid impedance is incorporated among other advanced robust control strategies into the control circuit of detailed PV system models [51], [52]. The question arising from complex modelling representations, is how these models are going to be used efficiently in the simulation of large power networks.

Until recently, the main research interest on PV system modelling has focused on steady-state models which are easier to use during load flow studies and PV produced power estimation. The model presented (MPV2) in [53] can simulate steady-state operation of PV systems when meteorological, PV system and power grid parameters are given. The simulation error of this model when compared with the actual PV system measurements indicated very small deviations during noon time and acceptable error during the afternoon. The model is built based on the principle of instantaneous power balance and it can be applied easily to a great number of topologies but it cannot perform simulations for transient analysis/harmonic studies. PV systems were simulated as negative constant power loads [54] or constant real power generators [26] (MPV3). These methods for model simplification are appropriate for static analyses but they are not suitable for dynamic studies and control strategy development.

Performance models (MPV4) which are able to predict the active power produced from PV systems by using the solar irradiance, temperature, efficiency of the system and/or measured performance coefficient (applicable to all commercial inverters) are found in the literature [55]–[57] but they cannot be used in transient and power quality studies as they do not consider the dynamics of the PV inverter [58]. Nevertheless, they have been used for defining the steady-state voltage levels in a distribution grid with varying PV concentrations [59], [60]. Additionally, the steady-state behaviour of PV systems has been characterized by recurrent neural networks (MPV5) in [61] and compared with the traditional component based model [62] mentioned previously (found in [55]). In a few cases, for simplification purposes, the dynamics of the PV array and the MPPT are replaced with a voltage source which is then connected to a detailed inverter model. The aforementioned simplified model (MPV6) has been used in power quality studies [63] and stability analysis [64] despite the

fact that part of the PV inverter dynamics is omitted. Average and phasor models (MPV7) are developed in [65]. A PV system is firstly simplified by reducing the whole circuit into a current source and then the high frequency from power electronics is removed. Further simplification is achieved by implementing a phasor model in which the fundamental frequency is disregarded for the sake of reducing the simulation effort and time. Moreover the results are compared with the average model instead of the detailed one. A simplified phasor model (MPV8) is also described in a National Renewable Energy Laboratory report [66] according to which the PV system is modelled as a current source and configured using only the current magnitude and angle of the fundamental frequency. A similar model is presented (MPV9) in [19] based on which the PV inverter is composed of a current source with grid synchronization and voltage control strategies under the assumption of fixed PV power and 100% converter efficiency. In this model representation, the current is defined by using the voltage RMS and angle at the connection point having as an input the apparent power needed to be produced by the PV system. As the scope of this work was to study the voltage rise in distribution grid feeders, the total generation efficiency of the inverters, harmonics, switching and network transients are neglected.

An analytical model (MPV10) for PV distributed generators is proposed in [67]. The PV system is initially represented by a voltage source and an inductor which is interfaced with a power source. The aim was to create a distribution grid equivalent circuit from which the dynamics of the PV system for the fundamental frequency are extracted and used to configure a voltage-controlled current source. Consequently, harmonic analysis cannot be performed when the models in [19], [66], [67] are used. Harmonic analysis is considered in [23], in which the PV plant is modelled as a set of current sources (MPV11) representing the generated output current and its harmonic component according to [68], [69]. The amplitude and harmonics of voltage are not taken into account in the modelling procedure thus increasing the uncertainty and error of the simulation results. In [70] the PV inverter was approximated by an averaged model, but the controls for MPPT were represented in detail (MPV12), including the dynamics of the phase-locked loop from which the sine wave reference was derived. The approximation for this specific average model is acceptable at the beginning of the cycle of the sine wave and as long as the hysteresis bandwidth is small. Also, the use of this model can lead to misleading results concerning the impact of high PV penetration if it is not configured and handled appropriately [71].

The work in [72] proposes a passive impedance network (current source in parallel and in series with two complex impedances) as a model (MPV13) that can capture effectively the PV system behaviour. The values of the complex impedances are calculated with the use

of experimental data for the fundamental frequency given that in the experimental topology only a linear load has been used and the harmonics were negligible in that case. With this modelling approach it has been observed that the PV inverter exhibits negative impedance characteristics which are commonly found in power electronic switching converters and also proves that the behaviour of the PV system can be successfully described by a first order transfer function [73]. In a recent work, a simplified PV system model for transient analysis is proposed but not validated experimentally [74]. A detailed model is simplified as a controlled current source having as an advantage that this model (MPV14) captures the dynamic behaviour of the PV system and at the same time preserves some of the control signals. This model, having the reactive support capability enabled, has been used further in voltage stability investigations [75] as it is suitable for fundamental frequency studies. Also, from this work another simplified approach has been developed which models the PV system as a voltage source (MPV15) that preserves all the control signals of the PV inverter. It is worth noting, however, that this can only simulate the fundamental frequency component with the harmonics being ignored and the controlled voltage source is defined by a signal that only contains the fundamental frequency component of the corresponding signal and any higher frequency harmonics observed during the analysis of the detailed model are ignored.

Verified models for PV generation suitable for transient response and stability analysis have been developed in [76] and used to assess the fault response of different PV penetration levels [77]. The dynamic model proposed (MPV16) in [76] was constructed to match experimental data from a certain PV panel and inverter, and the mathematical equations were developed regardless of the actual system configuration, which limits the control development. Moreover, the power quality response of distribution grids with PV systems under different solar irradiation conditions and with various concentrations of such systems was investigated by the authors using a steady-state modelling (MPV17) method [78]. Models (MPV18) appropriate for fast and accurate transient and steady-state simulation of PV systems are developed in [79], [80] but their drawback is that they require the impedance characteristics of the PV system and the distribution network to be completely defined. A simple dynamic PV system (MPV19) and a network topology are considered in [81] and represented using space vector theory. The transient PV system model is developed using d-q space vector representation to make the simulation simpler and computationally efficient. Its performance is satisfactory under steady-state conditions but presents a mismatch with the behaviour of the detailed model during transient conditions. An advanced version of d-q space vector PV system model (MPV20) with voltage regulation capability is used in [82]

for voltage stability studies. Impedance models (MPV21) are also becoming popular for their simplicity [83] but still no work describes how these models can represent accurately the PV inverters found on the market.

Summarizing, a large number of PV system models do exist in the literature, most of them do not realistically capture the dynamics introduced by the PV inverter control circuit and consequently they cannot be used for complete power quality studies. Furthermore, the majority of the models do not retain the control signals and they are mostly developed on the concept of full switching representation of the converter that imposes a high computational burden on power system simulations. On the other hand, a subset of PV system models requires parameters that are not calculated in a convenient way or are not readily available by the manufactures. Clearly, the impact of high penetration of PV systems is very important and appropriate modelling is required to reveal all the possible unwanted consequences of large deployment of PV systems [37]. A thorough research study conducted by Sandia National Laboratories states the need for accurate, flexible and standardized analysis in addressing new and more interactive distribution systems. Modifications to distribution engineering tools are necessary to take into consideration the transient behaviour and simplify their use to handle efficiently PV systems and distributed generation [84].

2.4 Equivalent Distribution Grid Models

Simulation studies are a powerful tool for engineers as they can provide significant insight into the operation of power systems. Quite often, detailed power grid representations are inserted into simulation software for power quality and stability investigations [85]–[88]. However, simplified simulation models of the power grid are very useful for many reasons if they can represent correctly a physical process. On one hand, simplified/universal power grid models can decrease the simulation time or/and scale down the computational power required for understanding complex systems. On the other hand, such models can be adopted and used by a wider group of engineers [89]. When medium/high voltage networks are quite large, parts of the network are replaced with Norton equivalent models obtained via coherency based techniques by grouping parts of the network behaving similarly [90]–[92]. Also, model order reduction methods are applied to replace large scale distribution grids of low importance with state-space models [93]. The formulation of both Norton equivalent and state-space models requires explicit knowledge of the power system and the characteristics of its components which may become a very challenging and difficult task due to lack of required/accurate data. Thevenin equivalent circuits are used in simulation studies in order to simplify the majority of the power network [94]–[99]. More specifically,

a Thevenin equivalent circuit (TEC) can be defined at the busbar of the distribution transformer or at the point of common coupling (PCC). Defining the TEC with adequate accuracy can have multiple benefits especially for integration/planning/stability analysis [99]–[103] and in particular for appropriately sizing the power generators according to the grid requirements prior their installation. The need stems from the fact that in low voltage networks the X/R ratios are lower than unity which means that in such a case voltage regulation via reactive absorption/injection may not be effective [104]. Great variability of Thevenin equivalent impedance (grid impedance) at PCCs [99] unavoidably leads to different voltage regulation requirements [105]. So far, an accurate TEC has been used for the calculation of the short circuit current [106] (at a connection point of interest) and for control purposes in an attempt to ensure the stability of the power system [107]. Additionally, in integration studies, the TEC is chosen randomly according to the needs of the investigation or on an empirical basis (taken from survey data [108]) giving useful but general results, which may differ from real case scenarios. Furthermore, despite the fact that online methods for defining TEC do exist [109], [110], they can only utilize the capabilities of an already installed distributed generator (as the aforementioned methods are incorporated into the inverter control circuit) and cannot contribute in distribution grid expansion and planning. This work moves one step forward by using a validated/accurate TEC for voltage quality studies and for evaluating voltage regulation schemes based on the actual distribution grid dynamics at the PCC. Finally, the work undertaken establishes a methodology which can be followed to assess the actual grid requirements with considerable precision.

2.5 Power Electronics – PV Inverter Capabilities

Power electronics are widely used for many applications as they can be found wherever there is a need to modify voltage levels, frequency characteristics or convert the DC energy into AC and vise versa. The conversion is not always done in a perfect way and depending on the control characteristics of the converter the absorption or injection of distorted current into the electricity grid can affect the normal operation of the electricity grid and may cause problems to utility customers [111]. Currently, the PV inverter manufacturers are obliged to produce inverters that comply with the standard IEC 61727 [112] limiting partly the injection of current harmonics into the electricity grid. Fortunately, the power inverters have the ability to suppress harmonics [113] and regulate the voltage levels if properly designed [114]. Up to now, different regulation methods have been used depending on the case and cost. Among them, power curtailment, installation of storage means and regulation of reactive power [107], [115] are the main methods available to help in maintaining the voltage

of distribution grids to desirable levels. The choice of the voltage regulation method should be preferably done based on the characteristics of the PV system installation. Power curtailment is an attractive option for voltage regulation as it can contribute in frequency control as well [116]–[118], but a significant waste of valuable energy may occur during long and often overvoltage events. Reactive power control can be used for effective voltage regulation but it may result in higher currents, losses in the feeder and lower power factors at the input of the feeder [119]–[123]. In addition, the apparent power of the inverters and/or the size of conductors might have to be increased to reduce the line impedances in order to fulfil the requirements for voltage regulation. Upgrading the conductors can be an expensive approach, especially for underground feeders [118]. Energy storage units are usually expensive and the benefit-cost ratio can be quite low if they are sized to store the surplus of energy produced by high penetration of RES [124].

It is apparent that as generation penetrates into the distribution network, voltage control is becoming necessary at distribution level hence, decentralized storage is gaining importance. Consequently, a lot of work is required to introduce such kind of power control schemes into the low and medium voltage distribution grid and subsequently to incorporate active control schemes into commercial PV inverters without increasing the cost. Currently investments in this direction are slow mainly due to cost and regulatory objections than availability of mature technology.

It is widely accepted that distributed generation and especially PV systems that incorporate fully functional inverters which can control quality at the connection point can contribute significantly in improving the levels of power quality of the future electricity grids [125].

2.6 Novelty of this PhD work

Initially, a unique measurement and analysis method has been formulated to configure the SPVSM with which the optimum number of cases is selected to assist simulations. Also, in this work, a novel PV system model using regression fit equations, which is computationally efficient has been developed. With this model the voltage levels and harmonic distortion of a proposed distribution grid can be assessed. From the literature findings it has been observed that such model that is capable of taking into consideration the voltage harmonics of the grid to perform calculation of the amplitude and phase of the injected current harmonics has not been proposed yet.

In order to produce simulation results with good accuracy, it is required for the network grid dynamics to be known. For this purpose, a new/practical method for defining the

network dynamics has been developed. In more detail, the distribution grid is replaced by an accurate Thevenin equivalent circuit which can be easily obtained via waveform or phasor measurements. Until now, researcher were using this equivalent circuit in some studies but they were not defining accurately its parameters. The accurate parameters of the Thevenin equivalent circuit has been used until now for the calculation of the short circuit current [106] (at a connection point of interest) and to track weak grid conditions [107] but not for building an accurate equivalent circuit for simulation studies. In this PhD thesis, an improved methodology is developed based on the existing knowledge found in literature in order to define an accurate distribution grid equivalent for simulation studies.

Furthermore, a Detailed PV system model (DPVSM) is tuned and validated using measurements from 150 kW_p PV systems and it is then used in the simulation of different concentration scenarios. Its response is verified by utilizing measurements obtained before and after the installation of the 150 kW_p PV system in an industrial area. It is one of the few attempts made to measure data before and after the installation of a PV system inside the distribution grid which are utilized for the development of a PV system model. Moreover, the DPVSM is further used in the evaluation of different voltage regulation algorithms and in the study of fault response of an industrial grid topology.

Another important novelty of this research work lies in the development of a generic and accurate PV system model, which is presented in chapter 7 of this thesis. This PV system model gains the ability to characterize the transient behaviour of PV systems in a generic way via a parameter estimation process. The proposed model gives the opportunity to analyse more aspects of power quality and voltage stability with higher accuracy under balanced and unbalanced conditions.

Chapter 3
Power Quality

3.1 Introduction

In this chapter, power quality is defined as it is directly related to the operation of PV systems. The importance of power quality in the operation of current and future power networks is stated briefly. In addition, common power problems and the main standards referring to power quality are presented along with the most important power quality indices and limits. Lastly, the recently adopted standards for voltage regulation are included in this chapter as they are one of the very early but important steps undertaken towards the smart grid concept aiming to maintain the voltage variation inside the acceptable range and contribute in the stability of the power system in the presence of localized energy production.

3.2 Power/Voltage Quality

Power (or Voltage) quality is an area of research that has been under investigation for the last two decades. A problem that belongs in the category of power quality is actually any kind of abnormal voltage or current condition that can cause economic or technical damage to the users of the power network. The changes in the distribution network imposed by the massive introduction of power electronic devices and distributed generation make power

quality problems very important nowadays. Normally, the conventional way of transferring the energy from the power stations to customers does not induce serious problems on the distribution network when the power supply is strong enough to absorb disturbances. Sometimes a few customers may experience power quality problems in a local area depending on the type of the load and the distance from the power generation.

The task of estimating the economic consequences of poor power quality in the daily activity of different utility users is quite difficult [126]. According to a survey conducted in the USA, the economic losses due to power quality range roughly between 119 to 188 billion dollars a year [5], [6]. It is estimated that power quality issues in Europe are causing serious and avoidable reduction in industrial performance with an economic impact exceeding 150 billion euros annually [127]. The causes of the economic losses are mainly the supply outages and power quality related problems across all business sectors. With the liberalization in the electricity market, power quality is becoming a critical matter for the future electricity grid as it can be transformed into a source of financial gain. Thereafter research on power quality may play a significant role in enhancing the economic performance of modern utilities and key companies and organizations [11].

Utility customers are becoming more and more demanding in terms of energy consumption and they need good supply to operate reliably. At the same time they tend to disturb the utility supply with the equipment used for their main daily activities. Such kind of equipment may include variable speed drives, computers, electronic ballasts and power electronic devices. This is imposing a higher burden on utilities to supply good quality electrical energy. On the other hand, the European Union has ambitious targets for electricity generation from RES in the upcoming years. Consequently, renewable energy sources and distributed generation (DG) will play a significant role in the energy mix in the future and further investigation is required to optimize the grid development strategies and improve power quality [8]–[10], [128], [129].

3.3 Power Quality Problems

In order to understand and solve the power quality problems it is important to classify them into categories. There are different classifications for power quality issues which are characterised by specific properties. Some of the properties (shown in Table 3.1) classify the power quality events as "steady-state" and "non-steady-state" phenomena. In some regulations/standards the most important factor is considered to be the duration of the power quality event. On the other hand, some standards use the waveform shape or the frequency range of the event to characterize the power quality problem and classify it into a specific

category. Table 3.2 shows the classification of electromagnetic phenomena used by the power quality community. Also, in the following subsections, the main power quality problems are discussed briefly.

Table 3.1. Properties used for the categorization of power quality events [130]

Steady-state phenomena	Non-steady-state phenomena
Amplitude	Rate of rise
Frequency	Amplitude
Spectrum	Duration
Modulation	Spectrum
Source impedance	Frequency
Notch depth	Rate of occurrence
Notch area	Energy potential
	Source impedance

Table 3.2. Definition of power system disturbances [130]–[132]

Disturbance	Category	Sub-category	Typical spectral content	Typical duration	Typical voltage magnitude
Transients	Impulsive	Nanosecond	5ns rise	<50 ns	
		Microsecond	1μs rise	50 ns–1 ms	
		Millisecond	0.1ms rise	>1 ms	
	Oscillatory	Low frequency	<5 kHz	0.3–50 ms	0–4 pu
		Medium frequency	5–500 kHz	20 μs	0–8 pu
		High frequency	0.5–5 MHz	5 μs	0–4 pu
Short-duration variations	Instantaneous	Interruption		0.5–30 cycles	<0.1 pu
		Sag (dip)		0.5–30 cycles	0.1–0.9 pu
		Swell		0.5–30 cycles	1.1–1.8 pu
	Momentary	Interruption		30 cycles–3 s	<0.1 pu
		Sag (dip)		30 cycles–3 s	0.1–0.9 pu
		Swell		30 cycles–3 s	1.1–1.4 pu
	Temporary	Interruption		3 s–1 min	<0.1 pu
		Sag (dip)		3 s–1 min	0.1–0.9 pu
		Swell		3 s–1 min	1.1–1.2 pu
Long-duration variations	Interruption, sustained			>1 min	0.0 pu
	Undervoltages			>1 min	0.8–0.9 pu
	Overvoltages			>1 min	1.1–1.2 pu
Voltage/Current unbalance				Steady state	0.5–2%
Waveform distortion	DC offset			Steady state	0–0.1%
	Harmonics		0–100th harmonic	Steady state	0–20%
	Interharmonics		0–6 kHz	Steady state	0–2%
	Notching			Steady state	
	Noise		Broadband	Steady state	0–1%
Voltage fluctuations			<25 Hz	Intermittent	0.1–7%
	Flicker				0.2–2 Pst
Power frequency variations				<10 s	

3.3.1 Transients

For a long time, the term “transients” has been used in the analysis of power system variations to denote events which are undesirable and momentary in nature. Another simple definition for the word “transient” adopted quite commonly in international standards is “a phenomenon or quantity which varies between two consecutive steady states during a time interval which is short compared with the time-scale of interest” [133]. Transients can be

classified into two categories: impulsive and oscillatory. An impulsive transient is a sudden frequency change in the steady-state condition of voltage, current, or both. Their characteristics and waveforms depend on the mechanism of generation and the distribution network parameters. Impulsive transients are normally characterized by their rise and decay times, which can also be revealed by their spectral content. The most common cause of impulsive transients is a lightning current surge. Such an example of a typical current impulsive transient caused by lightning is shown in Fig. 3.1.

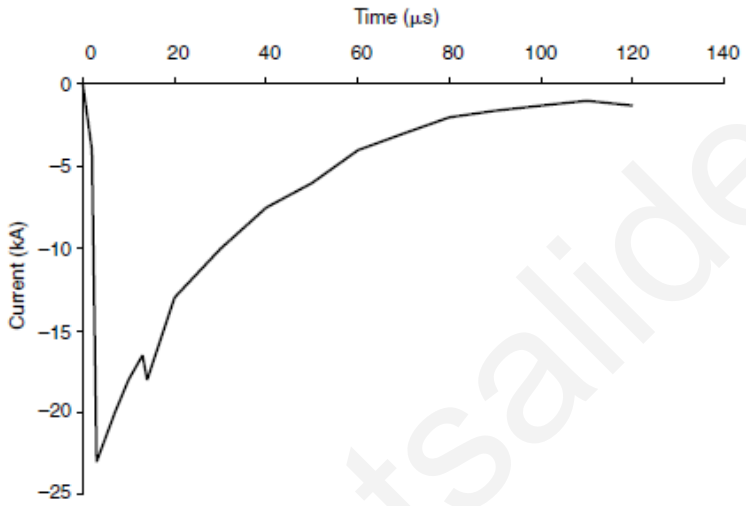

Figure 3.1. Lightning stroke current impulsive transient [130]

An oscillatory transient is a sudden frequency change in the steady-state condition of voltage, current, or both that includes both positive and negative polarity values. Oscillatory transients can be a result of appliance switching, fast acting overcurrent protective devices, capacitor bank switching and ferroresonance. An example of oscillatory transient voltage caused by back-to-back capacitor switching is shown in Fig. 3.2.

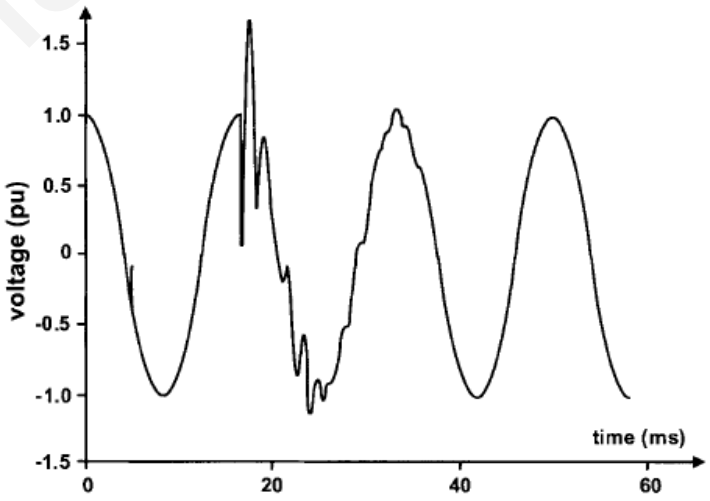

Figure 3.2. Oscillatory transient voltage caused by capacitor bank energisation [132]

3.3.2 Short-Duration Voltage Variations

In this category, there are three different types of short-duration events designated as instantaneous, momentary, and temporary. Each subcategory is divided into interruption, sag, and swell. Short-duration voltage variations are caused by fault conditions, large load energisation and loose wiring connections. In the case of a fault, the impact on the voltage is of short-duration variation because protective devices operate immediately to clear the fault. An interruption occurs when the supply voltage decreases to less than 0.1 pu for less than 1 minute. Some causes of interruption are equipment failures, control malfunction or breaker opening. The difference between interruption and long/sustained interruption is that in the former the supply is restored automatically in a few cycles, but during the latter the supply should be restored manually. Interruption is characterized based on its duration according to Table 3.2. An example of momentary interruptions due to a fault is shown in Fig. 3.3.

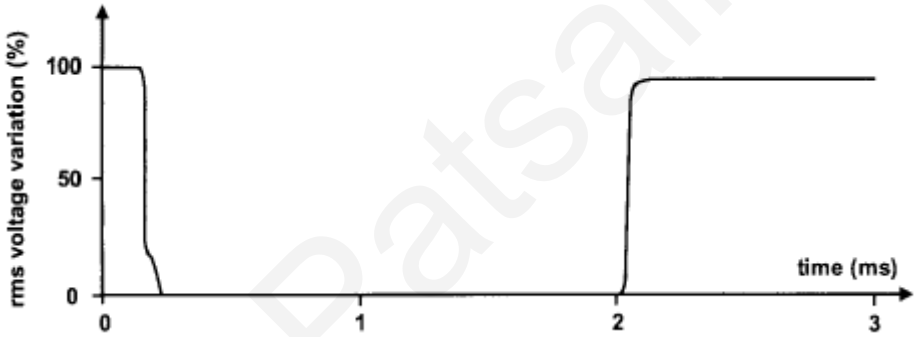

Figure 3.3. Momentary interruptions due to a fault [132]

A sag is a decrease to between 0.1 and 0.9 pu in rms voltage or current at the power frequency for durations from 0.5 cycle to 1 min. Voltage sags are the main reason for malfunction of electrical low-voltage devices which are usually caused by energisation of heavy loads, starting of large induction motors and single line-to-ground faults. Uninterruptible power supplies or power conditioners are mostly used to prevent voltage sags. A voltage sag caused by a single line-to-ground fault is depicted in Fig. 3.4.

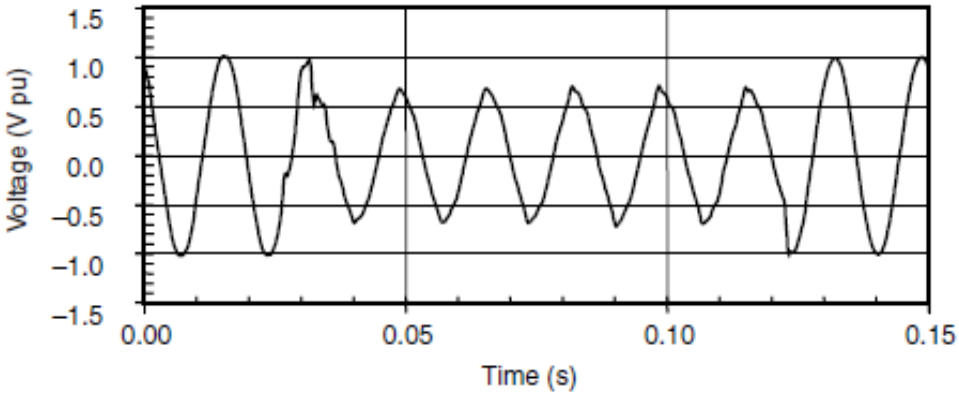

Figure 3.4. Voltage sag waveform for a single-line-to-ground fault [130]

The increase of voltage magnitude between 1.1 and 1.8 pu is called swell. The most accepted duration of a swell is from 0.5 cycles to 1 minute. Swells are not as common as sags and their main causes are switching off large loads, energising a capacitor bank, or single line-to-ground faults. If a single-line-to-ground fault is observed on one of the three phases, then voltage swells may arise on the other two phases. Such a voltage swell is represented graphically on Fig. 3.5.

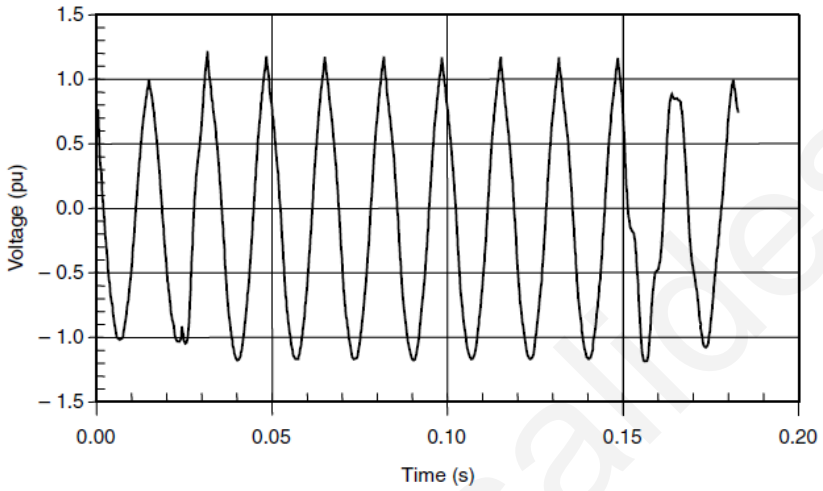

Figure 3.5. Instantaneous voltage swell caused by a single-line-to-ground fault [130]

3.3.3 Long-Duration Voltage Variations

The deviation of the rms value of voltage from the nominal value for longer than 1 minute is categorized as long-duration voltage variation. Long-duration voltage variations can be overvoltages, undervoltages or sustained interruption. Overvoltages and undervoltages generally are not the result of faults, but can be induced by load variations and switching operations. Inadequate voltage regulation or incorrect tap settings on distribution transformers can also result in overvoltage events. An overvoltage is an increase in the rms ac voltage greater than 110 percent for a duration longer than 1 min. On the other hand, an undervoltage is a decrease in the rms ac voltage to less than 90 percent for a duration longer than 1 min. Undervoltages are the result of switching events that are opposite to the events causing overvoltages. Specifically, a heavy load connection or a capacitor bank disconnection can both cause an undervoltage which is maintained until voltage regulation mechanisms of the power system restore the voltage back to its nominal value. Overloaded circuits can result in undervoltages as well. When the supply voltage has been zero for a period of time in excess of 1 min, the long-duration voltage variation is classified as sustained interruption. Voltage interruptions longer than 1 min are usually permanent events, which must be handle in a manual way by the utility personnel in order to resolve any problems and restore the voltage back to the nominal value.

3.3.4 Voltage/Current Unbalance

At the case when the voltages/currents of a three-phase system are not identical in magnitude and/or the phase difference between them is not exactly 120 degrees, voltage/current unbalance occurs. Voltage/Current unbalance is defined in standards with the help of symmetrical components. In more detail, the ratio of either the negative or zero sequence component to the positive-sequence component can be used to specify the percent of unbalance. Figure 3.6 shows an example of the aforementioned ratios obtained from a residential feeder. Sometimes voltage/current unbalance is defined as the maximum deviation from the average of the three-phase voltages/currents, divided by the average of the three-phase voltages/currents, expressed in a percentage.

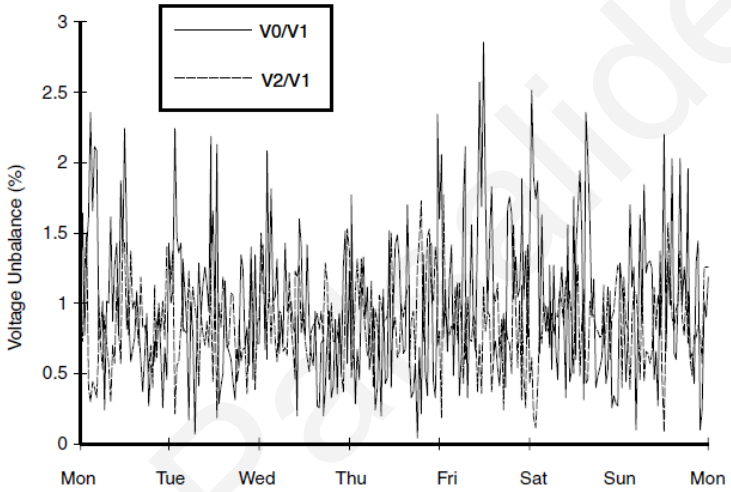

Figure 3.6. Voltage unbalance trend for a residential feeder [130]

The main causes of voltage imbalance in power systems are: a) the unbalanced single-phase loading in a three-phase system, b) overhead transmission lines that are not transposed, c) blown fuses in one phase of a three-phase capacitor bank, and d) severe voltage imbalance (more than 5%), which can result from single phasing conditions [132].

3.3.5 Waveform Distortion

A steady-state deviation from a sine wave of power frequency is called waveform distortion. The five primary types of waveform distortions are the DC offset, harmonics, interharmonics, notching, and the noise. A Fourier series is commonly used for the analysis of a non-sinusoidal waveform. The presence of a DC voltage or current in a power system is termed DC offset. This can occur as the result of a geomagnetic disturbance or asymmetry of electronic power converters. DC can have a harmful effect on transformer cores if it bias them so they saturate in normal operating conditions. This can cause additional heating and reduction of transformer life. Furthermore, DC may cause the erosion on grounding electrodes or other connectors. Harmonics are sinusoidal voltages or currents with

frequencies that are integer multiples of the fundamental frequency. Periodically distorted waveforms can be decomposed into a sum of fundamental component and harmonics. Harmonic distortion is created by nonlinear devices or loads connected on the power system. Harmonic distortion levels are described by the complete harmonic spectrum with magnitudes and phase angles for each individual harmonic component. It is also common to use the total harmonic distortion (THD) index to characterize the overall harmonic distortion.

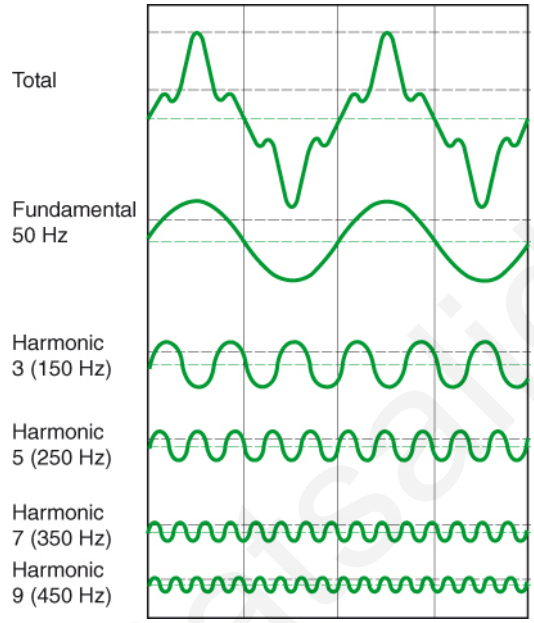

Figure 3.7. Distorted waveform and its harmonic components

Interharmonics are harmonic components which are not integer multiples of the fundamental frequency and they can appear as discrete frequencies or as a wideband spectrum. The main sources of interharmonics are the static frequency converters, the cycloconverters, the induction furnaces, and the arcing devices. Notching is a periodic voltage disturbance caused by the normal operation of power electronic devices when current is commutated from one phase to another (Fig. 3.8).

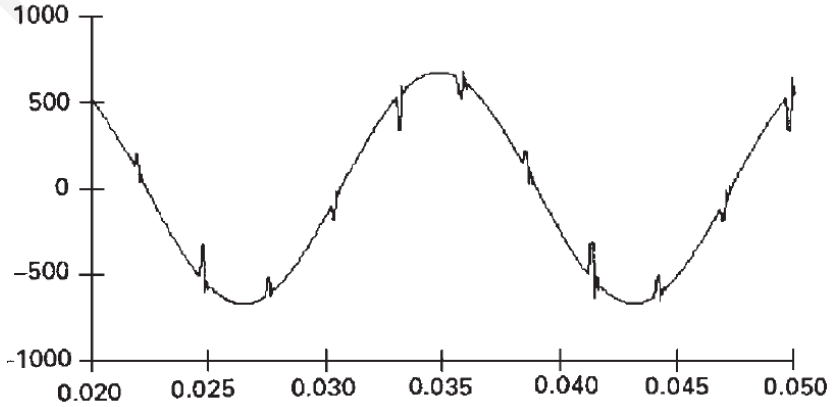

Figure 3.8. Example of voltage notching caused by a three-phase converter [130]

During the notching period, a momentary short-circuit is created between the commutating phases which reduces the line voltage (the amplitude of reduction is affected the system impedance). Finally, electric noise is defined as unwanted electrical signals with broadband spectral content lower than 200 kHz superimposed on the voltage/current waveform. Noise may result from faulty connections in transmission or distribution systems, arc furnaces, electrical furnaces, power electronic devices, control circuits, improper grounding etc.

3.3.6 Voltage Fluctuation and Flicker

Voltage fluctuations are systemic variations of the voltage envelope or random voltage changes, the magnitude of which does not normally exceed the voltage limits. Voltage fluctuations are divided into two categories. Those are the step-voltage changes which are regular/irregular in time and the cyclic/random voltage changes produced by load variations. Voltage fluctuations degrade the performance of electronic equipment and they may cause instability of its internal voltages/currents. Despite this, voltage fluctuations with an amplitude of less than 10% (in comparison to the nominal voltage) do not affect electronic equipment. Some of the main causes of voltage fluctuation are start-up of drives, arc furnaces, drives with rapidly changing loads, and rolling mills. A subcategory of voltage fluctuation is flicker which has been described as "continuous and rapid variations in the load current magnitude which causes voltage variations". The term “flicker” is derived from the impact of the voltage fluctuation on lamps in such a way that they are perceived by the human eye. An example of voltage fluctuation that can cause flicker are shown in Fig. 3.9.

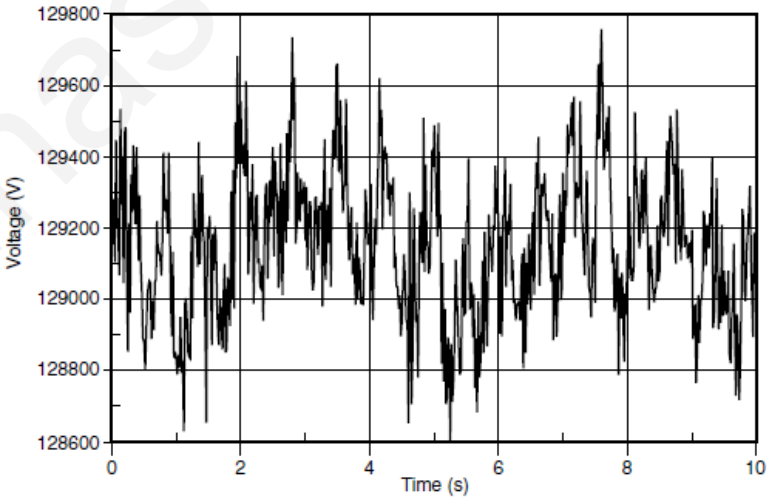

Figure 3.9. Example of voltage fluctuations caused by arc furnace operation [130]

3.3.7 Power Frequency Variations

Power frequency variations are defined as the deviation of the system fundamental frequency from it specified nominal value. The power system frequency is directly related to the rotational speed of the generators supplying the loads of the system. Normally, slight

variations in frequency arise in the attempt of balancing the generation with the load demand. The size of the frequency variations and its duration depend on the load characteristics and the response of the generation control system to load changes. Frequency variations that go outside of accepted limits for normal steady-state operation of the power system can be caused by faults on the bulk power transmission system, heavy load disconnection, or loss of significant power generation. For modern interconnected power systems, significant frequency variations are a rare phenomenon but they may appear on power systems which are isolated from the utility grid [130]–[132].

3.3 Power Quality Standards

The most common power quality standards in use nowadays are the EN 50160 [134], [135], the IEC 61000-4-30 [136] and the IEEE Standard 519-1992 [137]. The standard EN 50160 provides recommended levels of different power quality parameters, specifying also the time-based percentage during which levels should not be exceeded. The IEC 61000-4 provides the adequate methods for measuring voltage and current quantities, defines the aggregation periods, describes the measurement formulas and sets the accuracy levels. According to the European standard EN 50160 (IEC 50160), accommodated by most European Grid Codes, "Voltage characteristics of electricity supplied by public distribution systems", the voltage root-mean-square (RMS) should vary in the range of ±10% of the nominal voltage (230 V) for 95% of total operating time (at least one week). Also, the limit for total harmonic distortion should not exceed 8 %, including up to the 40th harmonic. More details are found on Tables 3.3 and 3.4.

Table 3.3. EN50160 power quality limits and acceptable time interval of tolerance

Power Quality Parameter	Supply voltage characteristicsaccording to EN 50160
Grid frequency	Mean value over 10 seconds ▪ -6% / +4% (47Hz to 52Hz) during 100% of the time ▪ ± 1% during 99.5% (49.5Hz to 50.5Hz) of the time
Supply voltage variations (under normal operating conditions, excluding situations arising from faults or voltage interruptions)	Mean value over 10 minutes ▪ U_n ±10% during 95% of one week (This report adopts a more restrictive limit opposed by Electricity Authority of Cyprus which actually is U_n -6%/+10%) ▪ U_n -15%/+10% during 100% of the time
Flicker severity	Plt≤1 for the 95% of the time
Rapid voltage changes	U_n ±5% normal, U_n ±10% infrequently with a short duration
Supply voltage dips	Duration < 1 seconds ,Depth <60% ▪ Locally limited dips caused by load switching on: Low Voltage (LV):10-50% and Medium Voltage (MV):10-15%
Short Interruptions of supply voltage	LV, MV: (up to 3 minutes) few tens –few hundreds / year
Long Interruptions of supply voltage	LV, MV: (longer than 3 minutes) < 10 - 50 /year
Temporary, power frequency overvoltages	LV: <1.5 kV rms MV: 1.7 Uc (solid or impedance earth) 2.0 Uc (unearthed or resonant earth)
Transient overvoltages	LV: generally < 6kV (Occasionally higher; rise time: ms – μs)
Supply voltage unbalanced	LV, MV: up to 2% for 95% of week, mean 10 minutes rms values
Harmonic voltage	8% Total Harmonic Distortion (THD) - LV, MV: For more details see Table 3.4

Table 3.4. Values of individual harmonic voltages at the supply terminals for orders up to 25, given in percent of U_n

Power Quality Parameter				Supply voltage characteristics according to EN 50160	
Not multiples of 3		Multiples of 3			
Order h	Relative voltage (%)	Order h	Relative voltage (%)	Order h	Relative voltage (%)
5	6	3	5	2	2
7	5	9	1.5	4	1
11	3.5	15	0.5	6....24	0.5
13	3	21	0.5		
17	2				
19	1.5				
23	1.5				
25	1.5				

U_n- Nominal voltage of the supply system (rms)

The IEEE Standard 519-1992 "Recommended Practices and Requirements for Harmonic Control in Electrical Power Systems" specifies the limits of harmonic voltage and current at the point of common coupling between end user and distribution utilities. The approach adopted in this standard requires the participation of both end users and utilities. The limits established by this standard are equal to 5 % for the voltage and current total harmonic distortion that the producer can provide to the customer. The limits for the maximum individual harmonic components are also determined and must be 3 % for voltage lower than 69 kV.

Table 3.5. Current Distortion Limits at STC

Current Distortion Limits at STC[a] (IEC 61727)	
Odd Harmonics	*Distortion Limit*
3rd through 9th	Less than 4.0%
11th through 15th	Less than 2.0%
17th through 21st	Less than 1.5%
23rd through 33rd	Less than 0.6%
Even Harmonics	*Distortion Limit*
2rd through 8th	Less than 1.0%
10th through 32nd	Less than 0.5%
Current Distortion	*Limit at STC[a]*
Total Harmonic Distortion (THD)	Less than 5.0%

a. STC - Standard Test Conditions

The European standard EN 61727 (IEC 61727) "Photovoltaic (PV) systems - Characteristics of utility interface" (Table 3.5) has established less restrictive limits for current harmonics. The total harmonic distortion shall be less than 5 % at rated inverter output and even individual harmonics shall be less than 25 % of the lower odd harmonic limits [112]. However, concerns about the shortfalls of current standards have started to emerge in the literature and the attempt to validate their usefulness in modern grids constitutes a significant issue that must be investigated [138]–[142]. Some standard which are related to power quality are found in Tables 3.6 and 3.7.

Table 3.6. IEEE and ANSI guidelines [131]

IEEE 4	Standard techniques for high-voltage testing
IEEE 100	Standard dictionary of electrical and electronic engineering
IEEE 120	Master test guide for electrical measurements in power circuits
IEEE 141	Recommended practice for electric power distribution for industrial plants with effect of voltage disturbances on equipment within an industrial area
IEEE 142	Recommended practice for grounding of industrial and commercial power systems
IEEE 213	Standard procedure for measurement of conducted emissions in the range of 300 kHz–25MHz from television and FM broadcast receivers to power lines
IEEE 241	Recommended practice for electric power systems in commercial buildings
IEEE 281	Standard service conditions for power system communication equipment
IEEE 299	Standard methods of measuring the effectiveness of electromagnetic shielding enclosures
IEEE 367	Recommended practice for determining the electric power station ground potential rise and induced voltage from a power fault
IEEE 376	Standard for the measurement of impulse strength and impulse bandwidth
IEEE 430	Standard procedures for the measurement of radio noise from overhead power lines and substations
IEEE 446	Recommended practice for emergency and standby systems for industrial and commercial applications (e.g., power acceptability curve, CBEMA curve)
IEEE 449	Standard for ferroresonance voltage regulators
IEEE 465	Test specifications for surge protective devices
IEEE 472	Event recorders
IEEE 473	Recommended practice for an electromagnetic site survey (10 kHz–10 GHz)
IEEE 493	Recommended practice for the design of reliable industrial and commercial power systems
IEEE 519	Recommended practice for harmonic control and reactive compensation of static power converters
IEEE 539	Standard definitions of terms relating to corona and field effects of overhead power lines
IEEE 859	Standard terms for reporting and analyzing outage occurrences and outage states of electrical transmission facilities
IEEE 944	Application and testing of uninterruptible power supplies for power generating stations
IEEE 998	Guides for direct lightning strike shielding of substations
IEEE 1048	Guides for protective grounding of power lines
IEEE 1057	Standards for digitizing waveform recorders
IEEE P1100	Recommended practice for powering and grounding sensitive electronic equipment in commercial and industrial power systems
IEEE 1159	Recommended practice on monitoring electric power quality. Categories of power system electromagnetic phenomena
IEEE 1250	Guides for service to equipment sensitive to momentary voltage disturbances
IEEE 1346	Recommended practice for evaluating electric power system compatibility with electronics process equipment
IEEE P1453	Flicker
IEEE/ANSI 18	Standards for shunt power capacitors
IEEE/ANSI C37	Guides for surge withstand capability (SWC) tests
IEEE/ANSI C50	Harmonics and noise from synchronous machines
IEEE/ANSI C57.110	Recommended practice for establishing transformer capability when supplying no sinusoidal load currents
IEEE/ANSI C57.117	Guides for reporting failure data for power transformers and shunt reactors on electric utility power systems
IEEE/ANSI C62.45	(IEEE 587) Recommended practice on surge voltage in low-voltage AC power circuits, including guides for lightning arresters applications
IEEE/ANSI C62.48	Guides on interactions between power system disturbances and surge protective devices
ANSI C84.1	American national standard for electric power systems and equipment voltage ratings (60 Hz)
ANSI 70	National electric code
ANSI 368	Telephone influence factor
ANSI 377	Spurious radio frequency emission from mobile communication equipment

Table 3.7. IEC guidelines [131]

IEC 38	Standard voltages
IEC 816	Guides on methods of measurement of short-duration transients on low-voltage power and signal lines. Equipment susceptible to transients
IEC 868	Flicker meter. Functional and design specifications
IEC 868-0	Flicker meter. Evaluation of flicker severity. Evaluates the severity of voltage fluctuation on the light flicker
IEC 1000-3-2	Electromagnetic compatibility Part 3: Limits Section 2: Limits for harmonic current emissions (equipment absorbed current <16 A per phase)
IEC 1000-3-6	Electromagnetic compatibility Part 3: Limits Section 6: Emission limits evaluation for perturbing loads connected to MV and HV networks
IEC 1000-4	Electromagnetic compatibility Part 4: Sampling and metering techniques
EN 50160	Voltage characteristics of electricity supplied by public distribution systems
EN 50438	Requirements for micro-generating plants to be connected in parallel with public low-voltage distribution networks
EC/EN 60868	Flicker meter implementation
IEC 61000	Electromagnetic compatibility (EMC)

3.4 Standards for Voltage Regulation

The need for voltage regulation in distribution grids with significant amount of distributed generators has been identified and added as a requirement in the latest standards for generating plants installed in public low-voltage distribution networks. According to the newly published European standard (EN) 50438:2013, which refers to micro-generators (sources of electrical energy designed to operate in parallel with a public low voltage distribution network with nominal currents up to and including 16 A per phase), the reactive power exchange with the electricity grid for voltage regulation purposes should follow the characteristic curve provided by the Distribution System Operator (DSO) within active factors $\cos\varphi = 0.9_{\text{under-excited}}$ to $\cos\varphi = 0.9_{\text{over-excited}}$ when the active power output of the micro-generator is more than or equal to 20 % of its nominal active power. Furthermore, the micro-generator is not allowed to exchange more reactive power than 10 % of the micro-generator's nominal power when the active power output is less than 20 % of its nominal active power [138]. A European standard that will set the requirements for connection of generators above 16 A per phase is still under development due to variations in the electricity grids of different European countries [139], [140]. Nevertheless, the requirements stated in EN 50438:2013 are in line with the German Guideline "Generating Plants Connected to the Medium-Voltage Network" [115].

Chapter 4
Simple PV System Model (SPVSM)

4.1 Introduction

The most straightforward method found in the literature for the PV systems modelling was adopted for the initial power quality investigations. More specificity, the PV system is modelled as a set of harmonic current sources which are connected in parallel at the point of common coupling with the utility. The harmonic current sources are configured either by using analysed or raw measurements data. The power related measurements are acquired using the power quality analysers ACE 4000 and Fluke 1760. The solar irradiance and temperature measurement data are taken from the measurement database of the PV Technology Laboratory, University of Cyprus. Furthermore, weather measurements were taken from the Metrological station in Akrotiri, Limassol (also operated by the PV Technology Laboratory). Simulation results for different PV concentrations are obtained by using the Simple PV System Model (SPVSM) and an evaluation is performed for the model, network topology and methods used in the simulation studies. More details about the distribution grid topology and methodology followed in the simulations while using the SPVSM are also presented in this chapter.

4.2 Measurements and Data Acquisition

4.2.1 Power Quality Analysers/Recorders

For the power quality measurements two powerful, versatile three-phase electric power quality analyser/recorders were used. Those are the ACE 4000 and the Fluke 1760. Both have enough processing power and robust data management capabilities that allow the acquisition of highly accurate measurements even on distorted waveforms. The intuitive Windows interface makes the setup of measurements and the analysis of data a simple procedure.

The measurements can be exported in text file or excel format for further analysis using other processing software. Measurement surveys can be performed by selecting either fully automatic or customizable setup options. All AC and DC measurements can be made without any programming required. Recording triggers can be specified for any power quality characteristic, and measurements can be made with multiple recording rates. All power quality measurements are simultaneously recorded in the instrument's high-capacity hard drive with true cycle-by-cycle measurement and a minimum of 256 samples per cycle on every channel.

Table 4.1. Main functionalities/Measurements of Power Quality Analyzers/Recorders

Measurement Types	
The instruments combine many different measurement types, also referred to as "virtual instruments":	
• **Digital recording of measured data (data logger)** • **Power measuring device (recording of load profiles)** • **Recording of power frequency** • **Power Quality Analyser**	• Fast transient recorder • Ripple control signal analyser • Harmonics analyser • Voltage disturbances analyser (events)
Measurements	
The following measurements can be made:	
• **RMS values of voltage and current as well as power values with programmable averaging time** • **Oscilloscope data (instantaneous value, sensing value)** • **Powerful and versatile triggering engine**	• Load and energy measurements • Analysis of voltage and current harmonics/interharmonics • Fast transient analysis • Signalling voltage, ripple control signal analysis

All recorded data (samples, phasors, waveforms, harmonic spectra and measurement text) can be displayed in real-time. Once a measurement survey has been completed, data may easily be exported for use in any spreadsheet or other data analysis application. Fluke 1760 can also perform statistical analysis on data based on the EN50160 standard. The main functionalities and measurements available are mentioned in Table 4.1.

4.2.2 Environmental Conditions Measurements Infrastructure

Both meteorological and PV system measurements are being acquired and stored through an advanced measurement platform at the PV Technology Laboratory. The platform comprises of meteorological and electrical sensors connected to a central data logging system that stores data at a resolution of 1-second and accumulation steps of 15-minute averages.

The monitored meteorological parameters include solar irradiance, wind direction and speed as well as ambient and module temperature. The electrical parameters measured include DC current and voltage, DC and AC power at MPP as obtained at each PV system output. The meteorological station in Akrotiri has the same capabilities in terms of weather measurement quantities from which data have also been obtained [108].

4.2.3 Data Collection - PV related Measurements

For proper modelling of the PV systems, measurements were undertaken at grid connected photovoltaic systems that are located in different locations around Cyprus. A power quality analyser was placed at the output of single or three phase photovoltaic systems to measure the appropriate power quality parameters.

Also solar irradiance was monitored using a pyranometer in some cases when the PV system was located nearby a meteorological station. The quantities recorded are the solar irradiance, power factor, the amplitude and angle of individual current harmonics, the Total Harmonic Distortion (THD), active and reactive power harmonics and RMS values of voltage and current for a time period of two weeks (one week before the connection of the PV system to the grid and one week after the connection). A typical example of the solar irradiance measurements for an average day in Cyprus is shown in Fig. 4.1a. The solar irradiance profile for a low irradiance day is shown in Fig. 4.1b. By comparing the results for current THD on an average day shown in Fig. 4.1c with that measured on a low irradiance day, Fig. 4.1d, it can be deduced that solar irradiance plays some role in the distortion of the current waveform and hence the quality of supplied energy. The current and voltage waveforms during different solar irradiance conditions are shown in Fig. 4.1e and 4.1f. Due to the fact that the energy input at low irradiance periods is low, the harmonic content of current waveform is getting significant in comparison to the fundamental frequency. The opposite applies for high solar irradiance conditions. Moreover, the current distortion observed on current waveforms does not affect the voltage significantly.

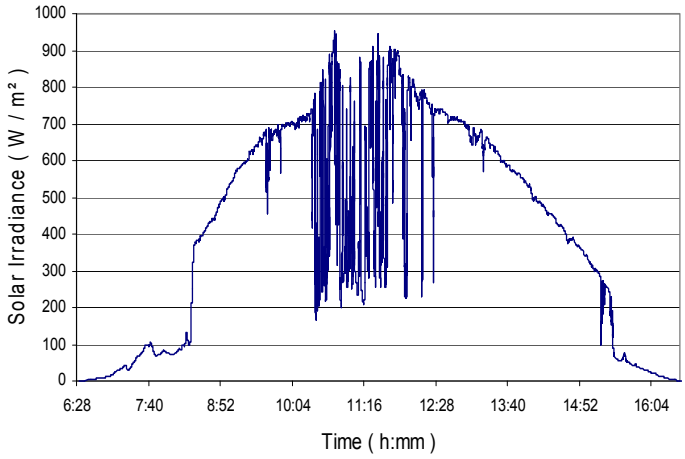

Fig. 4.1a. Solar Irradiance observed for an average day

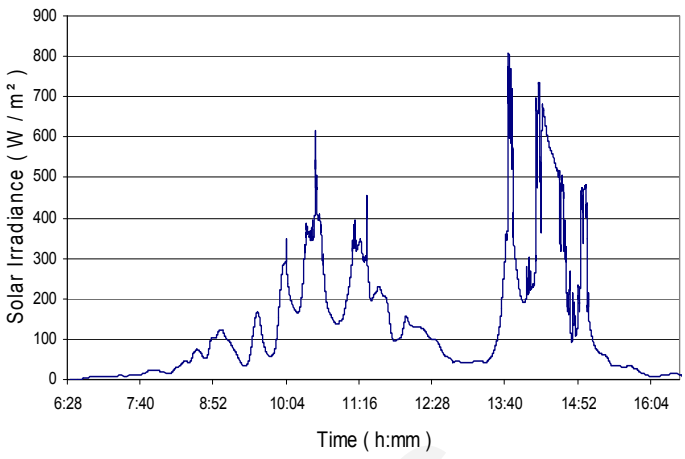

Fig. 4.1b. Solar Irradiance observed for a low solar irradiance day

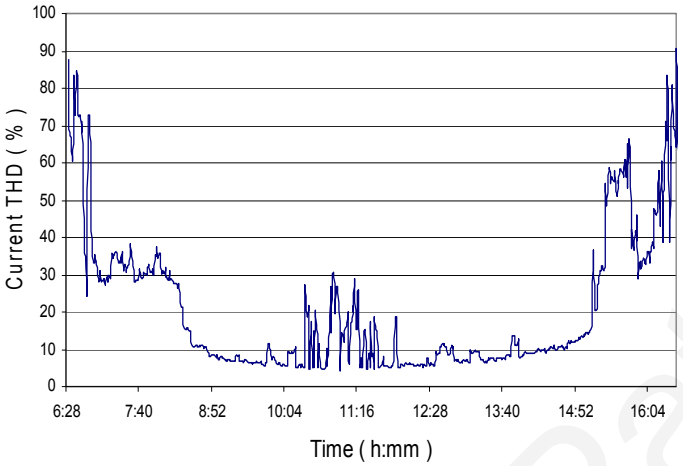

Fig. 4.1c. Current THD measured for an average day

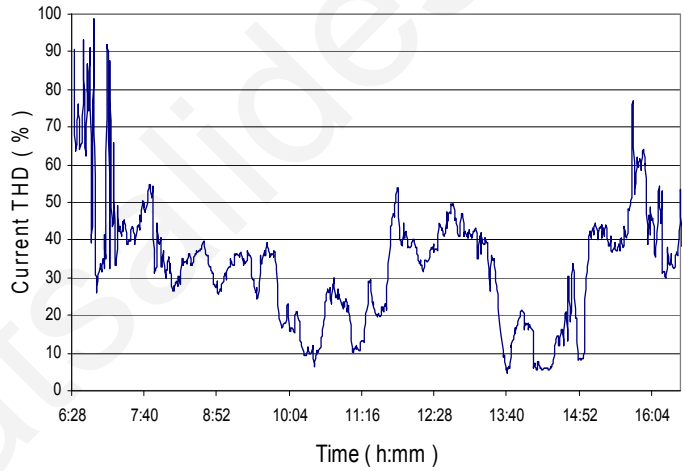

Fig. 4.1d. Current THD measured for a low solar irradiance day

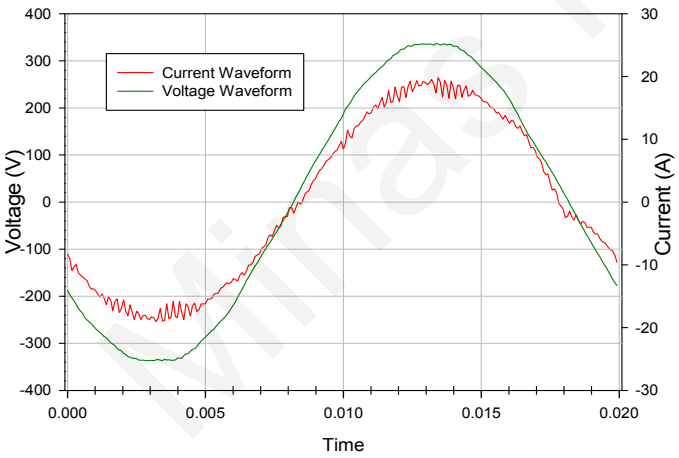

Fig. 4.1e. Voltage and Current Waveforms measured during high irradiance (950 W/m2)

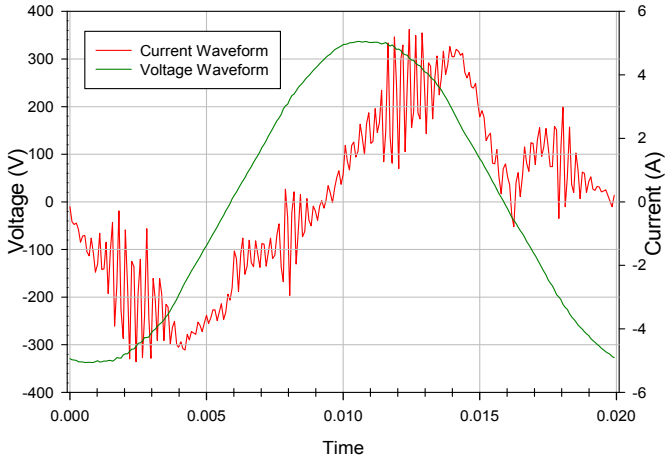

Fig. 4.1f. Voltage and Current Waveforms measured during low irradiance (250 W/m2)

Figure 4.1. Measurements observed during different solar irradiance conditions

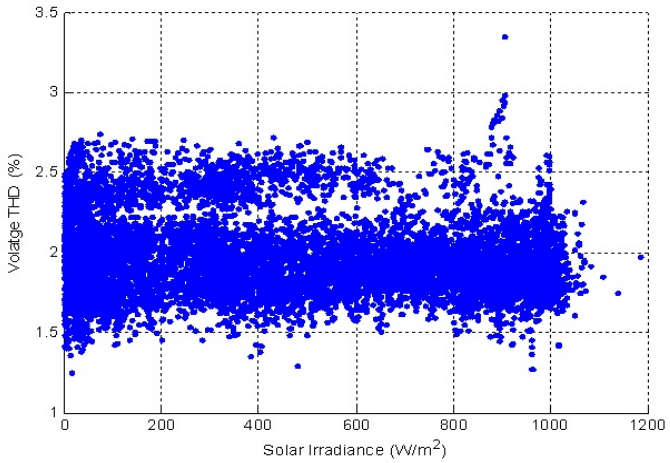

Fig. 4.2a. Measured Voltage THD vs Solar Irradiance measured at the PV Technology Laboratory

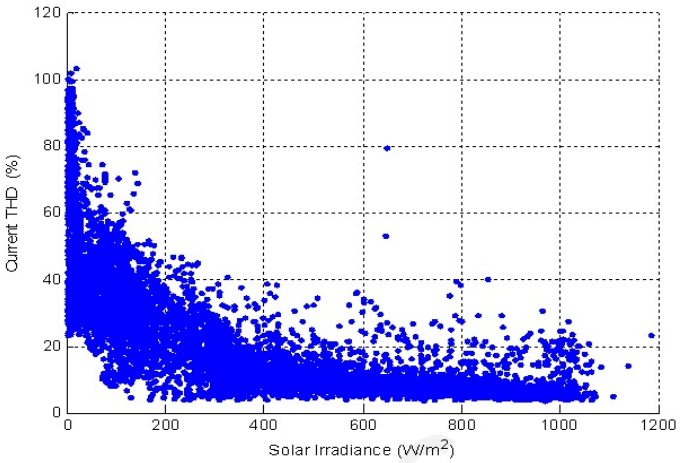

Fig. 4.2b. Measured Current THD vs Solar Irradiance Measured at the PV Technology Laboratory

Figure 4.2. Measured Voltage and Current THD vs Solar Irradiance Measured at the UCY PV Park

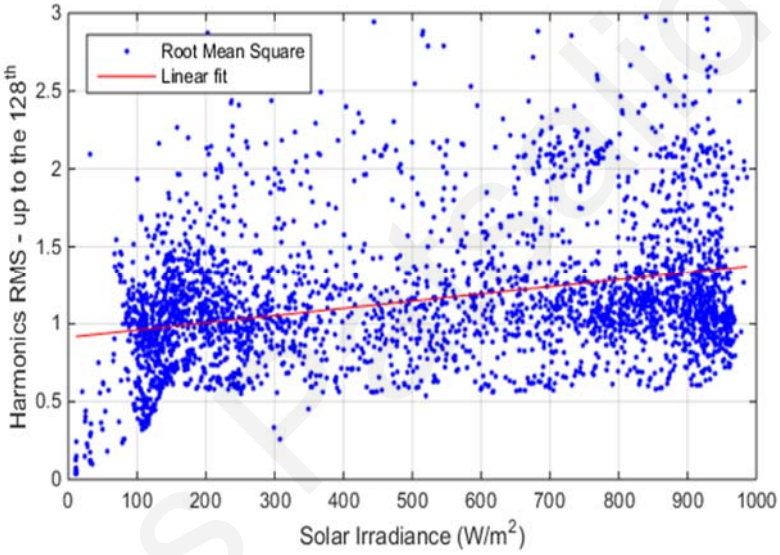

Figure 4.3. Harmonics RMS vs Solar Irradiance Measured at the PV Technology Laboratory

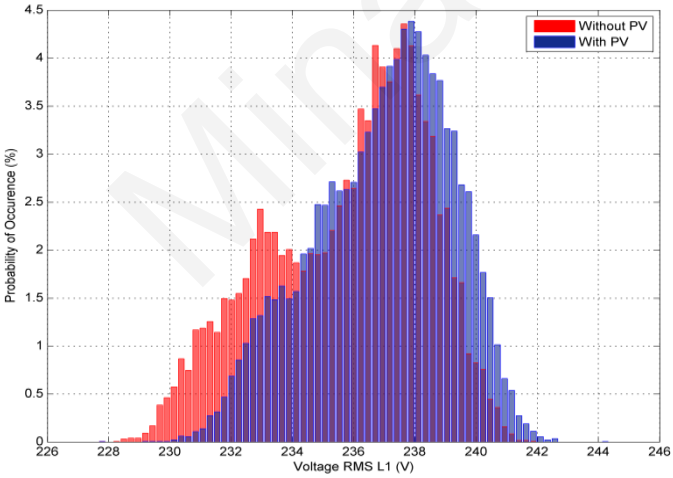

Figure 4.4a. Voltage RMS before and after the installation of the PV system

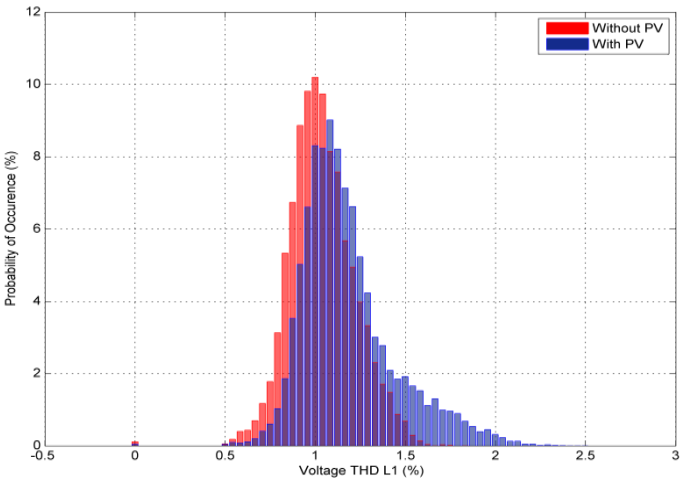

Figure 4.4b. Voltage THD before and after the installation of the PV system

Figure 4.4. Measurements obtained at the busbar of the distribution transformer before and after the installation of a 150kW$_p$ PV system in an industrial area under investigation

However, this will have a tremendous effect at high concentration scenarios. In order to formulate a clearer view of the effect of solar irradiance on voltage and current waveform, power quality quantities were correlated with the instantaneous solar irradiance measured during a two week period and the results are shown in Fig. 4.2a and 4.2b for the voltage and current THD respectively. The current THD measured at the output of the PV system under investigation is very sensitive to changes of incident radiation. This occurs because of two reasons: a) The THD index is inversely proportional to the current amplitude (as seen by equation (4.1)) and consequently inversely proportional to solar irradiance and b) The root mean square of current harmonics is promotional to the solar irradiance as depicted in Fig. 4.3. Both the THD index and the root mean square (RMS) value of the total harmonics of a signal are defined as follows:

$$THD^A = \frac{H_{RMS}}{A_1} = \frac{\sqrt{{A_2}^2 + {A_3}^2 + {A_4}^2 \cdots + {A_n}^2}}{A_1} \tag{4.1}$$

where H_{RMS} is the root mean square of harmonics up to the nth order, A_n is the RMS of nth harmonic and A_1 is the RMS of fundamental frequency. On the other hand, the voltage harmonics are not strongly dependent on the fluctuations of solar irradiance, as the impedance seen by the PV system is not significant to amplify the injected current harmonics and convert them into voltage harmonics. If the impedance was significant, the linear relationship between solar irradiance and current harmonic would be reflected on voltage THD index as well. The total voltage harmonic distortion is found to range from 1.2 % to 3.5 %, as shown in Fig. 4.2a. Also, the current total harmonic distortion has a larger range of values, from 3.8% to 103.4% (Fig. 4.2b). In general, the current distortion consists a result of switching operation of the inverter which can be boosted by the inability of control circuit and sensors of the inverter to measure and maintain the sinusoidal waveform shape of the output current. Furthermore, the nonlinearity of the inverter due to factors such as (i) the dead time, (ii) the delay in gate drive circuits, (iii) turn-on and turn-off delays, (iv) parasitic capacitance effects, (v) voltage drop in switching devices, (vi) zero-current clamping and (vii) short pulse dropping can play a significant role in the distortion of output current [141].

Fig. 4.4 shows the resulting voltage RMS and voltage distortion at the busbar of the distribution transformer of an industrial area with and without the presence of the PV systems (Phase A). Similar results are observed on all the three phases. The aforementioned results observed are similar in the majority of places where large PV systems are installed and consequently are used further in the modelling and simulation procedure explained in the next chapters.

4.3 SPVSM - Network - Methodology

4.3.1 SPVSM - Set of parallel Harmonic Current Sources

Firstly, the PV system has been modelled as a set of harmonic current sources and it has been configured using the measurements from the PV systems. Two different ways were adopted in using the aforementioned model depending on the simulation type and software used. The model used in PSCAD software is shown in Fig. 4.5. Details about the model formulated in DigSilent software are found in subsection 4.3.3.1.

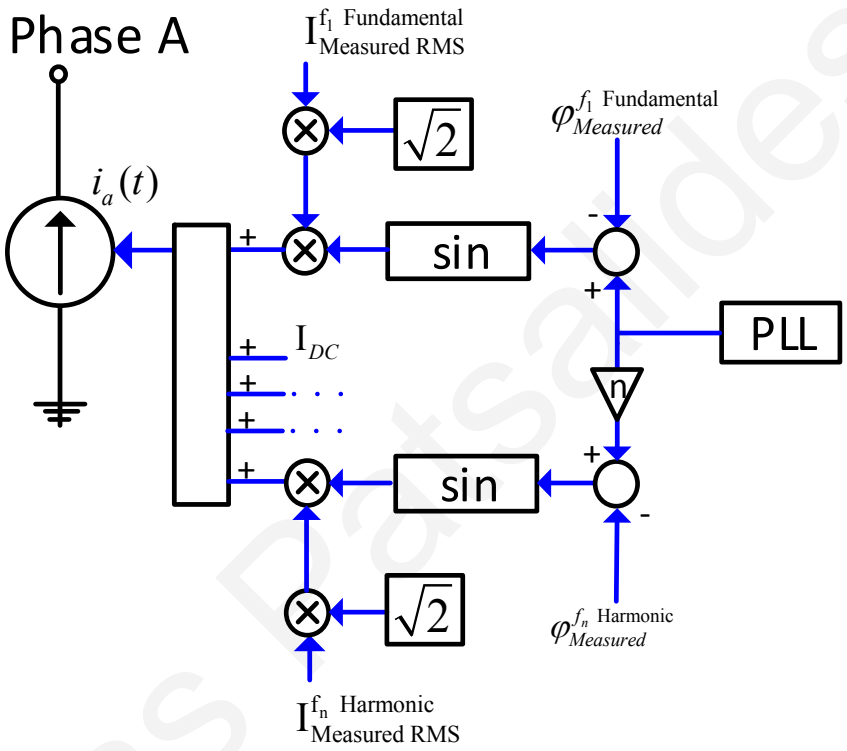

Figure 4.5. SPVSM - Three phase current source configured using measurements

At the beginning, the model was inserted into DigSilent software for performing steady-state simulations. In order to obtain the data required for configuring the current source, statistical analysis was performed on measurements from which three different simulation cases have been extracted based on solar irradiance. The phase of measured harmonic currents was modified according DigSilent requirements in order to be inserted into the aforementioned software having the right format. In the second phase, the model was inserted into PSCAD software and the simulation was repeated using the raw harmonic measurements. The correction for phasor angles has been provided from a Phase Lock Loop Element (PLL). An advanced version of the aforementioned model is found in [19] which takes into account also the voltage at the fundamental frequency to adjust the fundamental frequency current (but it does not model current harmonics) and it is further used in the study of the voltage levels in

a distribution grid with high PV penetrations. In [19], the voltage harmonic distortion is not considered.

4.3.2 Distribution Network under investigation - Radial Topology

The network configuration chosen for simulation while using the SPVSM is shown in Fig. 4.5. The topology is composed of linear loads (nonlinear loads are not considered as the investigation is focused only on the voltage distortion caused by PV systems), grid connected photovoltaic systems and a step down transformer. The representation of consumption has been done by linear loads to ensure that the produced distortion in the network will be due to the presence of the modelled PV systems. The external grid supplies the network at 11 kV. The voltage is stepped down to low voltage in a distribution substation to supply the energy needs of the loads. Two types of distribution substations were considered, having transformers of 500 kVA and 1000 kVA rated power respectively. Grid connected photovoltaic systems were added to the network topology to satisfy part of the energy demand (up to 70% of load demand). It must be mentioned that the distribution transformer operates in the linear region and consequently the distribution network itself (without the modelled PV systems) is linear.

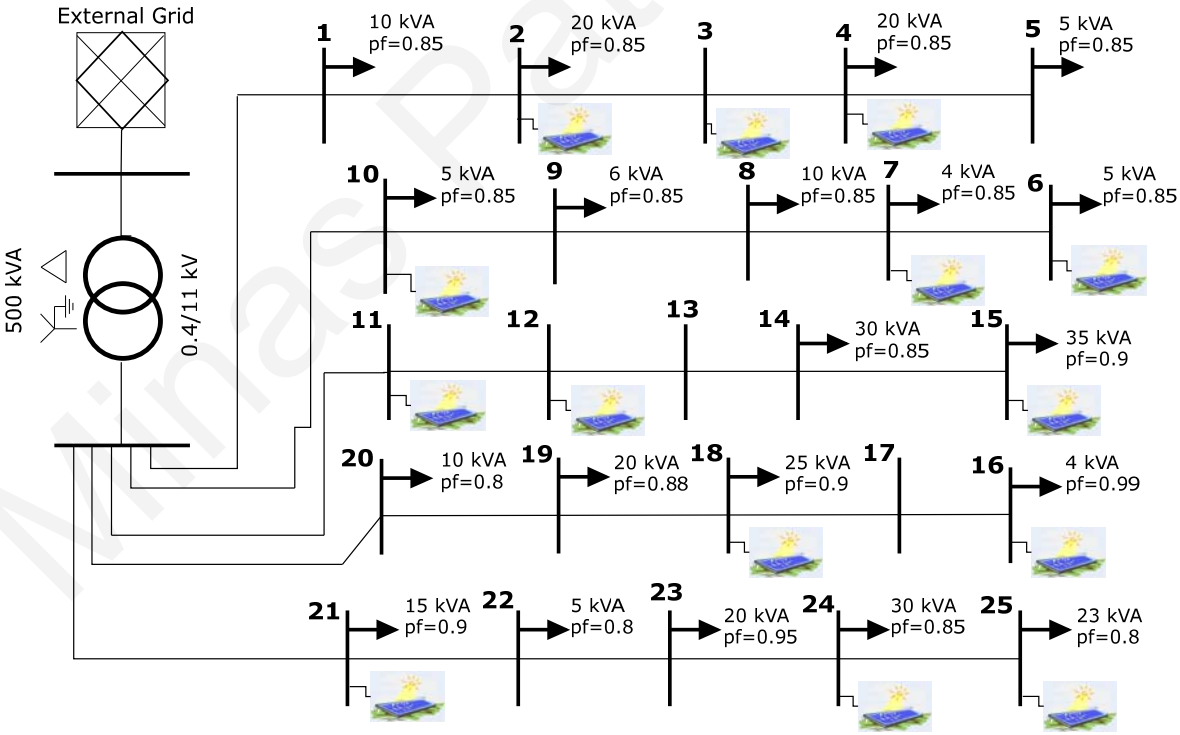

Figure 4.6. Radial Network Topology - SPVSM

The installed photovoltaic systems (two to three systems on each feeder) have a rated value of 15 kW_p each, exactly the same as the capacity of the PV Park where the measurements were taken from and statistically quantified. This is in line with the future

penetration scenarios of PV in Cyprus where the current feed-in-tariff scheme clearly favours installations of such size. Linear loads vary from 4 to 35 kVA and have a power factor that lies in the range of 0.8 to 0.99, according to the diagram shown in Fig. 4.6. It was felt that this is the most common situation that may arise in the typical low voltage grid.

The models of the transmission lines and transformers used by DigSilent PowerFactory Software are described in [142] and the calculation of power indices is defined in [143]. The equipment data used for the modelling of distribution lines, cables and transformers are those used for the analysis and simulation of the distribution network belonging to the Electricity Authority of Cyprus.

4.3.3 Methods adopted for the SPVSM

Measurements from the output of a 15 kW_p PV system located at the PV Technology Laboratory of the University of Cyprus are used to configure the PV system model developed and to extract the simulation cases. The measurements were acquired using a power quality analyser with a sampling time of one minute for a period of two weeks. Measurements of solar irradiance were also obtained from a pyranometer in a synchronized way with the power quality measurements.

Firstly, it was necessary to perform analysis on the measurements in order to observe the variation characteristics of power quality quantities and the main factors causing this variation. The measurements were analysed and subsequently subdivided into the optimum number of groups according to their variation using the k-mean cluster algorithm. After the analysis, it was observed that the variation of the current phasors has a strong correlation with the solar irradiance and hence the subdivision of the different cases was done based on the solar irradiance profile. This subdivision aims to create groups of measurements with small variations that can produce similar simulation results if randomly selecting a cycle measurement from the same group. It is important to mention that the definition "cycle measurement" refers to all the simultaneous measurements acquired during one time-cycle lasting for 0.02 s including all the individual current harmonic phasors.

The PV systems are modelled as current sources which are configured using the average measurement findings of the applied analysis for each case. Special attention was given to the proper amplitude and phase assessment of the current harmonics obtained from measurements, which were then used in the model. In particular, the harmonic angles were adjusted using the bus voltage and current angles, as described in the following section (4.3.4), before being inserted into the software [144]. The derived simulation cases are inserted into DigSilent PowerFactory to obtain the desirable simulation parameters of a

proposed distribution grid for the different cases. In that way, the solar irradiance dependent level of harmonic distortion due to PV generation is assessed.

In order to get a better sense of how the outcomes compare with the standard EN50160 it was necessary to perform simulations for each time measurement and analyse the results based on the requirements of the standard EN50160. For the aforementioned requirement, the PV system model (current source) was configured using the raw measurement data and the simulation was repeated using the PSCAD software. The outcomes of the simulation were analysed and it was found that the high solar irradiance case was giving the most representative results according to the EN50160 standard. As the high solar irradiance case was the most representative one and at the same time the worst case scenario (regarding voltage distortion observed on the buses of the simulated distribution topology), it was further used to investigate various PV concentration scenarios and concentration limits in chosen buses of the proposed distribution network using the high irradiance case in conjunction with DigSilent PowerFactory. Results for the voltage RMS and the voltage distortion are presented and analysed in an attempt to determine how power quality quantities are affected by changes in PV penetration in the adopted grid topology.

In this work it is assumed that all the PV systems are located in the same area close to each other and therefore are exposed to the same levels of solar irradiance and reacting in the same manner in terms of power quality. In practice, dispersed PV systems will usually experience different irradiance levels depending on where the systems are installed. Therefore, a more realistic approach would be to use solar irradiance data from all the installation points or perform Monte-Carlo simulation by statistically varying the solar irradiance [145]. However, the focus of this work to date has been to develop the appropriate model in order to be able to study the power quality behaviour of the PV systems and to predict the maximum penetration limits based on the worst case scenario, which is the case when all the systems produce at their maximum (i.e. a high solar irradiance day with completely clear weather) as has been seen by the findings. Also the following assumptions have been considered to be valid:

- No PV systems export reactive power into the system.
- The substation bus is a strong bus (low impedance supply – bus with voltage which is insensitive to load variations).
- Stability and transient phenomena are not considered.
- The loads are linear and consume constant active and reactive power (a constant power load model is used according to [146]).
- The power factor of the loads is considered to be in the range of 0.8 - 0.99.

- The PV systems are installed on feeders of the same distribution transformer.

The inverter under investigation complies with the following standards: EN 61000-6-3:2002-08, EN 61000-6-4:2002-08, EN 550222:003-09, EN 61000-3-3:2002-05, EN 61000-3-2:2001-12, EN 61000-6-1:2002-08, EN 61000-6-2:2002-08

4.3.3.1 Harmonic Origins and Power Flow

Since PV systems are connected to the grid via inverters, we usually talk about inverter related distortion. Theoretically the most commonly used Pulse-Width Modulation (PWM) inverters produce only high order harmonic distortion, mainly attenuated by the system, associated with switching frequency f_{sw} and given by:

$$f_h = k_1 f_{sw} \pm k_2 f_1 \tag{4.2}$$

where k_1, k_2 are integers and f_1 is the fundamental frequency.

However, low order harmonic currents are also produced from deficiencies in the inverter control loop and the connection of the inverters to weak or distorted grids. The distorted grid voltage behaves like an external disturbance resulting in a distorted output current. Therefore, measurement of the actual current harmonic content of the inverter output and its use in simulations is justified.

At the fundamental frequency, conventional methods such as "Newton-Raphson" are used for power flow analysis. Harmonic power flow modelling techniques include time-domain, harmonic domain and hybrid approaches. In the harmonic load flow calculation DigSilent PowerFactory software, for example, carries out a steady-state network analysis at each frequency defined by harmonic sources and then applies phase corrected superposition to calculate the harmonic currents. Thus a fundamental frequency load flow study needs to be performed before a harmonic penetration analysis, in order to determine fundamental voltage and current magnitudes as well as phase angles [143], [144]. Harmonic current sources are considered as:

$$I_h = k_h e^{i\Delta\varphi_h} \times I_1 e^{i\varphi_1} \tag{4.3}$$

where $\Delta\varphi_h = ((h-1)\varphi_1 + (\varphi_h - \varphi_1))$, h is the harmonic order, I_1 the fundamental frequency current and $k_h = I_h/I_1$ is the harmonic relative magnitude.

The current angle of each harmonic is referenced to the fundamental current angle at each bus. Obviously, harmonic currents are changed from absorbing to injecting when a change of 180^o is observed on the current harmonic phase.

4.3.4. Analysis of Measurements - Choice of Best Data Clusters

In order to obtain the best way of grouping and defining the effect of solar irradiance on produced current harmonics, and thus to make the simulations more computationally efficient, the k-means clustering algorithm was utilized to subdivide data into categories. The main objective is to define a certain number of centroids that are placed as far as possible from each other and to have objects belonging to each centroid with minimum variance. This task can be achieved by minimizing an objective function, which in this specific case is the squared error function (4.4), by reassigning the objects into the group with the closest centroid,

$$SE = \sum_{j=1}^{k} \sum_{i=1}^{n} \left\| x_i^{(j)} - c_i \right\|^2 \tag{4.4}$$

where $\left\| x_i^{(j)} - c_i \right\|$ is a distance measure method between a data point $x_i^{(j)}$ and the cluster center c_i [147], [148]. The Euclidean distance was used as a metric for classifying data into groups. Multiple runs of the k-means algorithm with different, randomly selected, initial conditions ensured that the solution obtained was close to the global minimum. Prior to applying the k-means method, it was also necessary to convert the phasors of the current harmonics from polar to Cartesian coordinates to avoid any discontinuities arising from the representation of the phase.

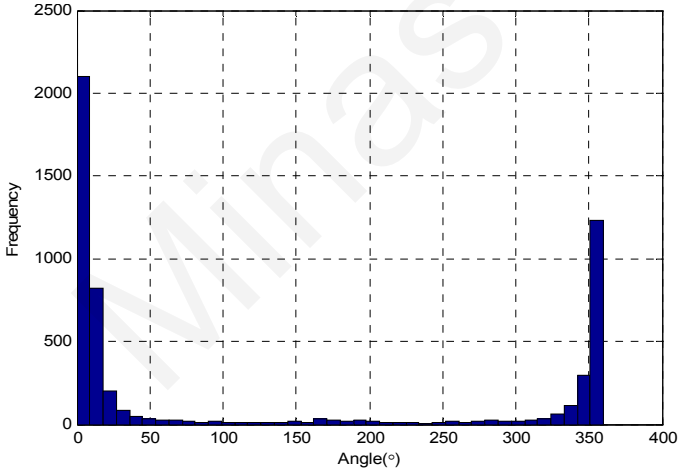

Figure 4.7a. 2nd Order Harmonic Angle on Phase L1 - Histogram

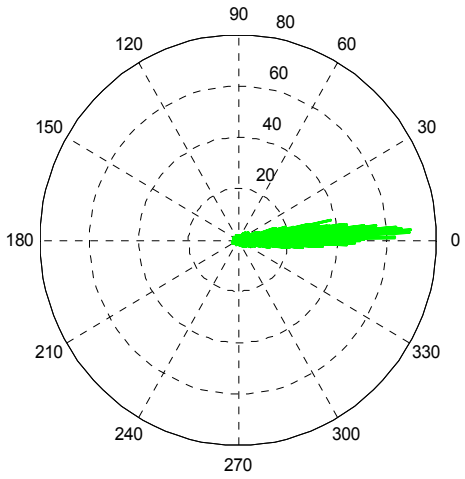

Figure 4.7b. 2nd Order Harmonic Angle on Phase L1 – Polar Coordinates

Figure 4.7. Variation of 2nd Order Harmonic Angle on Phase L1

In the histogram of the 2nd order harmonic angle (Fig. 4.7a), two different groups of values can be distinguished. By taking an average on the specific data, a misleading mean value is calculated. By looking at the polar form of the 2nd order harmonic angle (Fig. 4.7b),

it is clear that the values of the 2nd order harmonic angle vary around an area that includes both 0˚ and 360˚.

Consequently, it is more convenient if polar coordinates are used to preserve the continuity properties of the measurement data, otherwise the k-means partitioning method will divide the data into the wrong clusters.

The number of harmonic phasor groups has been chosen according to the average silhouette values after performing a k-means analysis for a different number of clusters [149]. The k-mean analysis was applied to a three dimensional space having as dimensions the real and imaginary part of the current harmonics and the solar irradiance. To achieve this task it was necessary to correlate the solar irradiance with each harmonic phasor.

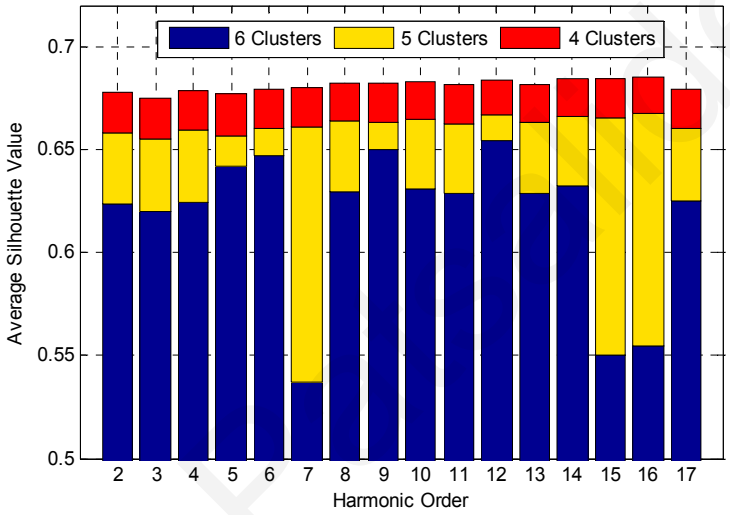

Figure 4.8. Average Silhouette value vs number of Clusters – Choice of harmonic phasor grouping

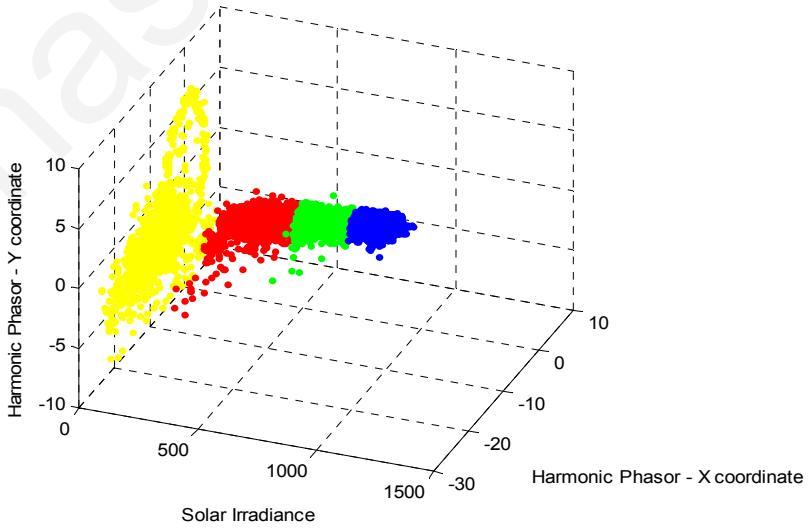

Figure 4.9. 4th Order harmonic phasor divided into four Clusters (Yellow: Extremely Low Solar Irradiance case, Red: Low Solar Irradiance Case, Green: Average Solar Irradiance Case, Blue: High Irradiance Case)

The methodology of calculating the mean silhouette value has been applied to each of the harmonic phasor measurements. In this work, harmonics up to the 17th order were considered

for the simulation as they were the most significant in amplitude. The average silhouette value for each harmonic is graphically presented for different number of clusters in Fig. 4.8. From this figure, it can be seen that as the number of clusters increases, the grouping of data is done in a less efficient way. Furthermore, it has been observed that if we choose to have four clusters, the data will group efficiently together and will be located close enough to the nearest centroid having in this way the minimum variance within the cluster. Therefore, harmonic phasor-solar irradiance measurements are subdivided into four groups using the k-means partitioning method as shown in Fig. 4.9.

4.3.5. Extraction of Simulation Cases

After the subdivision of data, a very useful observation was made with regard to the variation of the quantities in relation to the solar irradiance. It is obvious from Fig. 4.9 that the fluctuation of harmonic phasors is highly dependent on solar irradiance. Thereafter, the extraction of simulation cases can be effectively and efficiently done based on solar irradiance. The cluster of data with the highest variation referring to the situation where the solar irradiance reaches quite low levels (Extremely Low Solar Irradiance case) is not going to be considered in the simulations as these extreme fluctuations will give results of decreased accuracy and confidence.

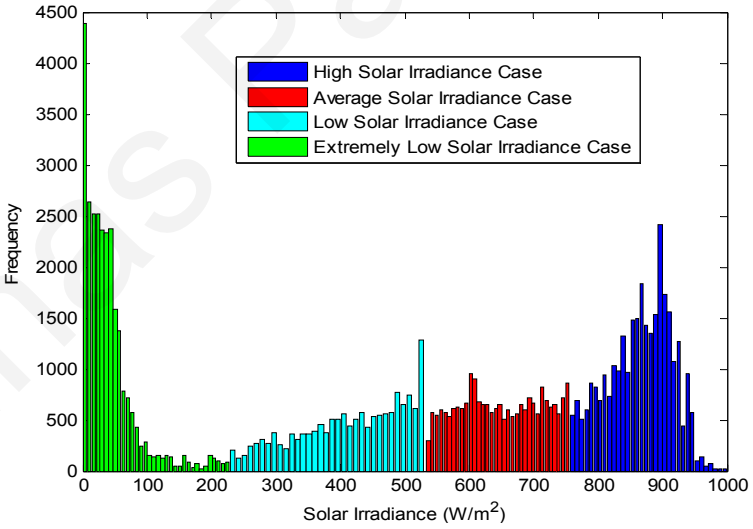

Figure 4.10. Density Distributions of the Four Solar Irradiance Cases

In the next step, the range of variation of each solar irradiance case was defined by creating a frequency distribution of solar irradiance for each grouping category considering all the harmonics up to the 17th order. The frequency distributions for the four solar irradiance cases are shown in Fig. 4.10. As the distributions of the four solar irradiance cases were overlapping slightly, it was necessary to isolate the overlapping data and calculate the median of their distribution to set the boundaries of each simulation case.

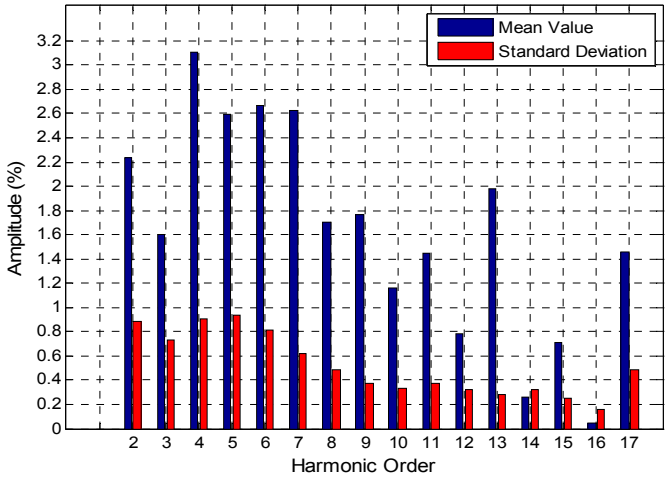

Figure 4.11a. Average Percentage of Current Harmonic Amplitude measured on Phase L1 (%) – High Solar Irradiance Case

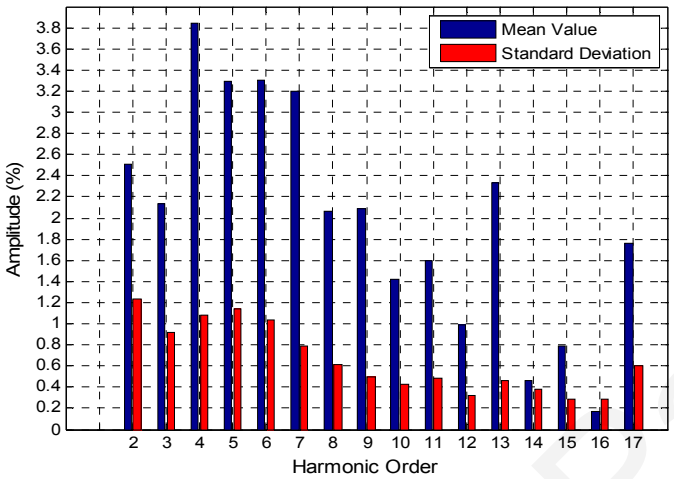

Figure 4.11b. Average Percentage of Current Harmonic Amplitude measured on Phase L1 (%) - Average Solar Irradiance Case

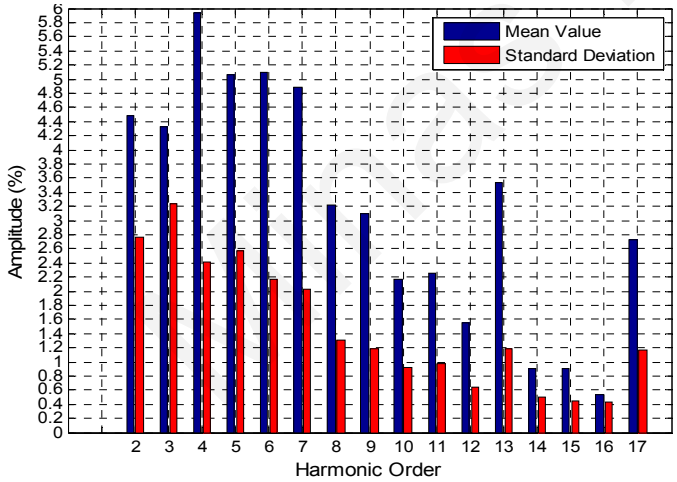

Figure 4.11c. Average Percentage of Current Harmonic Amplitude measured on Phase L1 (%) - Low Solar Irradiance Case

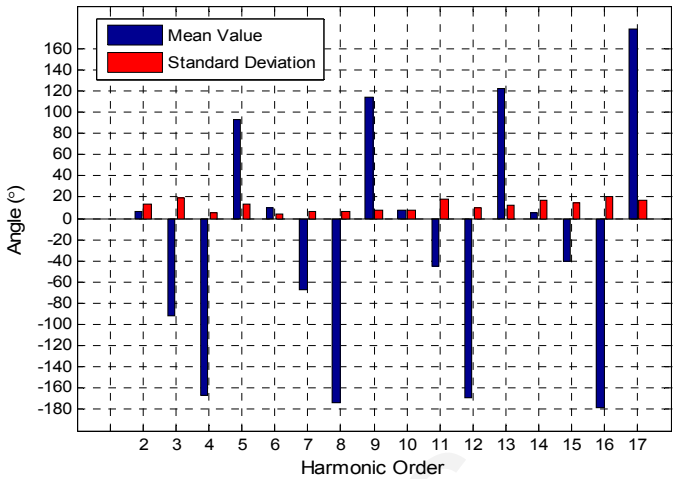

Figure 4.11d. Average Current Harmonic Angle on Phase L1 (˚) - High Solar Irradiance Case

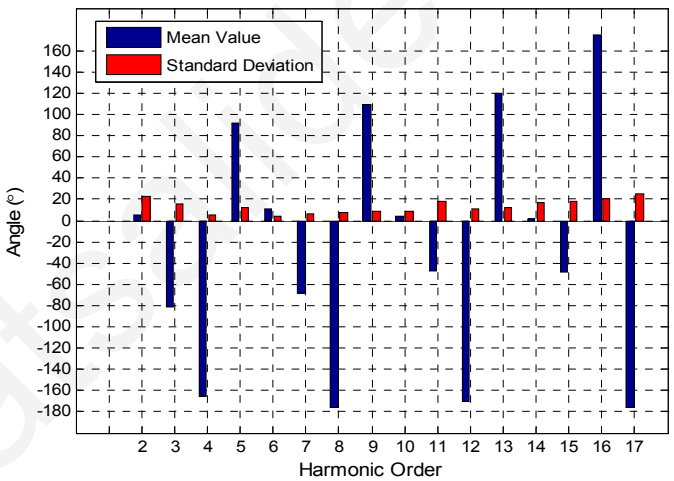

Figure 4.11e. Average Current Harmonic Angle on Phase L1 (˚) - Average Irradiance Case

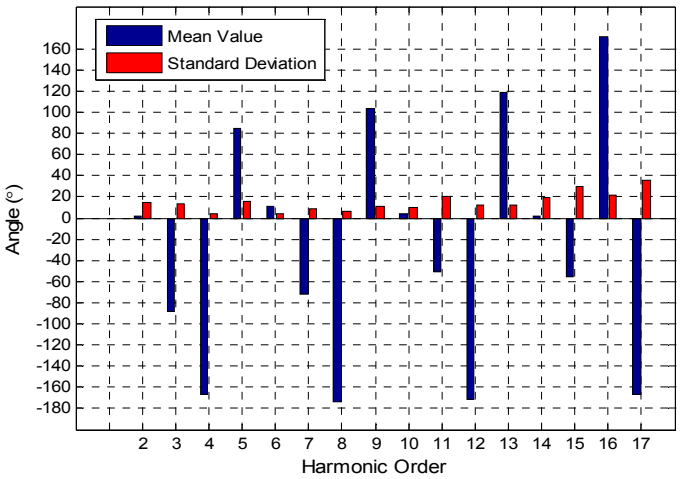

Figure 4.11f. Average Current Harmonic Angle on Phase L1 (˚) - Low Irradiance Case

Figure 4.11. Average Current Harmonic Amplitude and Angles used as an input to the simulator

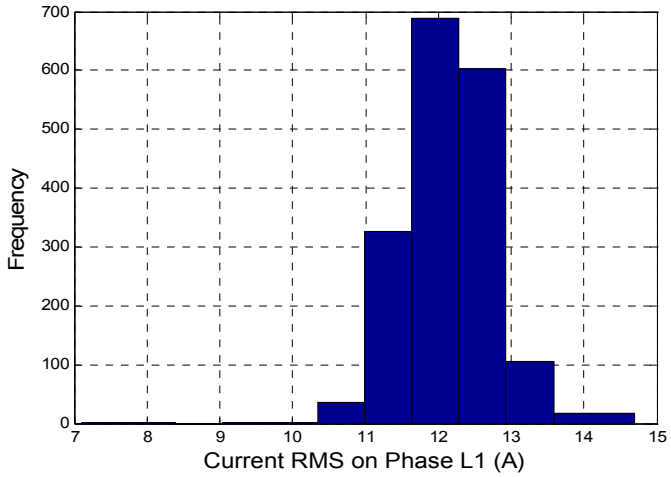

Figure 4.12a. High Irradiance Case – Mean = 12.123

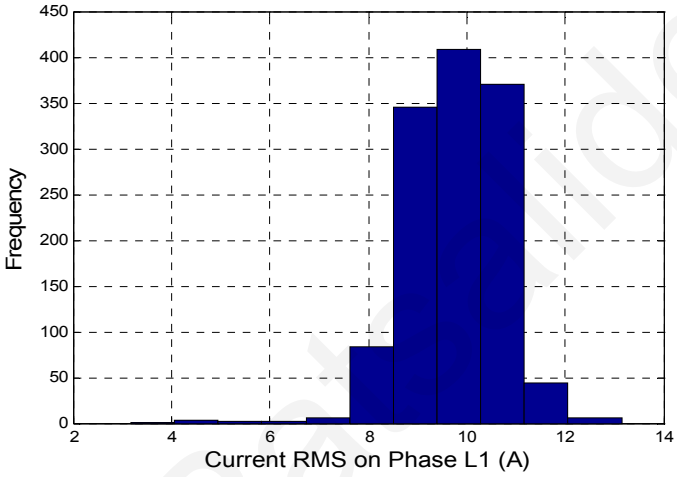

Figure 4.12b. Average Irradiance Case – Mean = 9.767

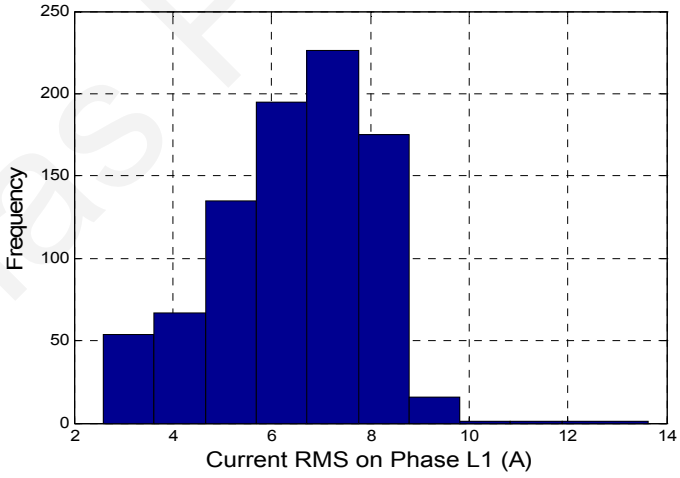

Figure 4.12c. Low Irradiance Case – Mean = 6.434

Figure 4.12. Current RMS measured on Phase L1 for the three simulation cases

Following the analysis of the data, three cases were extracted from measurements and the average values of each case for phase L1 are shown in Fig. 4.11. The three simulation cases are named:

- High Solar Irradiance Case (757.27 W/m^2 and above).
- Average Solar Irradiance Case (between 535.32 and 757.26 W/m^2).

- Low Solar Irradiance Case (between 230.27 and 535.31 W/m^2).

The average amplitudes of the first seventeen harmonics for the three simulation cases are presented in Figs. 4.11a-c. The mean of the individual current harmonics decreases as the solar irradiance increases. A similar observation applies for the variance of the amplitude of the current harmonics. The circular nature of harmonic angles prevents the use of commonly used statistical techniques, as the methods utilized by such techniques would provide inaccurate or misleading results. For the calculation of the average harmonic angles under investigation it was required to use Circular Statistics explained in [150] and [151]. The resulting angles are shown in Figs. 4.11d-f. From Figs. 4.11d-f, it can be noted that the variance of current harmonic angles decreases as the solar irradiance increases. The analysis presented in Fig. 4.11 has been done for all the three phases. The current amplitude (in amperes) was also needed to adjust fully the current sources that have been set using the mean value of each chosen simulation case. In Fig. 4.12, the distribution of the current measured at the output of the PV system is graphically presented. From the results in Fig. 4.12 it can be concluded that the mean value is considered to be a suitable representation for the most probable situation.

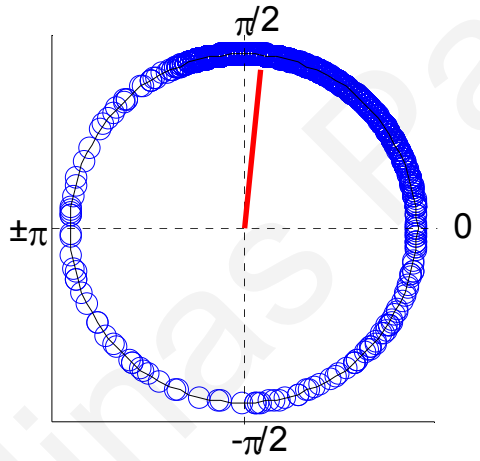

Figure 4.13a. Whole set of data (Raw Data)

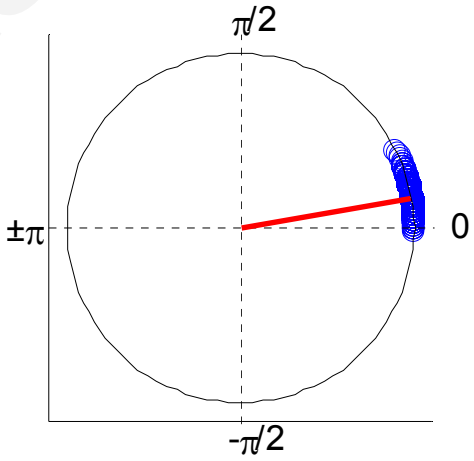

Figure 4.13b. High Irradiance Case (Raw Data)

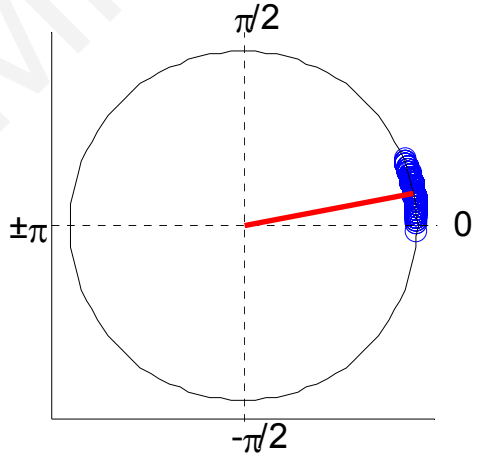

Figure 4.13c. Average Irradiance Case (Raw Data)

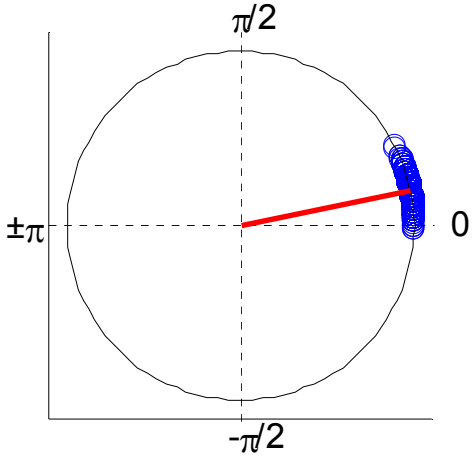

Figure 4.13d. Low Irradiance Case (Raw Data)

Figure 4.13. Variation of 5th Harmonic Angle on Phase L1 before and after subdivision of raw data

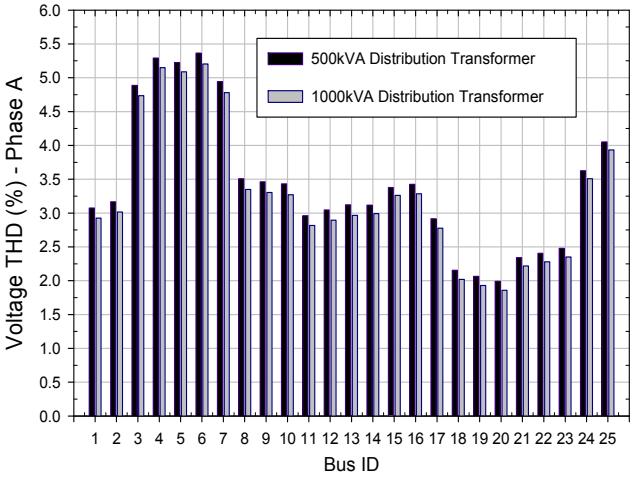

Figure. 4.14a. Voltage THD vs Bus ID - Low Irradiance Case

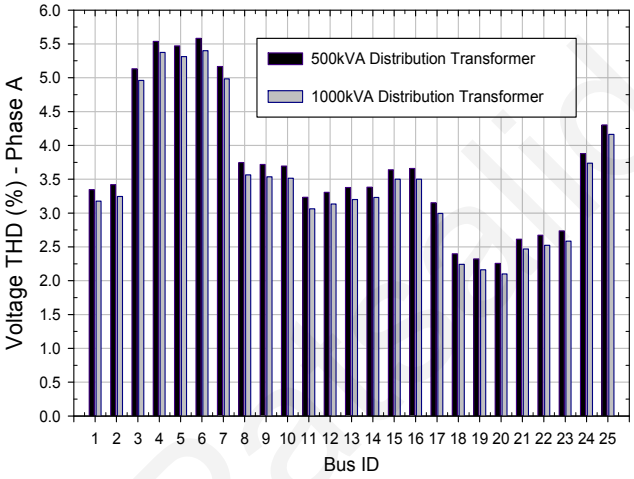

Figure. 4.14b. Voltage THD vs Bus ID - Average Irradiance Case

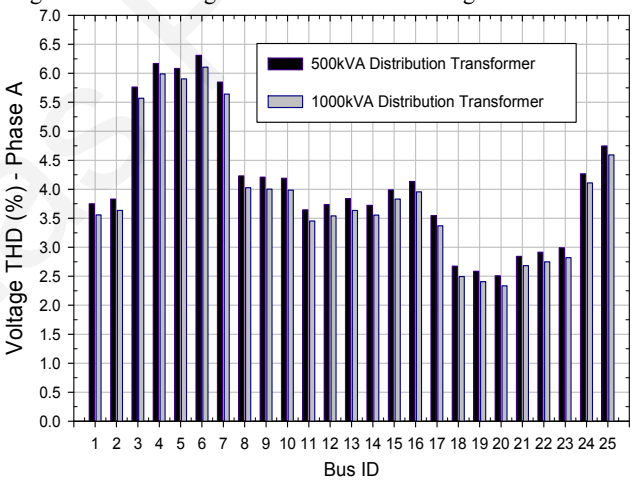

Figure. 4.14c. Voltage THD vs Bus ID - High Irradiance Case

Figure 4.14. Voltage THD vs Bus ID for different irradiance cases

The variation of the 5th harmonic angle is shown in Fig. 4.13 (The red line presented in each graph depicts the average value of the mentioned angular quantity). It is clear that the subdivision of data into clusters limits the variation of the angle into a smaller range. For the three different cases chosen in the specific study, the variation of angle within the clusters does not vary significantly. The variation of the harmonic angles increases only during

extremely low irradiation conditions whilst the inverter is not functioning in an optimum and proper way due to insufficient input energy. After obtaining all the required information to fully configure the current sources, the modelling of PV systems becomes feasible.

4.4 Simulation Results - Simple PV System Model

The Simple PV System was firstly simulated with the DigSilent PowerFactory Software. Voltage distortion caused by nearby installed inverters was not investigated due to the nature of modelling adopted. The results obtained from the simulation of the two topologies for a 500 kVA and 1000 kVA distribution transformer are shown in Fig. 4.14. In both cases, it is obvious that the THD of all buses increases as the solar irradiance increases. Nevertheless, the Average Current Harmonic Amplitudes in the high irradiance case are much lower than in the medium and low irradiance cases. Despite this fact, their effect on the voltage THD is more pronounced since the power contribution from the photovoltaic system is much higher during this period. Buses that are located at the end of the radial network and have photovoltaic systems connected are also experiencing problems with harmonics. The voltage THD obtains the highest value at the point of the network where the highest concentration of photovoltaic systems exists (Bus ID 6 - Fig. 4.6). In addition to this, the network with the high capacity distribution transformer has more immunity to voltage pollution caused by harmonics. In other words, the stronger the network at the point of connection to the medium voltage grid the better for the customers in terms of quality of supply.

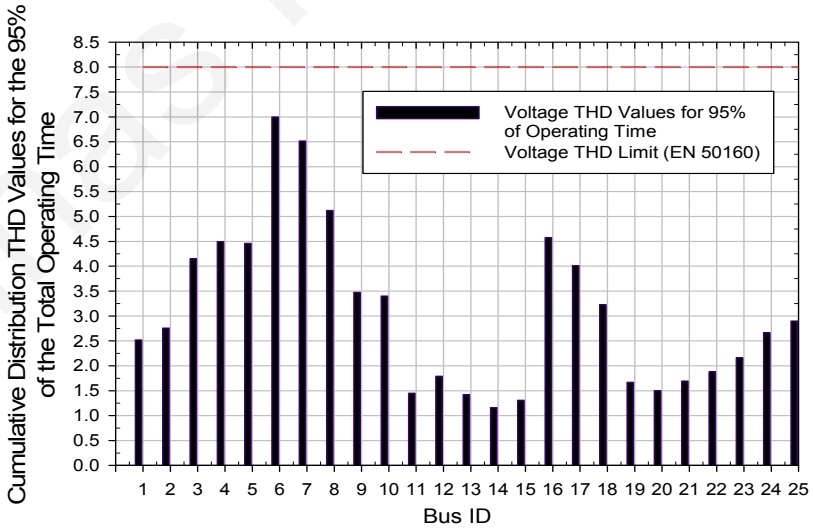

Figure 4.15. Cumulative distribution of Voltage THD vs bus ID for 95% of the total operating time

According to the EN 50160 standard the limit for voltage THD is 8% including up to the 40th harmonic. As can be seen in Fig. 4.14c, the voltage THD on Bus ID 6 is approaching 6.3%. A significant observation made is that the limits described in IEEE Standard 519-1992 "Recommended Practices and Requirements for Harmonic Control in Electrical Power

Systems" are exceeded. The EN 50160 standard sets the limit for voltage THD to 8% and the specific limit should not be exceeded for more than 5% of the total operating time. Fig. 4.14 shows that the limits are not exceeded. However, the most representative results are those shown in Fig. 4.14, according to which the limits of the EN 50160 standard are not exceeded for 95% of the total operating time. In order to obtain the results of Fig. 4.15-4.16, it was necessary to use the PSCAD software to perform the simulations.

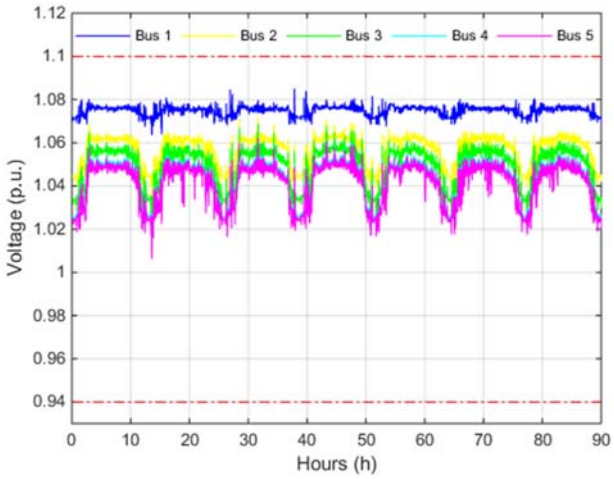

Figure. 4.16a. Voltage Variation on Buses 1-5

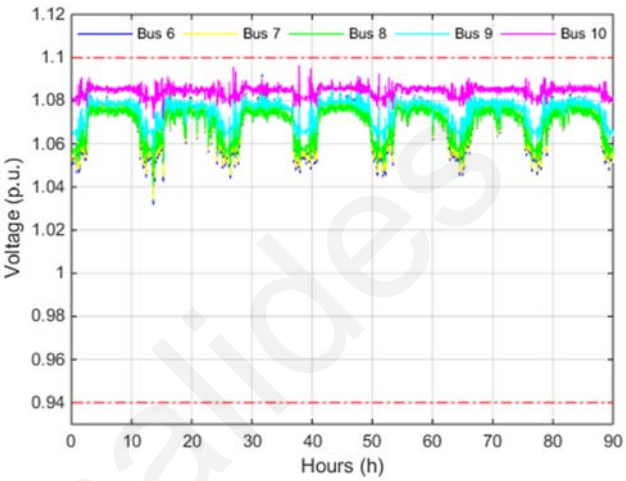

Figure. 4.16b. Voltage Variation on Buses 6-10

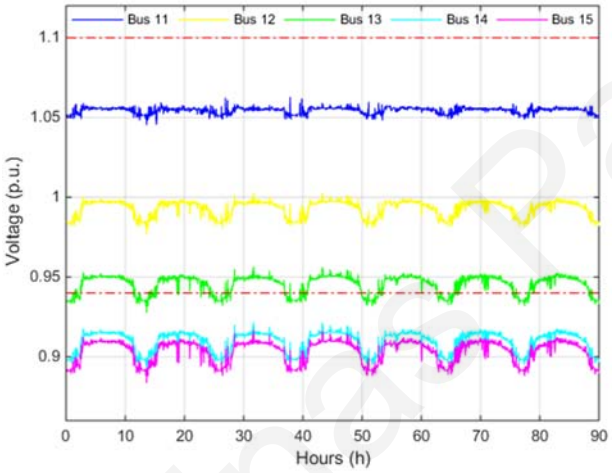

Figure. 4.16c: Voltage Variation on Buses 11-15

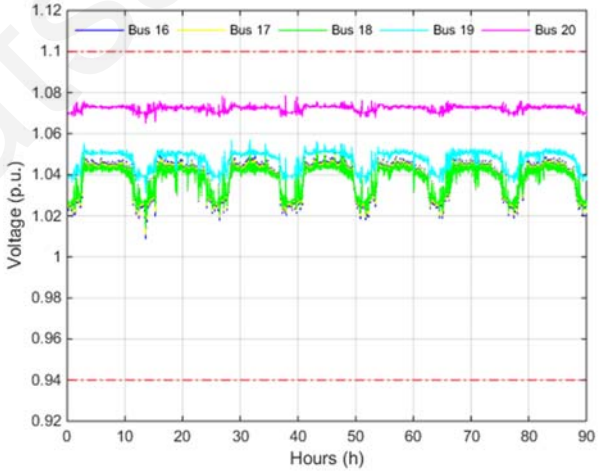

Figure. 4.16d: Voltage Variation on Buses 16-20

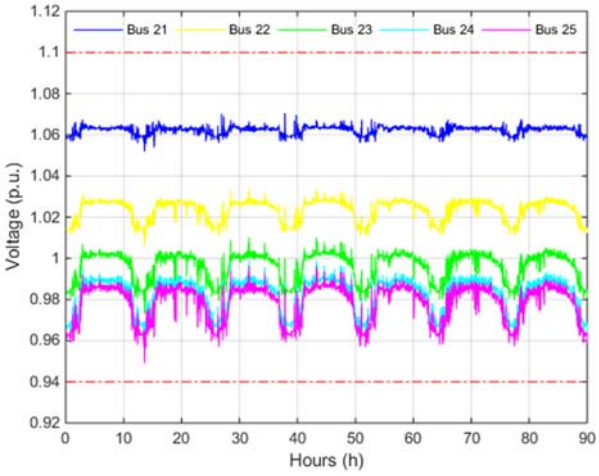

Figure. 4.16e. Voltage Variation on Buses 21-25

Figure 4.16. Voltage Variation on the Buses of the Proposed Distribution Network Topology

From the comparison of outcomes from DigSilent PowerFactory and PSCAD it is observed that the simulation case seen to be in line with the EN50160 standard analysis is the high solar irradiance one. During high solar irradiance conditions the PV inverters are operating at rated conditions so from the aforementioned observation it becomes clear that by using the characteristics of the inverter at rated conditions (high irradiance case) it is feasible to get a good estimate of how the distribution network will react in the presence of high PV penetrations.

By studying the voltage profile of the network buses using PSCAD software (Fig. 4.16), it can be noted that the voltage limits are exceeded for more than 5% of total operating time on a certain number of buses even if the taps of the transformer are adjusted to their maximum permissible level. The simulation time presented in Fig. 4.16 is actually equivalent to one week's operation of the distribution topology in the presence of PV systems considering only the daytime hours (approximately 13 hours per day).

4.4.1. Investigation of Concentration Limits

In this section, the high solar irradiance case has been chosen to be used in DigSilent PowerFactory for the simulation of the different concentration scenarios as it constitutes the worst case scenario and secondly because it gives results based on the EN50160 standard analysis as has been seen in the previous section.

Five different PV concentration scenarios were considered in order to observe the harmonic response of the proposed distribution network in each case. The busbars with PV systems are shown in Table 4.2. In each busbar only one PV system is connected. From the simulation results shown in Fig. 4.17, it is clear that the busbar voltage THD increases as the concentration of photovoltaic systems increases. The installation of a PV system on a certain bus gives rise to voltage THD on the specific bus and when PV systems are installed also on neighbouring buses, the value of voltage THD can also rise dramatically on neighbouring buses, exceeding the EN 50160 limits in some instances. It is important to mention at this point that the limit is exceeded only by the first seventeen harmonics and obviously the limits described in IEEE Standard 519-1992 are exceeded.

Generally, the effect of harmonics is not so pronounced with low concentrations of PV systems, but the situation gets worse as the installed PV capacity increases. The calculations show (Fig. 4.17), that the voltage THD limits are not exceeded even when the installed PV capacity reaches 24% (120 KVA Installed PV Capacity divided by the Power Rating of the Distribution Transformer) of the transformer size. Proper planning of PV system installation on the grid is therefore important to avoid severe voltage distortion.

The voltage variation on the busbars of the proposed distribution topology has also been considered after performing simulations in PSCAD (configuring the current sources using the raw measurements file) for the different concentration scenarios and is shown in Fig. 4.18. As the concentration of PV systems inside the distribution network increases, the voltage levels rise respectively. The plots of Fig. 4.18 present the upper and lower limits of voltage for 95% of total simulation time (one week period). The red line represents the limits for voltage that must not be exceeded for more than 5% of the total operating time. From Fig. 4.18 it can be observed that by increasing the concentration of PV systems inside the distribution network, the variation of voltage increases. Despite the fact that the voltage limits may be exceeded under high concentration of PV systems, it can be seen that in some cases PV systems improve the voltage levels.

Table 4.2. Different Concentration Scenarios

Bus ID	**Installed PV System Capacity**				
	15KVA (1 system)	60KVA (4 systems)	120KVA (8 systems)	240KVA (16 systems)	375KVA (25 systems)
1				√	√
2			√	√	√
3					√
4				√	√
5			√	√	√
6				√	√
7	√	√	√	√	√
8				√	√
9				√	√
10					√
11			√	√	√
12				√	√
13					√
14					√
15		√	√	√	√
16			√	√	√
17					√
18		√	√	√	√
19					√
20				√	√
21				√	√
22					√
23					√
24		√	√	√	√
25					√

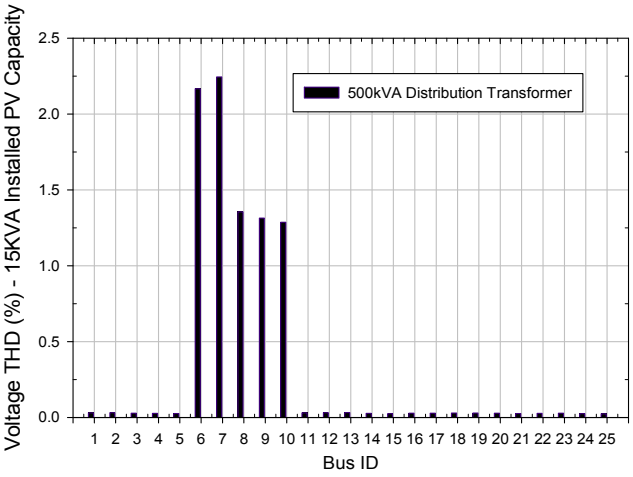

Figure 4.17a. Voltage THD vs Bus ID – 15 KVA Installed PV Capacity (1 system)

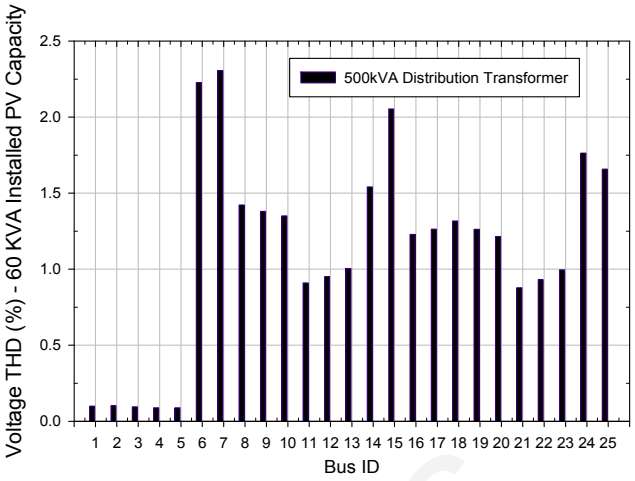

Figure 4.17b. Voltage THD vs Bus ID – 60 KVA Installed PV Capacity (4 systems)

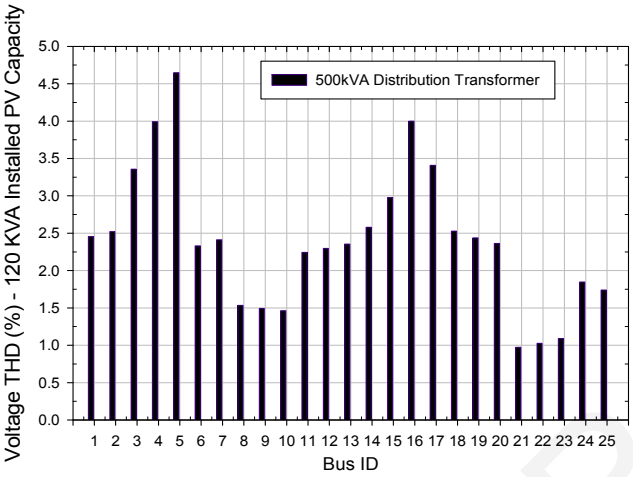

Figure 4.17c. Voltage THD vs Bus ID – 120 KVA Installed PV Capacity (8 systems)

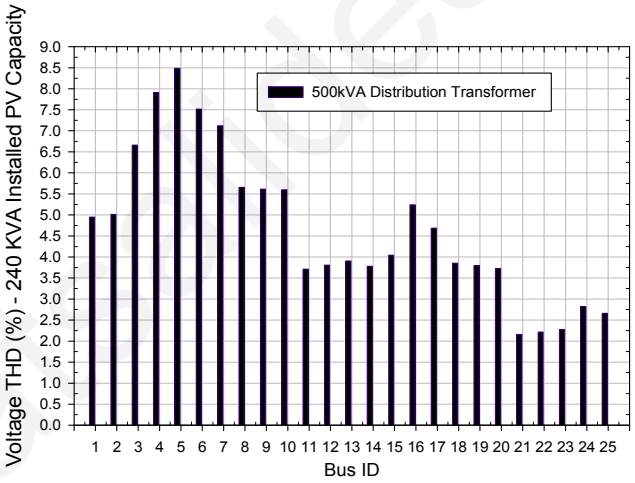

Figure 4.17d. Voltage THD vs Bus ID – 240 KVA Installed PV Capacity (16 systems)

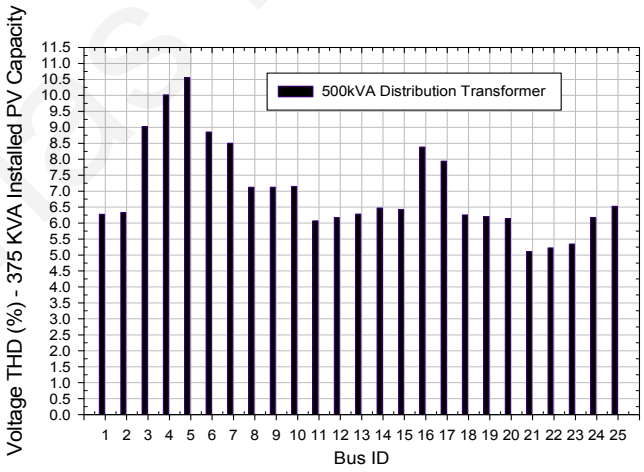

Figure 4.17e. Voltage THD vs Bus ID – 375 KVA Installed PV Capacity (25 systems)

Figure 4.17. Voltage THD vs Bus ID for different concentration scenarios

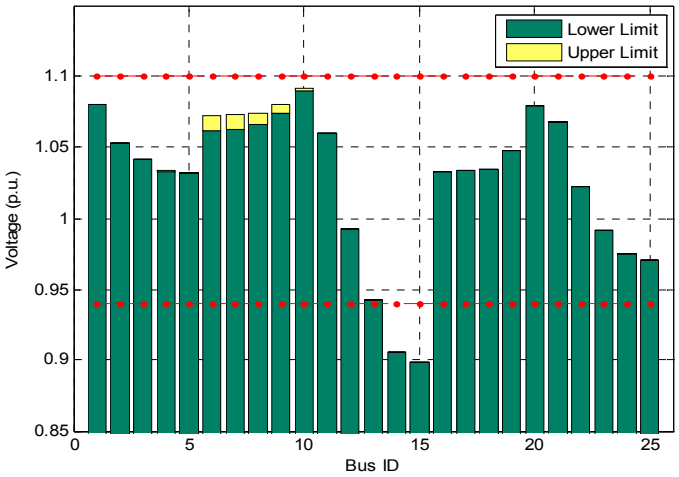

Figure 4.18a. Voltage Variation vs Bus ID – 15 KVA Installed PV Capacity (1 system)

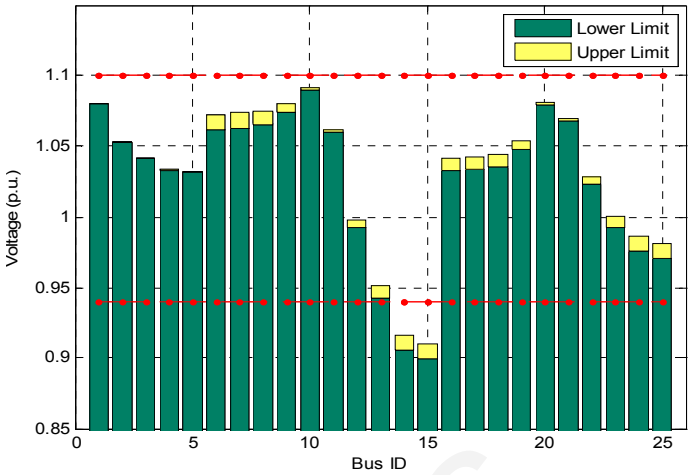

Figure 4.18b. Voltage Variation vs Bus ID – 60 KVA Installed PV Capacity (4 systems)

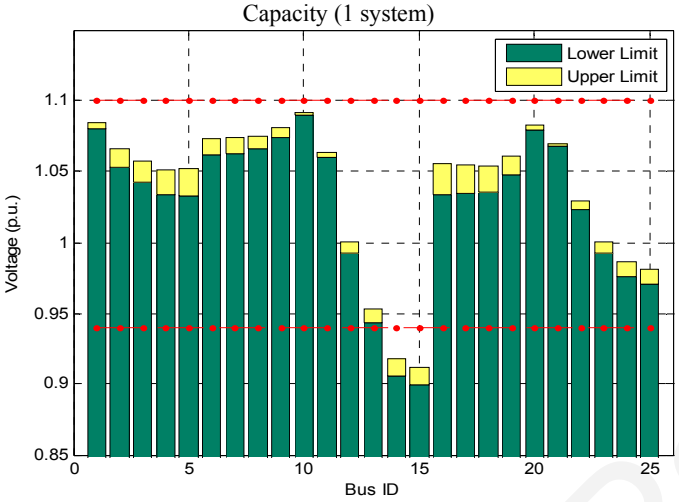

Figure 4.18c. Voltage Variation vs Bus ID – 120 KVA Installed PV Capacity (8 systems)

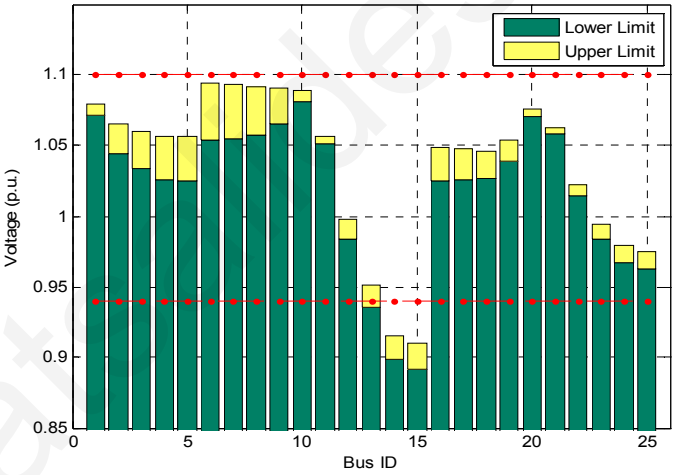

Figure 4.18d.Voltage Variation vs Bus ID – 240 KVA Installed PV Capacity (16 systems)

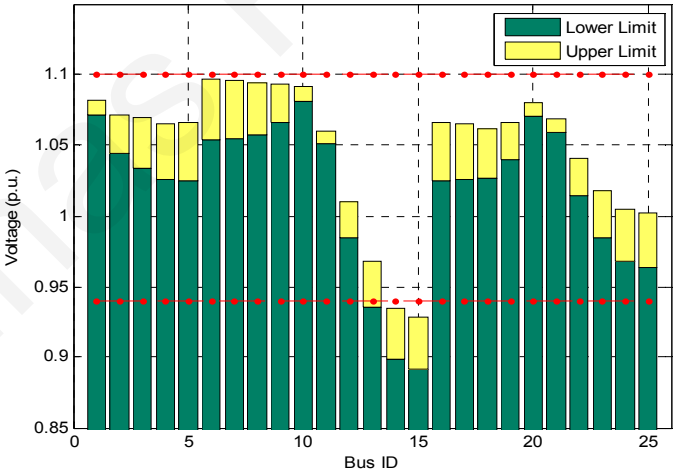

Figure 4.18e.Voltage Variation vs Bus ID – 375 KVA Installed PV Capacity (25 systems)

Figure 4.18. Voltage Variation vs Bus ID for different concentration scenarios

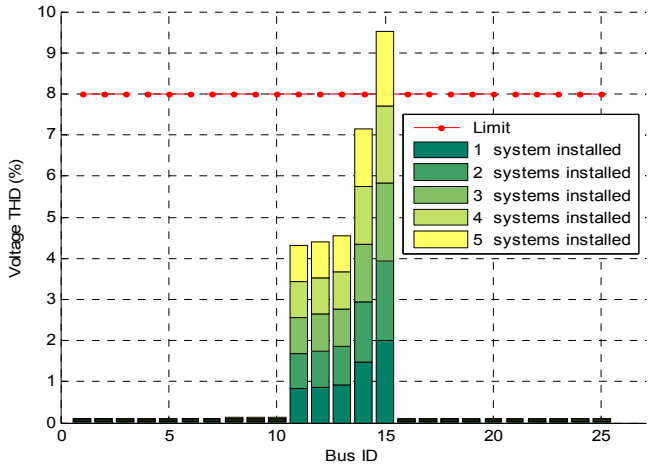

Figure 4.19a. Investigation of Concentration Limits on an Edge Bus

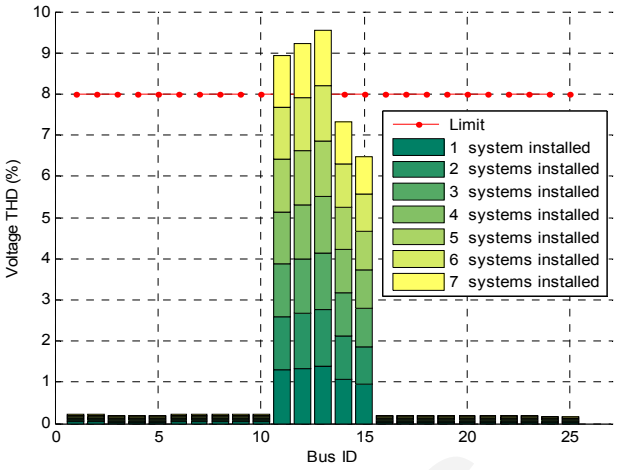

Figure 4.19b. Investigation of Concentration Limits on a Transformer's Neighbouring Busbar

Figure 4.19. Investigation of Concentration Limits on selected buses

Some busbars are less sensitive to voltage variations and consequently they are better candidates for the installation of PV systems. The voltage of buses that are already below the lower limit can be improved by installing PV systems and on buses that the voltage is approaching the upper limit PV systems must be avoided. For this purpose, the harmonic response of two types of buses of the proposed distribution network was simulated with DigSilent PowerFactory using the worst case scenario data. In order to obtain a feel of the concentration limits, single point PV installations of various sizes are further examined. In this part of the simulation, the capability of installing more than one PV system on one busbar, before exceeding the limits proposed by the EN 50160 and IEEE 519-1992 standards, is investigated.

The main parameter considered in this case was the immunity of certain buses to voltage disturbances. One bus with high and one with low immunity to voltage disturbances were chosen. Frequently, buses that are located at the end of a radial network (Bus ID 15 - Fig. 4.6) have lower immunity to voltage disturbances and buses that are connected close to the distribution substation, the beginning of a distribution line, (Bus ID 11 - Fig. 4.6) have higher immunity.

The simulation results for the low voltage immunity case are shown in Fig. 4.19a. The installation of photovoltaic systems was done on bus 15 (Fig. 4.6) and the maximum capacity was found to be four systems with 15 kVA rated power (60 kVA to 75 kVA). The fifth PV system forced the voltage THD of bus 15 to exceed the EN 50160 standard, whereas the limits described in IEEE Standard 519-1992 were exceeded after the installation of the third PV system (45 kVA). The maximum voltage THD value was observed on the bus where photovoltaic systems are connected. This is quite a straightforward result, having in mind that buses located at the edge of a radial power network are weaker in terms of short circuit

current and that a significant part of the energy required on that bus is provided mostly by PV systems with distorted characteristics on the same bus.

The simulation procedure was repeated for bus 11 (Fig. 4.6) and the results are shown in Fig. 4.19b. The maximum PV capacity for this case was found to lie in the range of 90 kVA to 105 kVA, whereas the limits described in IEEE Standard 519-1992 were exceeded after the installation of the sixth PV system. The maximum voltage THD is not observed on the same bus where the PV systems are installed due to the fact that the energy required for this bus is mainly supplied by the distribution transformer [8].

4.5 Conclusions

The main focus of the work above has been to develop a preliminary PV system model in order to be able to study the power quality behaviour of the PV systems and to predict the maximum penetration limits. The measurement based analysis presented, identifies that the maximum permissible concentration of PV can be reached under certain circumstances related to the distribution grid topology, inverter technology and the solar irradiance level. From the findings, it has been noted that the levels of power quality of busbars inside a distribution network decrease by installing higher concentrations of PV systems if proper planning is not taken into consideration. Also, an important observation made is that the buses located closer to the distribution transformer have higher immunity to voltage disturbances than those located at the end of the radial network. Finally, a general outcome obtained is that the case when all the systems produce at their maximum constitutes a representative scenario for evaluating the harmonic response of the distribution grid.

However, the simulation results can be improved if the voltage of fundamental frequency and harmonics are considered in the PV System Model. Moreover, the exact dynamics of the distribution grid under investigation are crucial in performing reliable power quality studies and consequently they should be modelled in a convenient and accurate way. Lastly, a validation/verification procedure is required to be developed to ensure that the simulation outcome yields credible results.

Chapter 5
Advanced PV System Model (APVSM)

5.1 Introduction

Modifications and additions to the simple model produced an advanced model which is essentially a power source configured using harmonic measurements of active and reactive power. The APVSM if compared to the SPVSM has the advantage of taking into account the voltage variations and it can adjust accordingly the output current of the power source based on the variation in the voltage level and phase.

On the other hand, the dynamics of the distribution grid in the industrial area are modelled via the harmonic distribution grid equivalent described in Chapter 9. It is inevitably evident that an accurate equivalent distribution grid model is required in order to assess correctly the impact of PV market deployment on the electricity grid network, imposed by the power quality constrains. Furthermore, the dynamics of the distribution grid should be known in order to define the PV penetration limit and proposed voltage regulation methods to increase the PV capacity. The proposed model describes adequately the distribution grid dynamics and it is used along with the APVSM in the simulation of different PV penetration levels. The simulation results and models utilized are evaluated at the end of this chapter.

5.2 APVSM - Network - Methodology

5.2.1 APVSM - Set of parallel Harmonic Power Sources

The APVSM has been built based on the SPVSM presented in the previous chapter. In general, the APVSM is a power source which is composed of a set of harmonic power sources that take into account the grid voltage and voltage harmonics (the output current of APVSM is the sum of harmonic currents produced by the individual harmonic power sources). The novelty of the proposed APVSM lies in the fact that the output current harmonics are calculated using the voltage harmonics of the grid. The PV system model developed is unique and it has not been proposed in literature before. Also, in the calculation of output current harmonics, both solar irradiance (G_H) and power measurements (P,Q for active and reactive power respectively) are considered.

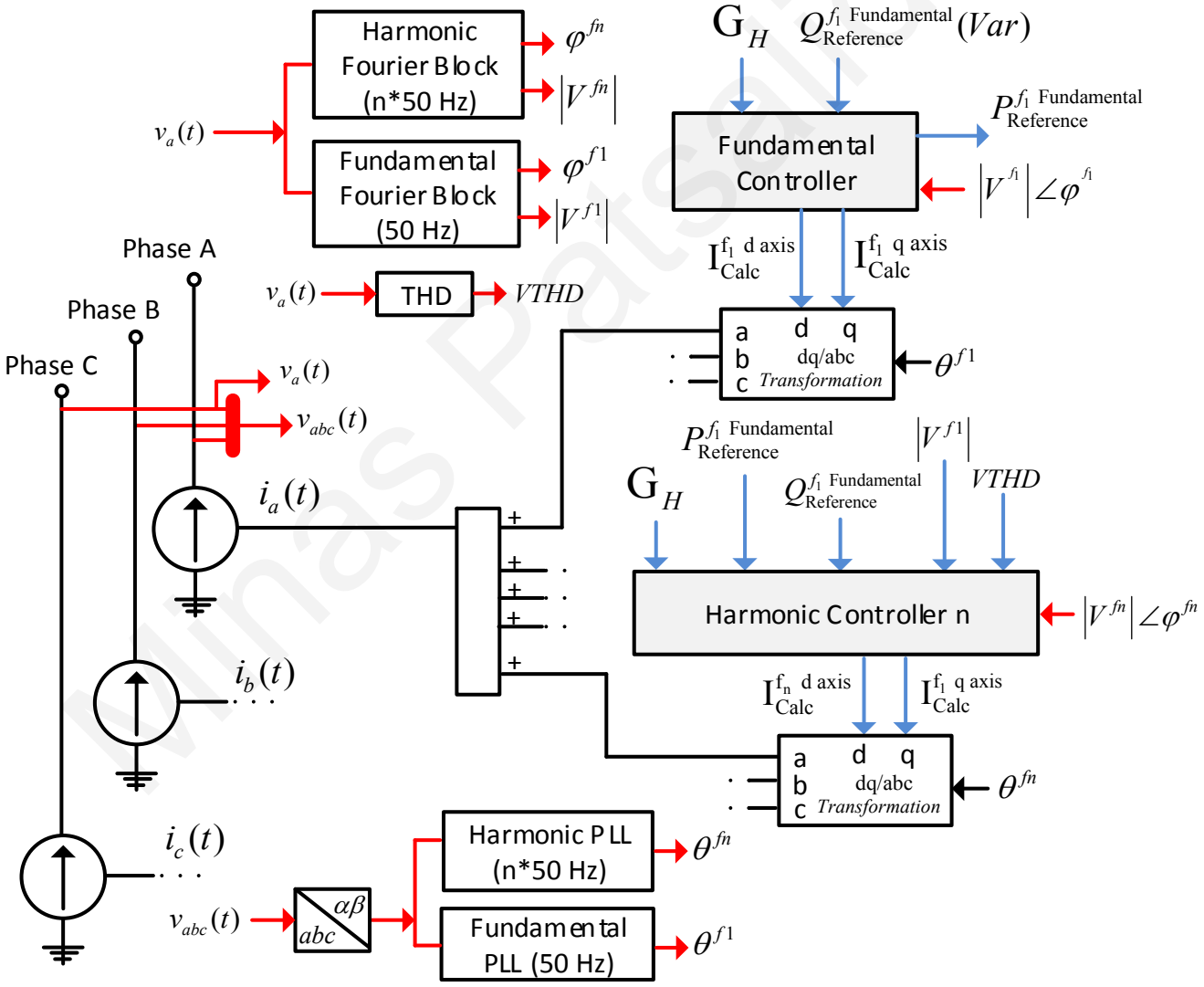

Figure 5.1. APVSM - Three phase power sources using regression fit polynomial models

The only problematic condition possible to occur while using the proposed model is the case when the amplitude of a voltage harmonic is exactly zero. At that situation, the issue is

resolved by setting the amplitude of the specific voltage harmonic to a very small nonzero value. It must be mentioned although that this situation has zero probability to occur in reality (due to the nonlinear loads which are connected on the electricity grid) therefore the aforementioned assumption is quite reasonable.

The power measurements needed for the development of the APVSM are taken from a 150 kW_p PV system and are further utilized to define the polynomial regression models with the highest possible accuracy. The internal model signals driving the current sources are defined based on the significance of measured power harmonics. The general diagram showing the structure of the APVSM is shown in Fig. 5.1. The measurements used for defining the regression models are the solar irradiance, the fundamental and harmonics of active and reactive power, the voltage RMS and Total Harmonic Distortion. The symbolic form of regression input variables is depicted in Table 5.1.

Table 5.1. Regression models input variables and their reduce symbolic form

Symbol	Input Variables
x_1	Solar Irradiance
x_2	Active Power Fundamental Reference
x_3	Reactive Power Fundamental Reference
x_4	Voltage RMS
x_5	Voltage THD

The current for the fundamental frequency is calculated by the Fundamental Controller shown in Fig. 5.2. The Fundamental Controller takes as input the solar irradiance (G_H) and the reference signal of reactive power ($Q_{Reference}^{f_1\ Fundamental}$).

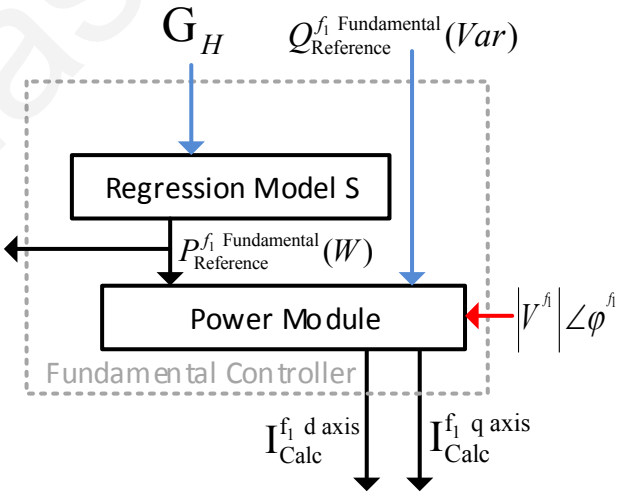

Figure 5.2. APVSM – Fundamental Controller

The solar irradiance is used as an input to the Regression Model S which is defined based on field measurements of solar irradiance and active power (of fundamental frequency) obtained from the 150 kW_p PV system. The generalized form of the adopted linear regression

model that represent the relationship between a response variable and one or more predictor variables is described by the equation (5.1):

$$y = \sum_{k=1}^{n} \beta_k f_k(x_1, x_2, \dots x_n) + \varepsilon \tag{5.1}$$

where y is the response variable, n is the number of linear component composing the response variable, x_k are the predictor variables, f_k is any function formulated by the predictors x_k, β_k are the unknown parameters to be estimated and ε is the error between the actual response and the estimated response. The regression model is defined by applying stepwise regression which is a systematic method for adding and removing terms from a multi-linear model based on their statistical significance. The method/algorithm begins with an initial model and then compares the explanatory power of incrementally larger and smaller models. The method terminates when no single step improves the regression model [152]. The unknown parameters itself are estimated by applying robust regression which minimizes the least-squares error via iterative methods [153]. The details for the regression model S (both statistics and parameter estimations) are depicted in Table 5.2.

Table 5.2. Regression model S

Active Power Reference – Regression model parameter and statistics						
Linear regression model: $y \sim \beta_0 + \beta_1 x_1$					**Confidence Interval of β_k**	
Parameter	**Estimated β_k**	**SE**	**tStat**	**pValue**	**Lower Bound**	**Upper Bound**
(Intercept)	-0.25261	0.01094	-23.091	4.64E-100	-0.2741	-0.2312
x_1	0.24107	0.000132	1827.4	0	0.2408	0.2413

From the table, it is evident that three measures of statistics are used for evaluating the validity of the regression model. Those are the standard error (SE), the t-statistic (tStat), and the p-value for the hypotheses tests (pValue) which are described by equations (5.2), (5.3) and (5.4) respectively.

$$SE = \sqrt{\frac{\sum \left(Y - \hat{Y}\right)^2}{N}} \tag{5.2}$$

where SE is the standard error of the estimate, N is the number of pairs of observations, Y is an actual response values, and $\hat{Y}$ is a predicted/estimated response values. The numerator is the sum of squared differences between the actual response values and the predicted response values. For a hypotheses test on coefficient k, with:

$H_0: \beta_k = 0$

$H_1: \beta_k \neq 0$

the t-statistic is:

$$t = \frac{\beta_k}{SE(\beta_k)} \tag{5.3}$$

where $SE(\beta_k)$ is the standard error of the estimated coefficient β_k. If there is no linear relationship between the predictor's function f_k and the response variable then $\beta_k = 0$. Alternatively, if there is a linear relationship then $\beta_k \neq 0$. In linear regression, the t-statistic index is useful for making inferences about the regression coefficients. The hypothesis test on coefficient k examines the null hypothesis according to which the corresponding term is not significant versus the alternate hypothesis that the coefficient is different from zero. The null hypothesis is evaluated by comparing the t-statistic index with the critical values of t-distribution having $N - (n + 1)$ degrees of freedom and a significance level (a). If the critical values of the t-distribution are lower than the t-statistic index then the null hypothesis is rejected. On the other hand, the p-value is the estimated probability of rejecting the null hypothesis (H_0) when the null hypothesis is true. In other words, the p-value represents the probability of observing a test statistic more extreme than what it has been observed assuming that the null hypothesis is true. If X the random variable representing the observed data, x a single instance and H the statistical hypothesis then the "more extreme than what was actually observed" can either mean $\{X \geq x\}$ (right tail event) or $\{X \leq x\}$ (left tail event) or the "smaller" of $\{X \geq x\}$ and or $\{X \leq x\}$ (double tailed event). Thus the p-value is given by

$$\text{p} - \text{value} = \begin{cases} \Pr(X \geq x|H)\ for\ a\ right\ tail\ event \\ \Pr(X \leq x|H)\ for\ a\ left\ tail\ event \\ 2 * minimum\{\Pr(X \geq x|H), \Pr(X \leq x|H)\}\ for\ a\ double\ tail\ event \end{cases} \tag{5.4}$$

The smaller the p-value, the larger the significance because it reveals that the hypothesis H may not be adequate to explain the observation. More specifically, the hypothesis H_0 is rejected if any of these probabilities is less than or equal to the significance level which is typically set to 0.05. Also, the accuracy of the regression models has been defined using the R-square (R^2) value to provide a measure of how reliably the trend is described by the polynomial fit (a high R^2 value shows good agreement between measurements and regression fit model while values close to unity denote perfect much between measurements and regression fit). In general R^2 is defined as:

$$R^2 = 1 - \frac{\sum_{i=1}^{n} M_i - F_i}{\sum_{j=1}^{k} M_i - \bar{M}} \tag{5.5}$$

where M_i are the observed values, F_i are the modelled values and $\bar{M}$ is the mean of the observed values. Lastly, the coefficient confidence intervals provide a measure of precision for linear regression coefficient estimates. A $100 * (1 - a)\%$ confidence interval gives the

range that the corresponding regression coefficient will be in with $100 * (1 - a)\%$ confidence. The $100 * (1 - a)\%$ confidence intervals for linear regression coefficients is given by:

$$CI_{Lower,Upper} = \beta_k \pm t_{(1-\frac{a}{2},n-p)} SE(\beta_k) \tag{5.6}$$

where β_k is the coefficient estimate, $SE(\beta_k)$ is the standard error of the coefficient estimate, and $t_{(1-\frac{a}{2},n-p)}$ is the 100(1–α/2) percentile of t-distribution with n – p degrees of freedom, n is the number of observations and p is the number of regression coefficients [154].

The d-q axis current for the fundamental frequency are calculated based on the schematic diagram shown in Fig. 5.3 which derives from equation (5.6).

$$\vec{S}_{L1} = \frac{1}{2}\vec{V}_{L1}\vec{I}^{*}_{L1} \Rightarrow \vec{I}^{*}_{L1} = \frac{2\vec{S}_{L1}}{\vec{V}_{L1}} \Rightarrow \vec{I}^{d}_{L1} + j\vec{I}^{q}_{L1} = \vec{I}^{f_1 \text{ d axis}}_{Calc} + j\vec{I}^{f_1 \text{ q axis}}_{Calc} = \left(\frac{2\vec{S}_{L1}}{\vec{V}_{L1}}\right)^{*} = \left(\frac{2|S|\angle a}{|V^{f_1}|\angle\varphi^{f_1}}\right)^{*} \tag{5.7}$$

where $\vec{S}_{L1}$ is the apparent power of phase L1, the $\vec{V}_{L1}$ is the voltage phase of phase L1, the $\vec{I}_{L1}$ is current phasor for phase L1 and the $\vec{I}^{*}_{L1}$ is the conjugate of current phasor $\vec{I}_{L1}$. It is considered that the three power system under consideration is balanced as the analysis is performed only for phase L1. Despite this, by applying modifications to the proposed model and by performing analysis on all phases it can become feasible to perform studies for unbalanced conditions as well.

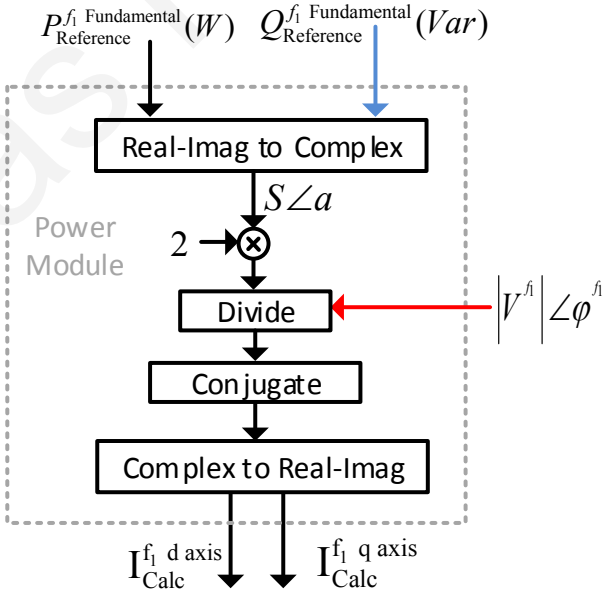

Figure 5.3. APVSM – Power Module

The voltage phasor $\vec{V}_{L1} = |V^{f_1}|\angle\varphi^{f_1}$ is obtained by applying Fourier analysis based on equation (5.7) on a running average window of one cycle.

$$f(t) = \frac{a_o}{2} + \sum_{n=1}^{\infty} a_n \cos(n\omega t) + b_n \sin(n\omega t) \quad (5.8)$$

where n represents the rank of the harmonics (n = 1 corresponds to the fundamental component.) The magnitude and phase of the selected harmonic component are calculated by equations:

$$|H_n| = \sqrt{a_n^2 + b_n^2} \quad (5.9)$$

$$\angle H_n = \tan^{-1}\left(\frac{b_n}{a_n}\right) \quad (5.10)$$

where

$$a_n = \frac{2}{T_n} \int_{t-T_n}^{t} f(t)\, a_n \cos(n\omega t) dt \quad (5.11)$$

$$b_n = \frac{2}{T_n} \int_{t-T_n}^{t} f(t)\, a_n \sin(n\omega t) dt \quad (5.12)$$

$$T_n = \frac{1}{f_n} \quad f_n - harmonic\ frequency \quad (5.13)$$

For the first cycle of simulation, the Fourier output is held to the values specified by the initial conditions and consequently the results are valid from the first cycle and after. The current for the chosen harmonic frequencies is calculated by the Harmonic Controller (n) shown in Fig. 5.4. The regression model (n) for selected harmonics (found in Table 5.3) is defined based on the concepts mentioned previously having as predictors the parameters of Table 5.1.

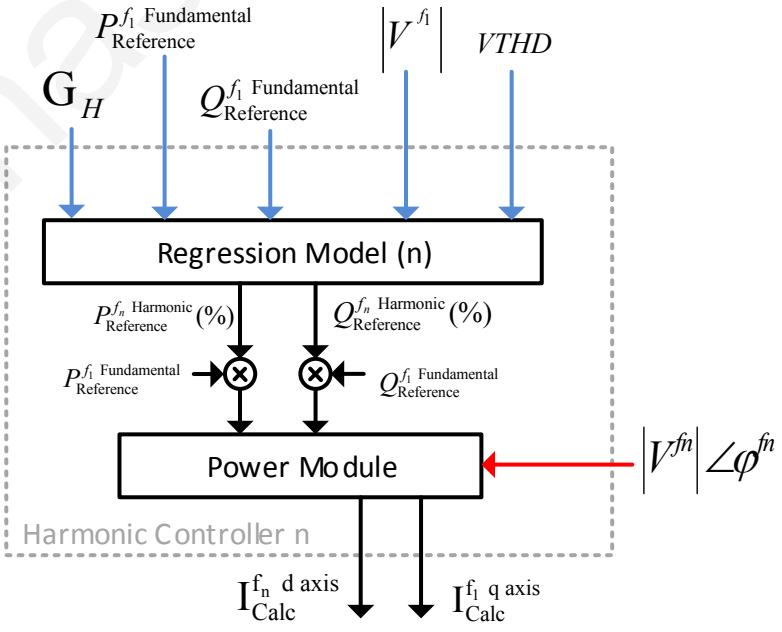

Figure 5.4. APVSM – Harmonic Controller (n)

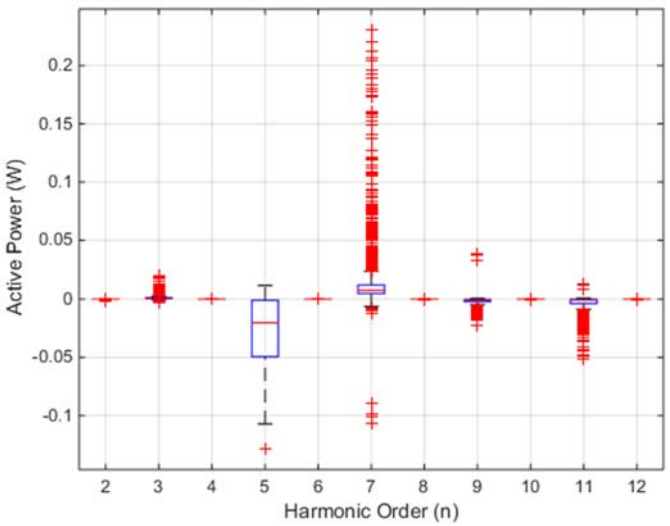

Figure 5.5a. Even/Odd harmonics of Active Power

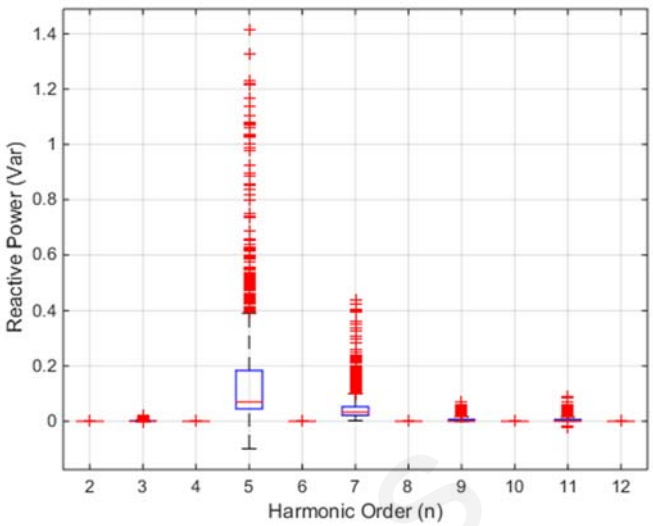

Figure 5.5b. Even/Odd harmonics of Reactive Power

Figure 5.5. Harmonics of Active and Reactive Power

As can be seen in table 5.3 the even harmonics and harmonics of order higher than the 11th are not considered in the modelling as their amplitude is insignificant. This observation can be seen from Probability of Occurrence of Power Harmonics in Fig. 5.5. The regression models and their estimated fit accuracy are shown in Table 5.3.

Table 5.3. Regression models used in the PV System modelling and their fit accuracy

Internal Model Signals	Input Variables	Accuracy (R^2)	Regression Model - Polynomial Degree
Active Power Fundamental	Solar Irradiance	1.000	Second Degree
Active Power 3rd Harmonic	Current RMS, Active Power Fundamental, Reactive Power Fundamental, Voltage RMS, Voltage THD	0.858	Four Degrees per variable
Active Power 5th Harmonic	Current RMS, Active Power Fundamental, Reactive Power Fundamental, Voltage RMS, Voltage THD	0.947	Four Degrees per variable
Active Power 7th Harmonic	Current RMS, Active Power Fundamental, Reactive Power Fundamental, Voltage RMS, Voltage THD	0.951	Four Degrees per variable
Active Power 9th Harmonic	Current RMS, Active Power Fundamental, Reactive Power Fundamental, Voltage RMS, Voltage THD	0.904	Four Degrees per variable
Active Power 11th Harmonic	Current RMS, Active Power Fundamental, Reactive Power Fundamental, Voltage RMS, Voltage THD	0684	Four Degrees per variable
Reactive Power 3rd Harmonic	Current RMS, Active Power Fundamental, Reactive Power Fundamental, Voltage RMS, Voltage THD	0.894	Four Degrees per variable
Reactive Power 5th Harmonic	Current RMS, Active Power Fundamental, Reactive Power Fundamental, Voltage RMS, Voltage THD	0.981	Four Degrees per variable
Reactive Power 7th Harmonic	Current RMS, Active Power Fundamental, Reactive Power Fundamental, Voltage RMS, Voltage THD	0.919	Four Degrees per variable
Reactive Power 9th Harmonic	Current RMS, Active Power Fundamental, Reactive Power Fundamental, Voltage RMS, Voltage THD	0.871	Four Degrees per variable
Reactive Power 11th Harmonic	Current RMS, Active Power Fundamental, Reactive Power Fundamental, Voltage RMS, Voltage THD	0.675	Four Degrees per variable

The voltage total harmonic distortion (VTHD) index is calculated by using equation (4.1). The amplitude of individual voltage harmonics is obtained by applying Fourier analysis on voltage waveforms. The regression model results for the 3rd Harmonic Active Power and the 3rd Harmonic Reactive Power are presented in Tables 5.4 and 5.5 respectively. Similar results are obtained for the remaining power harmonics found in Table 5.3.

Table 5.4. Regression models for the 3rd Harmonic Active Power

Active Power - 3rd Harmonic						
Linear regression model: y ~ Linear formula with 45 terms and 5 predictors					Confidence Interval of β_k	
Parameter	Estimated β_k	SE	tStat	pValue	Lower Bound	Upper Bound
(Intercept)	-0.5181	0.061543	-8.4185	9.68E-17	-0.6388	-0.3974
x_1	0.082704	0.037008	2.2347	0.025598	0.0101	0.1553
x_2	0.002345	0.000261	8.9877	8.39E-19	0.0018	0.0029
x_3	0.014678	0.000717	20.467	3.24E-81	0.0133	0.0161
x_4	-0.04747	0.003432	-13.831	9.11E-41	-0.0542	-0.0407
x_5	-1.8514	0.31019	-5.9686	3.06E-09	-2.4599	-1.2429
x_1^2	0.021833	0.005642	3.8696	0.000114	0.0108	0.0329
x_1x_2	-0.00057	0.000152	-3.7214	0.000206	-0.0009	-0.0003
x_1x_3	-0.00181	0.000421	-4.2996	1.83E-05	-0.0026	-0.001
x_3^2	-0.00016	7.55E-06	-21.758	4.13E-90	-0.0002	-0.0001
x_1x_4	0.010686	0.001899	5.6269	2.23E-08	0.007	0.0144
x_4^2	0.002725	0.000177	15.434	1.39E-49	0.0024	0.0031
x_1x_5	0.61674	0.16539	3.7289	0.0002	0.2923	0.9412
x_2x_5	0.007763	0.001294	6.0012	2.52E-09	0.0052	0.0103
x_3x_5	-0.02526	0.001735	-14.564	1.03E-44	-0.0287	-0.0219
x_4x_5	0.17785	0.013594	13.083	6.82E-37	0.1512	0.2045
x_5^2	1.9782	0.2598	7.6144	4.98E-14	1.4686	2.4879
x_1^3	-0.00347	0.001185	-2.9306	0.003441	-0.0058	-0.0011
$x_1^2x_4$	-0.00057	0.000207	-2.7335	0.00635	-0.001	-0.0002
$x_1x_4^2$	-0.00012	3.10E-05	-3.8777	0.000111	-0.0002	-0.0001
x_4^3	-0.00016	5.91E-06	-26.56	3.45E-125	-0.0002	-0.0001
$x_1^2x_5$	-0.0578	0.021106	-2.7385	0.006254	-0.0992	-0.0164
$x_1x_2x_5$	-0.00191	0.000626	-3.0583	0.00227	-0.0031	-0.0007
$x_1x_3x_5$	-0.00558	0.000946	-5.8981	4.65E-09	-0.0074	-0.0037
$x_1x_4x_5$	0.018938	0.005295	3.5766	0.00036	0.0086	0.0293
$x_2x_4x_5$	-0.00034	4.18E-05	-8.1713	7.00E-16	-0.0004	-0.0003
$x_3x_4x_5$	0.001987	0.000125	15.949	1.46E-52	0.0017	0.0022
$x_4^2x_5$	-0.00781	0.000514	-15.192	3.28E-48	-0.0088	-0.0068
$x_1x_5^2$	-0.0657	0.06387	-1.0286	0.30386	-0.191	0.0596
$x_2x_5^2$	-0.00755	0.001017	-7.428	1.96E-13	-0.0095	-0.0056
$x_3x_5^2$	0.019414	0.002928	6.6313	4.82E-11	0.0137	0.0252
$x_4x_5^2$	-0.08315	0.011523	-7.2163	8.92E-13	-0.1058	-0.0605
x_5^3	0.007141	0.036899	0.19354	0.84657	-0.0652	0.0795
$x_1^2x_4x_5$	0.002554	0.000862	2.9616	0.003114	0.0009	0.0042
$x_1x_4^2x_5$	-0.00016	3.95E-05	-4.0993	4.39E-05	-0.0002	-0.0001
$x_1^2x_5^2$	0.021413	0.012845	1.667	0.095745	-0.0038	0.0466
$x_1x_3x_5^2$	-0.00088	0.000348	-2.5112	0.012148	-0.0016	-0.0002
$x_3x_4x_5^2$	0.000529	8.44E-05	6.2658	4.99E-10	0.0004	0.0007
$x_4^2x_5^2$	-0.00202	0.00034	-5.9368	3.70E-09	-0.0027	-0.0014
$x_1x_5^3$	-0.04508	0.012883	-3.4994	0.000482	-0.0704	-0.0198
$x_3x_5^3$	0.013486	0.001553	8.686	1.08E-17	0.0104	0.0165
$x_4x_5^3$	-0.05335	0.006185	-8.6257	1.77E-17	-0.0655	-0.0412
x_5^4	0.011671	0.00522	2.2357	0.025534	0.0014	0.0219

Table 5.5. Regression models for the 3rd Harmonic Reactive Power

Reactive Power - 3rd Harmonic						
Linear regression model: y ~ Linear formula with 42 terms and 5 predictors					**Confidence Interval of β_k**	
Parameter	**Estimated β_k**	**SE**	**tStat**	**pValue**	**Lower Bound**	**Upper Bound**
(Intercept)	0.19434	0.10152	1.9143	0.055798	-0.0048	0.3935
x_1	-0.11936	0.060738	-1.9651	0.04961	-0.2385	-0.0002
x_2	-0.00122	0.000432	-2.8176	0.004909	-0.0021	-0.0004
x_3	0.00888	0.001154	7.6958	2.72E-14	0.0066	0.0111
x_4	-0.02837	0.008377	-3.3864	0.00072861	-0.0448	-0.0119
x_5	-0.5172	0.21994	-2.3515	0.01884	-0.9487	-0.0857
x_1^2	-0.0571	0.008808	-6.4824	1.27E-10	-0.0744	-0.0398
x_1x_2	0.001083	0.000255	4.2561	2.23E-05	0.0006	0.0016
x_1x_3	-0.00225	0.00066	-3.4121	0.0006638	-0.0035	-0.001
x_1x_4	0.01666	0.004679	3.5605	0.0003831	0.0075	0.0258
x_3x_4	-0.00097	4.61E-05	-21.088	1.88E-85	-0.0011	-0.0009
x_4^2	0.002433	0.000223	10.888	1.65E-26	0.002	0.0029
x_1x_5	0.3234	0.090849	3.5597	0.00038423	0.1452	0.5016
x_2x_5	0.001352	0.000916	1.4765	0.14005	-0.0004	0.0031
x_3x_5	-0.02622	0.003613	-7.2567	6.70E-13	-0.0333	-0.0191
x_4x_5	0.032735	0.01918	1.7068	0.088098	-0.0049	0.0704
x_5^2	-3.08	0.81979	-3.7571	0.00017932	-4.6882	-1.4718
x_1^3	0.006943	0.001625	4.2721	2.07E-05	0.0038	0.0101
$x_1^2x^4$	0.002103	0.000232	9.0505	4.89E-19	0.0016	0.0026
$x_1x_4^2$	0.000193	3.33E-05	5.8081	7.89E-09	0.0001	0.0003
x_4^3	-0.00018	8.32E-06	-21.96	1.60E-91	-0.0002	-0.0002
$x_1^2x_5$	-0.11872	0.046335	-2.5622	0.01051	-0.2096	-0.0278
$x_1x_3x_5$	-0.00757	0.002083	-3.636	0.00028746	-0.0117	-0.0035
$x_1x_4x_5$	0.027533	0.008754	3.145	0.0016973	0.0104	0.0447
$x_2x_4x_5$	0.000317	8.18E-05	3.8797	0.0001097	0.0002	0.0005
$x_3x_4x_5$	0.003377	0.00018	18.811	3.23E-70	0.003	0.0037
$x_4^2x_5$	-0.01406	0.000744	-18.908	7.50E-71	-0.0155	-0.0126
$x_1x_5^2$	-0.06483	0.026096	-2.4844	0.013097	-0.116	-0.0136
$x_2x_5^2$	0.014043	0.003445	4.0763	4.85E-05	0.0073	0.0208
$x_3x_5^2$	0.058466	0.004432	13.191	1.93E-37	0.0498	0.0672
$x_4x_5^2$	-0.25851	0.018387	-14.059	5.62E-42	-0.2946	-0.2224
x_5^3	-1.6889	0.33148	-5.0948	3.99E-07	-2.3391	-1.0386
$x_1^3x_5$	0.017728	0.00805	2.2021	0.027827	0.0019	0.0335
$x_1x_3x_5^2$	-0.00513	0.001455	-3.5222	0.00044239	-0.008	-0.0023
$x_1x_4x_5^2$	0.020212	0.006013	3.3613	0.00079755	0.0084	0.032
$x_3x_4x_5^2$	0.001082	0.000116	9.3315	4.19E-20	0.0009	0.0013
$x_4^2x_5^2$	-0.00403	0.000461	-8.7317	7.35E-18	-0.0049	-0.0031
$x_1x_5^3$	-0.03946	0.008946	-4.4103	1.11E-05	-0.057	-0.0219
$x_2x_5^3$	0.00667	0.001352	4.9327	9.13E-07	0.004	0.0093
$x_3x_5^3$	0.031749	0.002757	11.516	2.52E-29	0.0263	0.0372
$x_4x_5^3$	-0.12355	0.011115	-11.115	1.62E-27	-0.1454	-0.1017
x_5^4	0.051667	0.01169	4.4197	1.07E-05	0.0287	0.0746

For the proper synchronization of the fundamental/harmonic current signals, the CDSC-PLL is utilized. The CDSC-PLL is shown in Fig. 5.6 and it is used for detecting/tracking the phase angle of the grid voltage for both the fundamental frequency and the harmonics under consideration. More information about the CDSC, dqPLL and Phase correction modules composing the CDSC-PLL (Fundamental & Harmonic PLL Blocks) are found in [156]. The abc to Alpha-Beta (αβ) block performs a Clarke transformation on the three-phase abc voltage signal according to equation (5.14):

$$\begin{bmatrix} u_\alpha \\ u_\beta \end{bmatrix} = \begin{bmatrix} \frac{2}{3} & -\frac{1}{3} & -\frac{1}{3} \\ 0 & \frac{1}{\sqrt{3}} & -\frac{1}{\sqrt{3}} \end{bmatrix} \begin{bmatrix} u_a \\ u_b \\ u_c \end{bmatrix} \tag{5.14}$$

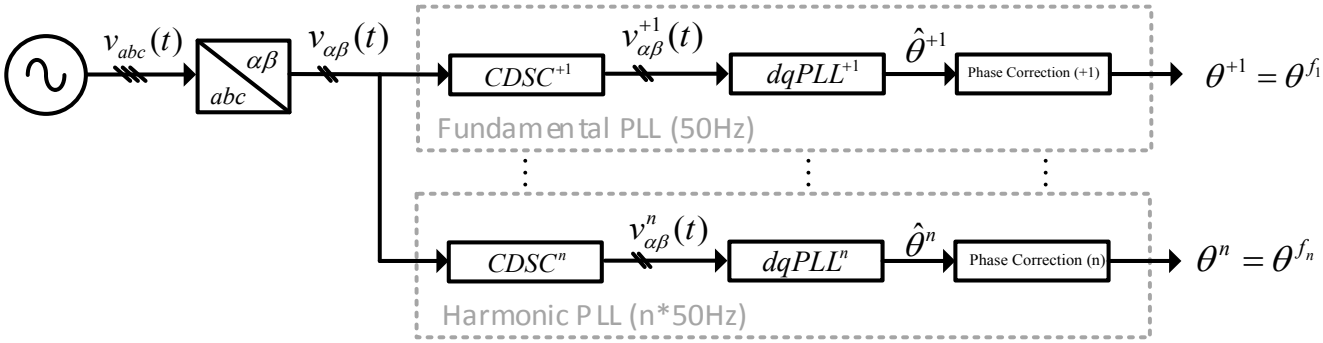

Figure 5.6. Fundamental and Harmonic PLL Modules

The input to the three phase current source has been calculated using the dq0/abc transformation described by equations (5.15). I_d and I_q represent the real and imaginary part of the calculated current phasor respectively.

$$\begin{bmatrix} I_a \\ I_b \\ I_c \end{bmatrix} = \frac{2}{3}\begin{bmatrix} \sin(\omega t) & \cos(\omega t) & 1 \\ \sin\left(\omega t - \frac{2\pi}{3}\right) & \cos\left(\omega t - \frac{2\pi}{3}\right) & 1 \\ \sin\left(\omega t + \frac{2\pi}{3}\right) & \cos\left(\omega t + \frac{2\pi}{3}\right) & 1 \end{bmatrix}\begin{bmatrix} I_d \\ I_q \\ I_o \end{bmatrix} \tag{5.15}$$

where I_a,I_b and I_c are the phase currents and the I_d,I_q are the d and q axis components of the calculated current phasor respectively. I_o is the zero-axis component which is equal to zero for balanced analysis.

5.2.2 Industrial Area Distribution Grid under Investigation

Different PV concentrations are investigated by using the APVSM to assess the power quality behaviour of a quite common distribution grid topology. The grid topology represents an industrial area in which power quality measurements were performed before and after the connection of a 150 kW_p PV system. The system topology of the distribution grid in the industrial area is shown in Fig. 5.7. Moreover, the response of the distribution grid before and after the installation of the 150 kW_p PV system is shown in Fig. 4.4. Based on measurements done in the industrial area the load power consumption follows the curve of Fig. 5.8. Subsequently, the data obtained from the measurements were further used in the simulation of the industrial area distribution grid. It is considered that the background total harmonic distortion (THD) of the voltage on the distribution transformer is approximately 1% (this assumption agrees with the measurements done on the distribution transformer).

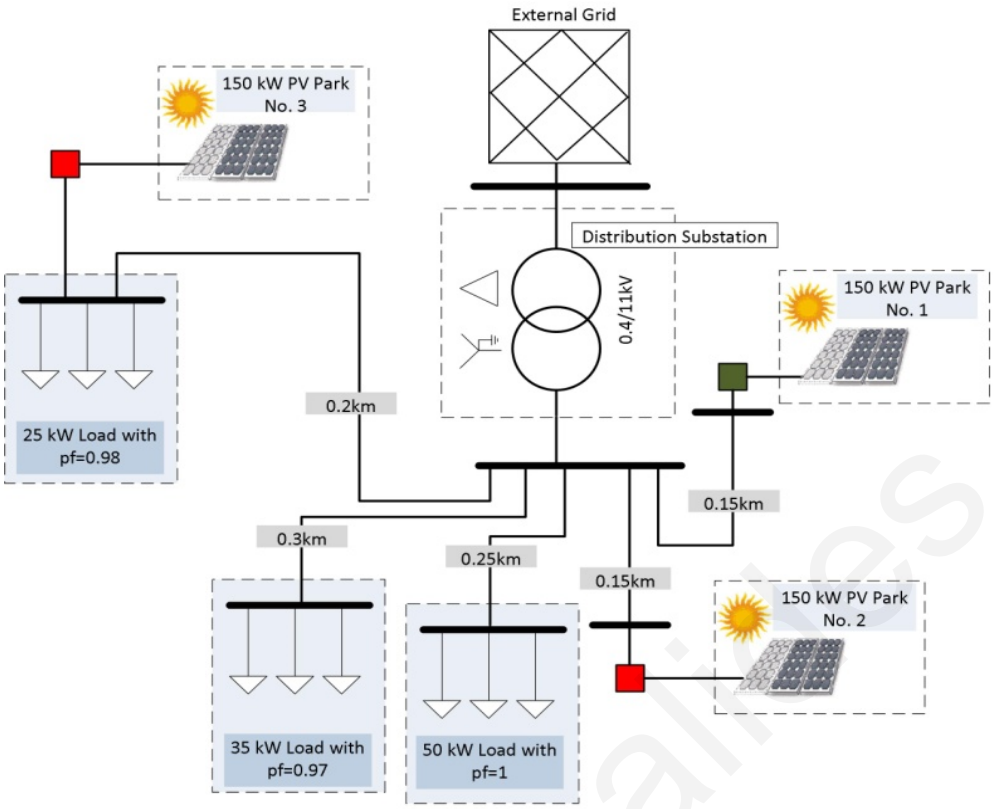

Figure 5.7. Industrial Area Network Topology under Investigation

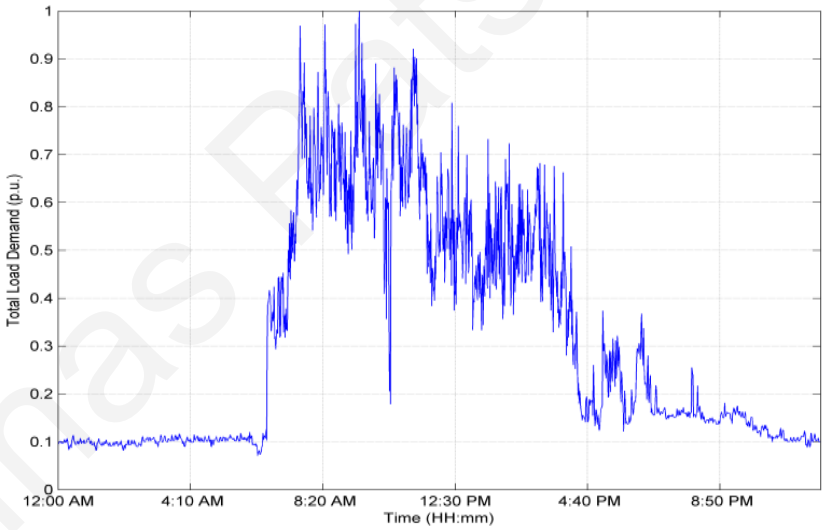

Figure 5.8. Load profiles for the cases under investigation

5.2.5 Methodology adopted for the APVSM

Measurements from the 150 kW_p PV System located in the industrial area under investigation are used to adjust the regression parameters required for the configuration of the APVSM. More specifically, data of one week are utilized to define the parameters of all the regression models of APVSM. The APVSM is then inserted into the electricity grid network of the industrial area to study the behaviour of different PV penetration scenarios. The distribution transformer and the medium voltage network are replaced by their equivalent circuit according to the methodology presented in Chapter 9. For simulation

purposes, up to three PV systems are installed on the distribution grid and the voltage distortion and voltage levels are considered.

5.3 Simulation Results - APVSM

The distribution grid topology of the industrial area is utilized for power quality investigations while using the APVSM as the specific circuit topology has been tuned and validated using experimental results. Three 150 kW_p PV systems are introduced inside the distribution grid topology and the simulation results are shown in Fig. 5.13. By comparing the response of the distribution grid before and after the installation of the 150 kW_p PV system shown in Fig. 4.4 with Fig. 5.9 it is evident that a good agreement exists between measured and simulated data. More specifically, from Fig. 5.9a it can be seen that the distribution grid will not experience problems with voltage harmonics as the injection of current harmonics is not significant (applies for EN 61727 compatible inverters). The dashed red line in Fig. 5.9b represents the EN 50160 limit of voltage RMS for the distribution grid.

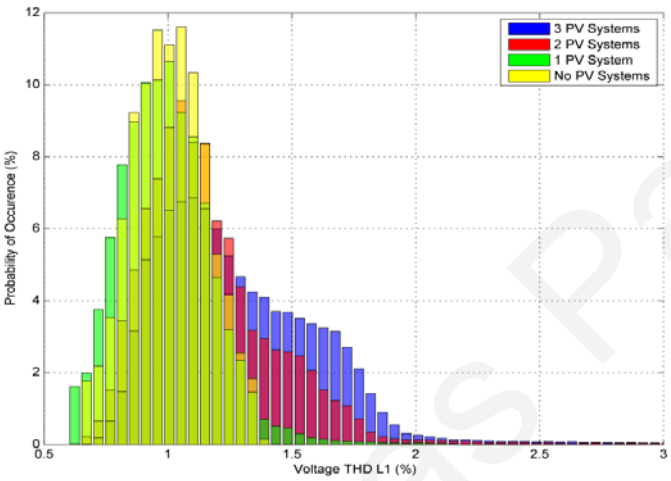

Figure 5.9a. Voltage THD obtained from the simulation of the industrial area distribution grid

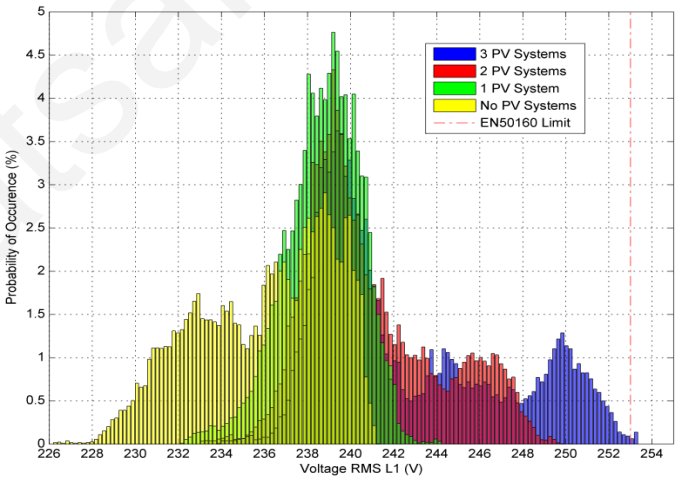

Figure 5.9b. Voltage RMS obtained from the simulation of the industrial area distribution grid

Figure 5.9. Simulation results for the industrial area case using the APVSM

As shown in Fig. 5.9b, the voltage limit is slightly exceeded with the installation of the third 150 kW_p PV system as the produced power during times of high solar irradiance is well above the demand of the local area loads.

5.4 Conclusions

In this chapter, a new PV system model for the study of power quality problems in distribution grids is developed based on the extension of SPVSM. The model is used for the study of varying PV penetrations in an industrial distribution grid network which is tuned and modelled using power measurements. Along with the new Advanced PV System model (APVSM), an accurate distribution grid model is proposed as well as an adequate validation procedure for comparing power quality measurements with simulation results. The

validation procedure is required in order to verify the accuracy of the models developed and to increase the confidence of simulation results. By comparing the response of the distribution grid before and after the installation of the 150 kW_p PV system it is evident that a good agreement exists between measured and simulated data. After the simulation results are verified, they are compared to the international standard EN 50160 which is adopted for power quality by many utilities worldwide. From the comparison, it has been observed that EN 61727 compatible inverters do not cause noticeable voltage distortion in distribution grids as the PV capacity increases up to almost four times the load demand. Furthermore, the voltage levels can be improved by installing the appropriate PV capacity depending on the local load demand. On the other hand when exceeding the aforementioned PV penetration limit, overvoltages can occur and loss of invaluable PV produced energy. In conclusion, the APVSM has been shown to produce acceptable steady-state response during solar irradiance variations. In addition, the transient response of the APVSM did not seem to react abnormally during the changes of solar irradiance and voltage grid variations but in order to get a more accurate view for the transient response of the PV systems a complete PV System Model representation is required to be developed.

Chapter 6
Detailed PV System Model (DPVSM)

6.1 Introduction

The third PV system model adopted for the simulations is a detailed circuit representation which includes a DC/DC converter, an AC/DC converter, a Maximum Power Point Tracking (MPPT), a filter and a Power/Protection Control Circuit. The specific model has been validated and tuned using measurements from a 150 kW_p PV system. The detailed model has been implemented to assess the steady-state/transient behaviour of PV systems and to provide the insight and data required for the simplification process with an ultimate aim to enable the ability of performing efficient power quality investigation on larger power systems. Thereafter, the work presented in this chapter focuses firstly on the accurate modelling of PV systems and secondly on the study of varying concentrations of photovoltaic (PV) systems on a proposed electricity grid with and without voltage regulation. Furthermore, apart from power quality investigations, the detailed PV system model has been used in fault studies in the presence of high PV penetrations. From simulations of varying concentrations of PV systems, it has been observed that no significant voltage distortion is caused when the inverters comply with standard EN 61727. The only problem seen while increasing the PV penetration levels above the load demand is the overvoltages

during high PV power production. For the latter case, different voltage regulation schemes are utilized to maintain the voltage quality at acceptable levels set by international standards.

Finally, the use of DPVSM made it possible to quantify the level of transient voltage levels by changing the load and solar irradiance conditions during the occurrence of a single-phase fault. It is important to be mentioned at this point that the modelling methods, presented earlier, cannot be used in the study of voltage regulation and faults as they do not take into account the additional functionalities incorporated into the control circuit of the PV inverter. Modifications to the PV System models presented in the previous chapters could enable the study of voltage regulation or even fault capability, but significant effort is required to make the models respond accurately during transient conditions.

6.2 DPVSM - Network - Methodology

6.2.1 DPVSM - Complete PV system circuit representation

The DPVSM proposed for the simulations consists of a PV array, a diode, an inverter and a power grid interface as shown in Fig. 6.1. The PV array is modelled according to its equivalent circuit shown in Fig. 6.2, by using the equations deriving from the circuit representation.

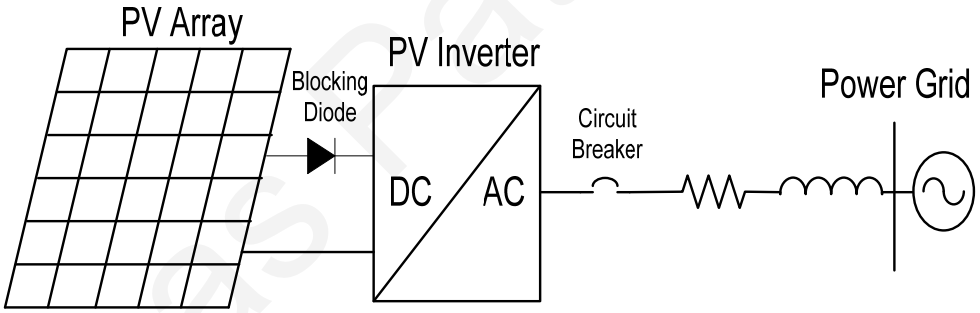

Figure 6.1. Proposed model for Grid-Connected Photovoltaic Systems

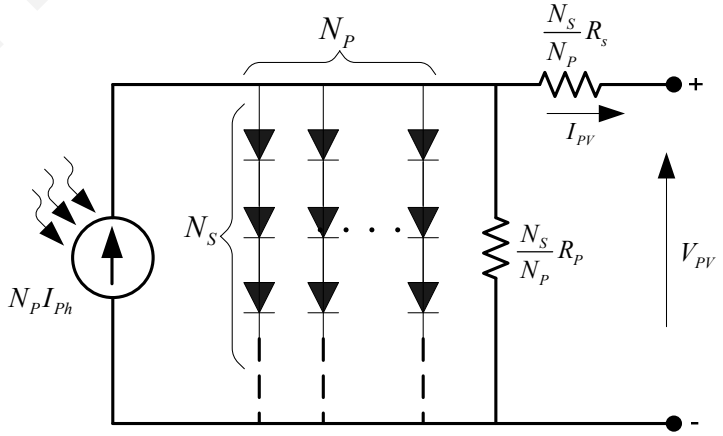

Figure 6.2. Equivalent circuit of a PV array

In particular, the behaviour of the PV array model is affected by the solar irradiance, the temperature and the specific characteristics of the chosen PV module technology. The PV

inverter circuit is composed of a DC to DC converter, which is necessary to track the maximum power point of the PV arrays, a DC to AC converter to transform the DC power into AC, means of energy transfer to absorb fast voltage variations and filters to eliminate undesirable harmonic components. The modular circuit configuration of the PV inverter is shown in Fig. 6.3 [155].

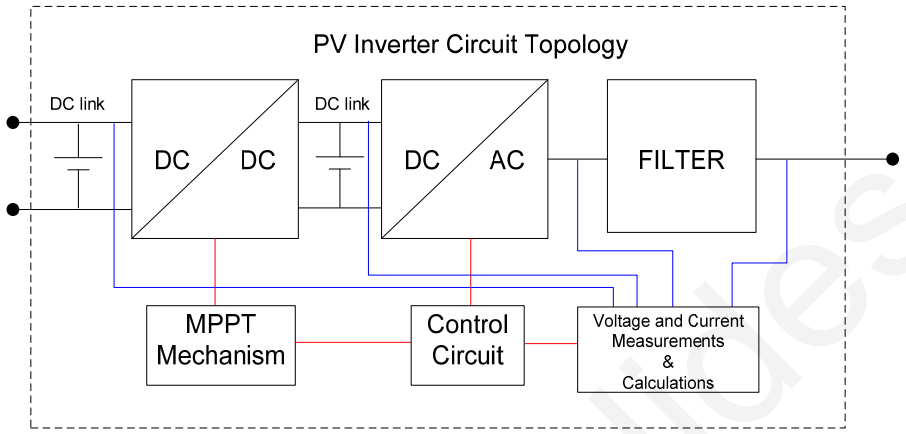

Figure 6.3. PV Inverter Circuit Topology

A maximum power point (MPP) tracking mechanism to extract the maximum power available from the PV array is also considered. The maximum power point tracking adopted is the incremental conductance method with an integral regulator to minimize the error in tracking the MPP. More information about the specific algorithm is found in [156] and [157]. The current controller is based on the feedback linearization scheme [158] according to the following equations expressed in the synchronously rotating d-q reference frame:

$$\mathrm{V_d} = \mathrm{E_d} \cdot \frac{\mathrm{N_1}}{\mathrm{N_2}} - \omega \cdot L \cdot \mathrm{I_q} - u_d \tag{6.1}$$

$$\mathrm{V_q} = \mathrm{E_q} \cdot \frac{\mathrm{N_1}}{\mathrm{N_2}} - \omega \cdot L \cdot \mathrm{I_d} - u_q \tag{6.2}$$

and

$$u_d = \left(K_p + \frac{K_i}{s}\right)(I_d^* - I_d) \tag{6.3}$$

$$u_q = \left(K_p + \frac{K_i}{s}\right)(I_q^* - I_q) \tag{6.4}$$

where $\mathrm{E_d}$ and $\mathrm{E_q}$ are the d- and q- axis components of the grid-side voltage, $\mathrm{V_d}$ and $\mathrm{V_q}$ are those of the inverter voltage, ω is the system angular frequency, L the reactance of the transformer, I_d^* and I_q^* the corresponding reference currents, I_d and I_q the actual currents at the inverter output, $\mathrm{N_1/N_2}$ the transformer ratio and K_p and K_i are the proportional and integral gains of the PI controller. The parameters u_d and u_q are the control rules (PI controller) for the d- and q- axis respectively.

The above model was chosen to be used as it represents, if properly tuned, the behaviour of the inverter during real time conditions that include variations in solar irradiance, temperature and supply voltage. In addition, the voltage regulation has been achieved via the PV inverter by controlling the amount of reactive power absorbed or injected into the grid. In this work, the performance of three different reactive power regulation methods is tested, two of them are static and one is dynamic. The regulation methods chosen are the following:

a) Fixed Power Factor: The power factor at the output of the PV system is pre-set to a certain value (-0.95) and it is kept constant during active power production.

b) Adaptive Power Factor: The power factor at the output of the PV system is defined according to the variation of active power production. The relationship of power factor with active power production is shown on Fig. 6.4 [159].

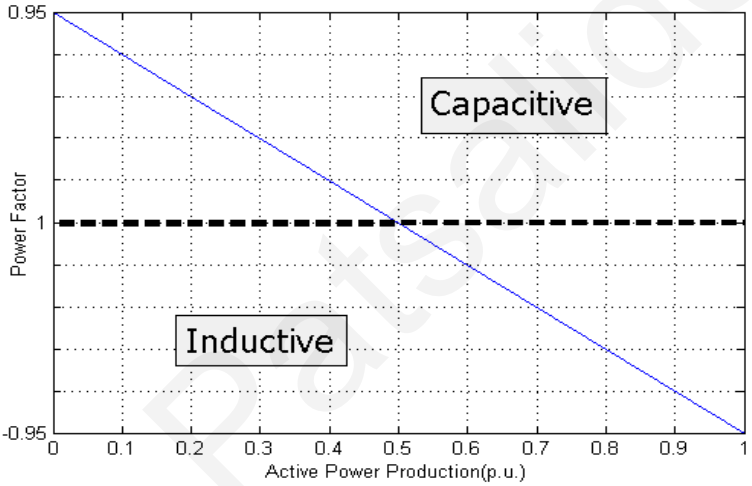

Figure 6.4. Adaptive Power Factor Method

c) Dynamic Power Factor Method: The power factor value is set dynamically according to the voltage level measured at the output of the PV system. The reactive power in this case is adjusted by changing the power factor based on the following algorithm (a similar voltage regulation scheme is found in [160] according to which the reactive power is varied in relation to the voltage level) :

$$PF = \begin{cases} 1 \; or \; -1 & \text{for } U_{Low}^{Dead\ Band} \le V_{grid} \le U_{High}^{Dead\ Band} \\ -1 + A_1 \times (V_{grid} - U_{High}^{Dead\ Band}) & \text{for } U_{High}^{Dead\ Band} < V_{grid} < U^{Upper\ Limit} \\ 1 + A_2 \times (V_{grid} - U_{Low}^{Dead\ Band}) & \text{for } U^{Lower\ Limit} < V_{grid} < U_{Low}^{Dead\ Band} \end{cases} \quad (6.5)$$

and

$$A_1 = \frac{1 - PF^{\min}}{U^{Upper\ Limit} - U_{High}^{Dead\ Band}} \qquad A_2 = \frac{1 - PF^{\min}}{U_{Low}^{Dead\ Band} - U^{Lower\ Limit}} \quad (6.6)$$

where V_{grid} is the RMS voltage measured on phase L1 (it is assumed that the power system is balanced), $U_{Low}^{Dead\ Band}$ and $U_{High}^{Dead\ Band}$ are the lower and upper limits of dead band zone

in which no voltage regulation is performed, $U^{Lower\ Limit}$ and $U^{Upper\ Limit}$ are the lower and upper limits of voltage range in which voltage regulation is performed and PF^{min} is the lower limit of the permissible power factor. A negative power factor value means absorption of reactive power. The above voltage regulation algorithms are based on voltage regulation methods described in [159]. It must be mentioned that the reactive power regulation methods adopted for the investigation are proposed by the German Guideline "Generating Plants Connected to the Medium-Voltage Network" [115].

6.2.2 Detailed PV System Model - Validation Procedure

The measurements taken from a 150 kW_p PV system using a power quality analyser are utilized for the modification/tuning and the verification of the proposed model. Specifically, the modification/tuning of the DPVSM has been done manually but likewise a parameter estimation procedure could be used for this purpose. Moreover, the solar irradiance during power quality measurements at the PV system was obtained from a Meteorological Station which is located nearby the system. The same solar irradiance profile was used for the simulations (Fig. 6.5).

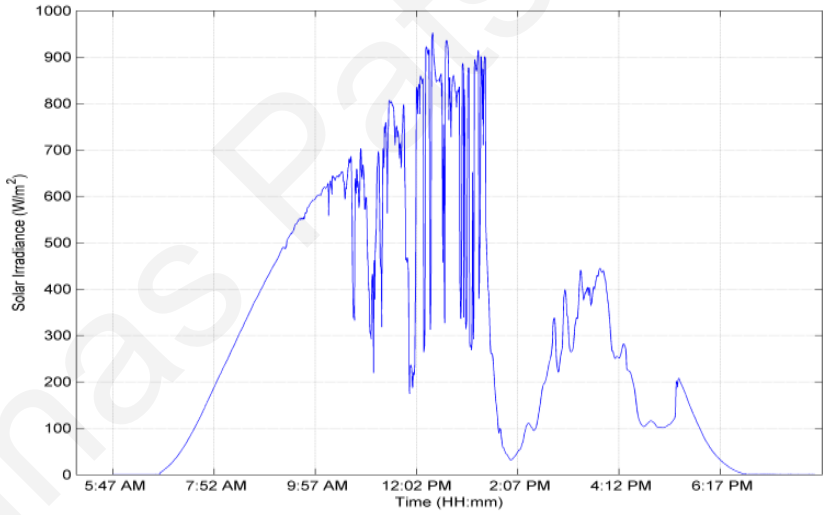

Figure 6.5. Solar Irradiance Profile vs Time

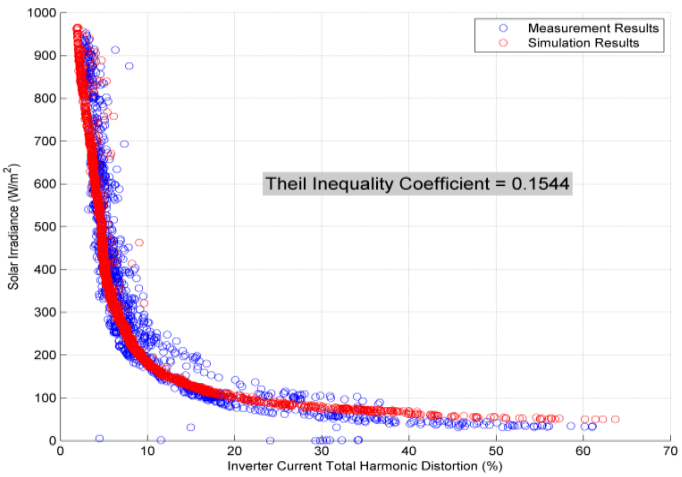

Figure 6.6a. Solar Irradiance vs Current Total Harmonic Distortion

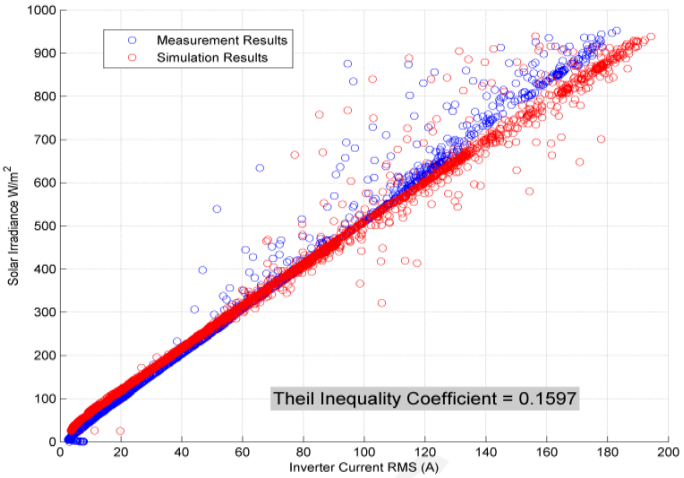

Figure 6.6b. Current RMS - Phase L1 vs Solar Irradiance

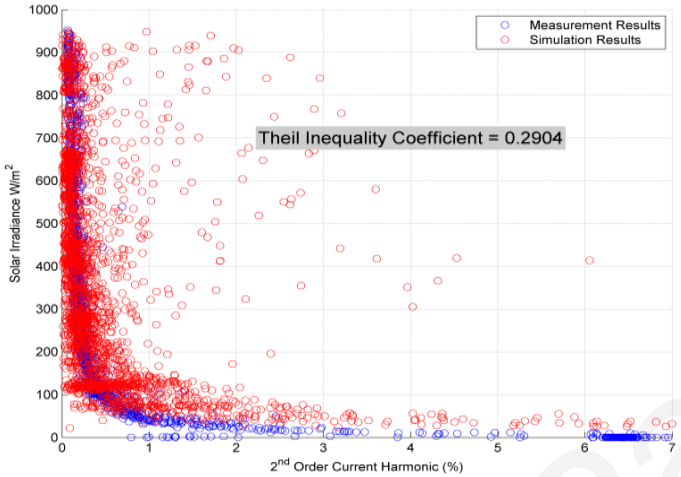

Figure 6.6c. 2nd Order Current Harmonic vs Solar Irradiance

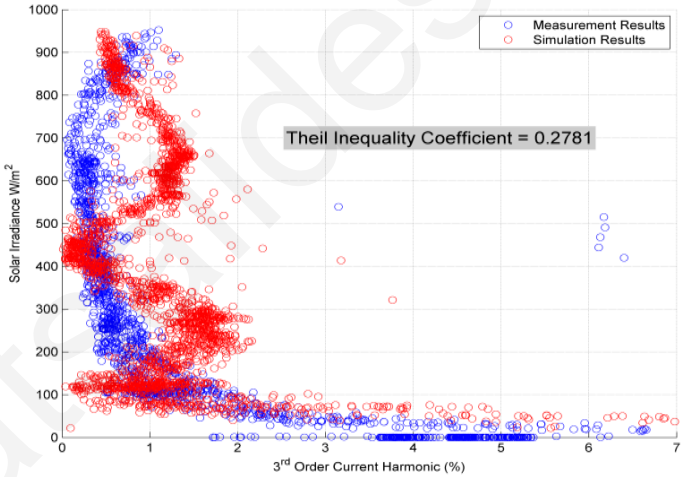

Figure 6.6d. 3rd Order Current Harmonic vs Solar Irradiance

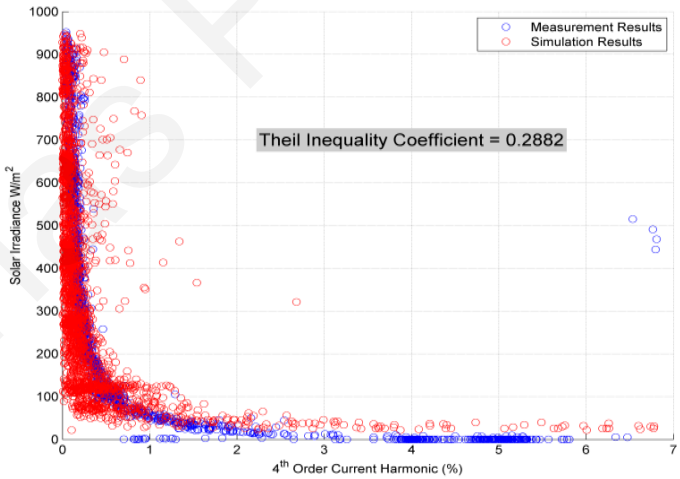

Figure 6.6e. 4th Order Current Harmonic Probability Distribution

Figure 6.6. Comparison between measured and simulated results

By using the measured irradiance as input to the simulation model a comparison between the simulation and experimental results was made possible as demonstrated in Fig. 6.6a-6.6e. The PV inverter model produced only odd harmonic currents at rated conditions as it is evident in Fig. 6.6c-6.6e. This is what expected from theory considering the operation of the power electronics during the conversion of DC power into AC. The current THD of the

inverter at rated operating conditions is lower than 5%. Also all individual harmonics up to the 17th have been checked and were found to be lower than the limits mentioned in Table 3.5. Consequently, the inverter under investigation complies with the standard EN 61727 (IEC 61727:2004) “Photovoltaic (PV) systems/ Characteristics of utility interface” (Table 3.5) as can be concluded from the measurement results. The actual comparison of the different measured and simulated quantities has been done with the "Theil inequality coefficient". The specific inequality coefficient provides a measure of how well a time series of observed values compares to a corresponding time series of estimated values. Values lower than 0.3 depict good agreement between estimated and observed data [161], [162]. As can be seen from the obtained results and inequality coefficients good agreement has been obtained between simulated and measured results. Following its validation, the detailed PV model can be used in the investigation of different PV concentration scenarios.

6.2.3 Distribution Grid Topologies under investigation

Different PV concentrations are also investigated by using the DPVSM to assess the power quality behaviour of two distribution grid topologies.

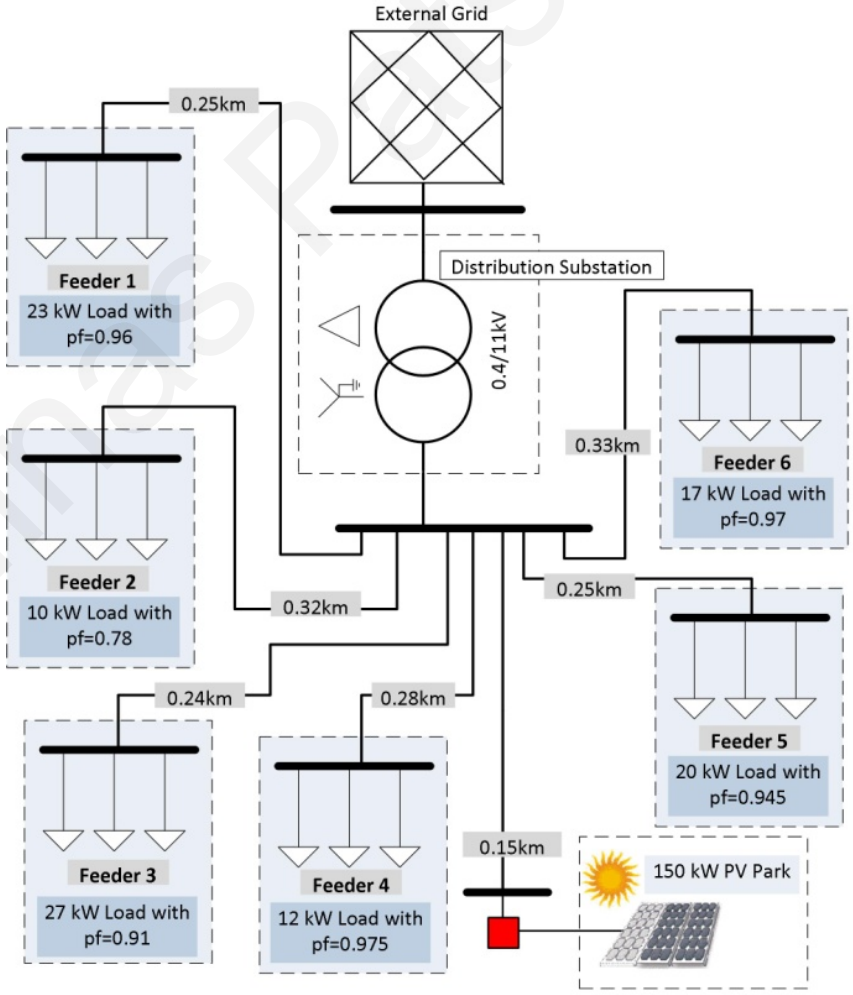

Figure 6.7. Distribution grid of the residential area

The first one represents the industrial area in which power quality measurements were performed before and after the connection of a 150 kW_p PV system and the second one is a residential area grid. The system topology of the distribution grids in the industrial and residential areas is shown in Fig. 5.7 and Fig. 6.7 respectively. It must be mentioned that the simulations for the industrial area have been undertaken in Chapter 5 using the APVSM. Due to this fact a comparison can be performed on the response of the industrial distribution grid for the two different models.

The load profile (Fig. 5.8) and the distribution grid topology (Fig. 5.7) for the industrial case are found in subsection 5.2.2. Measurements of load power consumption for summer and winter (Fig. 6.8) from a residential distribution transformer were also used for the simulation of the residential scenario. More information about the load variation in industrial and residential areas can be found in [163]–[165]. It is considered that the background total harmonic distortion (THD) of the voltage on the distribution transformer for both cases is approximately 1% (this assumption agrees with the measurements done on the distribution transformer for both areas).

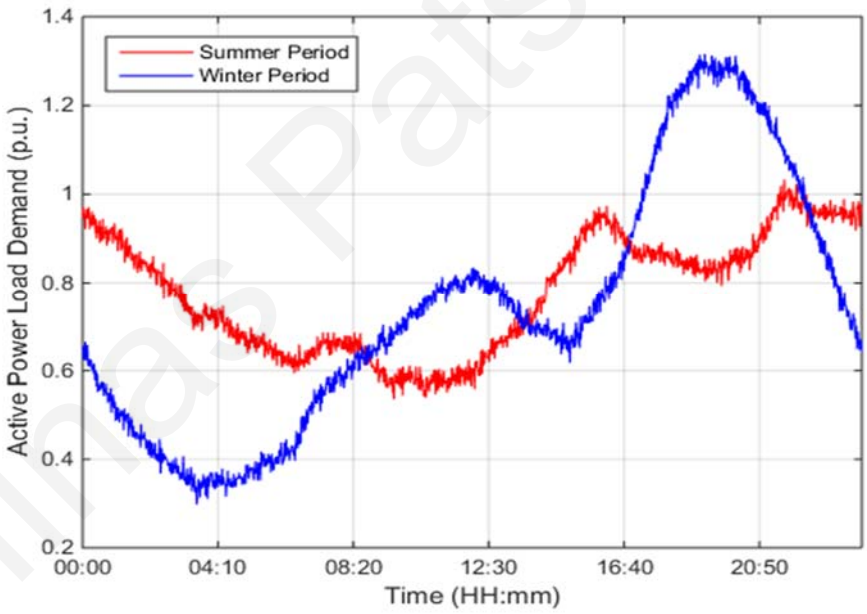

Figure 6.8. Load demand of the residential area

6.2.4 Methodology adopted for Detailed PV System Model

The measurements from the output of the 150 kW_p PV system located in the industrial area were used to develop a detailed PV system model. For the proper modelling of the PV system model, power quality measurements were undertaken at the grid connected PV system. The quantities recorded are the power factor, the amplitude and angle of individual current harmonics, the Total Harmonic Distortion (THD) and RMS values of voltage and current for a time period of two weeks. The solar irradiance was obtained also from a nearby

meteorological station and was employed in the development of the model after it was synchronized with the power quality data. The solar irradiance was monitored every minute and the power quality quantities every 30 seconds. Measurements of current amplitude and harmonics were then used to tune and validate the proposed PV system model. More information about the validation can be found in subsection 6.2.2.

The validated PV system model was further used in the simulation of two quite common distribution topologies. The first network represents an industrial area for which measurements are available before and after the installation of a 150 kW_p PV system and the second one is a residential area. The effect before and after the installation of the PV system observed from the measurements in the industrial area was utilized for the validation of the simulation results. For the industrial area case study, up to three 150 kW_p PV systems are connected to the distribution grid and the response of the distribution grid is evaluated. A residential distribution topology is then considered with 150 kW_p PV installed capacity and its response is simulated both for summer and winter load profiles. The distribution grid dynamics are determined by performing dedicated analysis on power quality measurements obtained at the busbar of the distribution transformer and appropriate modelling of the distribution grid is achieved based on the findings of the analysis. More details can be found in Chapter 9.

From the results it was obvious that no significant voltage distortion is caused if EN 61727 compatible inverters are installed. However, it has been observed that overvoltages can occur after exceeding a certain capacity of PV systems in the specific distribution grid topology. In addition, appropriate corrective actions able to keep the power quality within acceptable levels in the presence of high PV concentrations were considered. More specifically, three different voltage regulation algorithms found in the literature and in technical guidelines for the connection distributed generators on the low voltage network were employed to improve the voltage levels in the cases when more than one PV systems were installed in the grid. Finally, the response of the distribution grid during the occurrence of a fault was evaluated while changing the load conditions, the solar irradiance and PV penetration levels.

6.3 Simulation Results - DPVSM

Initially, the industrial area distribution grid was modelled properly and simulated in the presence of one 150 kW_p PV system. For this purpose, it was necessary to treat carefully the distribution grid dynamics as described in Chapter 9. The obtained simulated results are

compared with the measurements obtained before and after the installation of the 150 kW_p PV system shown in Fig. 6.9.

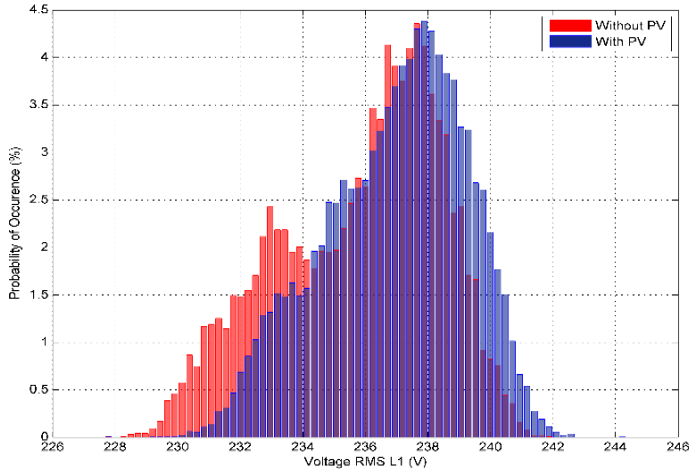

Figure 6.9a. Voltage RMS before and after the installation of the PV system

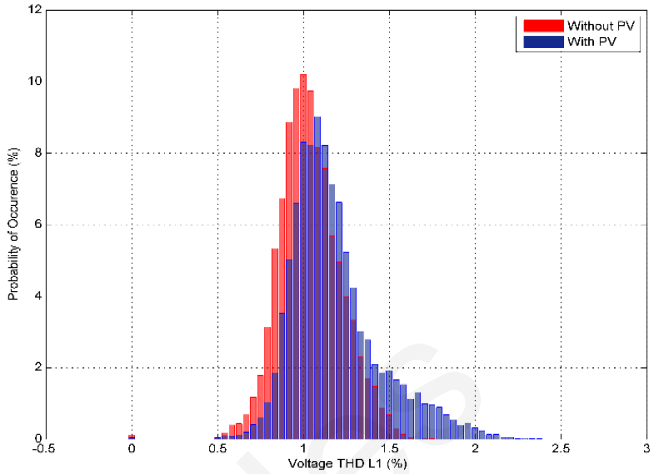

Figure 6.9b. Voltage THD before and after the installation of the PV system

Figure 6.9. Measurements obtained at the industrial area distribution grid

Then two more PV systems were introduced in order to investigate the effect of higher concentrations of PV systems on the grid. From the results in Fig. 6.10a it can be seen that the distribution grid will not experience problems with voltage harmonics as the injection of current harmonics is very low even during high solar irradiance conditions. The dashed red line in Fig. 6.10b represents the EN 50160 limit of voltage RMS for the distribution grids. This limit is exceeded with the installation of the third 150 kW_p PV system as the produced power during times of high solar irradiance is much more than the demand of the local distribution grid.

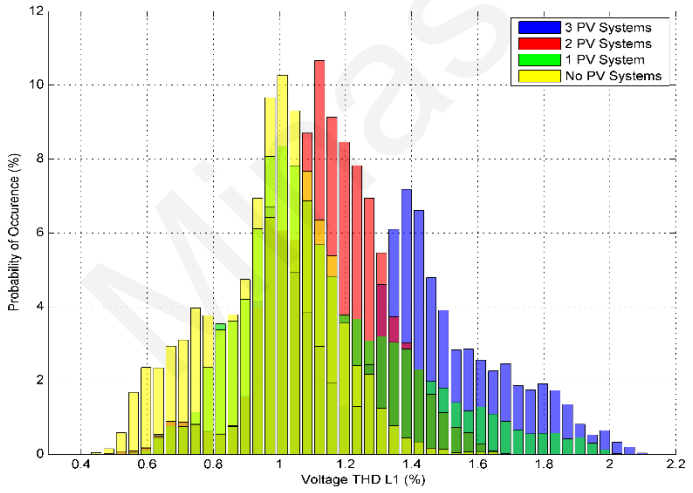

Figure 6.10a. Voltage THD obtained from the simulation of the industrial area distribution grid

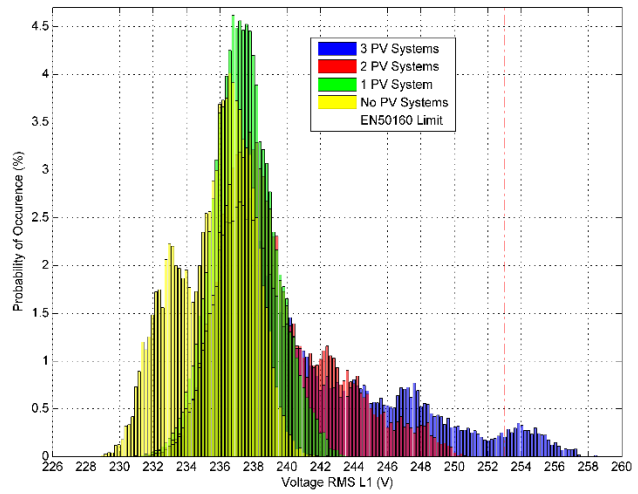

Figure 6.10b. Voltage RMS obtained from the simulation of the industrial area distribution grid

Figure 6.10. Simulation results for the industrial area case

The PV produced energy raises the grid voltage when the load is supplied by local PV generation and the excess of PV generated power is flowing thought the transformer into the medium voltage network.

In general, the violation of the voltage limit can have undesirable consequences for both energy producers and utility customers. On the one hand, it will force the inverters to trip and lead to loss of energy production each time the violation occurs and on the other hand it may cause malfunction or permanent damage to electrical devices and sensitive electronic equipment. For simulation purposes the inverter has not been designed to have a protection circuit and neither has been programmed to trip after exceeding certain voltage or frequency limits. This constitutes the main reason why overvoltage was allowed during the simulation process. Then a residential grid was considered in the presence of one PV system. The simulation results are shown in Fig. 6.11 and 6.12. It is important to be noted that the variation during winter load conditions is greater than the voltage variation during summer load conditions for the aforementioned PV installed capacity. The voltage THD index remains almost unaffected by the operation of the single 150 kW_p PV system installed on the residential distribution grid during the two seasons.

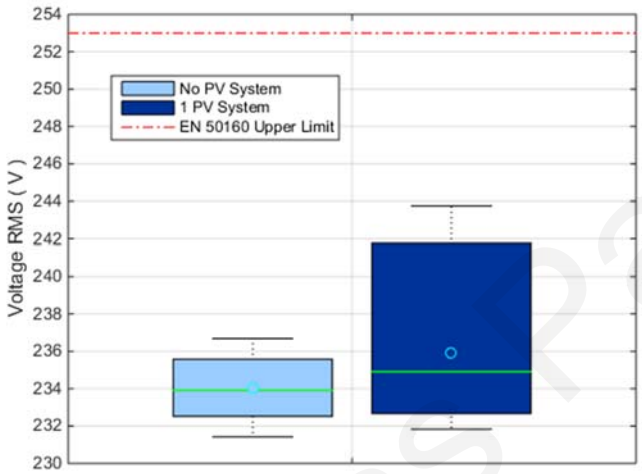

Figure 6.11a. Voltage RMS obtained from the simulation of the residential area distribution grid for summer load conditions

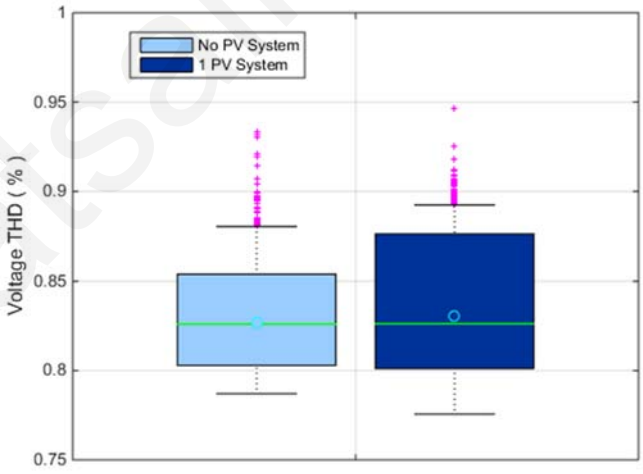

Figure 6.11b. Voltage THD obtained from the simulation of the residential area distribution grid for summer load conditions

Figure 6.11. Simulation results for the residential area for summer load conditions

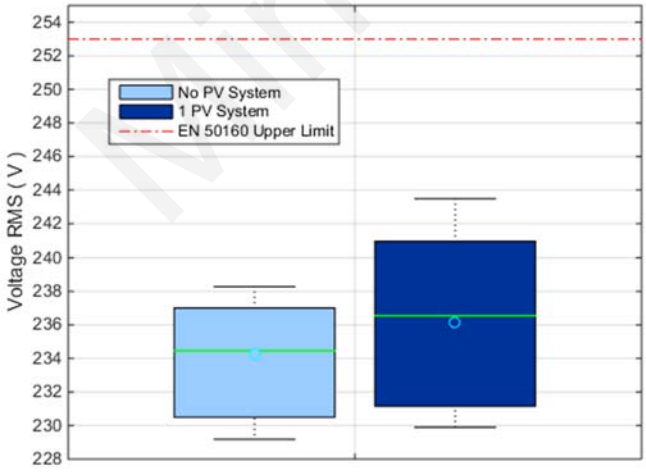

Figure 6.12a. Voltage RMS obtained from the simulation of the residential area distribution grid for winter load conditions

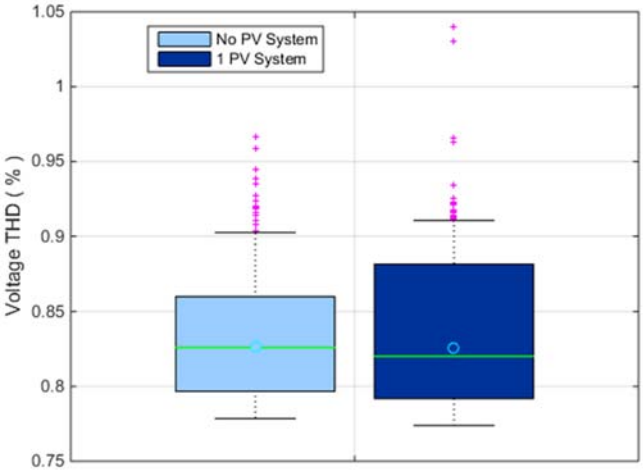

Figure 6.12b. Voltage THD obtained from the simulation of the residential area distribution grid for winter load conditions

Figure 6.12. Simulation results for the residential area for winter load conditions

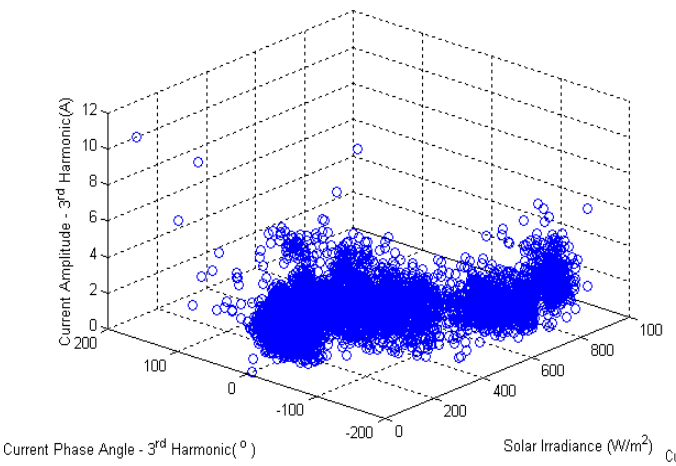

Figure 6.13a. 3rd Harmonic Phasor vs Solar Irradiance

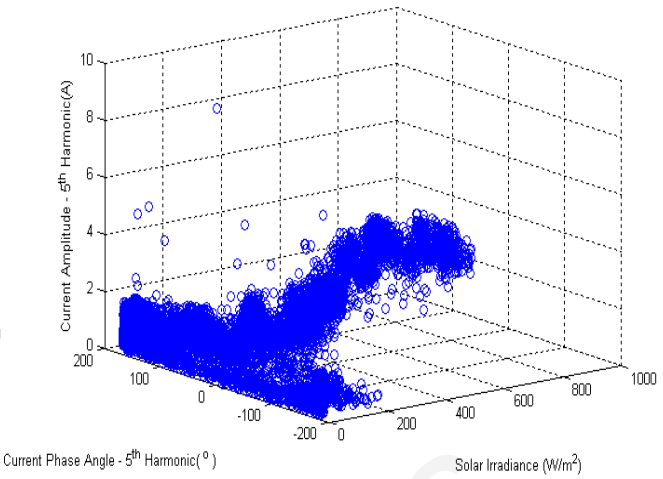

Figure 6.13b. 5th Harmonic Phasor vs Solar Irradiance

Figure 6.13. Harmonic Phasors vs Solar Irradiance

It is observed however that the voltage profile changes after the installation of a large PV system. The voltage variation increases from 6 to 12 volts in the summer as shown in Fig. 6.11a. On the other hand, in the winter the variation increases from 9 volts to 13 volts as observed in Fig. 6.12a. By observing the variation of the current harmonic phasors shown in Fig. 6.13, it can be concluded that in some instances the current harmonics may assist in improving the voltage THD when the harmonics of the grid have 180 degrees phase difference from the current harmonics of the inverter. This condition may be quite probable as the deficiencies in inverter control may cause harmonics of random phase and angle that may eliminate harmonics of the distribution grid voltage.

From Fig. 6.10b it is evident that in order to install more than two PV systems on the same distribution grid it is required to utilize a voltage regulation mechanism to maintain the voltage within acceptable levels since automatic voltage regulation is not an available option at the local distribution transformer. When the voltage regulation capability of the PV inverters is enabled, the voltage profile at the transformer's busbar can be improved only if the appropriate voltage regulation algorithm is selected based on network dynamics as can be seen on Fig.6.14. In Fig. 6.14a, the response of the grid voltage in the presence of two 150 kW_p PV systems with voltage regulation is presented. From the results of Fig. 6.14a it can be seen that the Adaptive Power Factor methods do not provide any improvement in the voltage behaviour. On the contrary, the aforementioned methods force the grid voltage to operate close to the allowable voltage limits and can cause voltage variations that can be harmful for the operation of the utility grid during solar irradiance fluctuations. This also applies to the three 150 kW_p PV capacity case (Fig. 6.14b). On the other hand, the Fixed Power Factor method achieves to set the voltage within an acceptable range but it can also cause large voltage deviations that are not desirable. The best performing voltage regulation

algorithm proved to be the Dynamic Power Factor method which not only it can lower the upper value of the voltage but additionally it can decrease the voltage variation in a quite small range even for the three 150 kW_p PV capacity. When the voltage regulation capability of some of the PV inverters is enabled, the voltage profile at the transformer's busbar can also be improved as can be seen in Fig. 6.15 (the dynamic power factor scheme is adopted which can achieve a power factor correction reaching at minimum 0.6). The comparison with the voltage limits described in EN 50160 standard can be done by referring to the cumulative distribution function (CDF) presented in the aforementioned graph.

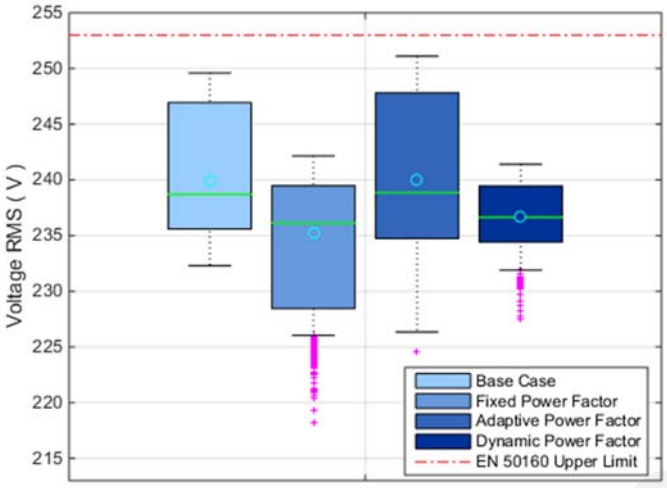

Figure 6.14a. Voltage RMS on transformer's busbar for two 150kW_p PV systems with and without voltage regulation

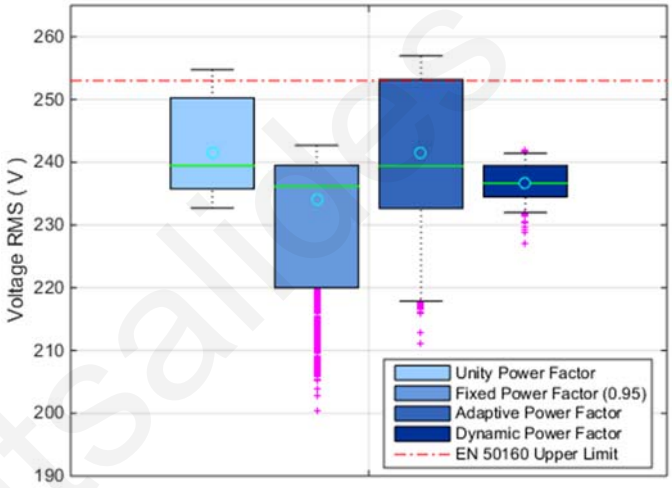

Figure 6.14b. Voltage RMS on transformer's busbar for three 150kW_p PV systems with and without voltage regulation

Figure 6.14. Voltage RMS on transformer's busbar with and without voltage

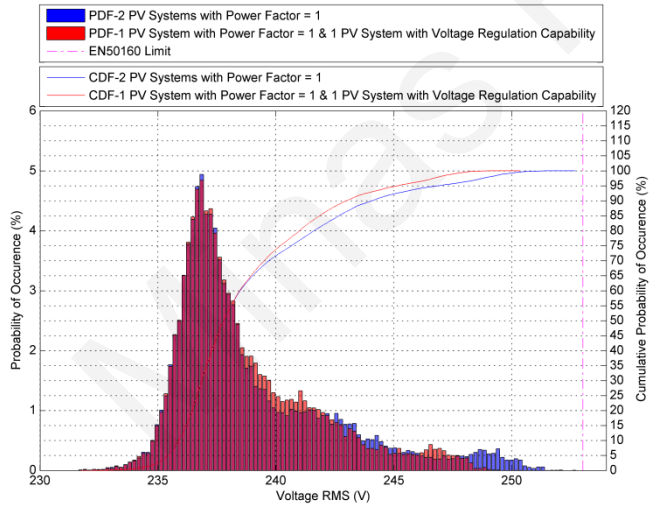

Figure 6.15a. Voltage RMS on transformer's busbar for two 150kW_p PV systems with and without voltage regulation

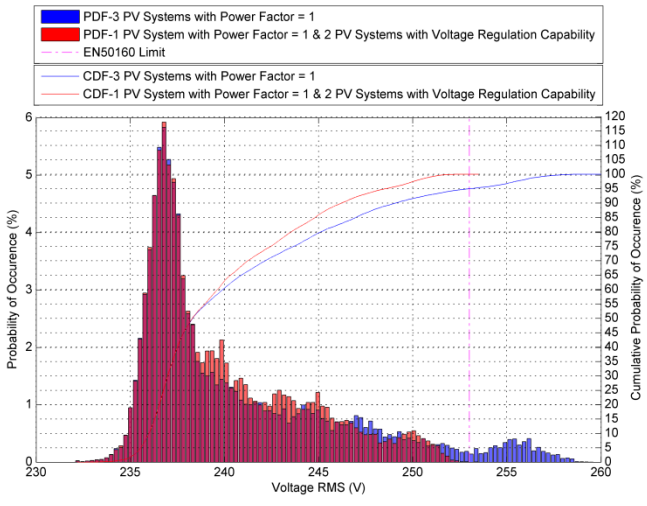

Figure 6.15b. Voltage RMS on transformer's busbar for three 150kW_p PV systems with and without voltage regulation

Figure 6.15. Voltage RMS on transformer's busbar with and without voltage regulation

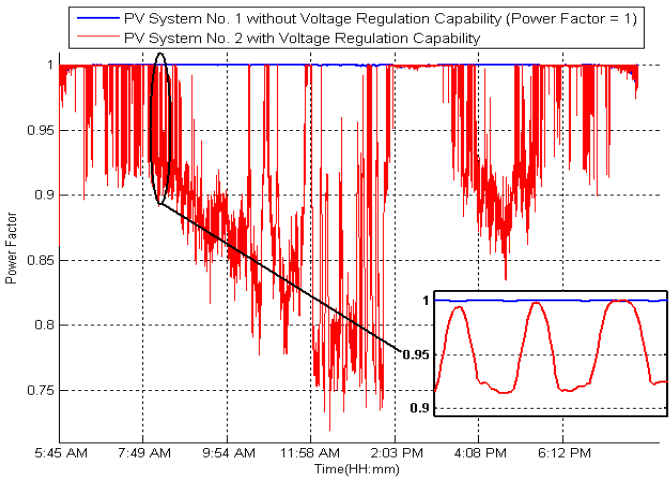

Figure 6.15a. Power Factor for two 150kW$_p$ PV systems installed capacity with voltage regulation capability

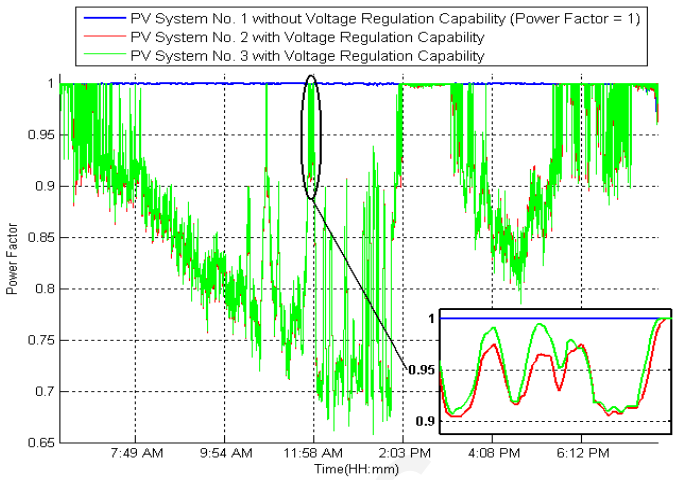

Figure 6.15b. Power Factor for three 150kW$_p$ PV systems installed capacity with voltage regulation capability

Figure 6.16. Power Factor at the output of PV systems during voltage regulation

The improvement for one PV system without voltage regulation capability (VRC) and one with (Fig. 6.15a) is only 4 volts but for two 150 kW$_p$ PV system with VRC (Fig. 6.15b) the improvement reaches 7 volts and it is essential for the healthy operation of the distribution grid. The power factor for the different PV concentration cases is shown in Fig. 6.16. For the two 150 kW$_p$ PV system installed capacity case, the inverter is performing correction on the voltage by decreasing the power factor to 0.7 (lagging) in order to enable the network to accept more active power (Fig. 6.16a). In the three 150 kW$_p$ PV system installed capacity case, the two PV systems with VRC need to operate with a power factor reaching the value of 0.65 (lagging) so that the voltage is maintained at the desirable limits described by international standards (Fig. 6.16b). Additionally, from Fig. 6.16b it can be observed that the operation of the two PV systems with VRC is very similar in terms of reactive power regulation. Deviation in behaviour is mostly due to the fact that there is a slight difference in the voltage levels observed on the buses where PV systems are installed (it is known that the reactive power sharing or the active power curtailment is not done in an equal way among DGs due to fact that each point of common coupling has different voltage/impedance characteristics [18], [105], [166], [167]). It is clear thus that over-sizing the PV inverters becomes a necessity when regulation of reactive power is required to be achieved [168], [169].

Finally, the fault behaviour of the industrial area distribution grid has been evaluated during the occurrence of a fault on Phase A of Feeder 3 as shown on Fig, 6.17. The fault lasts for 5 cycles until the protective relays of the distribution grid detect and clear it. The protection control circuit of the PV system detects the large deviation in frequency during the fault occurrence and terminates the operation of the PV system.

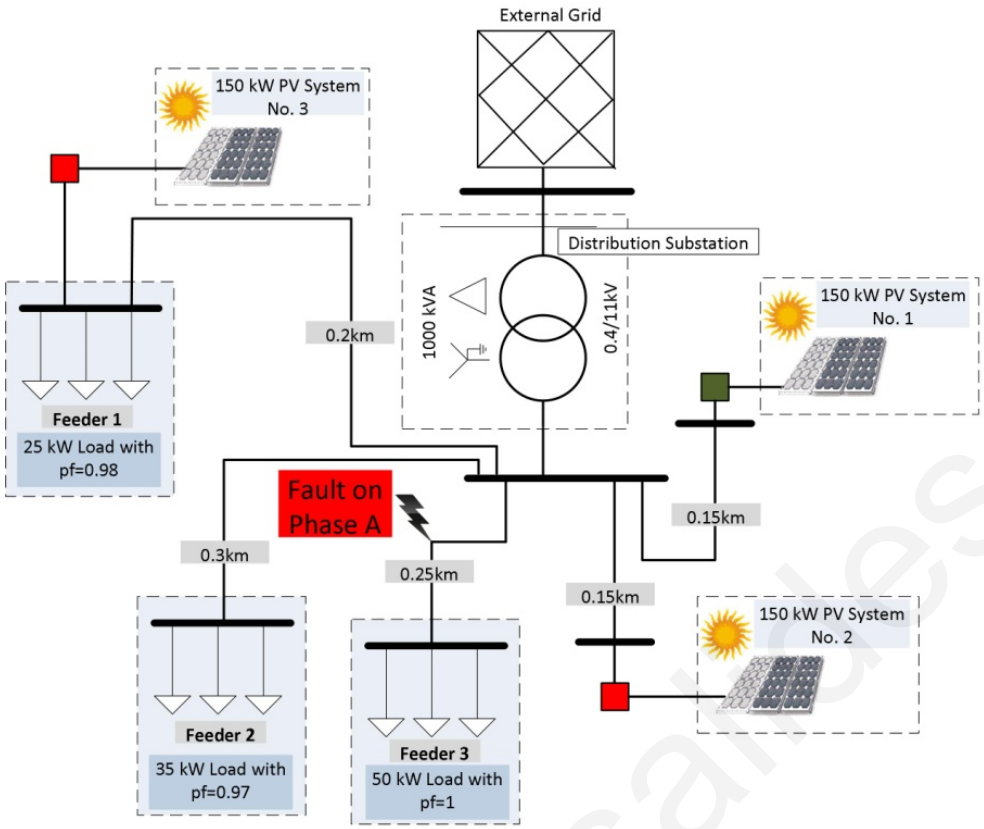

Figure 6.17. Introduction of Fault on Phase A of Feeder 3

As long as the fault is not cleared the PV system does not produce any power. When the grid voltage reaches again normal operation conditions, the PV system starts to generate power. Depending on the level of solar irradiance and local area load consumption, a transient is produced which may have an amplitude greater than the normal voltage operating condition in some instances. By performing parametric studies, it was possible to quantify the level of transient voltage levels by changing the load and solar irradiance conditions as can be seen in Fig. 6.18. The higher transient voltage occurs during high solar irradiance and no load conditions (Fig. 6.18a). The lower transient voltage is only affected by the load conditions as the PV system is deactivated while the fault is occurring (Fig. 6.18b). The maximum frequency value occurs mostly during medium solar irradiance conditions and it does not seem to be affected by the load consumption (Fig. 6.19a).

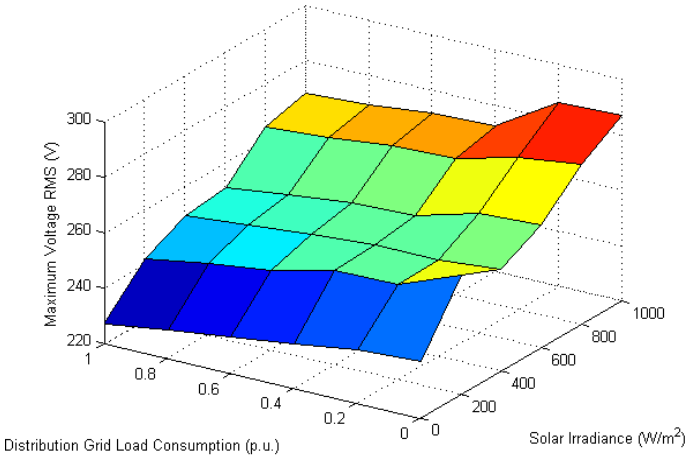

Figure 6.18a. Maximum Voltage value during the occurrence of the Fault on Feeder 3

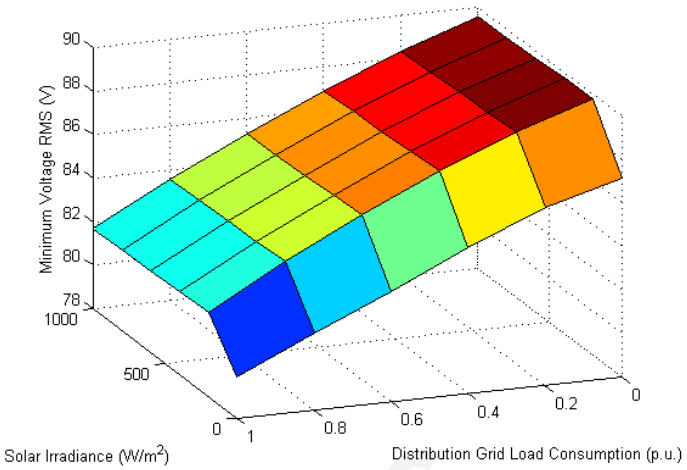

Figure 6.18b. Minimum Voltage value during the occurrence of the Fault on Feeder 3

Figure 6.18. Voltage Levels during the occurrence of the Fault on Feeder 3

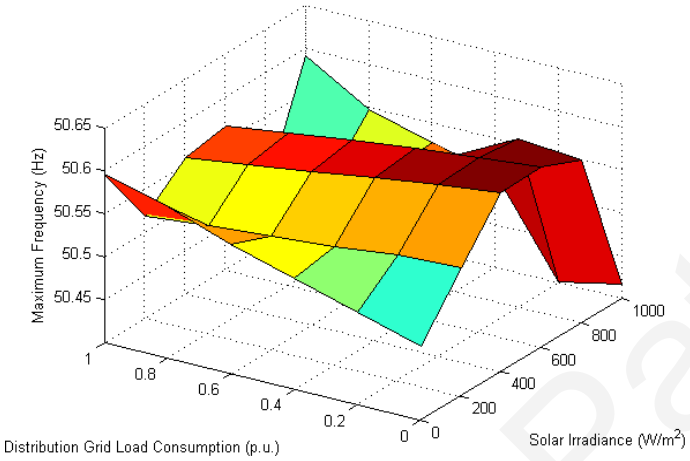

Figure 6.19a. Maximum Frequency value during the occurrence of the Fault on Feeder 3

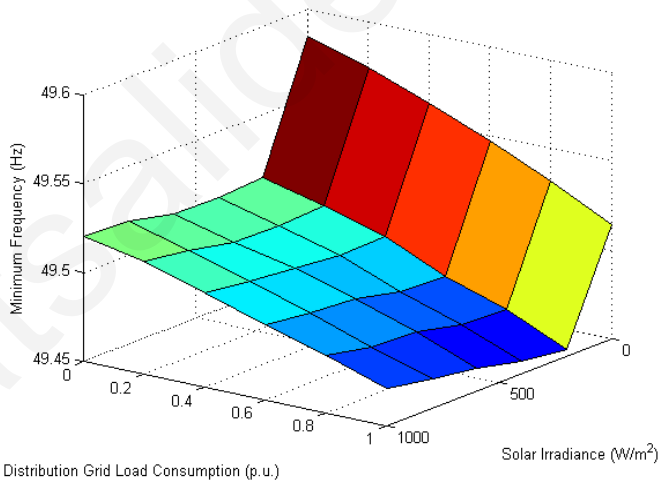

Figure 6.19b. Minimum Frequency value during the occurrence of the Fault on Feeder 3

Figure 6.19. Frequency Levels during the occurrence of the Fault on Feeder 3

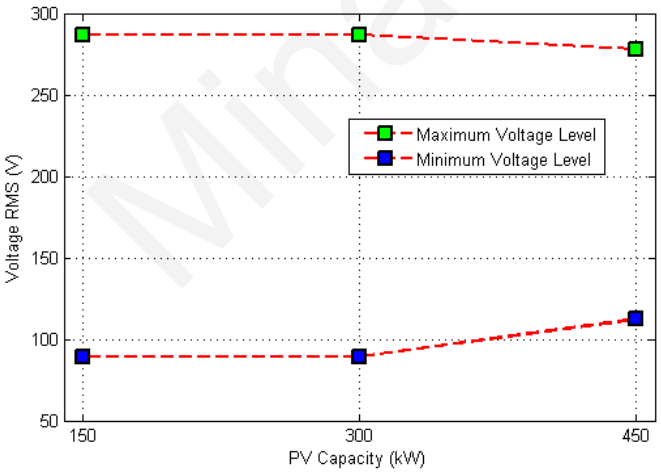

Figure 6.20a. Maximum and Minimum Voltage levels for different concentrations of PV during the occurrence of the Fault on Feeder 3

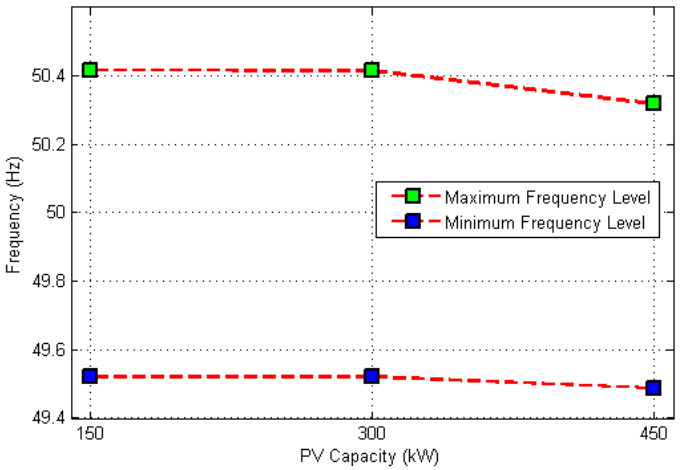

Figure 6.20b. Maximum and Minimum Frequency levels for different concentrations of PV during the occurrence of the Fault on Feeder 3

Figure 6.20. Voltage and Frequency Deviations levels for different concentrations of PV during the occurrence of the Fault on Feeder 3

On the contrary, the lower frequency level improved while the PV production is increasing as shown on Fig. 6.19b. The worst case in terms of voltage (no load and high solar irradiance conditions) is used to investigate different PV concentrations and results obtained are shown in Fig. 6.20. From Fig. 6.20a it can be observed that the voltage variations reduce as the PV capacity increases. On the other hand, the upper frequency value improves while increasing the PV capacity but the lower value gets even lower (Fig. 6.20b).

6.4 Conclusions

This chapter presents the Detailed Model Representation of the PV System as well as a voltage regulation algorithm able to maintain the voltage below the limits proposed by international standards. From the findings of the simulations it has been found that EN 61727 compatible inverters do not cause significant voltage distortion in distribution grids. However, it has been observed that overvoltage can occur during high PV production. In order to increase the installed PV capacity above the threshold imposed by the distribution grid dynamics and loading it is required to utilize the appropriate voltage regulation scheme. Apparently, the voltage regulation capability of the PV inverters will be enabled in future large PV installations to ensure the stability of power system operation and to maintain the good quality of supplied voltage.

On the other hand, it has been shown that the Detailed PV System Model can be used effectively in assessing the behaviour of the distribution grid during faults as modifications in the control circuit of the inverter to incorporate protection functionality is possible. Based on the observations made in this chapter it is evident that the use of PV system models operating at unity power factor will be limited. The most appropriate PV system model should not only consider the transient response of the inverter during changes of input power but also the transient response of the inverter during voltage variations. Any attempt for the development of simplified models should take into account the full functionality and capabilities of the inverters in order to be practical and useful in power studies of large power networks.

Chapter 7
Transient PV System Model (TPVSM)

7.1 Introduction

Photovoltaic (PV) technology is already one of the main alternative sources able to cover significant energy demand. The deployment of PV technology in local distribution grids is usually done in an uncontrolled way which may induce power quality issues as penetration increases. Simulation models and related studies are critical tools that reveal possible unwanted problems during the design stage prior to realization. The utilization of accurate simulation models is of great importance in an attempt to assess the real consequences of localized energy production from distributed energy sources and in particular PV. A generic PV system model for transient studies, the parameters of which can be tuned using transient data is proposed in this work. The model is tuned and validated using transient data obtained from a detailed PV system circuit topology developed in Matlab Simulink. The model is a three phase representation capable of simulating with sufficient accuracy normal/unbalanced operating conditions and voltage regulation. Harmonics are also incorporated into the model to reveal its capability for use in complete power quality studies. The main novelty of this work lies in the fact that the proposed model can be tuned in order to represent accurately the dynamic behaviour of PV systems for both balanced and unbalanced conditions. The

developed model is used along with the detailed PV system model to assess the voltage transient response of a distribution grid busbar. Finally, the transient behaviour of the distribution grid busbar having different grid impedance values is also evaluated utilizing the proposed model. The estimated and observed results are compared with the Theil Inequality coefficient depicting good agreement.

7.2 Transient PV System Model

7.2.1 Existing PV System Models - Comparison

The modelling capabilities of the PV system models presented in Chapter 2-Section 2.3 are summarized in Table 7.1. It is evident that a comparison is made feasible between the proposed PV system model and the existing models found in the literature via the main modelling capabilities shown in Table 7.1. An aspect derived from the literature search, which may not be so obvious, but it can be quite important for simulation studies, is the ability of a specific modelling capability to be tuneable. A considerable number of PV system models found in the literature cannot be tuned/adjusted in order to represent accurately the dynamics of each PV system found on the market constituting a great drawback for simulation studies. The adjustability of a specific modelling capability can help in representing accurately PV systems with different parameters.

Table 7.1. Capabilities of models found in the literature and comparison with the model proposed in this work

Model Name	Modelling Capabilities													
	Steady State Response		Transient Response		Balanced Conditions		Unbalanced Conditions		Filter Harmonics		Switching Harmonics		Control Harmonics	
		Tuneable		Tuneable		Tuneable		Tuneable		Tuneable		Tuneable		Tuneable
MPV1 (detailed PV System model)	√	Yes	√	Yes	√	Yes	√	No	√	Yes	√	Yes	√	No
MPV2	√	Yes	×	No	√	Yes	×	No	√	No	×	No	×	No
MPV3	√	Yes	×	No	√	Yes	×	No	×	No	×	No	×	No
MPV4	√	Yes	×	No	√	Yes	×	No	×	No	×	No	×	No
MPV5	√	Yes	×	No	√	Yes	×	No	×	No	×	No	×	No
MPV6	√	Yes	√	Yes	√	Yes	√	No	√	Yes	√	Yes	√	No
MPV7	√	Yes	√	Yes	√	Yes	×	No	×	No	×	No	×	No
MPV8	√	Yes	√	Yes	√	Yes	×	No	×	No	×	No	×	No
MPV9	√	Yes	×	No	√	Yes	×	No	×	No	×	No	×	No
MPV10	√	Yes	√	Yes	√	Yes	×	No	×	No	×	No	×	No
MPV11	√	Yes	×	No	√	Yes	×	No	×	No	√	Yes	×	No
MPV12	√	Yes	√	No	√	Yes	×	No	×	No	×	No	×	No
MPV13	√	Yes	√	Yes	√	Yes	×	No	×	No	×	No	×	No
MPV14	√	Yes	√	Yes	√	Yes	×	No	×	No	×	No	×	No
MPV15	√	Yes	√	Yes	√	Yes	×	No	×	No	×	No	×	No
MPV16	√	Yes	√	Yes	√	Yes	×	No	×	No	×	No	×	No
MPV17	√	Yes	×	No	√	Yes	×	No	×	No	√	Yes	×	No
MPV18	√	Yes	√	Yes	√	Yes	×	No	√	Yes	√	Yes	×	No
MPV19	√	Yes	√	Yes	√	Yes	×	No	×	No	×	No	×	No
MPV20	√	Yes	√	Yes	√	Yes	×	No	×	No	×	No	×	No
MPV21	√	Yes	√	Yes	√	Yes	×	No	√	Yes	√	Yes	×	No
Proposed Model	√	Yes	√	Yes	√	Yes	√	Yes	√	Yes	√	Yes	√	Yes

7.2.2 Methodology

A generic PV system model is developed based on the circuit topology and control scheme of a detailed three phase PV system. Analysis of the switching circuit representation in d-q synchronous frame is performed to extract the equations and transfer functions required for the formulation of the proposed model. The DC link of the PV inverter is considered to be constant and is omitted from the analysis as the dynamics of the DC link are much slower than the dynamics of the inverter. The transfer functions derived from the analysis for balanced and unbalanced conditions are used to define a parametrized/generic model of which the parameters are determined using the Nelder-Mead simplex estimation method. The specific parameter estimation method compares the performance of the proposed model with transient data from the detailed PV system model while varying its parameters in order to establish the correct transient behaviour. The new model is capable of simulating in an accurate and efficient way normal and unbalanced operating conditions. The novelty of this work lies in the fact that the transient behaviour of the PV inverter during unbalanced conditions can be tuned based on the inverter characteristics; an option that is not given by the other models found in literature. Finally, simplified modelling of harmonics is also undertaken in order to make the model more useful for power quality studies in an attempt to highlight the full capabilities of the proposed model.

7.2.3 Detailed PV System Model

A common detailed PV system model is formed by a PV array, an inverter and a power grid interface. The PV array is affected by the solar irradiance, the temperature and the specific characteristics of the chosen PV module technology. The PV array converts the solar irradiance into DC power which is then delivered to the distribution grid via the DC/AC inverter. A Maximum Power Point Tracking (MPPT) Controller consisting mainly of a DC/DC converter is used to extract the maximum available energy by adjusting the voltage at the output of the PV array. The PV array and DC/DC converter are connected to a DC link whose voltage is maintained constant by a DC/AC inverter circuit topology. In more detail, the DC/AC inverter is set to inject the power reaching at the DC link into the electricity grid and in that way the DC link remains constant. A filter is always placed at the output of the inverter to eliminate undesirable harmonic currents produced by the switching operation of the inverter. The modular circuit configuration of the PV system is shown in Fig. 7.1 [155].

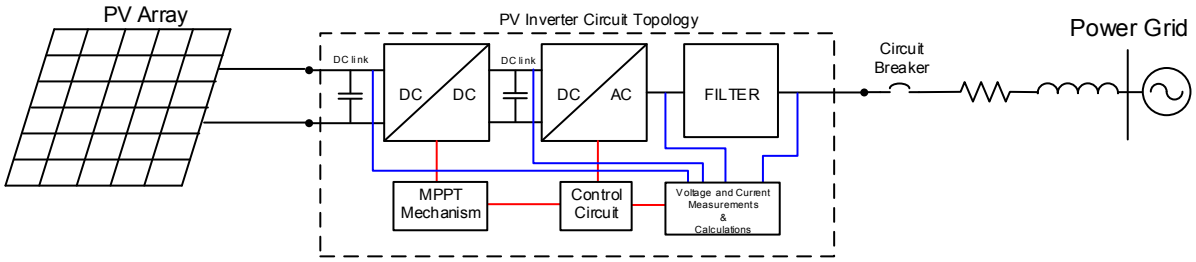

Figure 7.1. General schematic of a Detailed Photovoltaic System

Considering the large dc link capacitor, and the lower than fundamental frequency control bandwidth of the DC bus voltage [170], [171], the DC link can be assumed constant. The assumption of constant DC link is reasonable if it is also taken into account that the DC/AC inverter has a much faster current control loop response compared to the changes in solar irradiance and temperature [172].

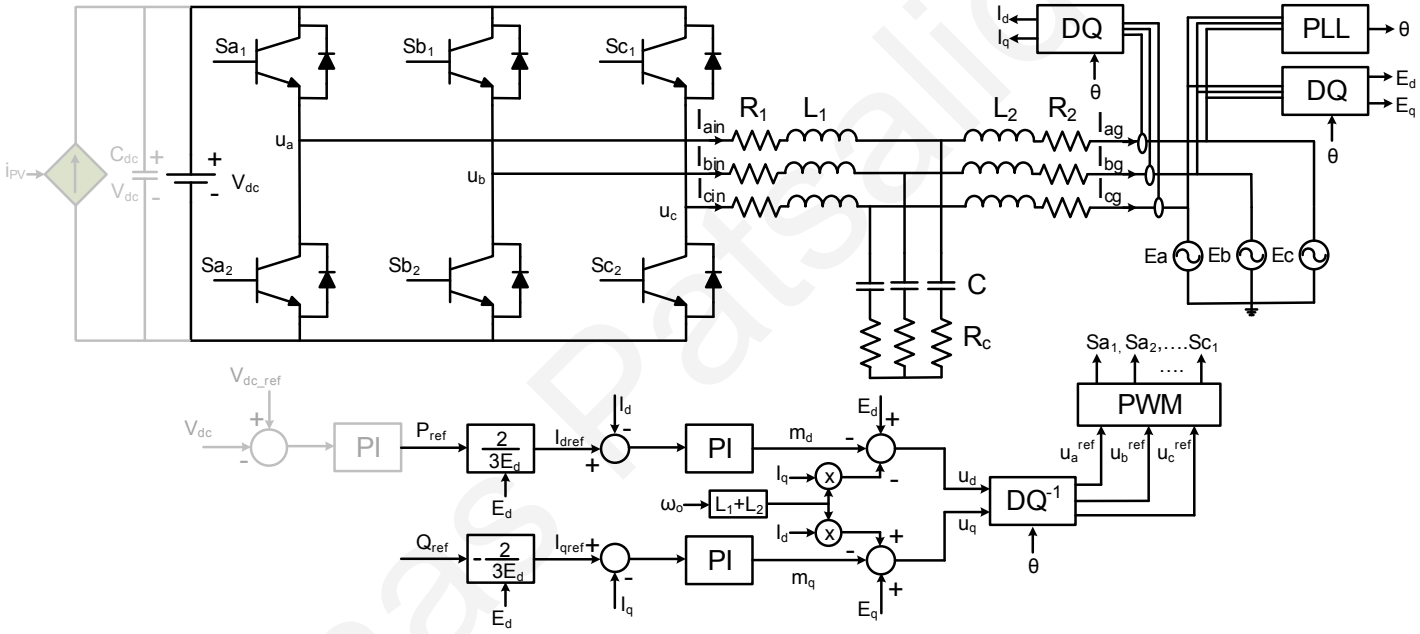

Figure 7.2. Detailed circuit topology of the adopted PV system [173]

The circuit topology of the detailed PV system model is shown in Fig. 7.2 [174], [175]. The current controller is based on the feedback linearization scheme [158] according to the following equations expressed in the synchronously rotating d-q reference frame:

$$u_d = E_d - \omega_o L I_q - m_d \tag{7.1}$$

$$u_q = E_q + \omega_o L I_d - m_q \tag{7.2}$$

and

$$m_d = (K_p + \frac{K_i}{s})(I_{dref} - I_d) \tag{7.3}$$

$$m_q = (K_p + \frac{K_i}{s})(I_{qref} - I_q) \tag{7.4}$$

where E_d and E_q are the d- and q- axis components of the grid-side voltage, u_d and u_q are those of the inverter voltage, ω_o is the system angular frequency, L the total inductance of the filter (L_1+L_2), I_{dref} and I_{qref} the corresponding reference currents, I_d and I_q the actual currents at the inverter output, and K_p and K_i are the proportional and integral gains of the PI controller. The parameters m_d and m_q are the control rules (PI controller) for the d- and q- axis respectively. Moreover, a Phase Lock Loop (PLL) is employed to track the phase angle of grid voltage for use in transforming AC quantities into the d-q synchronous reference frame and vise versa. The decoupling of active and reactive line current components, by projecting them onto a synchronously rotating d-q reference frame, allows the independent control of active and reactive power supply. The active (I_{dref}) and reactive (I_{qref}) current references are calculated by using the active (P_{ref}) and reactive (Q_{ref}) power references as follows:

$$I_{dref} = \frac{2}{3E_d} P_{ref} \quad \text{and} \quad I_{qref} = -\frac{2}{3E_d} Q_{ref} \tag{7.5}$$

The outer voltage loop is omitted due to the fact that it is assumed that the DC link is constant. Depending on the chosen voltage regulation method, the reactive power reference (Q_{ref}) is set or adjusted accordingly. The aforementioned detailed model was chosen to be used as it can represent the transient behaviour of the inverter during real time conditions that include variations in solar irradiance, temperature and supply voltage. The LCL filter is defined according to the guidelines given in [176].

7.2.4 Proposed PV System Model Description

The generalized schematic diagram of a PV system is shown in Fig. 7.3. The main components are the filter, the utility grid interface and the power stage interface. The power stage is managed by the control unit based on the grid synchronization and power measurement signals.

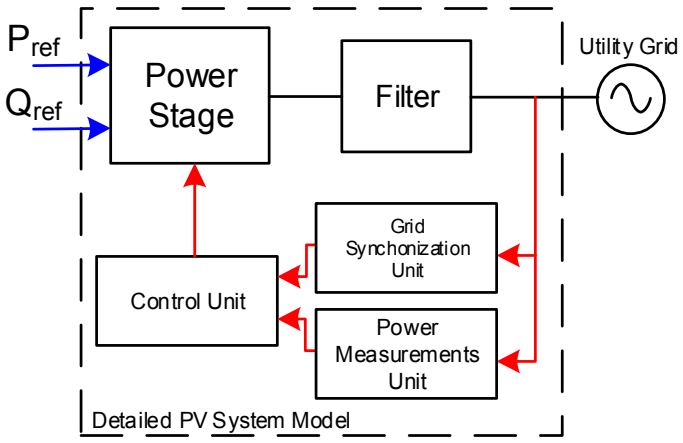

Figure 7.3. Generalized Schematic diagram of a PV System [173], [177]

The PV system model proposed in our work is depicted in detail in Fig. 7.4 and it is designed according to the generalized structure presented in Fig. 7.3. The PV system model is composed of a three-phase current source (power stage interface), an LCL filter and a control circuit defined in d-q synchronous frame (control unit) [173], [177].

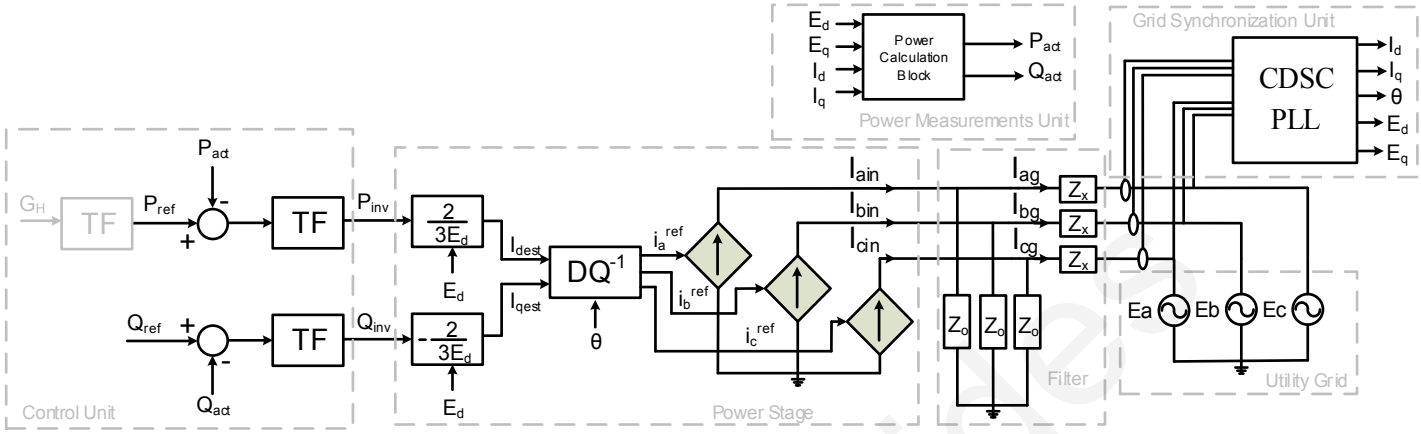

Figure 7.4. Detailed diagram of the proposed PV System Model

In the literature, a current source with a C/LC filter has been proposed in [175], [178] for simulation studies but the specific model does not have the ability to be tuned/adjusted in such a way to represent the transient behaviour of various inverters. The control circuit of the proposed model includes a specially formulated transfer function (TF) which can be tuned via an estimation method by only using transient data of current obtained from the output of a simulation PV system model or a real PV system. The estimation method varies the parameters of the TF, until the model current output matches the provided transient data. The LCL filter parameters can also be estimated via transfer function identification while using harmonic data of voltage and current phasors captured at the output of the inverter under test. The PLL dynamics are decoupled from the proposed model dynamics by utilizing a PLL with fast response. As the DC link is assumed constant [179], the dynamics of the DC/DC converter, the MPPT and the PV array are omitted from the analysis but it is possible to include their effect into the model by adding a transfer function that will relate the solar irradiance G_H with the active power reference (P_{ref}) signal of the control unit [180]–[185]. By replacing the DC link with a DC source, the nominal power of the model becomes unlimited which is a great advantage when needing to use the model to represent various PV systems. Finally, it is important to mention that the analysis presented in this work can be applied for proportional-resonant (PR) current controllers as well [186], [187]. The abstract representation of the proposed model including the input/output signals and the parameters required for balanced/unbalanced and harmonic modelling is shown in Fig. 7.5. When using the developed model, no prior knowledge is prerequisite about the modelling techniques applied for the formulation of the model, but just only the parameters characterizing a

specific PV system (shown in Fig. 7.5). The main advantage of the proposed model over the detailed PV system model is that it can be tuned and represent accurately the transient behaviour of the PV system under unbalanced conditions (something not possible when using the detailed PV system model).

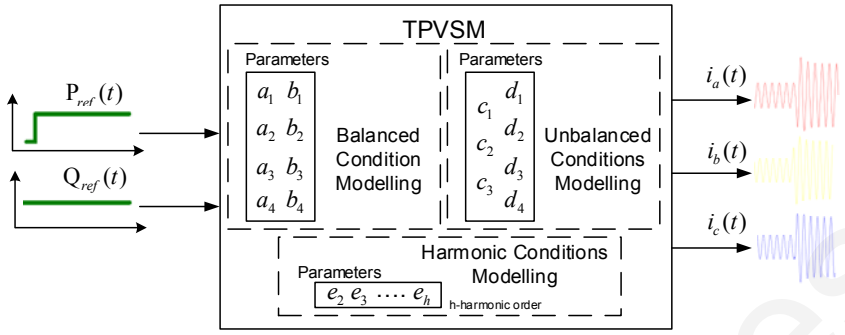

Figure 7.5. Proposed Transient Photovoltaic System Model (TPVSM)

7.2.4.1 LCL filter Parameters Estimation

Defining the parameters of the LCL filter can be done in various ways. The parameters are usually not available by the manufacturer and therefore accessing the internal circuit of the inverter can reveal the type of the filter and the values of filter elements. Another method for estimating the filter parameters can be the identification of the filter transfer function using harmonic impedance data. The harmonic impedance data can be obtained if the inverter is set at zero state in reference to the well-known space-vector pulse switching modulation and by performing simultaneous measurements of voltage and current phasors at different harmonic frequencies. The filter topology at zero state is shown in Fig. 7.6.

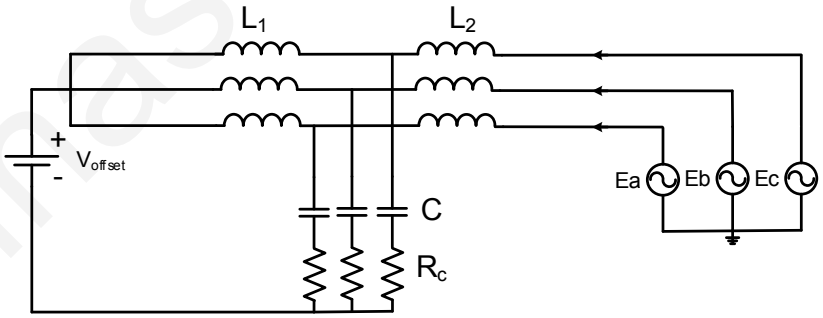

Figure 7.6. Filter topology at zero state [188]

By shorting the left side of inductor L_1 a connection is created between the L_1 and the common point of capacitor bank having a DC offset difference (assuming that the system is balanced). According to the superposition theorem [189], if analysis is performed on harmonics, the two points are electrically connected with a short circuit for harmonic frequencies. In this work, voltage and current phasors were employed from the first to the eleventh harmonic frequency and by dividing the voltage phasors with the current phasors it becomes possible to calculate the actual harmonic impedance values.

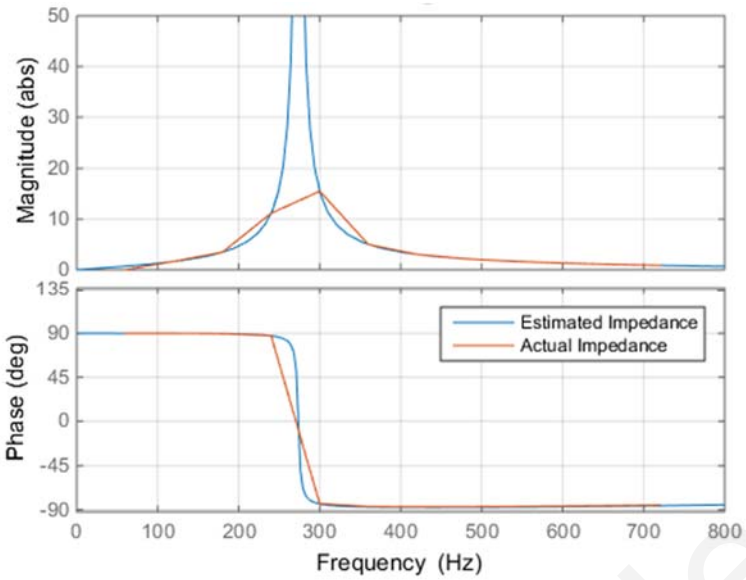

Figure 7.7. Bode Diagram of Filter Impedance

The estimated transfer function of the harmonic impedance is obtained by applying the estimation algorithm found in [190] and is then compared to the actual transfer function of an LCL filter. The actual harmonic impedance and the estimated transfer function response are both depicted in Fig. 7.7. The transfer function of the filter impedance is given by equation (7.6) and the estimation method provides a transfer function of the same form given by equation (7.7) [191].

$$Z_f^{act}(s) = \frac{s^3 L_1 L_2 C + s^2 (L_1 + L_2) \mathrm{CR}_c + s(L_1 + L_2)}{s^2 L_1 \mathrm{C} + s\,\mathrm{CR}_c + 1} \tag{7.6}$$

$$Z_f^{est}(s) = \frac{A_1 s^3 + A_2 s^2 + A_3 s}{B_1 s^2 + B_2 s + 1} \tag{7.7}$$

The mathematical formula (7.6) has four unknowns which can be easily calculated from the system of five equations obtained via equating equation (7.6) with (7.7).

$$\begin{cases} A_1 = L_1 L_2 C \\ A_2 = (L_1 + L_2)\mathrm{CR}_c \\ A_3 = L_1 + L_2 \\ B_1 = L_1 \mathrm{C} \\ B_2 = \mathrm{CR}_c \end{cases} \tag{7.8}$$

The estimated and actual values of the LCL filter impedance are shown in Table 7.2.

Table 7.2. Filter Parameters

LCL Filter Parameter	Detailed PV System Model Values	Estimated Values	Error
L_1 (H)	0.0017	0.0017	1.02%
L_2 (H)	9.6243e-05	9.287e-05	3.50%
R_C (Ohms)	0.0449	0.0453	0.89%
C (F)	2.0057e-04	1.9893e-04	0.81%

By applying the Thevenin to Norton transformation on the LCL circuit topology it is possible to derive the impedances Z_o and Z_x by using the following equations.

$$Z_o(s) = \frac{s^2 L_1 \mathrm{CR}_c + sL_1}{s^2 L_1 \mathrm{C} + s\,\mathrm{CR}_c + 1} \tag{7.9}$$

$$Z_x(s) = sL_2 \tag{7.10}$$

7.2.4.2 Transfer Function of the proposed PV system model for balanced conditions

The main core of the model formed to represent accurately the dynamic behaviour of PV systems is the transfer function shown in Fig. 7.4 for d and q synchronous reference frame respectively. In order to formulate the required transfer function it is first assumed that the filter at the output of the inverter is an L filter and not an LCL. This is reasonable due to the fact that the dynamic behaviour of an LCL filter is similar to the L filter at low frequencies which coincide with the current controller bandwidth [192]. It must also be mentioned that in order to design a PI current controller for an inverter it is recommended to neglect the filter capacitor using the L approximation mentioned above [193]. This approximation gives reasonable results and at the same time makes the analysis and derivation of the required transfer function simpler. The ac dynamics of the three phase inverter omitting the switching effects is derived from equation (7.11):

$$L_t \frac{d\vec{i}}{dt} + R\vec{i} = \vec{v} - \vec{E} \tag{7.11}$$

where L_t is the total inductance of the output filter, R_t is the total resistance of the output filter, $\vec{i}$ the instantaneous output current, $\vec{v}$ the instantaneous voltage at the inverter side and $\vec{E}$ is the instantaneous voltage of the grid side. Transforming equation (7.11) into d-q synchronous frame yields:

$$L_t \frac{di^c}{dt} + Ri^c + j\omega_o L i^c = v^c - E^c \tag{7.12}$$

where $i^c = I_d + jI_q$ is the d-q frame output current, $E^c = E_d + jE_q$ the d-q frame voltage of the grid side, $v^c = V_d + jV_q$ the d-q frame voltage at the inverter side and ω_o is the system angular frequency. A PI current controller with grid voltage feedforward and d-q cross coupling cancellation is utilized for the inverter control task [194]:

$$v^c_{ref} = G_{PI}(\mathrm{i}^c_{ref} - i^c) + j\omega_o L i^c + aE^c = (k_p + \frac{k_i}{s})(\mathrm{i}^c_{ref} - i^c) + j\omega_o L i^c + aE^c \tag{7.13}$$

where v^c_{ref} is the control rule for the d-q synchronous frame, $i^c_{ref} = I_{dref} + jI_{qref}$ is the d-q frame reference output current and a the feedforward cancellation factor which can either be a transfer function or a constant less than or equal to unity. For proper operation of the current controller the parameter a is considered to be unity which is valid for the DC variations

occurring in d-q frame. As discussed in the following subsection for unbalanced condition modelling, this is not valid if harmonics appear at the controller. Based on the above, the current controller diagram for d-axis is shown in Fig. 7.8 [195]. The same applies for the q-axis.

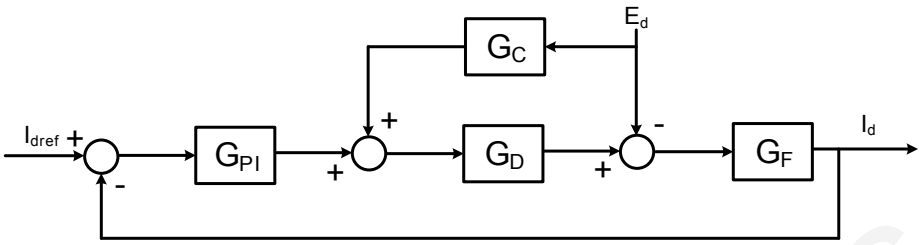

Figure 7.8. Current controller in d-q synchronous frame for d axis

From the diagram of the current controller, the transfer function relating the output current in the d-q frame with the reference current and the feedforward voltage is described by equation (7.14) [191].

$$i^c = \underbrace{\frac{G_{PI}G_DG_F}{G_{PI}G_DG_F+1}}_{g(s)} \mathrm{i}^c_{ref} - \underbrace{\frac{G_F(-G_DG_C+1)}{G_{PI}G_DG_F+1}}_{y(s)} E^c \tag{7.14}$$

where

$$G_{PI} = k_p + \frac{k_i}{s} \qquad G_F = \frac{1}{L_t s + R_t} \qquad G_D = e^{-sT_d} = \frac{1}{1+T_d s+0.5T_d{}^2 s^2} \qquad G_c = e^{sT_c} = 1+T_c s+0.5T_c{}^2 s^2$$

The inverter control delay G_D [195] is approximated by a second order Pade formula [196], [197]. G_D is the output filter transfer function and G_C the compensation/feedforward filter transfer function [194], [195]. As mentioned before, it is assumed that G_DG_C is exactly equal to unity (equivalent to a feedforward cancellation factor equal to unity) which is indeed valid for DC variations [194] and therefore equation (7.14) reduces to (7.15):

$$i^c = \frac{G_{PI}G_DG_F}{G_{PI}G_DG_F+1}\mathrm{i}^c_{ref} = \frac{k_p s+k_i}{s^3\frac{T_d^2}{2}L_t + s^2(L_tT_d+\frac{T_d^2}{2}R_t)+s(T_dR_t+k_p+L_t)+k_i+R_t}\mathrm{i}^c_{ref} \tag{7.15}$$

By considering also that the compensation/feedforward transfer function and the Pade formula transformations, it is possible to define a relationship between the actual grid voltage and the voltage passed into the controller given by (7.16):

$$v^c_{ref} = \frac{v^c}{G_D} = (1+T_d s+0.5T_d{}^2 s^2)\,\mathrm{v}^c \Rightarrow \mathrm{v}^c = (1-T_d s+0.5T_d{}^2 s^2)v^c_{ref} \tag{7.16}$$

Combining equation (7.15) with (7.16) it becomes possible to define the relationship between the reference active (P_{ref})/reactive (Q_{ref}) power with the actual inverter active (P_{inv}) /reactive (Q_{inv}) power:

$$P_{inv}+Q_{inv}j=v^c\cdot i^c=\underbrace{\frac{(k_ps+k_i)(1-T_ds+0.5T_d{}^2s^2)}{s^4\frac{T_d^2}{2}L_t+s^3(L_tT_d+\frac{T_d^2}{2}R_t)+s^2(T_dR_t+L_t)+(k_p+R_t)s+k_i}}_{TF_G}\cdot v_{ref}^c\cdot \mathrm{i}_{ref}^c=TF_G\cdot(P_{ref}+Q_{ref}j) \tag{7.17}$$

which yields:

$$\frac{P_{inv}}{P_{ref}}=TF_G \quad \text{and} \quad \frac{Q_{inv}}{Q_{ref}}=TF_G \tag{7.18}$$

The target transfer function (TF) required for the power control circuit of the proposed PV system model can be obtained by analysing the control diagram of Fig. 7.9. It is assumed that the power losses at the output filter are negligible as modern inverters are designed to have less than 3% power losses in total at their output in comparison to the input power.

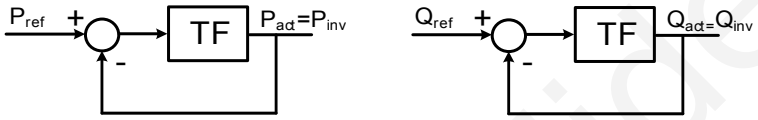

Figure 7.9. Power control circuit of the proposed PV system model

Finally, the target transfer function is given by (7.19):

$$TF=\frac{\frac{P_{inv}}{P_{ref}}}{1-\frac{P_{inv}}{P_{ref}}}=\frac{\frac{Q_{inv}}{Q_{ref}}}{1-\frac{Q_{inv}}{Q_{ref}}}=\frac{TF_G}{1-TF_G} \tag{7.19}$$

After substituting (7.17) into (7.19), a transfer function is obtained which has the same order as the transfer function in (7.17):

$$TF=\frac{s^3\frac{T_d^2}{2}k_p+s^2(\frac{T_d^2}{2}k_i-k_pT_d)+s(k_p-k_iT_d)+k_i}{s^4\frac{T_d^2}{2}L_t+s^3(L_tT_d+\frac{T_d^2}{2}R_t-\frac{T_d^2}{2}k_p)+s^2(T_dR_t+L_t-\frac{T_d^2}{2}k_i+k_pT_d)+s(R_t+k_iT_d)}=\frac{a_1s^3+a_2s^2+a_3s+a_4}{s(\mathrm{b}_1s^3+b_2s^2+b_3s+b_4)} \tag{7.20}$$

7.2.4.3 Phase Lock Loop (PLL) requirements

The phase lock loop (PLL) required for the realization of the model is an important element which must have quite fast response to minimize its transient effect on the proposed model. Also, it is required to have the capability of estimating d-q components for balanced and unbalanced conditions. For this purpose, three types of PLLs and a Discrete Fourier transform (DFT) sequence analyser [198], [199] are evaluated in order to identify which one has the most accurate and fast response. The three PLLs under test are: ddsrfPLL [200], [201], CDSC-PLL [202] and DSC-PLL [203]. The dynamic response of the d-q synchronization methods under consideration for a positive sequence voltage variation is shown in Fig. 7.10 (the same exact dynamic response is observed for negative positive

sequence voltage variations). From Fig. 7.10, it is evident that the CDSC-PLL is the most appropriate as it fulfils the application requirements.

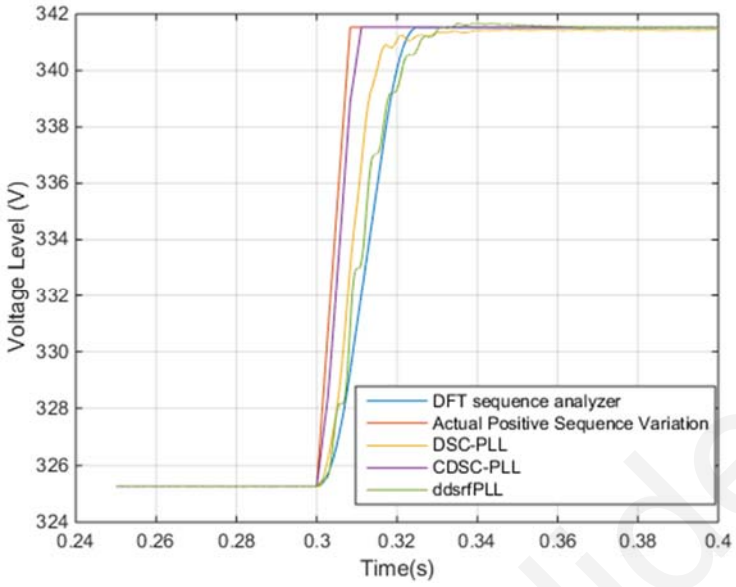

Figure 7.10. Dynamic response of d-q synchronization methods under consideration

7.2.4.4 Transfer Function of the proposed PV system model for unbalanced conditions

In order to model the transient behaviour of the inverter control circuit under unbalanced conditions an important observation must be taken into account. In d-q coordinates, the unbalancing in grid voltage is transformed into second order harmonic [201], [204] via the d-q transformation and therefore a second order harmonic is superimposed on the DC quantities if unbalanced voltage conditions occur. In [205], a current controller for unbalanced conditions is developed as well and in such a case the analysis presented in the previous subsection (subsection 7.2.4.2) should be repeated for obtaining the characteristic transfer function for unbalanced behaviour modelling of the inverter. For this case, as the transient behaviour of the inverter for balanced conditions has already been defined in subsection 7.2.4.2, superposition circuit analysis will be applied to study the control circuit only in the presence of the second order harmonic. Consequently, the current controller under unbalanced conditions is shown in Fig. 7.11. As can be seen from the circuit diagram, the reference currents are zero because the inverter is not designed to handle/react to unbalanced conditions. The part of the control diagram enclosed in the dashed rectangle reacts differently in the presence of the second order harmonic. More specifically, the product $G_D G_C$ is not unity for non-DC quantities if a slight difference exists between G_D and G_C or in the absence of the compensation transfer function G_C.

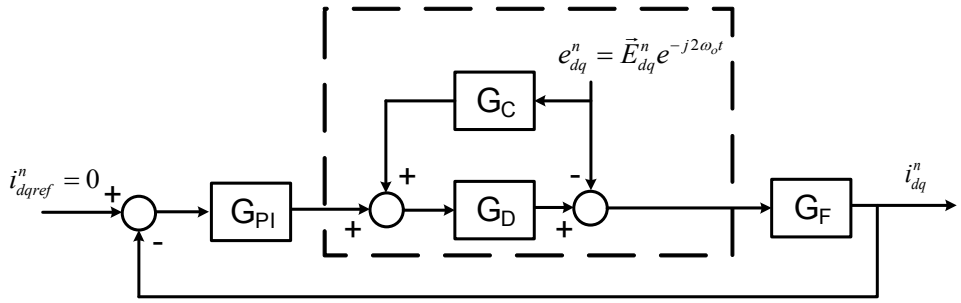

Figure 7.11. DQ synchronous frame current controller under unbalanced conditions

The product $G_D G_C$ is given by equation (7.21) based on which a sensitivity analysis is performed by increasing the difference between T_c and T_d .

$$G_D G_C = \frac{1 + T_c s + 0.5 T_c^2 s^2}{1 + T_d s + 0.5 T_d^2 s^2} \tag{7.21}$$

The frequency response of $G_D G_C$ is presented in Fig. 7.12 and it is evident that the presence of the second order harmonic enables the factor $y(\mathrm{s})$ of equation (7.14).

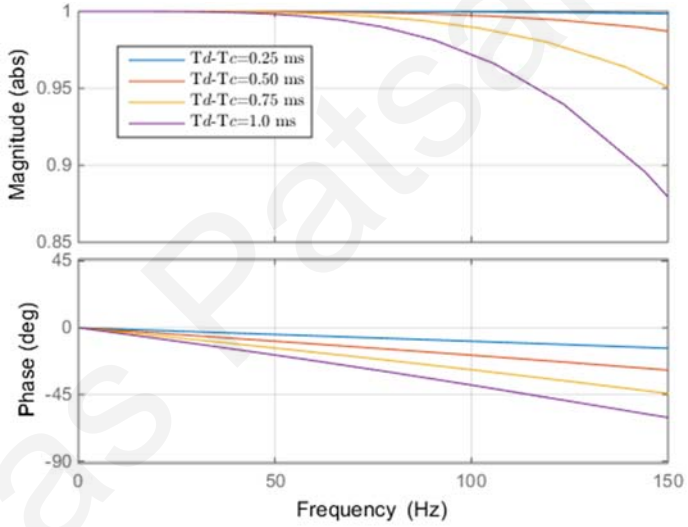

Figure 7.12. $G_D G_C$ Bode diagram

As a consequence, the transfer function of the negative sequence current is represented in the d-q frame with equation (7.22):

$$i^n_{dq} = \underbrace{\frac{G_F(-G_D G_C + 1)}{G_{PI} G_D G_F + 1}}_{y(s)} e^n_{dq} \tag{7.22}$$

where

$$i^n_{dq} = i^n_d + j i^n_q \quad \text{and} \quad e^n_{dq} = (E^n_d + jE^n_q) e^{-j2(\omega_o t + \varphi)} = (E^n_d + jE^n_q)(\cos(-2(\underbrace{\omega_o t + \varphi}_{\theta})) + j\sin(-2(\underbrace{\omega_o t + \varphi}_{\theta}))) \tag{7.23}$$

The parameter e^n_{dq} is the negative sequence grid voltage expressed in the d-q frame, θ is the angular frequency and E^n_d, E^n_q are the negative sequence components provided by the adopted PLL. Substituting (7.23) into (7.22) results in:

$$i_d^n = \frac{G_F(-G_D G_C + 1)}{G_{PI} G_D G_F + 1}(E_d^n \cos(2\theta) + E_q^n \sin(2\theta)) \tag{7.24}$$

$$i_q^n = \frac{G_F(-G_D G_C + 1)}{G_{PI} G_D G_F + 1}(E_d^n \cos(2\theta) - E_q^n \sin(2\theta)) \tag{7.25}$$

For simplification purposes, $G_D G_C$ and G_D are both approximated by the first order Pade formula as:

$$G_D G_C = \frac{1 + T_c s}{1 + T_d s} \quad \text{and} \quad G_C = \frac{1}{1 + T_d s} \tag{7.26}$$

Additionally it is assumed that the PI controller compensates exactly the effect of the output filter [195] yielding:

$$G_{PI} G_F = \frac{M}{s} \tag{7.27}$$

where M is a constant. Equations (7.26) and (7.27) are then substituted into (7.24) and (7.25), giving:

$$i_d^n = \frac{s^2(T_d - T_c)}{s^3 L_t M + s^2(R_t T_d + L) + s(M L_t + R_t) + R_t M}(E_d^n \cos(2\theta) + E_q^n \sin(2\theta)) = \frac{c_1 s^2 + c_2 s + c_3}{d_1 s^3 + d_2 s^2 + d_3 s + d_4}(E_d^n \cos(2\theta) + E_q^n \sin(2\theta)) \tag{7.28}$$

$$i_q^n = \frac{s^2(T_d - T_c)}{s^3 L_t M + s^2(R_t T_d + L) + s(M L_t + R_t) + R_t M}(E_d^n \cos(2\theta) - E_q^n \sin(2\theta)) = \frac{c_1 s^2 + c_2 s + c_3}{d_1 s^3 + d_2 s^2 + d_3 s + d_4}(E_d^n \cos(2\theta) - E_q^n \sin(2\theta)) \tag{7.29}$$

Finally, the complete circuit diagram of the proposed PV system model for balanced/unbalanced conditions is shown in Fig. 7.13.

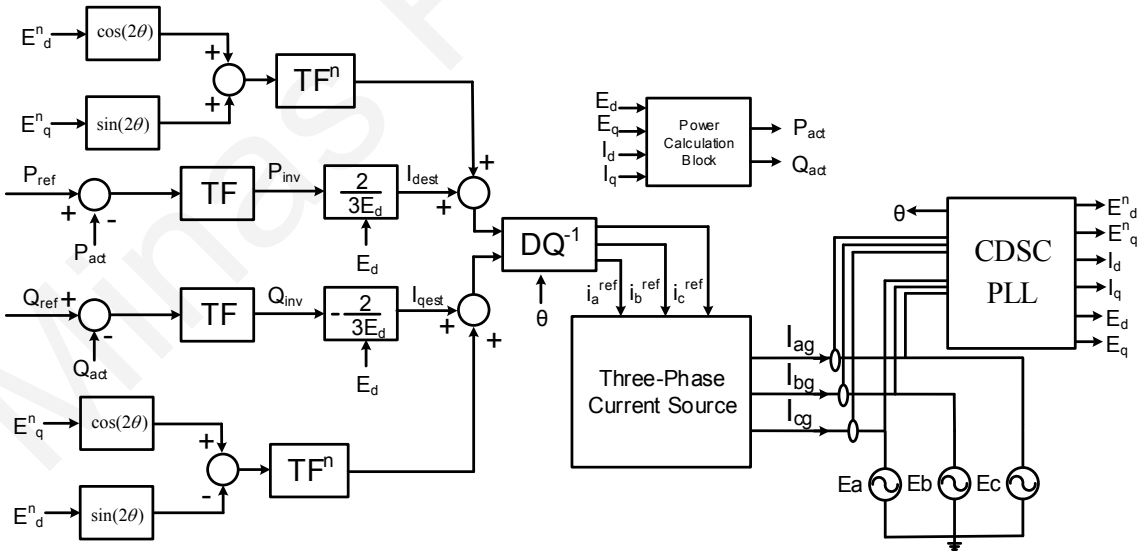

Figure 7.13. Proposed PV System Model for balanced/unbalanced conditions

7.2.4.5 Parameter Estimation via the Nelder-Mead algorithm

The generalized transfer functions obtained for balanced and unbalanced conditions representing the dynamics of the PV system can be further used along with current transient

data to form a parameter estimation problem. More specifically the transfer function for balanced conditions described by (20) can be represented by a PI controller in series with a weighted sum of poles lying in the left-half plane for the d and q axes respectively. This is valid for stable systems of which their poles always lie in the left-half plane. It is assumed that the oscillatory part (imaginary part) of complex poles is insignificant or less probable to occur (due to design constrains of PV system control) and therefore is omitted from the analysis. In general, oscillatory behaviour is not considered in this work in order to reduce the parameter estimation problem and for this reason equations (7.30) and (7.31) are proposed. If equation (7.30) does not perform as expected then equation (7.31) may be used (which has a double pole) or a parameter transfer function containing complex poles (equivalent to mathematical formula (7.18)). Equations (7.30) and (7.31) are obtained using the partial fraction decomposition/expansion method.

$$TF = (k_p^e + \frac{k_i^e}{s})(\frac{r_1^p}{s + p_1^p} + \frac{r_2^p}{s + p_2^p} + \frac{r_2^p}{s + p_2^p}) \tag{7.30}$$

$$TF = (k_p^e + \frac{k_i^e}{s})(\frac{r_1^p}{s + p_1^p} + \frac{r_2^p}{(s + p_2^p)^2}) \tag{7.31}$$

where all the unknowns in equations (7.30) - (7.31) are parameters to be estimated. Similarly, the parameter function for unbalanced conditions can be represented as:

$$TF^n = (\frac{r_1^n}{s + p_1^n} + \frac{r_2^n}{s + p_2^n} + \frac{r_2^n}{s + p_2^n})(E_d^n \cos(2\theta) - E_q^n \sin(2\theta)) \tag{7.32}$$

The parameter estimation is achieved with the Nelder-Mead simplex (NMS) algorithm. The target of the algorithm is to minimize a cost function (the sum of squared errors between estimated and simulated current RMS transient data) without employing a gradient calculation method, classifying the NMS technique in the category of direct search methods. The NMS simplex is a geometric shape of nonzero volume which is formed by n + 1 vertices. At first, the algorithm is started with an initial guess provided by the user and therefore the initial conditions play an important role in the duration and convergence of the estimation process. At every new iteration, NMS generates a new vertex based on the objective/cost function performance of simplex vertices. The algorithm then chooses to replace one of the existing vertices with the new vertex and so the technique progresses. As a consequence, the objective function value at each vertex is known at each iteration and the worst vertex with the highest value is replaced by the new vertex. The NMS simplex is rescaled by using four basic procedures: reflection, expansion, contraction, and shrinkage depicted in Fig 7.14. More information can be found in [206]–[208] .

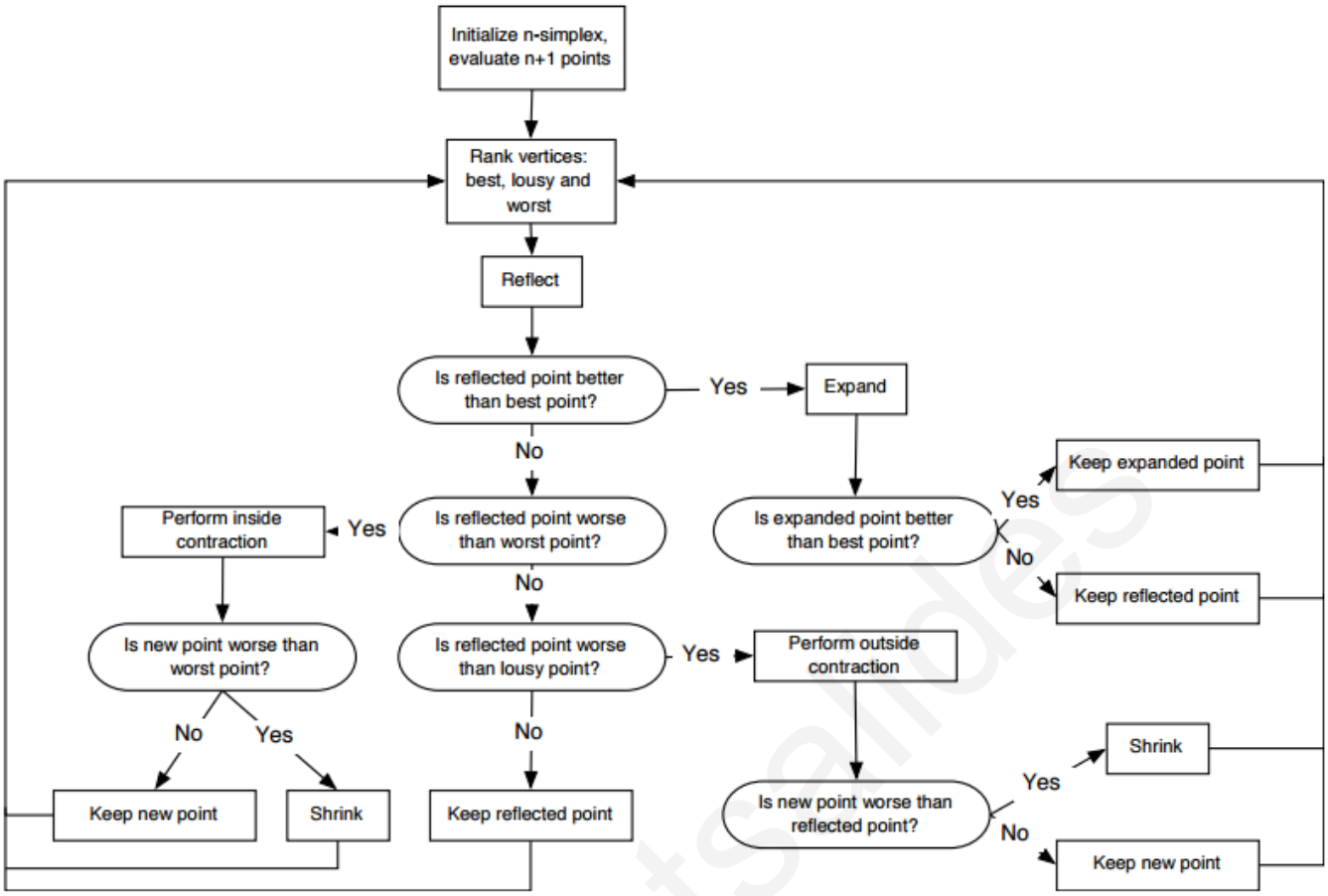

Figure 7.14. Flowchart of Nelder-Mead simplex algorithm

In brief, the transfer functions of balanced conditions for both d-q axes are estimated by applying a step change in active power input. The NMS tracks the transient response error between the detailed PV system model and the proposed model and adjusts the parameters of the transfer functions until the error is minimized. Comparison of current RMS transient data (of only phase L1 as the system is balanced and as the parameter transfer functions are equal for both d and q axes a slight difference between d and q axes parameter transfer functions may arise if the analysis of [194] is adopted) acquired during the active power step change are adequate for estimating the values of the parameter transfer functions. After that, a step change in reactive power input is applied to fine tune the parameter transfer function of q axis. Finally, a change in negative sequence components of the grid voltage is used to define the parameter transfer functions for unbalanced conditions. In this case, current transient data from two out of three phases are necessary for estimating and fine-tuning the d-q axes parameter transfer functions for the unbalanced conditions. Despite the fact that the NMS is an unconstrained estimation algorithm, its application in solving the aforementioned problem forces NMS to progress in the left-half plane (if initial conditions are set correctly) because the cost/objective function gets high values in the unstable region. The unstable

region consists of a barrier that limits correctly the values domain/range and desirably helps the NMS algorithm to converge faster.

7.2.4.6 Modelling of Current Harmonics

Current harmonics have their origin in two processes. The first one is the PWM switching and the second one is the influence of grid voltage harmonics on the inverter control circuit and output filter. As regards the first process, the variety of PWM switching methods can produce a current frequency spectrum which may differ depending on the type of the PWM algorithm. On the other hand, grid voltage harmonics pass through the control circuit and appear on the output current. More specifically, the second term of equation (7.14) is equivalent to an admittance component (as the case of unbalanced conditions) which transforms the voltage harmonics into current harmonics depending on the design parameters of the inverter. Based on this, it is possible to model the transient behaviour of selected harmonics. Alternatively, the steady-state behaviour of all the harmonics can be represented with an impedance element. In addition, it must be mentioned that the current harmonics injected into the grid are affected by the output filter as the impedance of the filter can interact with voltage harmonics. For this reason, the filter impedance of the proposed model (seen by the grid) is designed to be almost identical with the filter impedance of the detailed PV system model by utilizing the findings of subsection 7.2.4.1 and Norton's theorem [83], [209]. The model filter impedance seen by the grid in comparison to the actual filter impedance of the detailed PV system model is shown in Fig. 7.15.

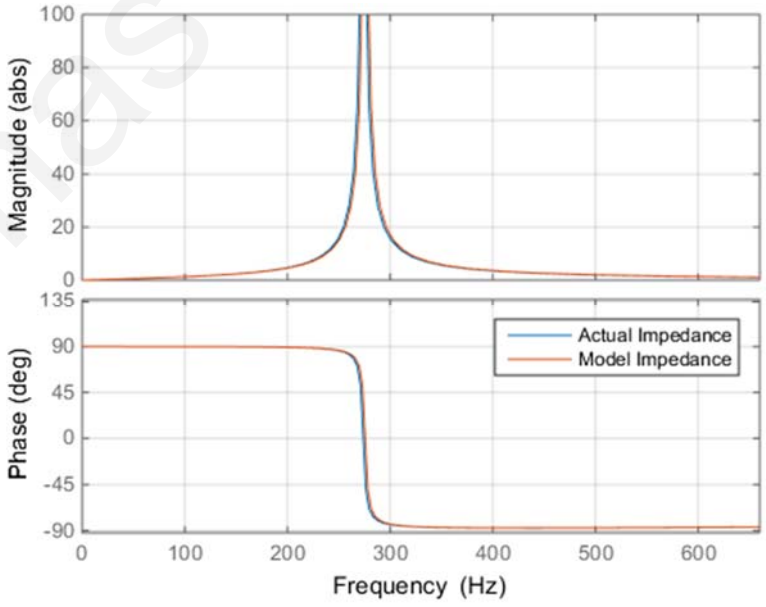

Figure 7.15. Comparison of model filter impedance with the actual filter impedance

Despite the fact that it is assumed that the grid voltage harmonics are low in this work and do not interact with inverter control or the output filter it is evident that the proposed model

can effectively be used in harmonic studies as both the model filter impedance and the control admittance (referring to equation (7.14)) seen by the grid are exactly the same as the detailed PV system model. Moreover, the switching harmonics can be incorporated into the model by adopting the procedure mentioned in the following paragraph. A more advanced procedure can be applied if it is required to achieve higher accuracy on modelled harmonics.

As stated in [210], [211], the current harmonics can be derived from an analytical mathematical expression if the PWM switching methodology is known and can have a unique value. As the PWM scheme is not always known it is chosen to represent the current harmonics by their mean value which is quite reasonable if the above statement is considered and by noting also the results of Fig. 7.16. The current harmonics are superimposed on the current source and they are transformed from the inverter side current to the grid side current by the following formula:

$$I_{inv}(h) = I_{out}(h)(1 + h^2\omega^2 CL_2) \tag{7.33}$$

where $I_{inv}(h)$ and $I_{out}(h)$ are the inverter side and grid side current at harmonic order h respectively.

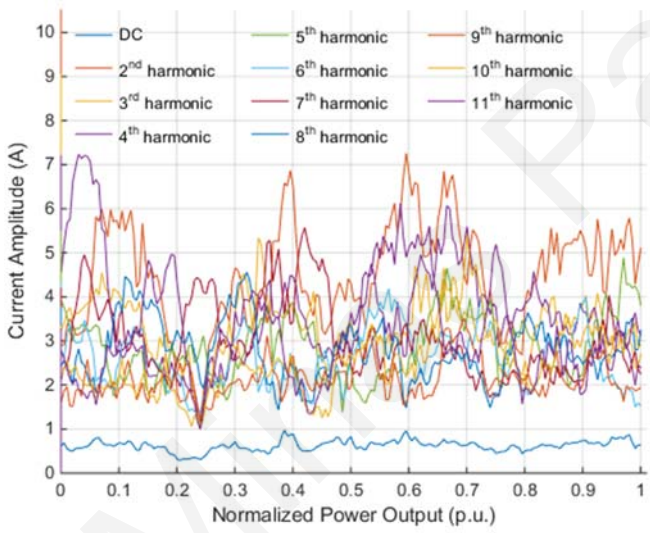

Figure 7.16a. Current Harmonics vs Normalized Power Output

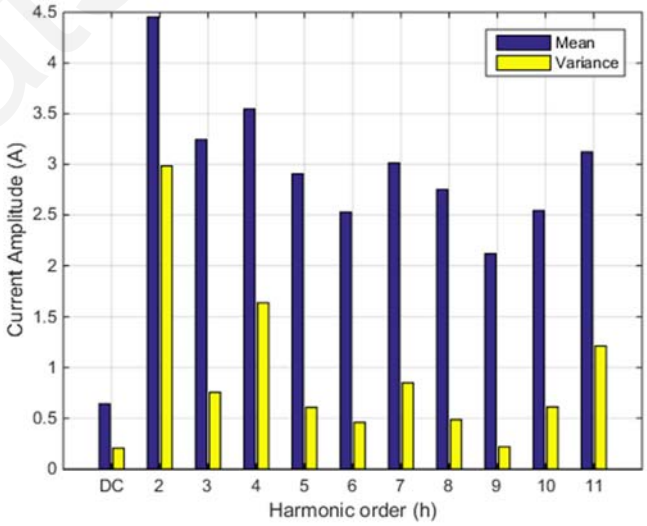

Figure 7.16b. Mean and Variance of inverter grid side current harmonics

Figure 7.16. Statistical analysis of inverter output current harmonics

7.2.4.7 Distribution Grid Topology

The system topology of the distribution grid used in the simulation is shown in Fig. 7.17a. In order to perform reliable studies about the power quality behaviour of a distribution grid in the presence of distributed generation, the electrical dynamics of the distribution grid is required to be known. For this reason, the distribution grid is modelled as a low voltage Thevenin Equivalent Circuit (TEC) according to [212]. The TEC shown in Fig. 7.17b replaces the high voltage network and the transformer.

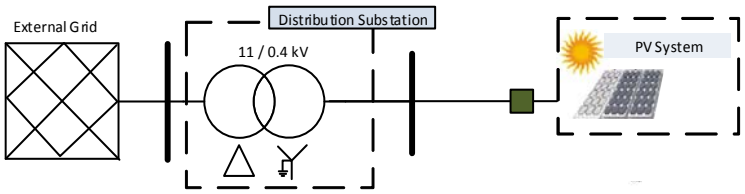

Figure 7.17a. Distribution Grid Topology

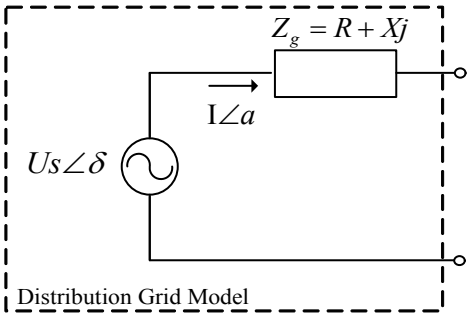

Figure 7.17b. Thevenin Equivalent Circuit

Figure 7.17. Equivalent Distribution grid model

7.3 Results

7.3.1 Results for balanced conditions

After applying the modelling procedure for balanced conditions found in the previous section it is possible to define accurately the transient behaviour of PV systems. More specifically, a step change of 0.3 p.u. in the active power input imposed a change in the output current which has a unique pattern depending on the design parameters and the dynamics of the detailed/actual PV system. The reactive power input is kept at a zero value. The transient response of both the detailed and the proposed PV system model during the step change in active power input is shown in Fig. 7.18a.

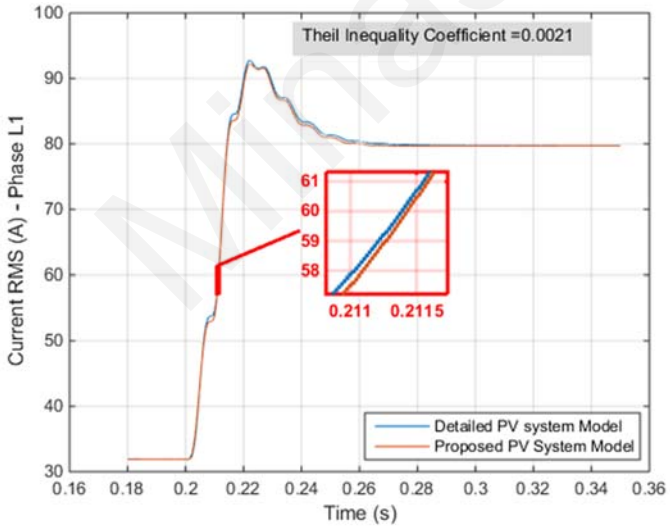

Figure 7.18a. Output current response to a step change in active power input

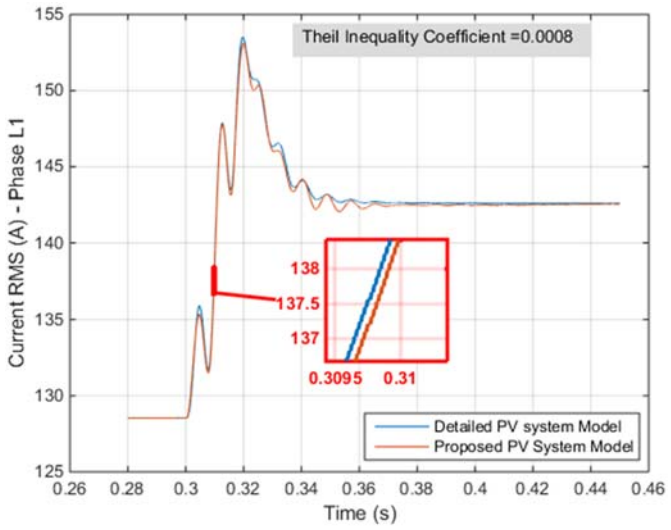

Figure 7.18b. Output current response to a step change in reactive power input

Figure 7.18. Transinet response comparison between the detailed and the proposed PV system model

The comparison is made with the "Theil inequality coefficient" [161], [162], [213]. As can be seen from the obtained results and inequality coefficient in Fig. 7.18a, good agreement

has been obtained between the detailed and the proposed PV system model. Similarly, the transient response of the output current to a step change in reactive power input of 0.3 p.u. is shown in Fig. 7.18b, depicting satisfactory results. In this case, the active power input is maintained at 0.8 p.u. and therefore the change in output current is dedicatedly done on the reactive current component due to the change in reactive power input.

7.3.2 Results for unbalanced condition

The proposed model is designed to model accurately the behaviour of PV systems during unbalanced conditions. For this purpose, the proposed model is tested under a 5% ramp and a 60% step change of the negative sequence component of grid voltage. The voltage waveforms during unbalanced conditions are graphically shown in Figs. 7.19 and 7.20.

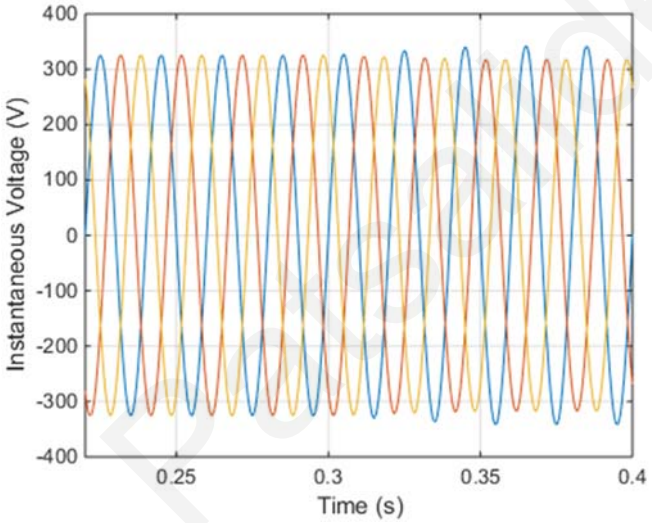

Figure 7.19. Voltage waveforms during unbalanced conditions - 5% ramp change

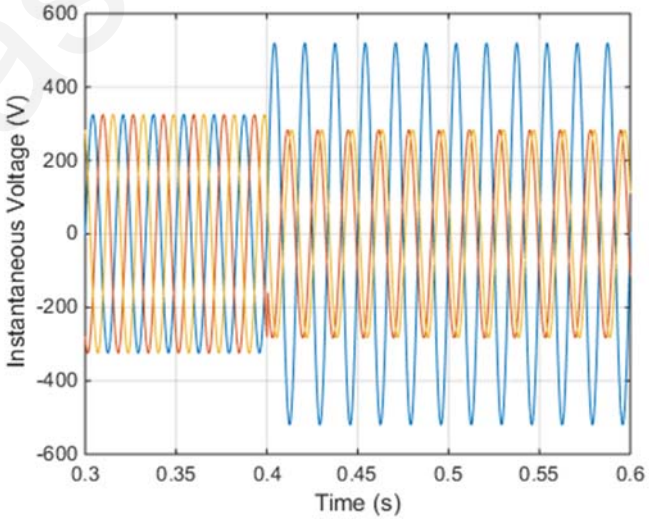

Figure 7.20. Voltage waveforms during unbalanced conditions - 60% step change

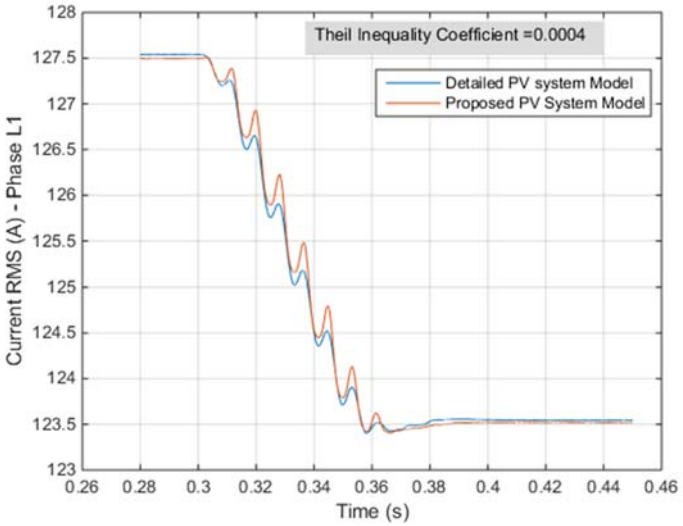

Figure 7.21a. Output current response of phase L1 during transient unbalancing conditions - 5% ramp change

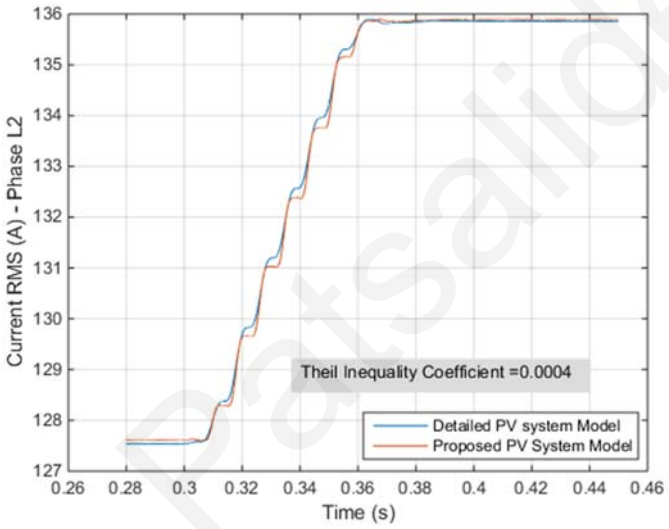

Figure 7.21b. Output current response of phase L2 during transient unbalancing conditions - 5% ramp change

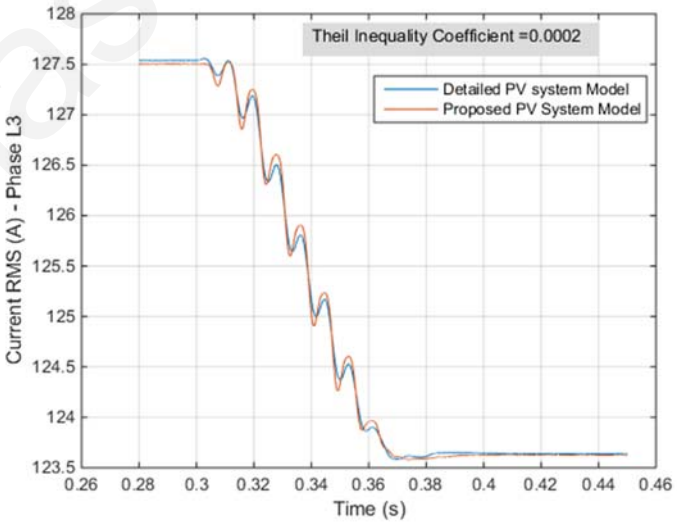

Figure 7.21c. Output current response of phase L2 during transient unbalancing conditions - 5% ramp change

Figure 7.21. Output current response during transient unbalancing conditions - 5% ramp change

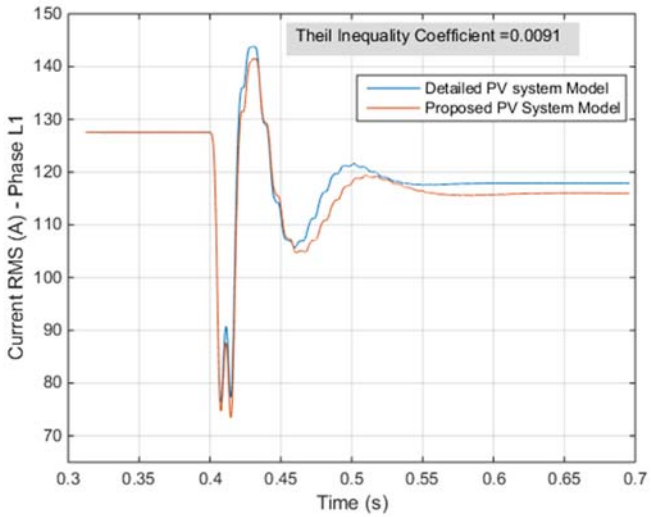

Figure 7.22a. Output current response of phase L1 during transient unbalancing conditions - 60% step change

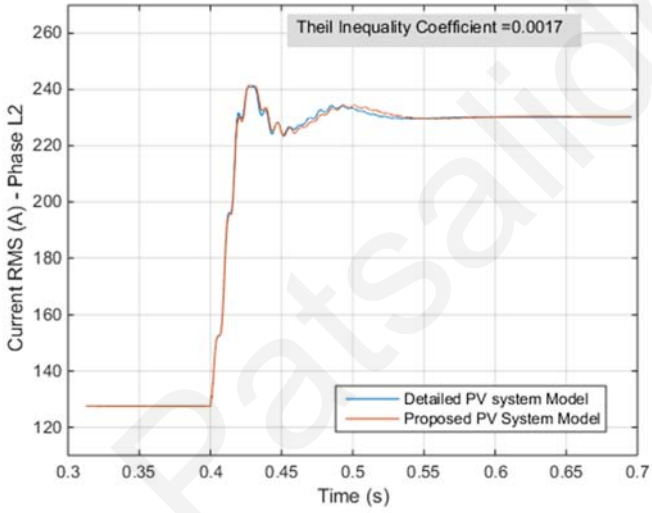

Figure 7.22b. Output current response of phase L2 during transient unbalancing conditions - 60% step change

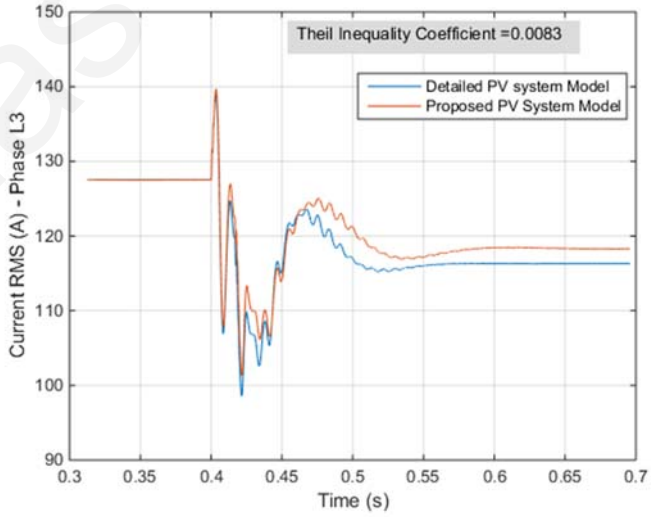

Figure 7.22c. Output current response of phase L2 during transient unbalancing conditions - 60% step change

Figure 7.22. Output current response during transient unbalancing conditions - 60% step change

The results for the unbalanced transient behaviour are shown in Figs. 7.21 and 7.22. As depicted in Figs. 7.21 and 7.22, the model manages to represent the behaviour of the detailed PV system adequately as the Theil inequality coefficient is almost zero.

7.3.3 Results for harmonics

Modelling of switching harmonics is also achieved in this work and it constitutes a first attempt of incorporating switching harmonics into the proposed model. The method adopted is simple but still it can provide results that can be useful for simulations. In Fig. 7.21, the variation of harmonics for both the detailed and the proposed PV system model is depicted. The Theil inequality coefficient for all the harmonics up to the 11th harmonic is below 0.3. Also it must be mentioned that the adopted modelling approach performs worse for low power outputs as the harmonic currents in that situation are comparable with the fundamental current. Further research will be undertaken in the future to formulate a more accurate model for switching harmonics.

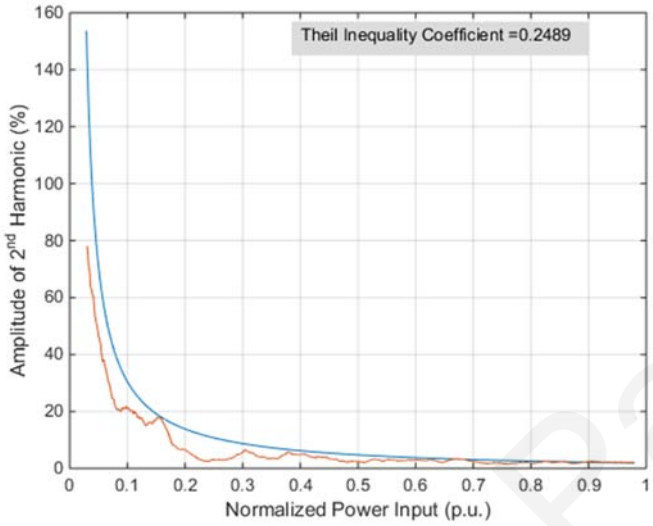

Figure 23a. Amplitude of 2nd harmonic vs normalized power output

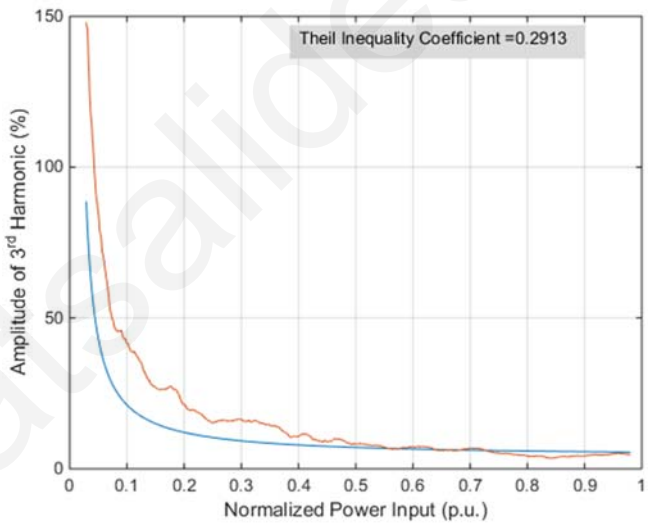

Figure 23b. Amplitude of 3rd harmonic vs normalized power output

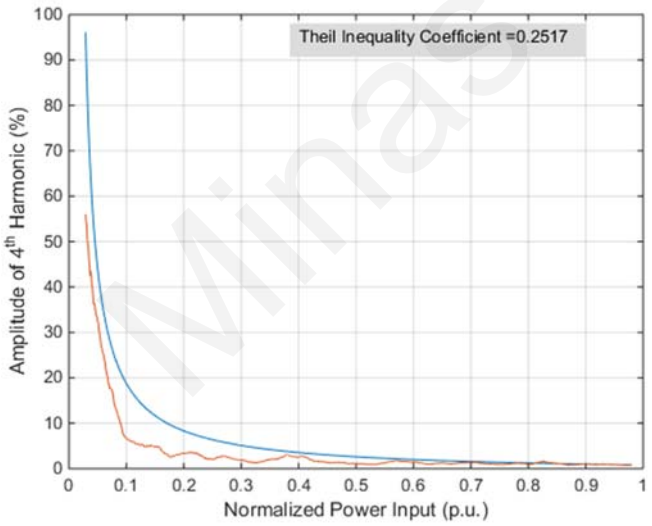

Figure 23c. Amplitude of 4th harmonic vs normalized power output

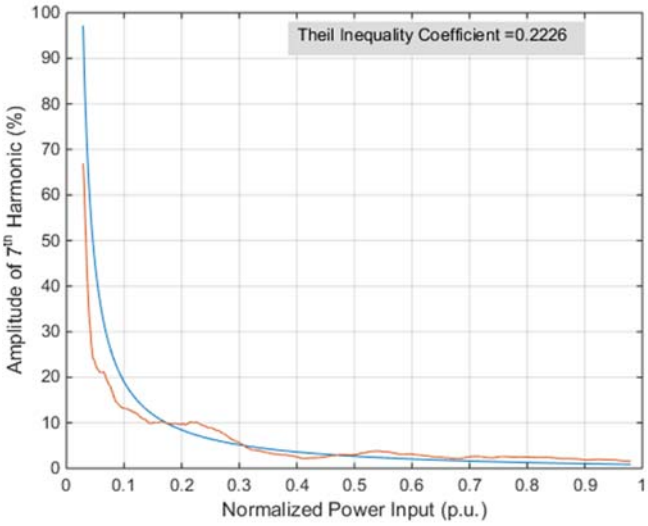

Figure 23d. Amplitude of 7th harmonic vs normalized power output

Figure 7.23. Amplitude of harmonics vs normalized power output

7.3.4 Power Quality Studies – Voltage Regulation

The proposed model and the detailed PV system model are both connected on the distribution grid topology presented in subsection 7.2.4.7. The grid impedance is chosen according to [212]. By imposing a step change in reactive power reference (the same step change as the one applied for the results presented on Fig. 7.18b) on both models then the voltage can be varied according to the reactive power reference and the dynamics of the distribution grid. The transient response of voltage though depends significantly on the transient behaviour of the PV system current as can be seen in Fig. 7.24 (compared to Fig. 7.18b). Via the aforementioned case study, it becomes possible to compare the proposed model with the detailed PV system model. From the results of Fig. 7.24, it can be clearly seen that the proposed model can produce simulation results of reasonable accuracy and importance.

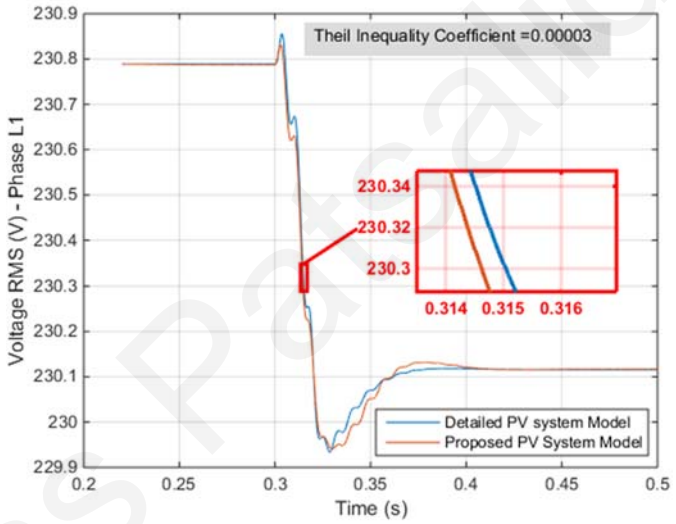

Figure 7.24. Transient response of voltage during a step change in reactive power reference

Finally, the voltage response for the distribution grid busbar for different grid impedance values is shown in Fig. 7.25. The values of grid impedance are chosen based on the range of values presented in [108].

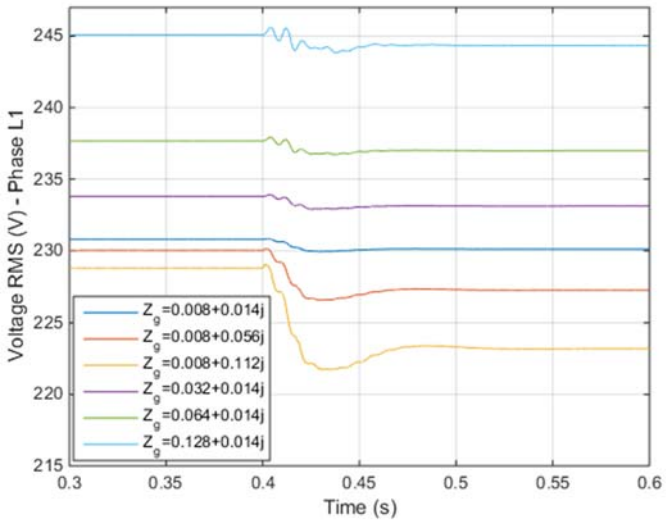

Figure 7.25. Transient response of voltage for different grid impedance values

From Fig. 7.25 it can be concluded that it is important to model in an accurate way the transient behaviour (as well as the steady-state response) of the PV systems as it can reveal the progress of power quality events which may be damaging for the operation of the distribution network or detrimental for the PV system operation itself.

7.4 Conclusions

A generic PV system model for transient studies is presented in this chapter. The proposed model is developed to fill a gap identified in literature referring to accurate PV system modelling. The adopted analysis utilizes existing knowledge to formulate an accurate transient model that considers the PV system control circuit and dynamics. The model can be fully defined and tuned using transient data obtained from a detailed PV system model via the Nelder-Mead simplex algorithm. The generic model can be applied for normal/unbalanced operating conditions and is in line with current DG standards as it can be used for studies of voltage regulation. The aim of the aforementioned research is to enhance the effort of assessing the consequences of high PV penetration and facilitate corrective action with appropriate technical solutions so as to enable the safe and unrestricted deployment of these technologies in electricity grids

Chapter 8
Equivalent Distribution Grid Model (EDGM)

8.1 Introduction

Renewable energy sources (RES) are expected to have a considerable share in the global energy mix over the next years and consequently further research is required to enhance the planning strategies, modify prudently the existing standards and set quality levels on delivered power in order to accommodate the penetration of these technologies. Depending on the distribution grid dynamics and the load demand, the amplitude of voltage may vary significantly and therefore proper simulation models are required for performing dedicated studies. In this chapter, a simplified and accurate model representing the distribution grid dynamics is introduced for power quality studies in the presence of distributed Photovoltaic (PV) generators. The proposed equivalent distribution grid model is validated using measurements and it is then used along with a verified PV system model to estimate the voltage variation and PV capacity of the distribution grid under investigation. Also a sensitivity analysis is performed by varying the parameters of the EDGM to assess how the PV capacity is altered. As a last step, common voltage regulation schemes are analyzed through the use of the proposed model, validating operational modes that can accommodate high distributed PV capacities.

8.2 Proposed Equivalent Distribution Grid Model

8.2.1 Thevenin's Theorem- Basic Theory

According to Thevenin's theorem, any linear electrical network with voltage/current sources and impedances can be replaced at chosen terminals (Fig. 8.1) by an equivalent voltage source V_{th} in series connection with an equivalent impedance Z_{th} [209].

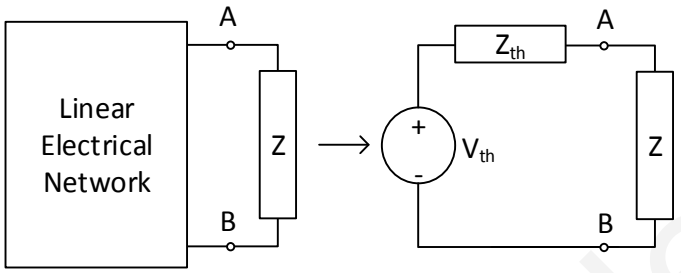

Figure 8.1. Graphical illustration of Thevenin's theorem

Thevenin's theorem is used when part of a large network/circuit needs to be simplified. More specifically it can be used for the simplification of any network before and/or after any specific busbar inside a distribution grid. The information is given as a voltage source but it is possible to tranform the voltage source into current source using Norton's Theorem.Via this method it is possible also to locate if other sources exist in the rest of the power network. For instance when there is a variation in the high voltage network (due to a fault), the Thevenin method finds the chatacteristics of the Thevenin impedance located at the side of the load [214].

8.2.2 Methodology

The formulation of the EDGM constitutes the starting point for performing the investigations for the permissible PV capacity and the voltage regulation in a typical distribution grid and in the presence of increased concentration of PV. The network topology was chosen for the investigations to represent a real case scenario for which the available measurements are able to define/reveal the distribution grid dynamics.

Firstly, the EDGM is determined by performing dedicated analysis on voltage/current measurements obtained at the busbar of the distribution transformer and appropriate modelling of the distribution grid is achieved based on the findings of the analysis. The EDGM is validated by using the measurements obtained before and after the installation of a 150 kW_p PV system. This is achieved while using the EDGM along with the verified PV system model developed in Chapter 6 by studying the power quality response of the distribution grid topology before and after the installation of the 150 kW_p PV system.

Following its validation, the EDGM is utilized in conjunction with the verified PV system model to simulate the behaviour of the distribution grid in the presence of increased PV penetrations. Through the simulations, it was assessed whether a violation of the voltage limit can occur after exceeding a specific PV capacity in the specific distribution grid topology under test.

Furthermore, appropriate corrective actions able to keep the power quality within acceptable levels were considered. More specifically, three different voltage regulation algorithms found in the literature and in technical guidelines for the connection of distributed generators on the low voltage network were employed to improve the voltage levels in the cases when the produced PV power pushes the voltage close or above the EN50160 upper limit [135]. Finally, the parameters of the EDGM were altered in such a way to evaluate the effectiveness of the applied corrective actions and to reveal their significance on the response of the distribution grid.

8.2.3 Mathematical Formulation of the Proposed Grid Model

In order to perform reliable studies about the power quality behaviour of a distribution grid in the presence of distributed generation, the electrical dynamics of the distribution grid are required to be known. For this reason, the distribution grid is modelled as a low voltage Thevenin Equivalent Circuit (TEC) as shown in Fig. 8.2a. In general, distribution feeders and transformers can be considered as a linear time invariant RLC equivalent circuit in transient simulations allowing simplifications to be made. Also, it can be assumed that the voltage in the medium-voltage network remains constant due to the operation of on-load tap changer transformer. In addition, the capacitance of medium-voltage lines is low and can be neglected [89], leaving only a small series RL impedance to be modelled which is included in the estimated Thevenin equivalent impedance. Due to the above, the distribution transformer and the medium-voltage network can be replaced by a TEC.

The formulation of a TEC provides insight into the voltage variation (of fundamental frequency) with regards to the flow of active and reactive power through the distribution transformer or the bus under consideration. The formula which actually represents the distribution grid dynamics and relates the active power, reactive power and buses voltage with the real and imaginary part of the Thevenin Equivalent Impedance (TEI) is shown below:

$$RP_{Load} + XQ_{Load} = U_s U_r \cos(\delta - \varphi) - U_r^2 \tag{8.1}$$

where P_{Load} is the consumed active power (consumed power is denoted with plus sign), Q_{Load} is the consumed reactive power, U_r and φ are the load RMS voltage and angle respectively,

U_s and δ are the source RMS voltage and angle respectively, R and X are the real and imaginary parts of the Z complex TEI.

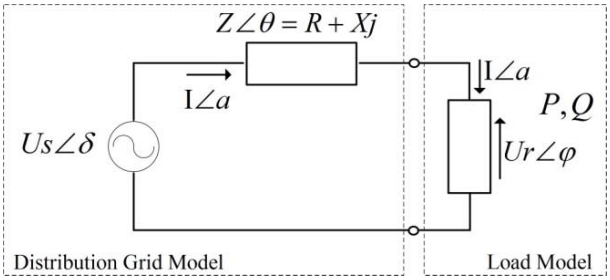

Figure 8.2a. Distribution grid model - Thevenin Equivalent Circuit

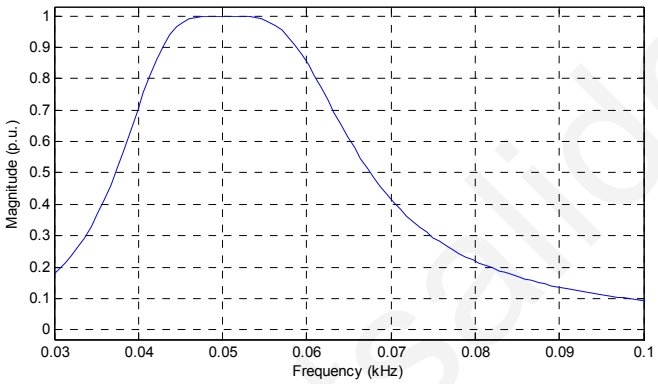

Figure 8.2b. Band-Pass Filter Frequency Response

Figure 8.2. Proposed distribution grid model

This new distribution grid model is defined according to the following procedure using voltage and current waveform measurements available from the bus under consideration. Initially, the voltage and current waveform data are de-noised and filtered. The de-nosing of the raw data is performed by wavelet coefficient thresholding using a global positive threshold to remove any Gaussian noise captured on voltage/current sensors due to environmental or load factors [215]. The filtering of the de-noised waveform data is then done with a dedicated band-pass filter able to reject any off-nominal frequency which is not close enough to the fundamental frequency. The frequency response of the band-pass filter is shown in Fig. 8.2b.

The filtered/de-noised data are used for the calculation of voltage and current phasors required for the estimation of the TEC parameters. The calculation of voltage/current phasors cannot be undertaken with the traditional Fourier method as the waveform data captured via measurements in real conditions do not exactly match the fundamental frequency but the frequency varies around it. Consequently, the Fourier method cannot be used for accurate phasor calculations at off-nominal frequencies neighbouring the fundamental frequency. In [216], different phasor estimation methods are evaluated for their ability to perform accurate phasor estimation at off-nominal conditions. From the aforementioned work it has been

shown that the dynamic methods are the most appropriate to achieve this task and introduce small errors at off-nominal and oscillatory conditions. For the estimation of the TEC parameters, the exact phasors for three successive instances are required. It is desirable to have the three successive instances be as close as possible in order to ensure that the upstream network remains constant [214]. Prony's [217] dynamic method is found to be the most appropriate for the estimation of TEC parameters as it can be implemented on short time intervals and give accurate phasor results (as short as one cycle). The voltage/current phasors calculated via Prony's dynamic method are further used for the estimation of the TEC parameters. In more detail, the TEC calculation concept derives from equation (8.2). By applying Kirchhoff's Voltage Law on the TEC, a fundamental equation is obtained as follows:

$$U_s \angle \delta = (R + jX) \times I \angle a + U_r \angle \varphi \tag{8.2}$$

Equation (2) is valid for a specific time instance and has eight variables four of which are unknown (Us,δ, R, X). The unknown variables cannot be obtained by direct measurements and are thus estimated by assuming that the grid side is constant for a number of successive cycles. Under this assumption, the load variation provides adequate data that can be used for the estimation of the remaining unknown parameters. Based on the ideas mentioned above, equation (8.2) is transformed into a more useful form, equation (8.3), which is used in the calculation of the grid impedance.

$$R + jX = \frac{U_r^{t_0} \angle \varphi^{t_0} - U_r^{t_1} \angle \varphi^{t_1}}{I^{t_0} \angle a^{t_0} - I^{t_1} \angle a^{t_1}} = -\frac{\Delta U_r}{\Delta I} \tag{8.3}$$

where t_0 and t_1 are two successive time moments. The main problem arising with the use of equation (8.3) is that it only applies if the frequency is constant. In practice, a phase drift is observed when the frequency is varying. This effect adds a small error in the voltage and current phase angles for each second cycle measurement when these are analysed with the Fourier method. More specifically, the reference angle is not the same between two consecutive cycles because the frequency variation forces it to drift. As the reference point is not the same between consecutive cycles, the voltage and current phasors used in equation (8.3) will give the wrong result and the estimated impedance phasor will be seen to rotate on the complex plane. By using Prony's method, for calculating the successive phasors instead, the phase drift phenomenon is significantly decreased compared with traditional phasor calculation methods (like Fourier). For the compensation of additional errors on the phase

angle, the triangulation method is used [218]. According to the triangulation method, any possible error in angle is found by calculating the phase drift angles between three consecutive cycles which are required to define a TEC. In general, for a TEC to exist and be valid, the following condition must be true for three successive time instances:

$$\det\begin{bmatrix} 1 & 1 & 1 \\ \vec{U}_r^{t_0} & \vec{U}_r^{t_1} & \vec{U}_r^{t_2} \\ \vec{I}^{t_0} & \vec{I}^{t_1} & \vec{I}^{t_2} \end{bmatrix} = 0 \tag{8.4}$$

The three successive time instances should be as close as possible (preferably three successive cycles) to ensure that the source voltage remains constant. If the phase drift due to frequency variation is taken into account then equation (8.4) becomes:

$$\det\begin{bmatrix} 1 & 1 & 1 \\ \vec{U}_r^{t_0} & \vec{U}_r^{t_1} e^{-j\varepsilon_1} & \vec{U}_r^{t_2} e^{-j\varepsilon_2} \\ \vec{I}^{t_0} & \vec{I}^{t_1} e^{-j\varepsilon_1} & \vec{I}^{t_2} e^{-j\varepsilon_2} \end{bmatrix} = \det\begin{bmatrix} 1 & e^{j\varepsilon_1} & e^{j\varepsilon_2} \\ \vec{U}_r^{t_0} & \vec{U}_r^{t_1} & \vec{U}_r^{t_2} \\ \vec{I}^{t_0} & \vec{I}^{t_1} & \vec{I}^{t_2} \end{bmatrix} = 0 \tag{8.5}$$

By further expanding the determinant of equation (8.5), the formulas necessary for the estimation of the TEI are obtained. In more detail:

$$A + B' + C' = A + B \cdot e^{j\varepsilon_1} + C \cdot e^{j\varepsilon_2} = 0 \tag{8.6}$$

where

$$A = \begin{bmatrix} \vec{U}_r^{t_1} & \vec{U}_r^{t_2} \\ \vec{I}^{t_1} & \vec{I}^{t_2} \end{bmatrix} \quad B = \begin{bmatrix} \vec{U}_r^{t_2} & \vec{U}_r^{t_0} \\ \vec{I}^{t_2} & \vec{I}^{t_0} \end{bmatrix} \quad C = \begin{bmatrix} \vec{U}_r^{t_0} & \vec{U}_r^{t_1} \\ \vec{I}^{t_0} & \vec{I}^{t_1} \end{bmatrix} \quad B' = B \cdot e^{j\varepsilon_1} \quad C' = C \cdot e^{j\varepsilon_2}$$

The vectors A, B' and C' should sum up to zero and consequently after using trigonometry the value of phase drift angles are defined by the following equations:

$$\varepsilon_1 = \pi + \angle\mathrm{A} - \gamma - \angle\mathrm{B} \tag{8.7}$$

$$\varepsilon_2 = \pi + \angle\mathrm{A} + \beta - \angle C \tag{8.8}$$

where

$$\beta = \cos^{-1}\left(\frac{|\mathrm{A}|^2 + |C|^2 - |B|^2}{2|\mathrm{A}||C|}\right) \qquad \gamma = \cos^{-1}\left(\frac{|\mathrm{A}|^2 + |B|^2 - |C|^2}{2|\mathrm{A}||B|}\right)$$

Finally, equation (8.9) is used for the calculation of TEI and equation (8.10) is used for the definition of the Thevenin Equivalent Source (TES) characteristics:

$$Z = R + jX = \frac{\vec{U}_r^{t_0} - \vec{U}_r^{t_1} \cdot e^{-j\varepsilon_1}}{\vec{I}^{t_0} - \vec{I}^{t_1} \cdot e^{-j\varepsilon_1}} \tag{8.9}$$

$$\vec{U}_s = \vec{U}_r^{t_0} - Z \cdot \vec{I}^{t_0} \tag{8.10}$$

where ε_1 is the frequency drift corrective factor, $\vec{U}_s$ the voltage phasor of the TES, $\vec{U}_r$ the voltage phasor of the point of common coupling (PCC) and $\vec{I}$ is the phasor of the current passing through the TEI Z. An important observation made and proven in [216] is that negative values of the real and imaginary part of the impedance depict the impedance on the load site and not the TEI. Based on that observation only the positive values of the real and imaginary part of the impedance are going to be considered. The results of the analysis are shown in the following section.

8.3 Simulation Study

8.3.1 Network Topology under Investigation

Different PV concentrations were investigated by using the EDGM to assess the power quality behaviour of the distribution grid topology and by applying the appropriate voltage regulation algorithm. The grid topology used in this work represents an industrial area in which power quality measurements were performed and used for modelling purposes. The system topology of the distribution grid in the industrial area is shown in Fig. 8.3a.

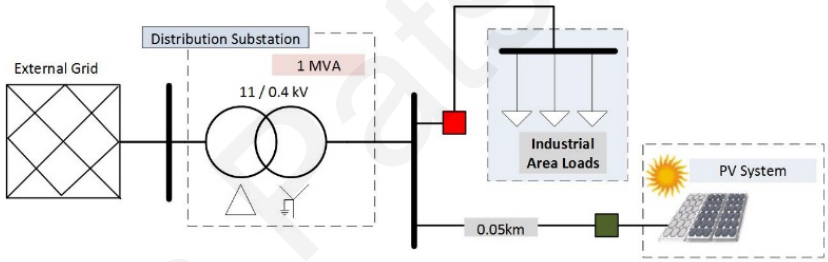

Figure 8.3a. Network topology under investigation

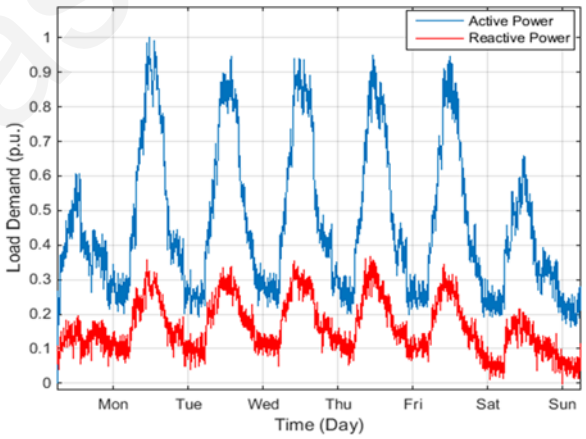

Figure 8.3b. Weekly Load Demand of the industrial area

Figure 8.3. Network topology and load demand

The distribution transformer and the medium voltage network are replaced by an accurate TEC. In addition, the loads in the distribution network are replaced by an aggregated load connected at the busbar of the distribution transformer. The aggregated load is defined by the active/reactive power measurements obtained from the industrial area under

consideration at a resolution of one second (shown in Fig. 8.3b) and therefore the actual load nature is fully accommodated in the aggregated load [99], [219]. The sinusoidal current output of the load model is calculated based on the active/reactive power measurements and the voltage at the output of the load [218]. Measurements of high resolution (having a sampling frequency of one Hz) are used in transient simulations and they are adequate for producing a realistic behaviour [220]. Results of the fundamental frequency are of interest in this investigation and consequently harmonics or nonlinear loads (loads which produce harmonics) are not represented by the model and are thus not considered during the simulations.

8.3.2 PV System Model Description

The PV system model used for the simulation study is the detailed PV system model described in Chapter 6.

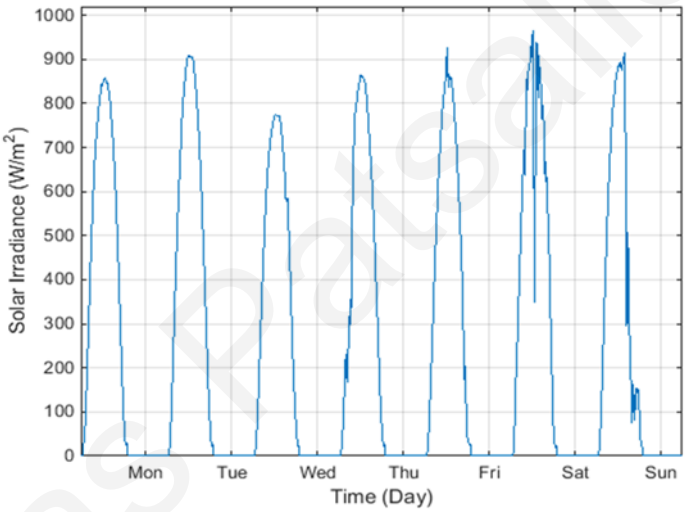

Figure 8.4. Sample solar irradiance profile acquired during the measurement

The solar irradiance used for the simulation having a resolution of one second is shown in Fig. 8.4. From the solar irradiance profile it can be observed that at specific time moments there is a decrease in solar irradiance due to shading from clouds. Consequently, the steady-state effect of shading at the output of the PV system is taken into account. However, it must be mentioned that in reality each PV panel experiences a decrease in output power with certain delay depending on the cloud direction and speed [221]. In such a case, more than one pyranometers can be used along with an interpolation method to obtain a solar irradiance profile that will match with less error the variations in PV system output [222]. In this contribution, the aggregated effect of shading during cloudy weather is modelled by varying the irradiance input to a single PV array component (it is assumed that the PV array is not subjected to shading from nearby objects). As only data from one pyranometer is available it is chosen to model the whole PV array as a single component with one solar irradiance

input (and a single temperature input as well). The total power output will be the same as having multiple PV panels experiencing uniform solar irradiance which is reasonable for the size of PV system adopted for the simulations. This stems from the fact that for PV panels placed in the same location, the decrease in solar irradiance will be similar and almost instantaneous for each PV panel and thereafter the transient effect caused by shading on the power output of the PV system is assumed negligible. If multiple PV systems located in different geographical areas are required to be modelled, then the shading effect due to clouds can be assessed by using solar irradiance profiles obtained from the pyranometers of each area.

In this case the adaptive power factor has been realized according to the following equation:

$$PF = \begin{cases} 1 & for\ 0 < P^{p.u.} \le 0.5 \\ -0.1 \times (P^{p.u.} - 0.5) + 1 \ \text{(under-excited)} & for\ 0.5 < P^{p.u.} \le 1 \end{cases} \quad (8.11)$$

where $P^{p.u.}$ is the active power production in per unit (p.u.).

8.4 Results

8.4.1 Estimation of EDGM parameters - TEI

The Voltage and current waveform measurements are analysed according to the proposed EDGM methodology. For the calculation of the grid impedance, acquisition of high resolution data is required and therefore a power quality analyser is utilized with 50 Hz timer synchronization capability.

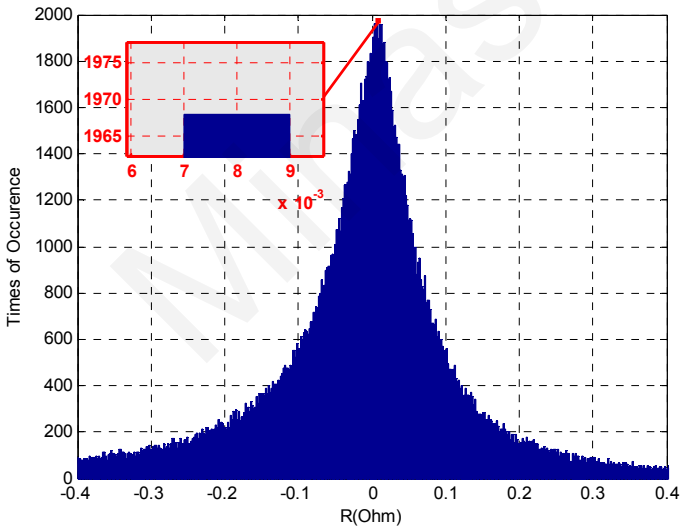

Figure 8.5a. Histogram of real part of grid impedance

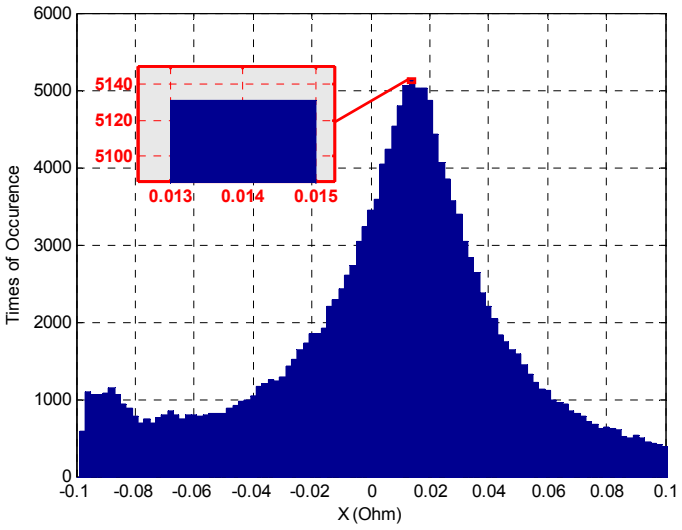

Figure 8.5b. Histogram of imaginary part of grid impedance

Figure 8.5. Statisitical analysis of grid impedance data

The power quality analyzer stores 256 samples per cycle for both voltage and current of phase L1. The phasors obtained from the proposed analysis are used to determine the real

and imaginary part of the grid impedance for the fundamental frequency. The probability distribution of both real and imaginary part of the grid impedance are shown in Fig. 8.5. From Fig. 8.5a, it is observed that the real part of the grid impedance ranges from 0.007 to 0.009 Ohms. On the other hand, from Fig. 8.5b, it can be seen that the imaginary part of the grid impedance ranges from 0.013 to 0.015 Ohms. Only the positive values of the real and imaginary part are considered because only these characterize the behaviour of the grid impedance [38]. The grid impedance is finally set equal to $0.008 + 0.014j = 0.0161\angle 60.3°$ Ohms by taking the mean value of the real and imaginary parts.

8.4.2 Validation of EDGM

The EDGM is validated by using the measurements obtained before and after the installation of a 150 kW_p PV system.

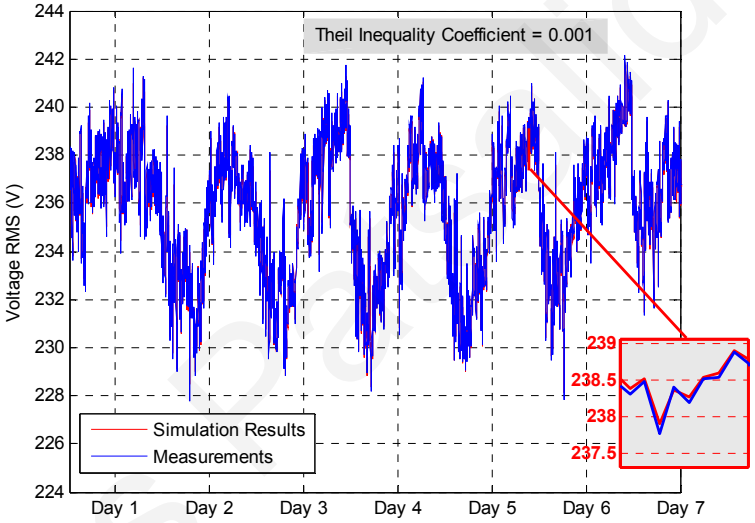

Figure 8.6a. Results obtained before the integration of the PV system

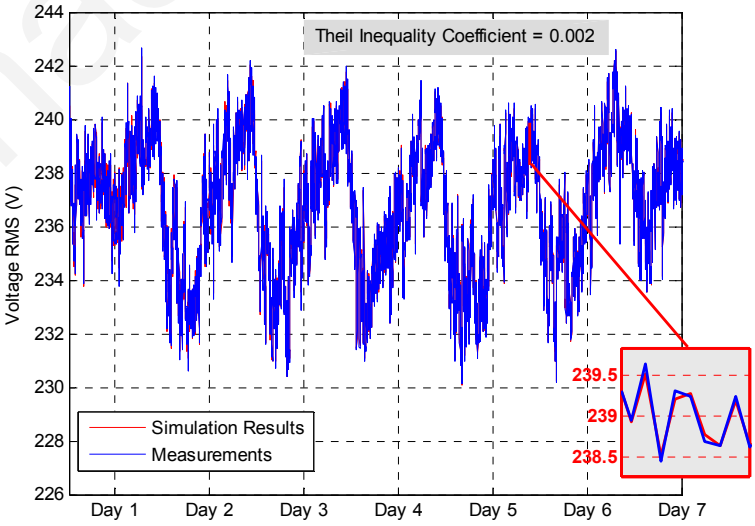

Figure 8.6b. Results obtained after the integration of the PV system

Figure 8.6. Results obtained before/after the integration of the PV system

This is achieved by using the EDGM along with the verified PV system model developed in Chapter 6 for studying the power quality response of the distribution grid topology before and after the installation of the PV system. Both measurements and simulation results are compared with the "Theil inequality coefficient" [161], [162], [213]. As can be seen from the obtained results and inequality coefficients in Fig. 8.6, good agreement has been obtained between simulated and measured results. Following its validation, the EDGM was further used in the investigation of different PV concentration scenarios.

8.4.3 Simulation Study Results

Up to 1.5 MWp capacity of PV systems was introduced in the distribution grid topology under investigation. The simulation results for the voltage RMS for different PV penetrations are shown in Fig. 8.7. It must be noted that only results for the fundamental frequency are presented in this section. The dashed red line represents the EN 50160 upper limit for voltage RMS. The lower limit of EN 50160 (207 V) is not depicted in the graphs because the voltage does not go below 210 V. As shown in Fig. 8.7, the voltage upper limit has been nearly reached with the installation of the 1.5 MWp PV system as the produced power during times of high solar irradiance is much more than the demand of the local distribution grid. The PV produced energy increases the grid voltage since the load is supplied by local generation and the surplus flows in the reverse direction to satisfy load beyond the local transformer, hence a voltage rise on the transformer busbar is unavoidable. It should be mentioned at this point that the capacity of the transformer is 1 MVA.

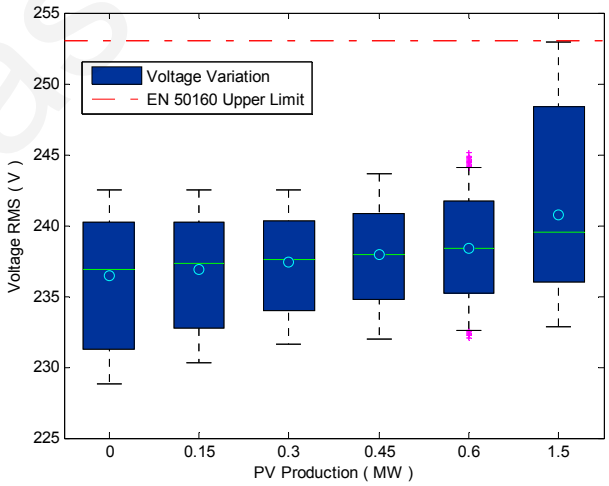

Figure 8.7. Voltage variation for different PV concentrations

It is evident from the results that in order to operate a PV capacity which is comparable to the nominal power of the transformer it is required to utilize a voltage regulation mechanism for maintaining the voltage within acceptable levels since automatic voltage regulation is not an available option at the local distribution transformer.

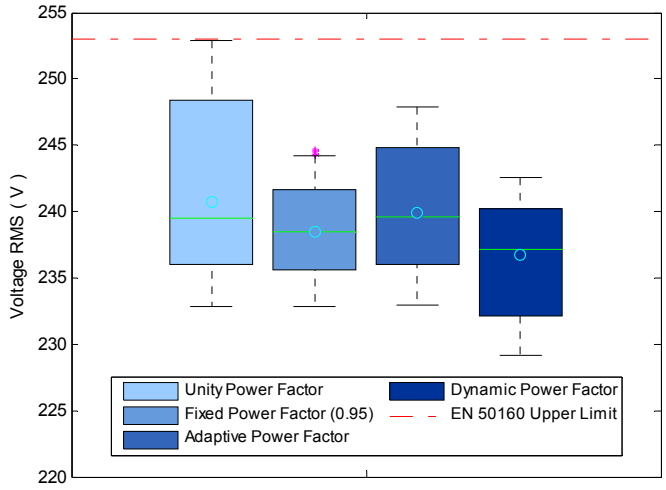

Figure 8.8a. Response of adopted voltage regulation methods

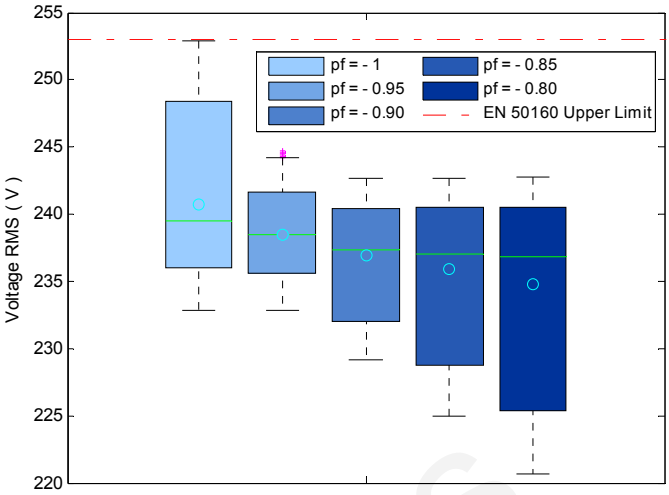

Figure 8.8b. Fixed Power Factor Scheme set to different values

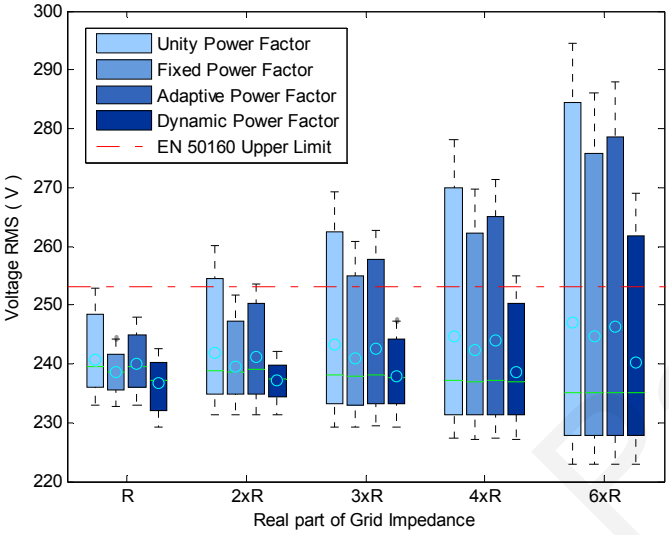

Figure 8.8c. Response of voltage regulation methods as a function of the real part of TEI

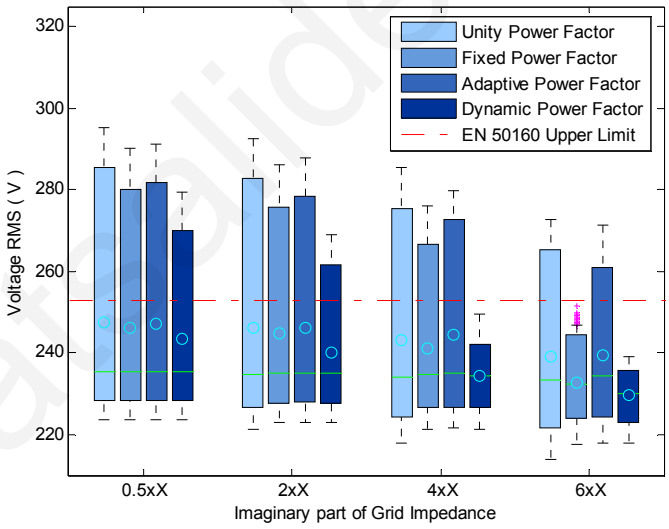

Figure 8.8d. Response of voltage regulation methods as a function of the imaginary part of TEI

Figure 8.8. Simulation results for different voltage regulation schemes

As can be seen in Fig. 8.8a, the voltage profile at the transformer's busbar can only be improved adequately if the appropriate voltage regulation algorithm is selected. In more detail, Fig. 8a shows the response of the grid voltage in the presence of 1.5 MWp PV system with the voltage regulation capability being enabled. From the results, it can be observed that the Adaptive Power Factor scheme provides the least improvement as the voltage has a wider variation range which is also closer to the EN 50160 upper limit. Also, the aforementioned method can create larger voltage variations that can be harmful for the operation of the utility grid during solar irradiance fluctuations. On the other hand, the Fixed Power Factor method achieves to set the voltage within an acceptable range but the best performing voltage regulation algorithm is the Dynamic Power Factor method which can lower sufficiently the upper value of the voltage and can maintain it well below the

acceptable limit. Additionally, the Fixed Power Factor method can narrow the voltage variation.

Next, the fixed power factor scheme is considered with different values (inductive) and the voltage at the busbar of the distribution transformer is considered. From Fig. 8.8b, it can be concluded that it is sufficient to set the power at a fixed value of -0.95 for the voltage quality to be kept within the required levels. Furthermore it can be seen that the power factor should not be set lower than -0.85 as the voltage variance reaches unacceptable values.

The effect of TEI on the voltage quality is then assessed by varying its real and imaginary part. The results are shown in Fig. 8.8c and 8.8d. From Fig. 8.8c it can observed that a higher real part of the TEI makes voltage regulation more difficult. The power factor must be set to a lower value than -0.95 when the real part of the TEI obtains higher values. On the other hand, it is apparent that the dynamic power factor method has the ability to regulate the voltage better even in the case when the real part of the grid impedance is 3 times the estimated value (0.024 Ohms). The choice of the particular TEI values that are examined is reasonable if we take into consideration the standard VDE 0126-1-2006 [223]. According to this standard, the threshold for islanding conditions was initially set to 0.5 Ohm but this limit was too tight/unrealistic as observed from field experience especially in cases where many inverters were operating close to each other. The value has eventually been set to 1 Ohms to avoid false detection of islanding phenomena.

As can be seen in Fig. 8.8d, the imaginary part of TEI plays an important role in the voltage regulation process. If the imaginary part of the TEI is too low then the regulation of the voltage becomes difficult. It can also be seen that the voltage decreases more than desired with a slight reactive power absorption in the case when the imaginary part of the grid impedance is significant.

From the above it is obvious that knowledge of the TEI and the availability of a simplified/accurate distribution grid model will be crucial for planning studies and for the future development of distribution grids. As the penetration of distributed PV grows, the ability to measure the grid impedance during real time operation is of utmost importance in order to be able to apply the appropriate regulation method using optimization techniques. This ability will be very useful in the situation when the grid impedance varies due to changes in the local distribution network. In some cases, phasor/waveform measurements may be adequate to define the grid dynamics and help in applying the correct measures for voltage regulation. As smart grids evolve and the concentration of distributed generators increases, such functionality will assist in maintaining the voltage envelope within system needs and achieve the required quality of supply.

8.5 Conclusions

A new simplified distribution grid model for the assessment of the behaviour of high PV concentration is presented in this chapter. Furthermore, the simplified distribution grid model is used for the evaluation of different voltage regulation algorithms able to maintain the voltage within the limits proposed by international standards. From the results, it has been shown that in order to facilitate higher penetration of distributed generation and avoid the loss of invaluable RES energy due to overvoltages, the utilization of an appropriate voltage regulation scheme is required when the local ratio of PV penetration to the local load exceeds a predetermined threshold that depends on the characteristics of the local network. From the findings of this work, it is also apparent that appropriate/accurate simulation tools and models should be readily available to achieve successful deployment of distributed generators.

Chapter 9
Application of the Distribution Grid Model

9.1 Introduction

The equivalent distribution grid model (EDGM) proposed in the previous chapter can have various applications of which three are realized and presented in this chapter. Firstly, the DGM is employed for the study of the voltage regulation capability of both the conventional adaptive power factor (CAPF) scheme and its generalized form. Secondly, a new voltage regulation scheme inspired by Thevenin's Theorem (which is directly related to DGM) is developed and presented. The well-known dynamic power factor method is modified accordingly to provide a variable lower limit, which is defined by the Thevenin Equivalent Impedance (TEI) measured at the point of common coupling with the electricity grid. The new voltage regulation scheme is incorporated into the control circuit of the detailed Photovoltaic (PV) system model for its further evaluation via computer simulations. Lastly, the DGM theory is used for defining the Harmonic Thevenin equivalent impedance (HTEI) measured at the point of common coupling which has the ability to characterize the response of the distribution grid for the harmonic frequencies of interest.

9.2 Generalized Adaptive Power Factor Method (GAPF)

9.2.1 Methodology

The models developed in the previous chapters are utilized for the evaluation of the conventional adaptive power factor voltage regulation scheme and its generalized form. In more detail, the DPVSM was inserted into the industrial distribution grid topology presented in subsection 8.3.1, the parameters of which are known and can be represented with the help of the DGM. The performance of the GAPF is then evaluated by assessing the levels of voltage variation in the presence of PV generation.

9.2.2 GAPF description

According to the conventional adaptive power factor (CAPF) scheme described by equation (8.11), the reactive/voltage regulation is enabled when the output active power is greater than half the nominal power. In order to investigate if the proposed curve of the adaptive power factor is the optimum, this is expressed in a generalized form represented by equations (9.1) and (9.2).

$$PF = \begin{cases} 1 \; or \; -1 & \text{for } 0 \le P \le P_{set} \\ -1 + A \times (P - P_{set}) & \text{for } P_{set} < P \le 1 \end{cases} \tag{9.1}$$

and

$$A = \frac{1 - PF^{\min}}{1 - P_{set}} \tag{9.2}$$

where P_{set} is the minimum active power set point at which voltage regulation is active and $PF^{\min}$ is the lower limit of the permissible power factor. The generalized adaptive power factor (GAPF) scheme is shown graphically in Fig. 9.1.

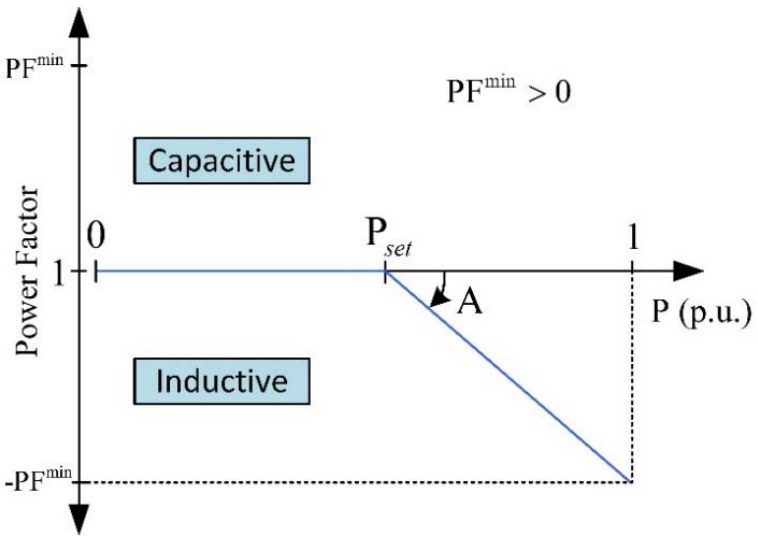

Figure 9.1. Generalized Adaptive Power Factor Method (GAPF)

By varying the parameters P_{set}, A and PF^{min} of the GAPF, the response of the voltage at the busbar of the distribution transformer is evaluated via simulation. It must be mentioned that the GAPF scheme can be converted to the CAPF scheme by setting the parameter P_{set} equal to 0.5.

9.2.3 Simulation Case Outcomes

A PV installation with 1.5 MWp nominal PV capacity is introduced into the distribution grid topology under investigation. The PV installation is equipped with a voltage regulation function which absorbs reactive power depending on the active power output. The simulation results for the voltage RMS of the distribution transformer busbar with and without voltage regulation are shown in Fig. 9.2. The dashed red line represents the EN 50160 upper limit for voltage RMS. The lower limit of EN 50160 (207 V) is not depicted in the graphs because the voltage does not go below 230 V. As shown in Fig. 9.2, with the 1.5 MWp PV system operating at unity power factor the voltage upper limit is almost reached, as the produced power during times of high solar irradiance was more than the demand of the local distribution grid. By applying the CAPF scheme, the voltage profile improves significantly. The PF^{min} of CAPF is set to 0.95 in this case.

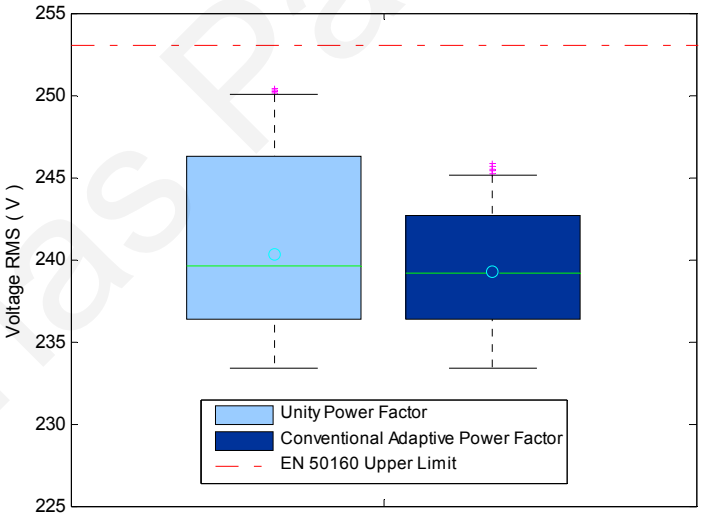

Figure 9.2. Voltage Profile with and without voltage regulation

After choosing different values of P_{set} (instead of 0.5 used in the CAPF), it can be observed that the variation of the voltage can decrease even more as shown in Fig. 9.3.

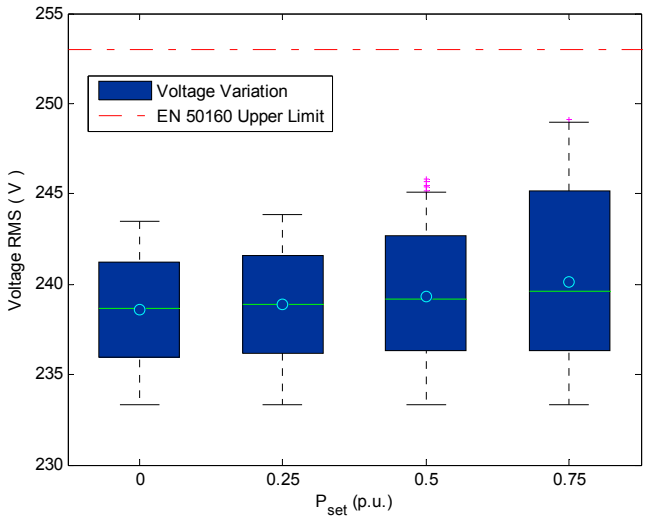

Figure 9.3. Generalized Adaptive Power Factor with $\boldsymbol{PF^{min} = 0.95}$

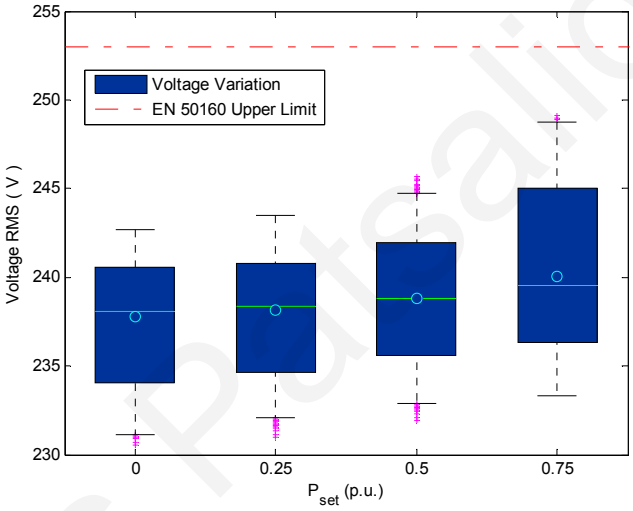

Figure 9.4. Generalized Adaptive Power Factor with $\boldsymbol{PF^{min} = 0.90}$

Furthermore, it can be seen that if the voltage regulation function is enabled a P_{set} equal to zero while maintaining the PF^{min} equal to 0.95, the voltage is kept to a lower level due to the early and adequate reactive power absorption. If the PF^{min} is set to a lower value (0.9), the voltage variation increases (as shown in Fig. 9.4) since excessive reactive power absorption is taking place which is not required by the distribution grid dynamics (this is determined by the imaginary part of the Thevenin equivalent impedance) and specific load consumption. It must be mentioned that parameter A in equations (9.1) and (9.2) is calculated by using the chosen PF^{min} and P_{set} values as presented in the previous subsection.

9.3 New Voltage Regulation Scheme based on the DGM

9.3.1 Methodology

A new voltage regulation scheme is developed based on the DGM theory presented in chapter 8. The proposed voltage regulation scheme is incorporated into the control circuit of the DPVSM for further investigation. The distribution grid on which the PV system model is coupled to, is represented by a DGM. Also, the impedance of the DGM is designed to experience a step change while the PV system is operated at its nominal conditions (at Standard Test Conditions). The voltage regulation scheme is based on the conventional dynamic power factor method described in technical guideline/standards, which is modified to have a variable power factor lower limit. The lower limit is calculated by using the parameters of the DGM measured at the point of common coupling with the electricity grid. The proposed modification improves the performance of the conventional dynamic power factor method and at the same time it can quantify the reactive power needed for proper regulation of the voltage level without losing valuable active power unless this is of utmost importance to preserve voltage quality and stability.

9.3.2 New Voltage Regulation Scheme Description

The proposed voltage regulation scheme is based on the Dynamic Power Factor method, which is represented by equations (9.3) and (9.4).

$$PF=\begin{cases} 1\ or\ -1 & \text{for } U_{Low}^{Dead\ Band} \le V_{grid} \le U_{High}^{Dead\ Band} \\ -1+A_1\times(V_{grid}-U_{High}^{Dead\ Band}) & \text{for } U_{High}^{Dead\ Band} < V_{grid} < U^{Upper\ Limit} \\ 1+A_2\times(V_{grid}-U_{Low}^{Dead\ Band}) & \text{for } U^{Lower\ Limit} < V_{grid} < U_{Low}^{Dead\ Band} \end{cases} \tag{9.3}$$

and

$$A_1=\frac{1-PF^{\min}}{U^{Upper\ Limit}-U_{High}^{Dead\ Band}} \qquad A_2=\frac{1-PF^{\min}}{U_{Low}^{Dead\ Band}-U^{Lower\ Limit}} \tag{9.4}$$

where V_{grid} is the RMS voltage measured on phase A (it is assumed that the power system is balanced), $U_{Low}^{Dead\ Band}$ and $U_{High}^{Dead\ Band}$ are the lower and upper limits of dead band zone in which no voltage regulation is performed, $U^{Lower\ Limit}$ and $U^{Upper\ Limit}$ are the lower and upper limits of voltage range in which voltage regulation is performed and $PF^{\min}$ is the lower limit of the permissible power factor. The proposed voltage regulation scheme is shown graphically in Fig. 9.5. The lower limit of the permissible power factor is determined as shown below. A negative power factor value means absorption of reactive power.

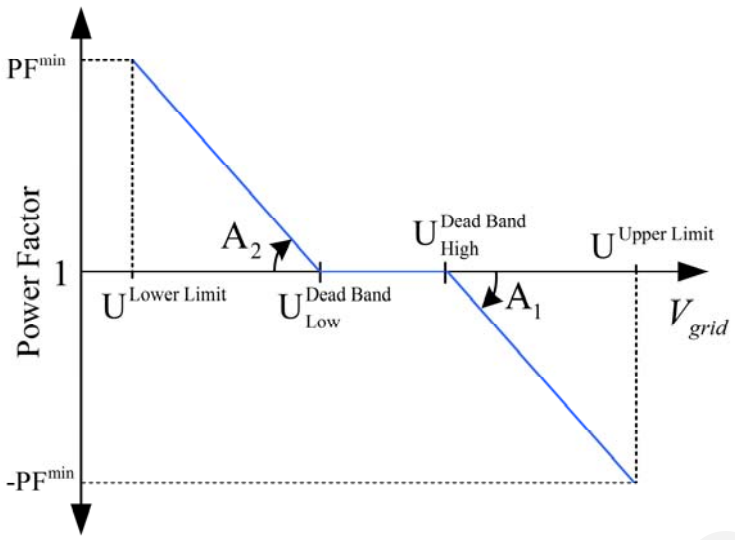

Figure 9.5. Proposed voltage regulation scheme

By setting the reactive power component of equation (8.1) to zero it becomes feasible to predict the level of voltage at the PCC when injecting a certain amount of active power into the PCC. Also it is assumed that the $\cos(\delta-\varphi)$ factor in equation (8.1) is equal to unity which holds true for zero reactive power absorption/injection.

$$\left(U_r^{Q=0}\right)^2 - U_S \cdot U_r^{Q=0} - R \cdot P_{PV} = 0 \tag{9.5}$$

The required solution to the above quadratic equation is obtained by finding the positive root using equation (9.6).

$$U_r^{Q=0} = \frac{U_s + \sqrt{U_s^2 + 4R \cdot P_{PV}}}{2} \tag{9.6}$$

By combining equations (8.1) and (9.5) a formula is derived which can define the maximum reactive power able to regulate adequately the voltage at PCC using a desirable voltage reference point.

$$Q_{PV}^{\max} = \frac{\left(U_r^{set}\right)^2 - \left(U_r^{Q=0}\right)^2 + U_S(U_r^{Q=0} - U_r^{set} \cdot \cos(\delta-\varphi))}{X} \tag{9.7}$$

where U_r^{set} is the desirable voltage reference point which is set to 245 V. The $\cos(\delta-\varphi)$ factor for non-zero reactive power absorption/injection is estimated by equation (9.8).

$$\cos(\delta-\varphi) = \frac{RP_{PV} + XQ_{PV} - U_r^2}{U_s U_r} \tag{9.8}$$

Finally, PF^{min} can be calculated from equation (9.9).

$$PF^{\min} = \frac{1}{\sqrt{1+\left(\frac{Q_{PV}^{\max}}{P_{PV}}\right)^2}} \tag{9.9}$$

From equations (9.5)-(9.7) it can be noticed that in order to calculate the maximum required reactive power, the real and imaginary part of the TEI are necessary. For this purpose, a module is incorporated into the inverter's control circuit responsible for estimating the parameters of the Thevenin Equivalent Circuit based on equations (8.9) and (8.10).

The PV system model has been simulated for only 10 seconds as this duration is more than enough to study the behaviour of the PV inverter during a change in distribution grid conditions (the inverter can change its output and reach a steady state in just a few cycles).

9.3.2 Simulation Case Outcomes

The developed model has been simulated and its response is evaluated for different conditions. Firstly, the model was simulated with a constant TEI of which the value is properly set in order for the voltage level to remain below the EN 50160 upper limit (shown in Fig. 9.6). It can be observed that the high solar irradiance conditions force the voltage to reach the maximum value of 251 V. Then, the real part of the TEI is increased by 0.06 and 0.09 Ohm respectively, approximating in that way a significant change in the topology of the distribution grid and different dynamic power factor schemes are tested for their ability to perform adequate voltage regulation. A significant increase in grid impedance can occur when a part of the distribution grid (which includes power generators) is isolated due to a fault or probably due to a sudden loss of generating power (loss of power delivered by storage or renewables). Transformer tap operations can cause less significant changes in the grid impedance as well. The initial grid impedance value has been chosen to be 0.06 Ohms as this was the result of field measurements during normal conditions. The choice of the final values of the grid impedance is also reasonable if we take into consideration that during islanding conditions or disconnection of a large part of the distribution network the impedance can experience a step change of 1 Ohm as required by VDE 0126-1-2006 [223]. The threshold described in the standard was initially set to 0.5 Ohm but this limit was too tight/unrealistic as observed from field experience especially in cases where many inverters were operating close to each other. The inverter sees a higher impedance in such case due to the fact that the produced active energy by the inverter needs to travel more distance before it is consumed. The actual and estimated (by the inverter) values of the TEI during the simulation are shown in Fig. 9.7. As can be seen there is a good match between actual and estimated values of TEI.

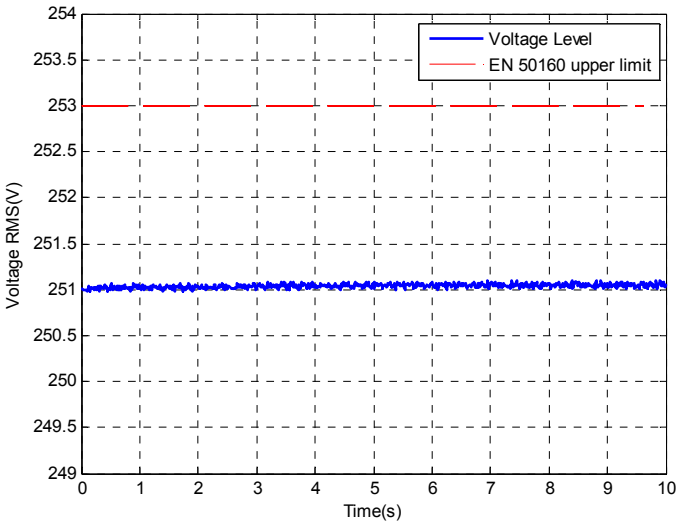

Figure 9.6. Voltage RMS at PCC vs Time – Constant TEI

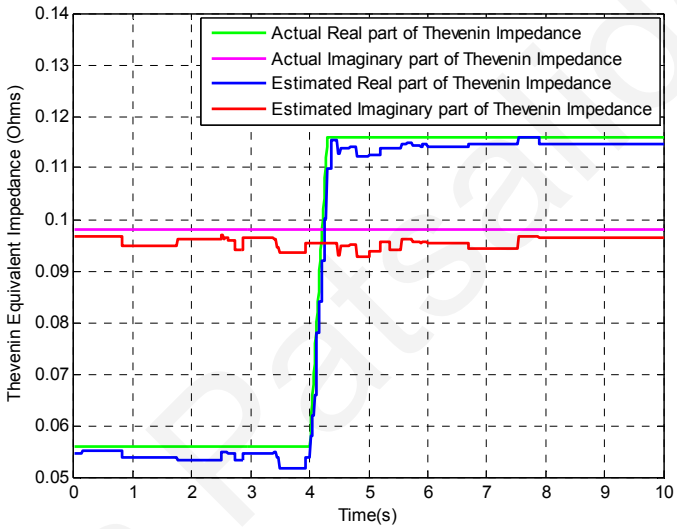

Figure 9.7. Actual and Estimated values of the TEI during a step change in the real part of TEI

A small error in tracking the grid impedance is observed due to the presence of harmonics produced by the inverter. The aforementioned error can be further reduced by using more advanced methods for estimating the voltage/current phasors similar to the ones used in synchrophasors theory. It must also be mentioned that the inverter is oversized in such a way so that it does not decrease/limit the active power output when it is required to absorb reactive power up to the nominal power of the PV system. Furthermore, the $U_{\text{High}}^{\text{Dead Band}}$ and $U^{\text{Upper Limit}}$ parameters are set to 245 V and 253 V respectively for all the voltage regulation schemes under test. By definition, the reactive power set point acts linearly with respect to PCC voltage in the voltage range between $U_{\text{High}}^{\text{Dead Band}}$ and $U^{\text{Upper Limit}}$ (see Fig. 9.5). Additionally, it is ensured that the aforementioned voltage range is not too tight to cause an overshoot on voltage during the operation of voltage regulation mechanism. The parameter U_r^{set} of the proposed method is chosen in such a way to reduce the magnitude of voltage overshoots

while keeping the voltage level well below the EN 50160 limit. The voltage behaviour for the different voltage regulation schemes is shown in Fig. 9.8.

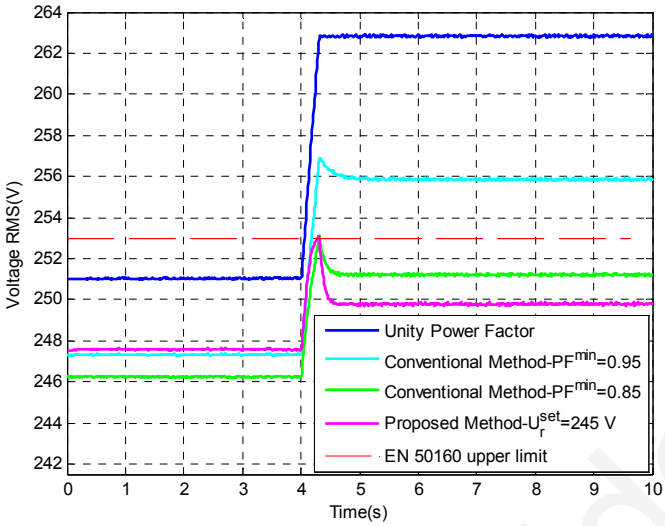

Fig. 9.8a. Voltage RMS at PCC vs Time for different voltage regulation schemes during a step change of 0.06 Ohm

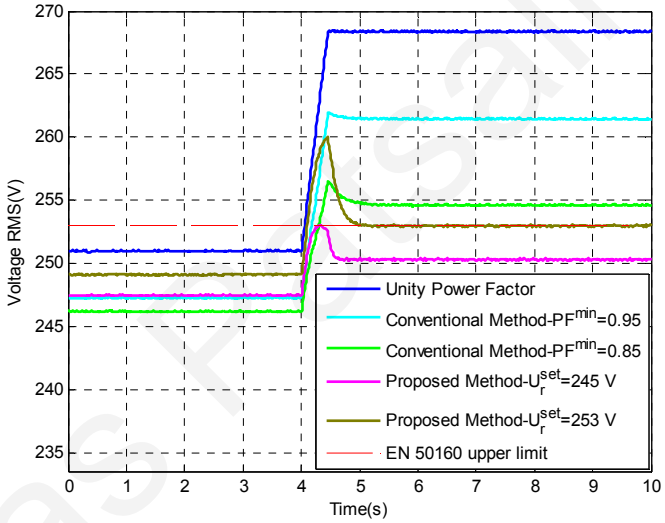

Fig. 9.8b. Voltage RMS at PCC vs Time for different voltage regulation schemes during a step change of 0.09 Ohm

Figure 9.8. Voltage RMS at PCC vs Time for different voltage regulation schemes

It is evident from the figure that the imposed step changes in the real part of TEI set the voltage above the upper limit of EN 50160 and consequently the voltage regulation function is necessary in such a case. When adjusting the lower limit of the permissible power factor to 0.95, it is clear that the voltage regulation mechanism is not capable of keeping the voltage within the acceptable levels. On the other hand by setting the lower limit of permissible power factor to 0.85 it has been shown via the simulation that the voltage remains below the limit of EN 50160 as long as the magnitude of the step change does not exceed a certain threshold. From the results, it is clear that the proposed voltage regulation method has performed quite well as it has the capability to estimate the lower limit of the permissible power factor to achieve adequate regulation of the voltage. The power factor variation

measured at the output of the PV inverter for the different voltage regulation schemes is depicted in Fig. 9.9. From this figure it can be seen that prior to the change in the real part of the TEI (see Fig. 9.7) the power factor does not need to go lower than 0.97.

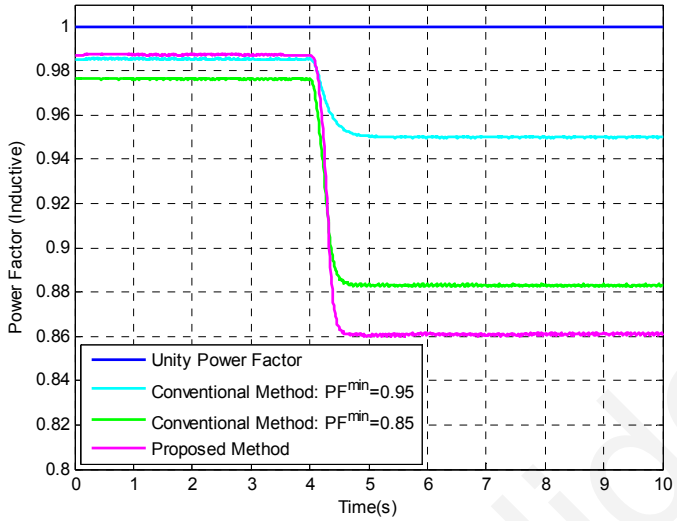

Fig.9.9a. Power Factor vs Time for different voltage regulation schemes during a step change of 0.06 Ohm

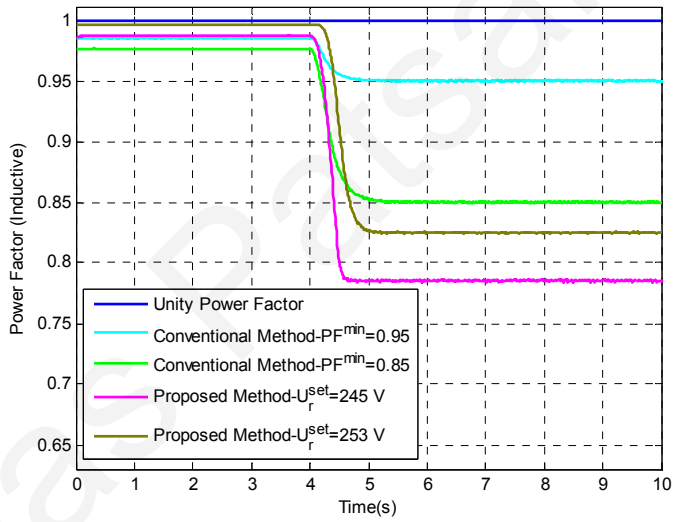

Fig.9.9b. Power Factor vs Time for different voltage regulation schemes during a step change of 0.09 Ohm

Figure 9.9. Power Factor vs Time for different voltage regulation schemes

However in the case when a significant increase in the TEI seen by the inverter occurs then a lower limit of the permissible power factor must be used. More specifically, in conventional distribution grids, it is not expected to have such a significant increase in the TEI, but this can be a possible case for a smart grid / microgrid topology in which the connection with the upstream power grid can experience abrupt sizeable changes (as the local load demand will be covered mostly by distributed generators and distributed storage). Despite this, the DSO is responsible for maintaining the voltage within the acceptable limits and thus it can utilize such dynamic methods as the one presented in this work if no other measures are effective during abnormal operating conditions.

9.4 Harmonic Distribution Grid Model (HDGM)

9.4.1 Methodology

Based on the theory presented in chapter 8, the harmonic impedance seen by a specific point of common coupling is possible to be found. This can be achieved by repeating the methodology of calculating the TEI for each harmonic frequency up to a specific harmonic order. The transfer function of the harmonic equivalent impedance is then obtained by applying estimation algorithms and subsequently the transfer function is built into a circuit using basic network synthesis techniques. In that way a more advance and complete distribution grid model is formulated (named HDGM) for use in accurate harmonic studies. The HDGM along with the DPVSM are both used to assess the harmonic response of the distribution grid topology depicted in subsection 8.3.1. For this purpose, simulation results for voltage THD are obtained from the point of common coupling (of the HDGM and the DPVSM) and are presented.

9.4.2 Formulation of HDGM

By taking into account the values of impedance for harmonic frequencies, it becomes possible to formulate the harmonic impedance seen by the point of common coupling and hence represent this harmonic impedance via a Thevenin Equivalent Circuit. As a consequence, the schematic diagram of Fig. 8.2a is changed to the schematic diagram of Fig. 9.10 to include not only the fundamental frequency but the harmonic frequencies up the desired harmonic order (h).

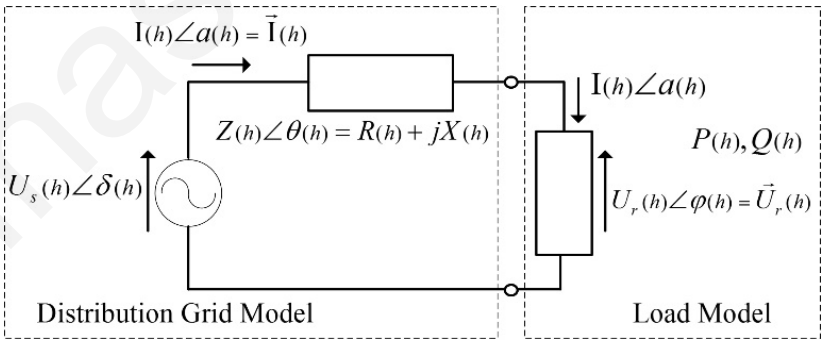

Figure 9.10. Complete Distribution grid model – Harmonic Thevenin Equivalent Circuit

Also, equation (8.9) is converted to equation (9.10) to include harmonic frequencies as well.

$$Z_{HDGM} = R_{HDGM}(h) + jX_{HDGM}(h) = \frac{\vec{U}_r(h)^{t_0} - \vec{U}_r(h)^{t_1} \cdot e^{-j\varepsilon_1}}{\vec{I}(h)^{t_0} - \vec{I}(h)^{t_1} \cdot e^{-j\varepsilon_1}} \tag{9.10}$$

More specifically, the harmonic impedance is calculated by applying the DGM theory presented in chapter 8 for each harmonic frequency under consideration. The mean value of

the impedance amplitude obtained from the analysis for each harmonic frequency is depicted graphically in Fig. 9.11.

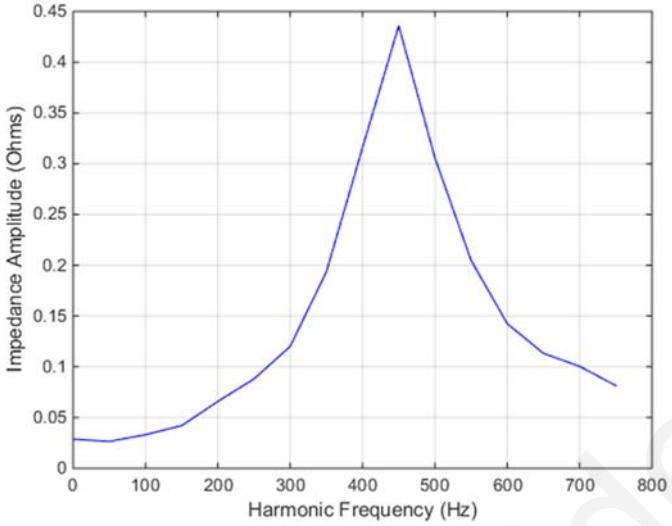

Figure 9.11. Amplitude of Harmonic Impedance

The transfer function of the harmonic impedance is obtained by applying estimation techniques on the calculated harmonic impedance values as described in [190]. From the results of the estimation process it has been found that two types of transfer functions can fit well the harmonic impedance data. The two types of transfer function models are described by equations (9.11) and (9.12) respectively.

$$Z^{1}{}_{HDGM}(s) = \frac{A_1 s + A_o}{B_2 s^2 + B_1 s + B_o} \tag{9.11}$$

$$Z^{2}{}_{HDGM}(s) = \frac{A_2 s^2 + A_1 s + A_o}{B_2 s^2 + B_1 s + B_o} \tag{9.12}$$

The first transfer function model represented by equation (9.11) can fit the harmonic impedance data with an accuracy (R^2) of fit estimation (defined by equation (5.5)) of 90.57%. On the other hand, the second transfer function model represented by equation (9.12) can fit the harmonic impedance data with an accuracy (R^2) of 93.2%. The amplitude and phase of the transfer function models $Z^{1}{}_{HDGM}(s)$ and $Z^{2}{}_{HDGM}(s)$ are shown in Figs. 9.12 and 9.13 respectively. From the aforementioned graphs it is evident that both transfer function models can represent the calculated harmonic impedance with good accuracy. After transforming the impedances described by equations (9.11) and (9.12) into admittances and by applying basic network synthesis techniques it becomes feasible to obtain the admittance equations in relation to RLC circuit components [224]. Equations (9.13) and (9.14) are the ones derived from applying the network synthesis techniques. Subsequently, the admittance equations can then be converted into electrical circuits as exactly depicted in Fig. 9.14.

$$Y^{1}{}_{HDGM}(s) = sC + \frac{1}{R_L + sL} \tag{9.13}$$

$$Y^{2}{}_{HDGM}(s) = \frac{1}{R_c + \frac{1}{sC}} + \frac{1}{R_L + sL} \tag{9.14}$$

More specifically, the circuit topologies shown in Figs. 9.14 are actually the Thevenin Equivalent Circuits which can represent with quite good accuracy the harmonic impedance data obtained from the DGM analysis of the first fifteen harmonics. For the simulations, however, the $Z^{2}{}_{HDGM}(s)$ Thevenin Equivalent Circuit is adopted as it provides higher fitting accuracy (R^2) than the $Z^{1}{}_{HDGM}(s)$ Thevenin Equivalent Circuit.

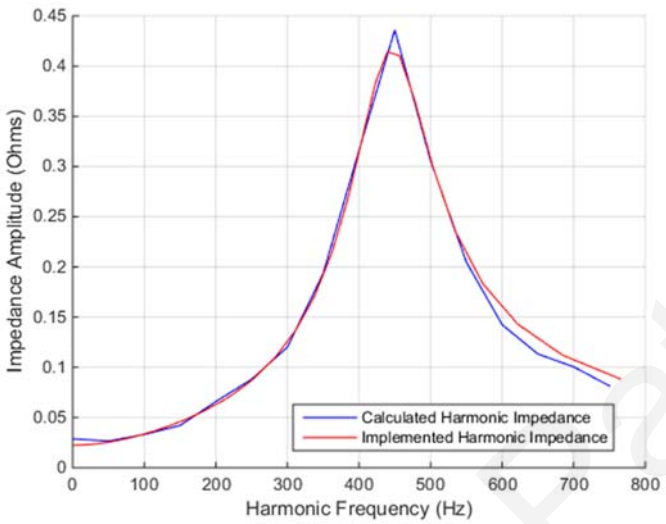

Figure 9.12a $Z^{1}{}_{HDGM}(s)$ - Amplitude

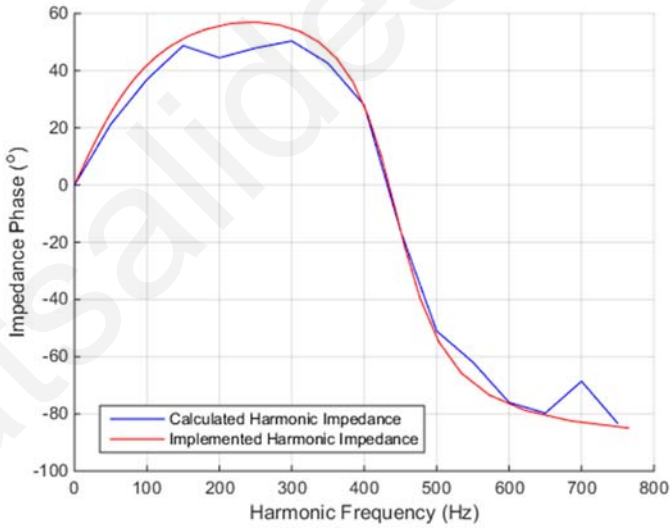

Figure 9.12b $Z^{1}{}_{HDGM}(s)$ - Phase

Figure 9.12. $Z^{1}{}_{HDGM}(s)$ transfer function model vs Calculated Harmonic Data

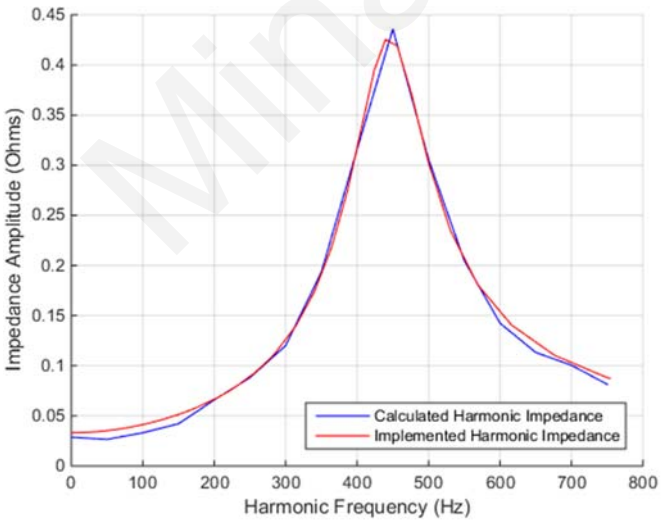

Figure 9.13a $Z^{2}{}_{HDGM}(s)$ - Amplitude

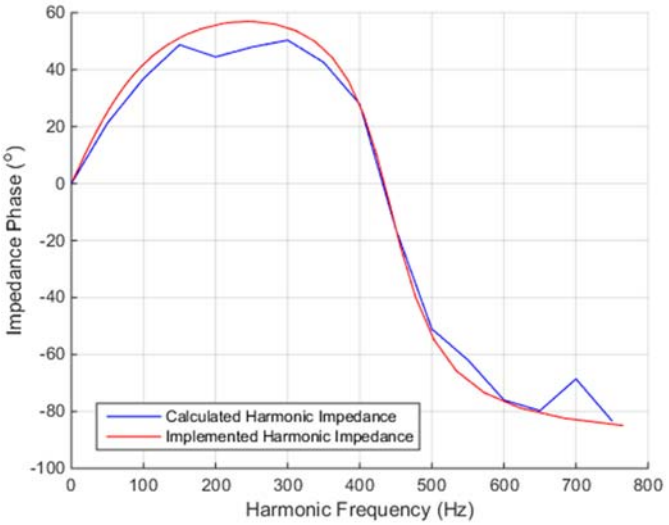

Figure 9.13b $Z^{2}{}_{HDGM}(s)$ - Phase

Figure 9.13. $Z^{2}{}_{HDGM}(s)$ transfer function model vs Calculated Harmonic Data

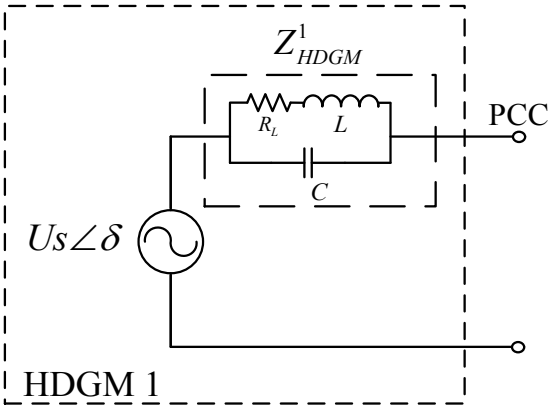

Figure 9.14a $Z^1_{HDGM}(s)$ - Circuit representation

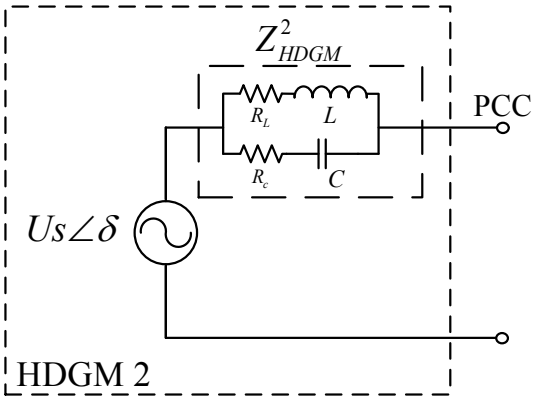

Figure 9.14b $Z^2_{HDGM}(s)$ - Circuit representation

Figure 9.14. $Z^1_{HDGM}(s)$ and $Z^2_{HDGM}(s)$ transformed into Thevenin Equivalent Circuits

9.4.2 Simulation Case Outcomes

While using the HDGM in simulations, the results of Fig. 9.15 are obtained which are quite similar with measurements recorded from PV systems in the field. From the aforementioned figure it can be seen that during times of high solar irradiance the amplitude of voltage harmonics increases. Under these conditions, the PV system produces harmonic currents with a higher amplitude, able to interact with the harmonic impedance of the distribution grid.

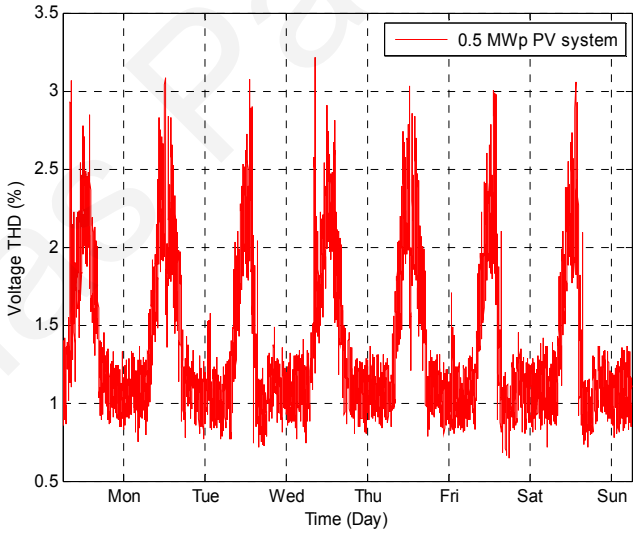

Figure 9.15. Voltage Total Harmonic Distortion (THD) vs time

9.5 Conclusions

In this chapter, a generalized adaptive power factor (GAPF) scheme is presented and evaluated. By choosing appropriately the parameters of the GAPF scheme, it is possible to decrease the voltage variation within a small range. However, the above conclusion may not be valid with different distribution grid dynamics and different load consumption and therefore simulation studies are required to establish the optimum configuration that will achieve improved voltage behaviour in distribution grids. Also, a new voltage regulation

scheme is presented able to vary the lower limit of the permissible power factor depending on the power production and the distribution grid dynamics. The proposed method improves the performance of the common dynamic power factor and at the same time it can quantify the reactive power needed for proper regulation of the voltage level at the PCC without wasting valuable active power when the PV system is not adequately sized. Future work includes the investigation of the applicability of the proposed algorithm for decentralized voltage control in the presence of high PV penetration. Finally, a harmonic distribution grid model is formulated which can be used in accurate harmonic studies. The advantage of the proposed harmonic distribution grid model is that it can produce accurate results for both the voltage variation of the fundamental frequency and the harmonic response of the distribution grid busbar under consideration.

Chapter 10
Conclusions and Future Work

10.1 Conclusions

Power quality problems are considered to be the main thread for any kind of distribution network, limiting also the unconditional installation of PV generation. The quest for increasing the energy produced by renewable sources will make the situation worse, giving rise to power quality problems, if appropriate protective proactive actions are not taken in the near future. Further research is necessary to understand the behaviour of renewable sources, improve the design of power electronics, establish effective guidelines for the proper installation of grid connected photovoltaic systems in distribution networks and develop the right tools to perform power quality studies. The analysis presented, identifies that with current inverters, maximum permissible concentrations of PV can be reached under certain circumstances. From this work, it has been observed that the levels of power quality of busbars inside a distribution network can decrease by installing higher concentrations of PV systems. Further research is necessary to establish effective guidelines for the proper installation of grid connected photovoltaic systems in distribution networks, and the optimum voltage regulation schemes should be defined clearly for each case. Additionally,

proper planning is required, which should also consider means of voltage and harmonic compensation as well as filtering when necessary.

Initially, the Simple PV System model (SPVSM) was developed for performing steady-state investigations on distribution grid topologies to assess the voltage levels and voltage harmonics. As the steady-state response of the Simple PV System model was not complete due to the fact that the grid voltage was not considered in the Simple PV System model, the Advanced PV System model (APVSM) was required to be developed. The Advanced PV System model could be effectively used in steady-state simulations but the control dynamics of the PV inverter were not represented by this model. In order to have the ability to study the transient behaviour of PV systems and perform complete power quality studies, considering also the dynamics of the PV inverter, it was necessary to develop the Detailed PV System model (DPVSM). However, the Detailed PV System model cannot be used in accurate power quality studies of large power networks for both balanced and unbalanced conditions. For this purpose, an accurate/universal PV system model for transient simulations is developed for balanced and unbalanced studies which is tuneable and can represented the dynamics of various inverters. The switching operation is omitted from the proposed model making the model computationally efficient for large networks.

Mainly, it has been found that EN 61727 compatible inverters do not cause intolerable voltage distortion in distribution grids and that the only important problem needed to be treated carefully when the PV capacity increases more than the load demand is the overvoltage. In order to facilitate higher penetration of distributed generation and avoid the loss of invaluable RES energy due to overvoltages, the utilization of an appropriate voltage regulation scheme is required when the local ratio of PV penetration to the local load exceeds a predetermined threshold that depends on the characteristics of the local network. The new generation of inverters offers this capability and it is up to Distribution System Operators and regulators, when the price is right, to transfer this requirement in the technical specifications for connection. More comforting however, is the fact that in real systems the DG planned currently to be installed is just the amount required to meet the demand of customers, hence within the rating of the local network. From the findings of this research work, it is apparent that both harmonic injection and changes in voltage profile from local DG up to the full rating of the local system, are not violating the thresholds set out in the EN50160 standard.

Through the procedure adopted in this work, new knowledge relative to the PV system modelling has been produced. Firstly, for the configuration of the Simple PV System model, a unique measurement analysis method has been formulated with which the optimum

number of case studies is selected. Also, a new PV system model using regression fit equations, which is computationally efficient has been developed. With this model (APVSM) the voltage levels and harmonic distortion of a proposed distribution grid can be assessed. Furthermore, the Detailed PV System model is tuned and validated using measurements from a 150kW$_p$ PV system and it is then used in the simulation of different concentration scenarios. Its response is verified by utilizing measurements obtained before and after the installation of the 150kW$_p$ PV system in an industrial area. Moreover, the Detailed PV System model is further used in the evaluation of different voltage regulation algorithms and lastly in the study of fault response of the industrial grid topology and outcomes are presented. In order to have simulation results with good accuracy, it is required for the network grid dynamics to be known. For this purpose, a method for defining the network dynamics has been defined. Power measurements from the distribution transformer busbar were used to extract the required information needed to calculate the equivalent impedance of the grid. Based on the equivalent distribution grid model presented in this PhD thesis, a new voltage regulation method is formulated capable of adapting at different grid/impedance conditions. The new voltage regulation method manages to maintain voltage into the permissible voltage range even at extreme grid conditions. Finally, an accurate transient PV system model is developed for performing power quality studies according to the requirements imposed by the trends in future decentralized power generation.

10.2 Future Work

As a future step, an experimental PV system setup will be developed which will be monitored by a state-of-art data acquisition system. The results obtained by the experimental setup are going to be used for the validation of the proposed transient PV system model. Both the experimental setup and the simulation model are going to be exposed to the same varying conditions to compare their response and make modifications to the proposed PV model if deviations exist between measured and simulated data. The interaction between simulations and experiment will lead in the finalization of the proposed transient PV system model. As a next step, further simplification of the proposed transient PV system model will be undertaken to enable the efficient and fast simulation of larger power networks. Additionally, statistical analysis on both weather and simulation data will be done in an attempt to minimize the simulation time needed by defining the appropriate input data to the simulations. The complete investigation of the impact of PV generation on power quality and fault studies in electricity grids with different PV penetration levels and proposal of a procedure for handling faults is going to be considered in more detail using the developed

transient PV system model. Also, a small battery will be considered to assess the benefits gained from charging and discharging the battery during the "right time". Further investigation will be performed to find the appropriate battery size which will minimize the voltage variations inside the distribution grid. As an extension of this work, a comparison with power curtailing techniques will be made. Concluding, voltage regulation methods will be tested for their ability to maintain the stability of voltage in large power networks with high PV penetrations (when the PV systems are operated either in a centralized or in a decentralized manner).

.

References

[1] J. F. G. Cobben, W. L. Kling, and J. M. a. Myrzik, "Power quality aspects of a future micro grid," in *2005 International Conference on Future Power Systems*, 2005, pp. 1–5.

[2] D. Galzina, "Grid Integration of Distributed Energy Sources Regarding Power Quality," in *IEEE International Energy Conference (ENERGYCON)*, 2014, pp. 1320–1324.

[3] A. Sallam and O. Malik, *Electric Power Quality*. Wiley-IEEE Press, 2015.

[4] V. Calderaro, V. Galdi, F. Lamberti, S. Member, and A. Piccolo, "A Smart Strategy for Voltage Control Ancillary Service in Distribution Networks," *IEEE Trans. Power Syst.*, vol. 30, no. 1, pp. 494–502, 2015.

[5] S. Bhattacharyya, J. M. a Myrzik, and W. L. Kling, "Consequences of poor power quality - An overview," in *Proceedings of the Universities Power Engineering Conference*, 2007, no. 1, pp. 651–656.

[6] M. I. Muhamad, N. Manm, and M. A. M. Radzi, "The Effects of Power Quality to the Industries," in *2007 5th Student Conference on Research and Development*, 2007, no. December, pp. 1 – 4.

[7] Y. J. Wang, R. M. O'Connell, and G. Brownfield, "Modeling and prediction of distribution system voltage distortion caused by nonlinear residential loads," *IEEE Trans. Power Deliv.*, vol. 16, no. 4, pp. 744–751, 2001.

[8] M. Patsalides, A. Stavrou, V. Efthymiou, and G. E. Georghiou, "Towards the establishment of maximum PV generation limits due to power quality constraints," *Int. J. Electr. Power Energy Syst.*, vol. 42, no. 1, pp. 285–298, 2012.

[9] M. C. Alvarez-Herault, R. Caire, B. Raison, N. Hadjsaid, and W. Bienia, "Optimizing traditional urban network architectures to increase distributed generation connection," *Int. J. Electr. Power Energy Syst.*, vol. 35, no. 1, pp. 148–157, 2012.

[10] R. P. S. Leão, G. C. Barroso, R. F. Sampaio, J. B. Almada, C. F. P. Lima, M. C. O. Rego, and F. L. M. Antunes, "The future of low voltage networks: Moving from passive to active," *Int. J. Electr. Power Energy Syst.*, vol. 33, pp. 1506–1512, 2011.

[11] B. Howe, "A new vision of PQ research for the next 10 years," *2007 9th Int. Conf. Electr. Power Qual. Util. EPQU*, pp. 1 – 5, 2007.

[12] P. J. M. Heskes, J. F. G. Cobben, and H. H. C. de Moor, "Harmonic Distortion in Residential Areas Due To Large Scale PV Implementation is Predictable," *Int. J. Distrib. Energy Resour.*, vol. 1, no. 1, pp. 7138–7138, 2005.

[13] J. F. G. Cobben, W. L. Kling, P. Heskes, and H. Oldenkamp, "Predict the level of harmonic distortion due to dispersed generation," in *Electricity Distribution, 2005. CIRED 2005. 18th International Conference and Exhibition on*, 2005, no. 2, pp. 1–4.

[14] M. C. Benhabib, J. M. a Myrzik, and J. L. Duarte, "Harmonic effects caused by large scale PV installations in LV network," in *2007 9th International Conference on Electrical Power Quality and Utilisation, EPQU*, 2007, pp. 1 – 6.

[15] Y. Miyamoto and H. Sugihara, "Demonstrative research on clustered PV systems," in *Conference Record of the IEEE Photovoltaic Specialists Conference*, 2009, pp. 512–516.

[16] S. Ueda, Y., Oozeki, T., Kurokawa, K., Itou, T., Kitamura, K., Miyamoto, Y., Nishikawa, "Detailed performance analysis results of grid-connected clustered PV systems in Japan–First 200 Systems Results of Demonstrative Research on Clustered PV Systems," in *20th European PVSEC*, 2005, pp. 3–6.

[17] E. Nakashima, Y. Miyamoto, N. Fukuoka, H. Sugihara, T. Tanabe, and K. Kitamura, "The characteristics of higher harmonics in clustered PV systems," in *Conference Record of the 2006 IEEE 4th World Conference on Photovoltaic Energy Conversion, WCPEC-4*, 2007, vol. 2, pp. 2423–2426.

[18] R. Tonkoski and L. a C. Lopes, "Impact of active power curtailment on overvoltage prevention and energy production of PV inverters connected to low voltage residential feeders," *Renew. Energy*, vol. 36, no. 12, pp. 3566–3574, 2011.

[19] E. Demirok, D. Sera, R. Teodorescu, P. Rodriguez, and U. Borup, "Clustered PV inverters in LV networks: An overview of impacts and comparison of voltage control strategies," in *2009 IEEE Electrical Power and Energy Conference, EPEC 2009*, 2009, pp. 1–6.

[20] N. Jayasekara and P. Wolfs, "Analysis of power quality impact of high penetration PV in residential feeders," in *Universities Power Engineering Conference (AUPEC), 2010 20th Australasian*, 2010, pp. 1–8.

[21] M. Oshiro, K. Tanaka, A. Uehara, T. Senjyu, Y. Miyazato, A. Yona, and T. Funabashi, "Optimal voltage control in distribution systems with coordination of distribution installations," *Int. J. Electr. Power Energy Syst.*, vol. 32, no. 10, pp. 1125–1134, 2010.

[22] M. Oshiro, K. Tanaka, T. Senjyu, S. Toma, A. Yona, A. Y. Saber, T. Funabashi, and C.-H. Kim, "Optimal voltage control in distribution systems using PV generators," *Int. J. Electr. Power Energy Syst.*, vol. 33, no. 3, pp. 485–492, 2011.

[23] K. Fekete, Z. Klaic, and L. Majdandzic, "Expansion of the residential photovoltaic systems and its harmonic impact on the distribution grid," *Renew. Energy*, vol. 43, pp. 140–148, 2012.

[24] V. Hengsritawat, T. Tayjasanant, and N. Nimpitiwan, "Optimal sizing of photovoltaic distributed generators in a distribution system with consideration of solar radiation and harmonic distortion," *Int. J. Electr. Power Energy Syst.*, vol. 39, no. 1, pp. 36–47, 2012.

[25] J. Wong, P. Baroutis, R. Chadha, R. Iravani, M. Graovac, and X. Wang, "A methodology for evaluation of permissible depth of penetration of distributed generation in urban distribution systems," in *IEEE Power and Energy Society 2008 General Meeting: Conversion and Delivery of Electrical Energy in the 21st Century, PES*, 2008, pp. 1–8.

[26] A. Canova, L. Giaccone, F. Spertino, and M. Tartaglia, "Electrical impact of photovoltaic plant in distributed network," *IEEE Trans. Ind. Appl.*, vol. 45, no. 1, pp. 341–347, 2009.

[27] J. C. Hernández, a. Medina, and F. Jurado, "Impact comparison of PV system integration into rural and urban feeders," *Energy Convers. Manag.*, vol. 49, pp. 1747–1765, 2008.

[28] K. Yoshida, K. Kouchi, Y. Nakanishi, H. Ota, and R. Yokoyama, "Centralized control of clustered PV generations for loss minimization and power quality," in *IEEE Power and Energy Society 2008 General Meeting: Conversion and Delivery of Electrical Energy in the 21st Century, PES*, 2008, pp. 1–6.

[29] S. Phuttapatimok, A. Sangswang, M. Seapan, D. Chenvidhya, and K. Kirtikara, "Evaluation of fault contribution in the presence of PV grid-connected systems," in *Conference Record of the IEEE Photovoltaic Specialists Conference*, 2008, pp. 1 – 5.

[30] Y. Zhou, L. Liu, and H. Li, "Autonomous control integrating fast voltage regulation and islanding detection for high penetration PV application," in *Conference Proceedings - IEEE Applied Power Electronics Conference and Exposition - APEC*, 2011, pp. 606–612.

[31] B. Verhoeven, "Utility aspects of grid-connected photovoltaic power systems," *Int. Energy Agency-Implementing Agreem. Photovolt. Power Syst.*, no. Tech. Rep. IEA PVPS T5–0, p. 168, 1998.

[32] E. Vasanasong and E. D. Spooner, "The effect of net harmonic currents produced by numbers of the Sydney Olympic Village's PV systems on the power quality of local electrical network," in *PowerCon 2000. 2000 International Conference on Power System Technology. Proceedings (Cat. No.00EX409)*, 2000, vol. 2, pp. 1001–1006.

[33] W. Yan, M. Braun, J. Von Appen, E. Kämpf, M. Kraiczy, C. Ma, T. Stetz, and S. Schmidt, "Operation strategies in distribution systems with high level PV Penetration," in *ISES Solar World Congress*, 2011, pp. 2–6.

[34] P. Kirawanich and R. M. O'Connell, "Potential harmonic impact of a residential utility-interactive photovoltaic system," in *Ninth International Conference on Harmonics and Quality of Power. Proceedings*, 2000, vol. 3, pp. 983–987.

[35] M. Bollen and C. Schwaegerl, "Distributed energy resources and waveform distortion," in *19th International Conference on Electricity Distribution*, 2007, pp. 1–4.

[36] D. Parmar and L. Yao, "Impact of unbalanced penetration of single phase grid connected photovoltaic generators on distribution network," in *Proceedings of 2011 46th International Universities' Power Engineering Conference (UPEC)*, 2011, pp. 1 – 8.

[37] "Photovoltaic Power Systems Programme: Task 14 - High Penetration PV in Electricity Grids," *Int. Energy Agency*, vol. Tech. Rep., 2013.

[38] P. E. Kakosimos and A. G. Kladas, "Implementation of photovoltaic array MPPT through fixed step predictive control technique," *Renew. Energy*, vol. 36, no. 9, pp. 2508–2514, 2011.

[39] G. C. Pyo, H. W. Kang, and S. I. Moon, "A new operation method for grid-connected PV system considering voltage regulation in distribution system," in *2008 IEEE Power and Energy Society General Meeting - Conversion and Delivery of Electrical Energy in the 21st Century*, 2008, pp. 1–7.

[40] L. Hassaine, E. Olias, J. Quintero, and M. Haddadi, "Digital power factor control and reactive power regulation for grid-connected photovoltaic inverter," *Renew. Energy*, vol. 34, pp. 315–321, 2009.

[41] A. Mohamed, M. Elshaer, and O. Mohammed, "Control enhancement of power conditioning units for high quality PV systems," *Electr. Power Syst. Res.*, vol. 90, pp. 30–41, 2012.

[42] B. Li, X. Tian, and H. Zeng, "A grid-connection control scheme of PV system with fluctuant reactive load," in *DRPT 2011 - 2011 4th International Conference on Electric Utility Deregulation and Restructuring and Power Technologies*, 2011, pp. 786–790.

[43] Y. Huang, M. Shen, F. Z. Peng, and J. Wang, "Z-source inverter for residential photovoltaic systems," *IEEE Trans. Power Electron.*, vol. 21, no. 6, pp. 1776–1782, 2006.

[44] S. Balathandayuthapani, C. S. Edrington, S. D. Henry, and J. Cao, "Analysis and control of a photovoltaic system: Application to a high-penetration case study," *IEEE Syst. J.*, vol. 6, no. 2, pp. 213–219, 2012.

[45] B. W. Bin Wang, T. H. T. Huang, B. J. B. Jiang, X. D. X. Dong, and Z. B. Z. Bo, "Dynamic modeling and transient fault analysis of feeder in distribution system with MW PV substation," in *2010 45th International Universities Power Engineering Conference (UPEC)*, 2010, no. 1, pp. 1 – 5.

[46] A. Ravi, P. S. Manoharan, and J. Vijay Anand, "Modeling and simulation of three phase multilevel inverter for grid connected photovoltaic systems," *Sol. Energy*, vol. 85, no. 11, pp. 2811–2818, 2011.

[47] R. Bhatt and B. Chowdhury, "Grid frequency and voltage support using PV systems with energy storage," in *North American Power Symposium (NAPS)*, 2011, pp. 1–6.

[48] I. M. El-Amin and M. S. Ali, "Impact of PV System on Distribution Networks," in *IEEE PES Conference on Innovative Smart Grid Technologies - Middle East (ISGT Middle East)*, 2011, pp. 1–6.

[49] A. Abdul Salam, I. Adam, F. Z. Hamidon, and A. M. a. Haidar, "Behaviour of grid connected photovoltaic systems," in *2011 IEEE Symposium on Industrial Electronics and Applications*, 2011, pp. 481–485.

[50] J. T. Bialasiewicz, "Renewable Energy Systems With Photovoltaic Power Generators: Operation and Modeling," *IEEE Trans. Ind. Electron.*, vol. 55, no. 7, pp. 2752–2758, 2008.

[51] L. Asiminoaei, R. Teodorescu, F. Blaabjerg, and U. Borup, "A digital controlled PV-inverter with grid impedance estimation for ENS detection," *IEEE Trans. Power Electron.*, vol. 20, no. 6, pp. 1480–1490, 2005.

[52] L. Asiminoaei, R. Teodorescu, F. Blaabjerg, and U. Borup, "Implementation and test of on-Line embedded grid impedance estimation for PV-inverters," in *PESC Record - IEEE Annual Power Electronics Specialists Conference*, 2004, vol. 4, no. 4, pp. 3095–3101.

[53] W. Yi-bo, W. Chun-sheng, L. Hua, and X. Hong-hua, "Steady-state model and power flow analysis of grid-connected photovoltaic power system," in *2008 IEEE International Conference on Industrial Technology*, 2008, no. 6, pp. 1–6.

[54] Y. Liu, J. Bebic, B. Kroposki, J. De Bedout, and W. Ren, "Distribution system voltage performance analysis for high-penetration PV," in *2008 IEEE Energy 2030 Conference, ENERGY 2008*, 2008, pp. 1–2.

[55] D. L. King, S. Gonzalez, G. M. Galbraith, and W. E. Boyson, "Performance Model for Grid-Connected Photovoltaic Inverters, SAND2007-5036," *Sandia Natl. Lab.*, vol. 38, no. September, pp. 655–660, 2007.

[56] W. Yi-bo, L. Hua, W. U. Chun-sheng, and X. U. Hong-hua, "Large-scale grid-connected photovoltaic power station's capacity limit analysis under chance-constraints," in *2009 International Conference on Sustainable Power Generation and Supply*, 2009, pp. 1–6.

[57] S. K. Firth, K. J. Lomas, and S. J. Rees, "A simple model of PV system performance and its use in fault detection," *Sol. Energy*, vol. 84, no. 4, pp. 624–635, 2010.

[58] S. Rahman and B. H. Chowdhury, "Simulation of photovoltaic power systems and their performance prediction," *IEEE Trans. Energy Convers.*, vol. 3, no. 3, pp. 440–446, 1988.

[59] A. Woyte, V. Van Thong, R. Belmans, and J. Nijs, "Voltage fluctuations on distribution level introduced by photovoltaic systems," *IEEE Trans. Energy Convers.*, vol. 21, no. 1, pp. 202–209, 2006.

[60] V. Acquaviva, P. Poggi, M. Muselli, and a. Louche, "Grid-connected rooftop PV systems for reducing voltage drops at the end of the feeder—a case study in Corsica Island," *Energy*, vol. 25, pp. 741–756, 2000.

[61] D. Riley and G. Venayagamoorthy, "Characterization and modeling of a grid-connected photovoltaic system using a Recurrent Neural Network," in *The 2011 International Joint Conference on Neural Networks (IJCNN)*, 2011, pp. 1761–1766.

[62] D. M. Riley and G. K. Venayagamoorthy, "Comparison of a recurrent neural network PV system model with a traditional component-based PV system model," in *Conference Record of the IEEE Photovoltaic Specialists Conference*, 2011, pp. 2426–2431.

[63] I. T. Papaioannou, M. C. Alexiadis, C. S. Demoulias, D. P. Labridis, and P. S. Dokopoulos, "Modeling and measurement of small Photovoltaic systems and penetration scenarios," in *2009 IEEE Bucharest PowerTech: Innovative Ideas Toward the Electrical Grid of the Future*, 2009, pp. 1–7.

[64] R. Shah, N. Mithulananthan, A. Sode-Yome, and K. Y. Lee, "Impact of large-scale PV penetration on power system oscillatory stability," in *IEEE PES General Meeting, PES 2010*, 2010, pp. 1–7.

[65] X. Mao and R. Ayyanar, "Average and Phasor Models of Single Phase PV Generators for Analysis and Simulation of Large Power Distribution Systems," in *2009 Twenty-Fourth Annual IEEE Applied Power Electronics Conference and Exposition*, 2009, pp. 1964–1970.

[66] S. Achilles, S. Schramm, and J. Bebic, "Transmission System Performance Analysis for High-Penetration Photovoltaics," 2008.

[67] N. P. Papanikolaou, E. C. Tatakis, and A. C. Kyritsis, "Analytical model for PV — Distributed generators, suitable for power systems studies," in *EPE '09. 13th European Conference on Power Electronics and Applications*, 2009, pp. 1–10.

[68] Task Force on Harmonics Modeling and Simulation, "Modeling and simulation of the propagation of harmonics in electric power networks. I. Concepts, models, and simulation techniques," *IEEE Trans. Power Deliv.*, vol. 11, no. 1, pp. 452–465, 1996.

[69] a. Bonner, T. Grebe, E. Gunther, L. Hopkins, M. B. Marz, J. Mahseredjian, N. W. Miller, T. H. Ortmeyer, V. Rajagopalan, S. J. Ranade, P. F. Ribeiro, B. R. Spherling, T. R. Sims, and W. Xu, "Modeling and simulation of the propagation of harmonics in electric power networks. Part II: sample systems and examples," *IEEE Trans. Power Deliv.*, vol. 11, no. 1, pp. 466–472, 1996.

[70] M. E. Ropp and S. Gonzalez, "Development of a MATLAB/simulink model of a single-phase grid-connected photovoltaic system," *IEEE Trans. Energy Convers.*, vol. 24, pp. 195–202, 2009.

[71] M. Mills-Price, M. Scharf, S. Hummel, M. Ropp, D. Joshi, G. Zweigle, K. G. Ravikumar, R. Moxley, and B. Flerchinger, "Interconnection control of distributed generation with time-synchronized phasors," in *2011 IEEE/PES Power Systems Conference and Exposition, PSCE 2011*, 2011, pp. 1–8.

[72] C. Limsakul, A. Sangswang, D. Chenvidhya, M. Seapan, B. Meunpinij, N. Chayavanich, and C. Jivacate, "An impedance model of a PV grid-connected system," *PVSC '08. 33rd IEEE Photovolt. Spec. Conf.*, pp. 1 – 4, 2008.

[73] F. L. Luo, H. Ye, and M. Rashid, *Digital Power Electronics and Applications*. Elsevier Academic Press, 2005.

[74] R. Yan and T. K. Saha, "Development of Simplified Models for a Single Phase Grid Connected Photovoltaic System," in *Universities Power Engineering Conference (AUPEC), 2010 20th Australasian*, 2010, pp. 1–6.

[75] R. Yan and T. K. Saha, "Investigation of voltage stability for residential customers due to high photovoltaic penetrations," *IEEE Trans. Power Syst.*, vol. 27, no. 2, pp. 651–662, 2012.

[76] Y. T. Tan, D. S. Kirschen, and N. Jenkins, "A model of PV generation suitable for stability analysis," *IEEE Trans. Energy Convers.*, vol. 19, no. 4, pp. 748–755, 2004.

[77] Y. T. Tan and D. S. Kirschen, "Impact on the power system of a large penetration of photovoltaic generation," in *2007 IEEE Power Engineering Society General Meeting, PES*, 2007, pp. 1–8.

[78] M. Patsalides, A. Stavrou, G. Makrides, V. Efthimiou, and G. E. Georghiou, "Power Quality Response of Distribution Grids with Connected Photovoltaic Systems under Different Solar Irradiation Conditions and Various Concentration Scenarios," in *6th Mediterranean, Conference and Exhibition on Power Generation, Transmission, Distribution and Energy Conversion, MEDPOWER 2008*, 2008, pp. 1–7.

[79] A. Menti, T. Zacharias, and J. Milias-Argitis, "Harmonic distortion assessment for a single-phase grid-connected photovoltaic system," *Renew. Energy*, vol. 36, no. 1, pp. 360–368, 2011.

[80] J. . Milias-Argitis and T. Zacharias, "A transformation method for the solution of power switching circuits based on network topological concepts," *Int. J. CIRCUIT THEORY Appl.*, vol. 18, no. May 1988, pp. 33–51, 1990.

[81] F. Fernandez-Bernal, L. Rouco, P. Centeno, M. Gonzalez, and M. Alonso, "Modelling of photovoltaic plants for power system dynamic studies," *Power Syst. Manag. Control*, vol. 1, pp. 17–19, 2002.

[82] B. Tamimi, C. Cañizares, and K. Bhattacharya, "Modeling and Performance Analysis of Large Solar Photo-Voltaic Generation on Voltage Stability and Inter-area Oscillations," in *Power and Energy Society General Meeting, 2011 IEEE*, 2011, pp. 1–6.

[83] F. Wang, "Output impedance modeling of grid-connected inverters considering nonlinear effects," in *2012 IEEE 13th Workshop on Control and Modeling for Power Electronics (COMPEL)*, 2012, vol. 3, no. 1, pp. 1–7.

[84] T. Ortmeyer, R. Dugan, D. Crudele, T. Key, and P. Barker, "Sandia report-Renewable Systems Interconnection Study : Utility Models , Analysis , and Simulation Tools," 2008.

[85] S. Jazebi, M. M. Hadji, S. Member, and R. A. Naghizadeh, "Distribution Network Reconfiguration in the Presence of Harmonic Loads: Optimization Techniques and Analysis," *IEEE Trans. Smart Grid*, vol. 5, no. 4, pp. 1929–1937, 2014.

[86] J. Morato, T. Knuppel, and J. Ostergaard, "Residue-based evaluation of the use of wind power plants with full converter wind turbines for power oscillation damping control," *IEEE Trans. Sustain. Energy*, vol. 5, no. 1, pp. 82–89, 2014.

[87] R. Eriksson, J. Beerten, M. Ghandhari, and R. Belmans, "Optimizing DC voltage droop settings for AC/DC system interactions," *IEEE Trans. Power Deliv.*, vol. 29, no. 1, pp. 362–369, 2014.

[88] L. Vanfretti, "Specification and Implementation of a Reference Grid for Distribution Network Dynamics Studies," in *2014 IEEE PES General Meeting | Conference & Exposition*, 2014, pp. 1 – 5.

[89] T. Noda, "Standard Models for Smart Grid Simulations," in *2014 International Power Electronics Conference (IPEC-Hiroshima 2014 - ECCE-ASIA)*, 2014, pp. 2175–2182.

[90] S. T. Cha, Q. Wu, and J. Ostergaard, "A generic danish distribution grid model for smart grid technology testing," in *IEEE PES Innovative Smart Grid Technologies Conference Europe*, 2012, pp. 1–6.

[91] Y. Liang, X. Lin, A. M. Gole, and M. Yu, "Improved coherency-based wide-band equivalents for real-time digital simulators," *IEEE Trans. Power Syst.*, vol. 26, no. 3, pp. 1410–1417, 2011.

[92] H. Yizhong, W. Wenchuan, Z. Boming, and G. Qi, "Development of an RTDS-TSA hybrid transient simulation platform with frequency dependent network equivalents," in *2013 4th IEEE/PES Innovative Smart Grid Technologies Europe, ISGT Europe 2013*, 2013, pp. 9–13.

[93] P. Li, H. Yu, C. Wang, C. Ding, C. Sun, Q. Zeng, B. Lei, H. Li, and X. Huang, "State-space Model Generation of Distribution Net works for Model Order Reduction Application," in *IEEE Power and Energy Society General Meeting*, 2013, pp. 1–5.

[94] S. Lefebvre, J. Prevost, and L. Lenoir, "Distribution state estimation: A necessary requirement for the smart grid," in *2014 IEEE PES General Meeting | Conference & Exposition*, 2014, pp. 1–5.

[95] M. H. Namin and V. G. Agelidis, "Voltage sensitivity study of LV/MV networks under high penetration of photovoltaic generation considering residential and industrial load profiles," in *2013 IEEE 39th Photovoltaic Specialists Conference (PVSC)*, 2013, pp. 2309–2314.

[96] D. F. Frame, G. W. Ault, and S. Huang, "The uncertainties of probabilistic LV network analysis," in *IEEE Power and Energy Society General Meeting*, 2012, pp. 1–8.

[97] P. J. Douglass, R. Garcia-Valle, J. Ostergaard, and O. C. Tudora, "Voltage-Sensitive Load Controllers for Voltage Regulation and Increased Load Factor in Distribution Systems," *IEEE Trans. Smart Grid*, vol. 5, no. 5, pp. 2394–2401, 2014.

[98] S. Hashemi, J. Ostergaard, and G. Yang, "Effect of reactive power management of PV inverters on need for energy storage," in *Conference Record of the IEEE Photovoltaic Specialists Conference*, 2013, pp. 2304–2308.

[99] G. Y. Yang, M. Mattesen, S. B. Kjaer, R. D. Lazar, A. Constantin, J. Ostergaard, and C. Stephansen, "Analysis of thevenin equivalent network of a distribution system for solar integration studies," in *IEEE PES Innovative Smart Grid Technologies Conference Europe*, 2012, pp. 1–5.

[100] M. Duckheim, J. Reinschke, P. Gudivada, and W. Dunford, "Voltage and power flow oscillations induced by PV inverters connected to a weak power distribution grid," in *IEEE Power and Energy Society General Meeting*, 2013, pp. 1 – 5.

[101] B. K. Perera, S. R. Pulikanti, P. Ciufo, and S. Perera, "Simulation model of a grid-connected single-phase photovoltaic system in PSCAD/EMTDC," in *2012 IEEE International Conference on Power System Technology, POWERCON 2012*, 2012, pp. 1 – 6.

[102] B. K. Perera, P. Ciufo, and S. Perera, "Point of common coupling (PCC) voltage control of a grid-connected solar photovoltaic (PV) system," in *IECON Proceedings (Industrial Electronics Conference)*, 2013, pp. 7475–7480.

[103] Y. Yang, H. Wang, and F. Blaabjerg, "Reactive power injection strategies for single-phase photovoltaic systems considering grid requirements," in *Conference Proceedings - IEEE Applied Power Electronics Conference and Exposition - APEC*, 2014, pp. 371–378.

[104] K. De Brabandere, B. Bolsens, J. Van Den Keybus, A. Woyte, J. Driesen, and R. Belmans, "A voltage and frequency droop control method for parallel inverters," in *PESC Record - IEEE Annual Power Electronics Specialists Conference*, 2004, vol. 4, no. 0, pp. 2501–2507.

[105] R. Tonkoski, L. a C. Lopes, and T. H. M. El-Fouly, "Coordinated active power curtailment of grid connected PV inverters for overvoltage prevention," *IEEE Trans. Sustain. Energy*, vol. 2, no. 2, pp. 139–147, 2011.

[106] M. Dilek, R. Broadwater, and R. Sequin, "Calculating short-circuit currents in distribution systems via numerically computed Thevenin equivalents," in *2003 IEEE PES Transmission and Distribution Conference and Exposition (IEEE Cat. No.03CH37495)*, 2003, vol. 3, pp. 984–990.

[107] T. An, S. Zhou, J. Yu, and Y. Zhang, "Tracking of Thevenin equivalent parameters on weak voltage load bus groups," *2006 IEEE PES Power Syst. Conf. Expo. PSCE 2006 - Proc.*, pp. 1570–1576, 2006.

[108] "Electromagnetic Compatibility (EMC) - Consideration of reference impedances and public supply network impedances for use in determining the disturbance characteristics of electrical equipment having a rated current ≤ 75 A per phase," IEC/TR 60725, 2012.

[109] F. W. Fuchs, F. Gebhardt, N. Hoffmann, A. Knop, R. Lohde, J. Reese, and C. Wessels, "Research laboratory for grid integration of distributed renewable energy resources - design and realization -," in *2012 IEEE Energy Conversion Congress and Exposition (ECCE)*, 2012, pp. 1974–1981.

[110] N. Hoffmann and F. W. Fuchs, "Online grid impedance estimation for the control of grid connected converters in inductive-resistive distributed power-networks using extended kalman-filter," in *2012 IEEE Energy Conversion Congress and Exposition, ECCE 2012*, 2012, pp. 922–929.

[111] J. Van Wyk, *Power quality, power electronics and control*, Fifth ed. 2002.

[112] "Photovoltaic (PV) systems – Characteristics of the utility interface," IEC 61727, 2004.

[113] D. Chen, J. Zhang, and Z. Qian, "Research on fast transient and 6n±1 harmonics suppressing repetitive control scheme for three-phase grid-connected inverters," *IET Power Electron.*, vol. 6, no. 3, pp. 601–610, 2013.

[114] A. Garces and A. Trejos, "A voltage regulator based on matrix converter for smart grid applications," in *2011 IEEE PES CONFERENCE ON INNOVATIVE SMART GRID TECHNOLOGIES LATIN AMERICA (ISGT LA)*, 2011, pp. 1–6.

[115] BDEW, "Generating Plants Connected to the Medium-Voltage Network: Guideline for generating plants' connection to and parallel operation with the medium-voltage network," BDEW Bundesverband der Energie- und Wasserwirtschaft e.V., Berlin, Germany, Technical Guideline, Jun. 2008.

[116] K. De Brabandere, A. Woyte, R. Belmans, and J. Nijs, "Prevention of inverter voltage tripping in high density PV grids," in *Proceedings of 19th Photovoltaic solar energy conference*, 2004, no. June, pp. 4–7.

[117] R. Tonkoski and L. A. C. Lopes, "Voltage Regulation in Radial Distribution Feeders with High Penetration of Photovoltaic," in *2008 IEEE Energy 2030 Conference*, 2008, vol. 1, no. 1, pp. 1–7.

[118] C. L. Masters, "Voltage rise: the big issue when connecting embedded generation to long 11 kV overhead lines," *Power Engineering Journal*, vol. 16, no. 1. p. 5, 2002.

[119] D. N. Gaonkar, P. C. Rao, and R. N. Patel, "Hybrid method for voltage regulation of distribution system with maximum utilization of connected distributed generation source," in *2006 IEEE Power India Conference*, 2005, vol. 2005, pp. 261–265.

[120] A. H. Rafa, O. Anaya-Lara, and J. R. McDonald, "Power factor control for inverter-interfaced microgeneration," in *Proceedings of the Universities Power Engineering Conference*, 2008.

[121] J. C. Vasquez, R. a. Mastromauro, J. M. Guerrero, and M. Liserre, "Voltage support provided by a droop-controlled multifunctional inverter," *IEEE Trans. Ind. Electron.*, vol. 56, no. 11, pp. 4510–4519, 2009.

[122] M. H. J. Bollen and A. Sannino, "Voltage control with inverter-based distributed generation," *IEEE Trans. Power Deliv.*, vol. 20, no. 1, pp. 519–520, 2005.

[123] P. M. S. Carvalho, P. F. Correia, and L. a F. Ferreira, "Distributed Reactive Power Generation Control for Voltage Rise Mitigation in Distribution Networks," *IEEE Trans. Power Syst.*, vol. 23, no. 2, pp. 766–772, 2008.

[124] Y. Ueda, K. Kurokawa, T. Itou, K. Kitamura, K. Akanuma, M. Yokota, H. Sugihara, and A. Morimoto, "Advanced Analysis of Grid-connected PV System's Performance and Effect of Battery," *IEEJ Trans. Power Energy*, vol. 127, no. 1, pp. 247–258, 2007.

[125] R. Kumar, "Assuring transient stability in the smart grid," in *2012 IEEE PES Innovative Smart Grid Technologies, ISGT 2012*, 2012, pp. 1 – 6.

[126] S. Bhattacharyya, M. Van Lumig, S. Cobben, J. Myrzik, and W. Kling, "Consequences of poor power quality for grid operators," in *Electricity Distribution, 2009 20th International Conference and Exhibition on*, 2009, pp. 1–4.

[127] R. Targosz and J. Manson, "Pan-European power quality survey," in *2007 9th International Conference on Electrical Power Quality and Utilisation*, 2007, pp. 1–6.

[128] M. Patsalides, A. Stavrou, G. E. Georghiou, and V. Efthymiou, "Assessing the level of harmonic distortion due to PV generation in mini grids," in *4th European PV-hybrid and Mini-Grid Conference*, 2008, pp. 328–335.

[129] "Roadmap 2010-18 and Detailed Implementation Plan 2010-12," The European Electricity Grid Initiative, Tech. Rep., May 2010.

[130] R. C. Dugan, M. F. McGranaghan, S. Santoso, and H. Wayne Beaty, *Electrical Power Systems Quality*, 2nd ed. McGraw-Hill, 2003.

[131] M. Chattopadhyay, Surajit Mitra and S. Sengupta, *Electric power quality*. Springer Science-Business Media, 2011.

[132] Ewald F. Fuchs and M. A. S. Masoum, *Power Quality in Power Systems and Electrical Machines*, Second Edi. Elsevier Academic Press, 2008.

[133] "Electromagnetic compatibility (EMC) - Part 4-4: Testing and measurement techniques - Electrical fast transient/burst immunity test," EN 61000-4-4, 2012.

[134] C. Masetti, "Revision of European Standard EN 50160 on power quality: Reasons and solutions," in *ICHQP 2010 - 14th International Conference on Harmonics and Quality of Power*, 2010, no. December 2006, pp. 3–9.

[135] "Voltage characteristics of electricity supplied by public electricity networks," EN 50160, 2010.

[136] "Electromagnetic compatability (EMC). Testing and measurement techniques. Power quality measurement methods," EN 61000-4-30:2009, 2009.

[137] "IEEE Recommended Practices and Requirements for Harmonic Control in Electrical Power Systems," *IEEE Std 519-1992*, 1993.

[138] "Requirements for micro generating plants to be connected in parallel with public low voltage distribution networks," EN 50438, 2013.

[139] "Requirements for the connection of generators above 16 A per phase - Part 1: Connection to the LV distribution system," CLC/FprTS 50549-1, 2014.

[140] D. G. and W. H. T. Degner, G. Arnold, M. Braun, "Utility-scale PV systems: Grid connection requirements, test procedures and European harmonization," Second Quarter, Fourth Edition, 2009.

[141] L. M. Gong and Z. Q. Zhu, "A novel method for compensating inverter nonlinearity effects in carrier signal injection-based sensorless control from positive-sequence carrier current distortion," *IEEE Trans. Ind. Appl.*, vol. 47, no. 3, pp. 1283–1292, 2011.

[142] J. Wasilewski, W. Wiechowski, and C. L. Bak, "Harmonic domain modeling of a distribution system using the DIgSILENT PowerFactory software," in *2005 International Conference on Future Power Systems*, 2005.

[143] G. Atkinson-Hope and W. C. Stemmet, "Assessing harmonic penetration in terms of phase and sequence component indices," in *10th International Conference on Harmonics and Quality of Power. Proceedings*, 2002, vol. 1, no. 3, pp. 86 – 92.

[144] G. A. Hope and W. C. Stemmet, "Assessing harmonic current source modelling and power definitions in balanced and unbalanced networks," *Int. J. Energy Technol. Policy*, vol. 4, no. 1/2, p. 85, 2006.

[145] J. M. Lujano-Rojas, R. Dufo-López, and J. L. Bernal-Agustín, "Probabilistic modelling and analysis of stand-alone hybrid power systems," *Energy*, vol. 63, pp. 19–27, 2013.

[146] A. Chandrasekaran and A. Khurshid, "Analysis of influence of load characteristics on distribution system modeling," in *Proceedings of the 32nd Midwest Symposium on Circuits and Systems,* 1989, pp. 4–7.

[147] S. N. S. Na, L. X. L. Xumin, and G. Y. G. Yong, "Research on k-means Clustering Algorithm: An Improved k-means Clustering Algorithm," in *Intelligent Information Technology and Security Informatics (IITSI), 2010 Third International Symposium on*, 2010, pp. 2–3.

[148] G. Hamerly, E. Perelman, and B. Calder, "Comparing multinomial and k-means clustering for {SimPoint}," in *2006 {IEEE} International Symposium on Performance Analysis of Systems and Software*, 2006, pp. 131–142.

[149] P. J. Rousseeuw, "Silhouettes: A graphical aid to the interpretation and validation of cluster analysis," *J. Comput. Appl. Math.*, vol. 20, pp. 53–65, 1987.

[150] P. Berens, "CircStat: A MATLAB toolbox for circular statistics," *J. Stat. Softw.*, vol. 31, no. 10, pp. 1–21, 2009.

[151] W. W. Cochran, H. Mouritsen, and M. Wikelski, "Migrating songbirds recalibrate their magnetic compass daily from twilight cues.," *Science*, vol. 304, no. 5669, pp. 405–408, 2004.

[152] N. R. Draper and H. Smith, *Applied Regression Analysis*, 3rd Editio. Wiley, 1998.

[153] P. W. Holland and R. E. Welsch, "Robust regression using iteratively reweighted least-squares," *Commun. Stat. - Theory Methods*, vol. 6, no. 9, pp. 813–827, 2007.

[154] S. Weisberg, *Applied Linear Regression*, Third Edit., vol. 528. Wile, 2005.

[155] S.-K. Kim, J.-H. Jeon, C.-H. Cho, E.-S. Kim, and J.-B. Ahn, "Modeling and simulation of a grid-connected PV generation system for electromagnetic transient analysis," *Sol. Energy*, vol. 83, no. 5, pp. 664–678, May 2009.

[156] M. Salhi and R. El-Bachtiri, "A maximum power point control photovoltaic system," in *18th Mediterranean Conference on Control and Automation, MED'10 - Conference Proceedings*, 2010, pp. 1579–1584.

[157] M. a G. De Brito, L. P. Sampaio, G. Luigi, G. a. E Melo, and C. a. Canesin, "Comparative analysis of MPPT techniques for PV applications," in *3rd International Conference on Clean Electrical Power: Renewable Energy Resources Impact, ICCEP 2011*, 2011, pp. 99–104.

[158] C. Schauder and H. Mehta, "Vector analysis and control of advanced static VAR compensators," in *IEE Proceedings - Generation, Transmission and Distribution*, 1993, pp. 299–306.

[159] M. B. T. Stetz, W. Yan, "Voltage Control in Distribution Systems with High Level PV-Penetration -Improving Absorption Capacity for PV Systems by Reactive Power Suppl," in *25th European Photovoltaic Solar Energy Conference and Exhibition / 5th World Conference on Photovoltaic Energy Conversion*, 2010, no. September, pp. 5000 – 5006.

[160] B. I. Craciun, D. Sera, E. A. Man, T. Kerekes, V. A. Muresan, and R. Teodorescu, "Improved voltage regulation strategies by PV inverters in LV rural networks," in *Proceedings - 2012 3rd IEEE International Symposium on Power Electronics for Distributed Generation Systems, PEDG 2012*, 2012, pp. 775–781.

[161] D. J. Murray_smith, "Methods for the external validation of contiuous system simulation models:a review," *Math. Comput. Model. Dyn. Syst.*, vol. 4, no. March 2015, pp. 5–31, 1998.

[162] F. Y. Min, M. Yang, and Z. C. Wang, "Knowledge-based method for the validation of complex simulation models," *Simul. Model. Pract. Theory*, vol. 18, no. 5, pp. 500–515, 2010.

[163] S. Y. S. Yang and Y. Z. Y. Zhang, "Short-term load forecast based on decomposition of daily load curve," in *Computer, Mechatronics, Control and Electronic Engineering (CMCE), 2010 International Conference on*, 2010, vol. 3, pp. 65 – 68.

[164] P. Mandal, T. Senjyu, K. Uezato, and T. Funabashi, "Forecasting several-hours-ahead electricity demand using neural network," in *2004 IEEE International Conference on Electric Utility Deregulation, Restructuring and Power Technologies. Proceedings*, 2004, vol. 2, pp. 515 – 521.

[165] M. Y. Cho and Y. W. Chen, "Fixed/switched type shunt capacitor planning of distribution systems by considering customer load patterns and simplified feeder model," *IEE Proceedings - Generation, Transmission and Distribution*, vol. 144, no. 6. p. 533, 1997.

[166] J. He, Y. W. Li, J. M. Guerrero, F. Blaabjerg, and J. C. Vasquez, "Microgrid reactive and harmonic power sharing using enhanced virtual impedance," in *Conference Proceedings - IEEE Applied Power Electronics Conference and Exposition - APEC*, 2013, pp. 447–452.

[167] D. Reeves, G. Nourbakhsh, G. Mokhtari, and A. Ghosh, "A distributed control based coordination scheme of household PV systems for overvoltage prevention," *IEEE Power Energy Soc. Gen. Meet.*, no. 1, 2013.

[168] M. Patsalides, G. E. Georghiou, A. Stavrou, and V. Efthimiou, "Assessing the power quality behaviour of high photovoltaic (PV) penetration levels inside the distribution network," in *Proceedings - 2012 3rd IEEE International Symposium on Power Electronics for Distributed Generation Systems, PEDG 2012*, 2012, pp. 709–716.

[169] M. Patsalides, G. E. Georghiou, A. Stavrou, and V. Efthimiou, "Voltage regulation via photovoltaic (PV) inverters in distribution grids with high PV penetration levels," in *Power Generation, Transmission, Distribution and Energy Conversion (MEDPOWER 2012), 8th Mediterranean Conference*, 2012, pp. 5–10.

[170] M. Cespedes and J. Sun, "Impedance modeling and analysis of grid-connected voltage-source converters," *IEEE Trans. Power Electron.*, vol. 29, no. 3, pp. 1254–1261, 2014.

[171] S. Golestan, M. Ramezani, M. Monfared, and J. M. Guerrero, "A D-Q synchronous frame controller for single-phase inverter-based islanded distributed generation systems," *Int. Rev. Model. Simulations*, vol. 4, pp. 42–54, 2011.

[172] A. Roshan, R. Burgos, A. C. Baisden, F. Wang, and D. Boroyevich, "A D-Q frame controller for a full-bridge single phase inverter used in small distributed power generation systems," in *Conference Proceedings - IEEE Applied Power Electronics Conference and Exposition - APEC*, 2007, pp. 641–647.

[173] S. Alepuz, S. Busquets-Monge, J. Bordonau, J. Gago, D. González, and J. Balcells, "Interfacing renewable energy sources to the utility grid using a three-level inverter," *IEEE Trans. Ind. Electron.*, vol. 53, no. 5, pp. 1504–1511, 2006.

[174] A. Yazdani and R. Iravani, *Voltage-Sourced Converters in Power Systems: Modeling, Control, and Applications*. 2010.

[175] A. Yazdani, "Electromagnetic transients of grid-tied photovoltaic systems based on detailed and averaged models of the voltage-sourced converter," in *IEEE Power and Energy Society General Meeting*, 2011, pp. 1–8.

[176] M. Liserre, F. Blaabjerg, and S. Hansen, "Design and control of an LCL-filter-based three-phase active rectifier," *IEEE Trans. Ind. Appl.*, vol. 41, no. 5, pp. 1281–1291, 2005.

[177] R. Teodorescu, F. Blaabjerg, M. Liserre, and P. C. Loh, "Proportional-resonant controllers and filters for grid-connected voltage-source converters," *IEE Proceedings - Electric Power Applications*, vol. 153, no. 5. p. 750, 2006.

[178] X. Wang, M. Ieee, Y. Li, S. M. Ieee, F. Blaabjerg, and F. Ieee, "Virtual-Impedance-Based Control for Voltage-Source and Current-Source Converters," *IEEE Trans. Power Electron.*, vol. PP, no. 99, 2014.

[179] N. A. Ninad and L. a. C. Lopes, "A Vector-controlled Single-phase Voltage Source Inverter Based Grid Interface Suitable for Variable Frequency Operation in Autonomous Microgrids," *Electr. Power Components Syst.*, vol. 40, no. 11, pp. 1266–1284, 2012.

[180] J. Puukko and T. Suntio, "Dynamic properties of a voltage source inverter-based three-phase inverter in photovoltaic application," *IET Renew. Power Gener.*, vol. 6, no. 6, pp. 381–391, Nov. 2012.

[181] M. Hankaniemi and T. Suntio, "Small-signal models for constant-current regulated converters," in *IECON Proceedings (Industrial Electronics Conference)*, 2006, pp. 2037–2042.

[182] T. Suntio, J. Huusari, and J. Leppäaho, "Issues on solar-generator interfacing with voltage-fed MPP-tracking converters," in *EPE Journal (European Power Electronics and Drives Journal)*, 2010, vol. 20, no. 3, pp. 40–47.

[183] A. Mäki, S. Valkealahti, and T. Suntio, "Dynamic terminal characteristics of a photovoltaic generator," in *Proceedings of EPE-PEMC 2010 - 14th International Power Electronics and Motion Control Conference*, 2010, no. 1, pp. 76–80.

[184] T. Messo, J. Jokipii, and T. Suntio, "Minimum DC-link capacitance requirement of a two-stage photovoltaic inverter," in *2013 IEEE Energy Conversion Congress and Exposition, ECCE 2013*, 2013, pp. 999–1006.

[185] T. Messo, J. Jokipii, J. Puukko, and T. Suntio, "Determining the value of DC-link capacitance to ensure stable operation of a three-phase photovoltaic inverter," *IEEE Trans. Power Electron.*, vol. 29, no. 2, pp. 665–673, 2014.

[186] D. Zammit, C. S. Staines, and M. Apap, "Comparison between PI and PR Current Controllers in Grid Connected PV Inverters," vol. 8, no. 2, pp. 224–229, 2014.

[187] W. Zhang, C. Citro, A. M. Cantarellas, D. Remon, A. Luna, and P. Rodriguez, "Tuning of Proportional Resonant Controllers for Three Phase PV Power Converters with LCL + trap Filter," in *2014 IEEE PES T&D Conference and Exposition*, 2014, pp. 1 – 5.

[188] G. Gohil, L. Bede, R. Teodorescu, T. Kerekes, and F. Blaabjerg, "Line Filter Design of Parallel Interleaved VSCs for High Power Wind Energy Conversion Systems," *IEEE Trans. Power Electron.*, vol. PP, no. 99, pp. 1–16, 2015.

[189] C. K. Alexander and M. N. O. Sadiku, *Fundamentals of Electric Circuits*, Fifth ed. McGraw-Hill, 2001.

[190] H. Garnier, M. Mensler, and a. Richard, "Continuous-time model identification from sampled data: Implementation issues and performance evaluation," *Int. J. Control*, vol. 76, no. March 2015, pp. 1337–1357, 2003.

[191] H. C. H. Cha, T.-K. V. T.-K. Vu, and J.-E. K. J.-E. Kim, "Design and control of Proportional-Resonant controller based Photovoltaic power conditioning system," in *2009 IEEE Energy Conversion Congress and Exposition*, 2009, pp. 2198–2205.

[192] J. Dannehl, C. Wessels, and F. W. Fuchs, "Limitations of voltage-oriented PI current control of grid-connected PWM rectifiers with LCL filters," *IEEE Trans. Ind. Electron.*, vol. 56, no. 2, pp. 380–388, 2009.

[193] M. Liserre, A. Dell'Aquila, and F. Blaabjerg, "Genetic algorithm-based design of the active damping for an LCL-filter three-phase active rectifier," *IEEE Trans. Power Electron.*, vol. 19, no. 1, pp. 76–86, 2004.

[194] L. Harnefors, M. Bongiorno, and S. Lundberg, "Input-admittance calculation and shaping for controlled voltage-source converters," *IEEE Trans. Ind. Electron.*, vol. 54, no. 6, pp. 3323–3334, 2007.

[195] M. Liang and T. Q. Zheng, "Synchronous PI control for three-phase grid-connected photovoltaic inverter," in *2010 Chinese Control and Decision Conference, CCDC 2010*, 2010, no. 2, pp. 2302–2307.

[196] C. Moler, *Experiments with MATLAB*. MathWorks, Inc., 2011.

[197] G. Baker and P. Graves, *Pade Approximants*, 2nd ed. New York: Cambridge University Press, 1996.

[198] T. Funaki and S. Tanaka, "Error estimation and correction of DFT in synchronized phasor measurement," in *IEEE/PES Transmission and Distribution Conference and Exhibition*, 2002, vol. 1, pp. 448–453.

[199] B. P. McGrath, D. G. Holmes, and J. J. H. Galloway, "Power converter line synchronization using a discrete Fourier transform (DFT) based on a variable sample rate," *IEEE Trans. Power Electron.*, vol. 20, no. 4, pp. 877–884, 2005.

[200] L. Hadjidemetriou, E. Kyriakides, and F. Blaabjerg, "A new hybrid PLL for interconnecting renewable energy systems to the grid," *IEEE Trans. Ind. Appl.*, vol. 49, pp. 2709–2719, 2013.

[201] P. Rodríguez, J. Pou, J. Bergas, J. I. Candela, R. P. Burgos, and D. Boroyevich, "Decoupled double synchronous reference frame PLL for power converters control," *IEEE Trans. Power Electron.*, vol. 22, no. 2, pp. 584–592, 2007.

[202] Y. F. Wang and Y. W. Li, "Three-phase cascaded delayed signal cancellation PLL for fast selective harmonic detection," *IEEE Trans. Ind. Electron.*, vol. 60, no. 4, pp. 1452–1463, 2013.

[203] Z. Xueguang, X. Dianguo, and L. Weiwei, "A novel PLL design method applied to grid fault condition," in *Conference Proceedings - IEEE Applied Power Electronics Conference and Exposition - APEC*, 2008, pp. 2016–2020.

[204] A. V. Timbus, R. Teodorescu, F. Blaabjerg, M. Liserre, and P. Rodriguez, "PLL algorithm for power generation systems robust to grid voltage faults," in *PESC Record - IEEE Annual Power Electronics Specialists Conference*, 2006.

[205] H. Cao, H. Zhang, W. Jiang, and S. Wei, "Research on PQ control strategy for PV inverter in the unbalanced grid," in *Asia-Pacific Power and Energy Engineering Conference, APPEEC*, 2012, pp. 1–3.

[206] W. Bao, X. Zhang, and L. Zhao, "Parameter estimation method based on parameter function surface," *Sci. China Technol. Sci.*, vol. 56, no. 6, pp. 1485–1498, 2013.

[207] N. Pham and B. M. Wilamowski, "Improved Nelder Mead ' s Simplex Method and Applications," *J. Comput.*, vol. 3, no. 3, pp. 55–63, 2011.

[208] J. C. Lagarias, J. a. Reeds, M. H. Wright, and P. E. Wright, "Convergence Properties of the Nelder--Mead Simplex Method in Low Dimensions," *SIAM J. Optim.*, vol. 9, no. 1, pp. 112–147, 1998.

[209] I. D. Mayergoyz and W. Lawson, *Basic Electric Circuit Theory*. Academic Press, 1997.

[210] W. Wu, Y. He, and F. Blaabjerg, "An LLCL power filter for single-phase grid-tied inverter," *IEEE Trans. Power Electron.*, vol. 27, no. 2, pp. 782–789, 2012.

[211] D. G. Holmes and T. a Lipo, *Pulse Width Modulation For Power Converters*. IEEE PRESS/WILEY- INTERSCIENCE, 2003.

[212] M. Patsalides, V. Efthymiou, A. Stavrou, and G. E. Georghiou, "A Simplified Distribution Grid Model for Power Quality Studies in the presence of Photovoltaic Generators."

[213] K. R. Dixon, *Modeling and Simulation in Ecotoxicology with Applications in MATLAB® and Simulink®*. CRC Press, Taylor & Francis Group, 2012.

[214] S. M. Abdelkader and D. J. Morrow, "Online Tracking of Thévenin Equivalent Parameters Using PMU Measurements," *IEEE Trans. Power Syst.*, vol. 27, no. 2, pp. 975–983, 2012.

[215] D. L. Donoho, "De-noising by soft-thresholding," *IEEE Trans. Inf. Theory*, vol. 41, no. 3, pp. 613–627, 1995.

[216] P. Castello, M. Lixia, C. Muscas, and P. A. Pegoraro, "Impact of the model on the accuracy of synchrophasor measurement," *IEEE Trans. Instrum. Meas.*, vol. 61, no. 8, pp. 2179–2188, 2012.

[217] J. A. de la O Serna, "Synchrophasor Estimation Using Prony's Method," *IEEE Trans. Instrum. Meas.*, vol. 62, no. 8, pp. 2119–2128, 2013.

[218] H. Hooshyar, F. Mahmood, and L. Vanfretti, "Specification and implementation of a reference grid for distribution network dynamics studies," in *2014 IEEE PES General Meeting | Conference & Exposition*, 2014, pp. 1–5.

[219] H. Mahmood, D. Michaelson, and J. Jiang, "Accurate Reactive Power Sharing in an Islanded Microgrid Using Adaptive Virtual Impedances," *IEEE Trans. Power Electron.*, vol. 30, no. 3, pp. 1605–1617, 2015.

[220] C. I. Ciontea, D. Sera, and F. Iov, "Influence of resolution of the input data on distributed generation integration studies," in *2014 International Conference on Optimization of Electrical and Electronic Equipment (OPTIM)*, 2014, pp. 673–680.

[221] H. Moaveni, D. K. Click, and A. Pappalardo, "Development of an irradiance sensor network to model photovoltaic plant-average irradiance time series," in *2014 IEEE 40th Photovoltaic Specialist Conference (PVSC)*, 2014, pp. 0788–0790.

[222] N. Kawasaki, A. Usami, K. Nishioka, T. Shimakage, J. Sumita, and H. Yamane, "Spatial interpolation of the solar irradiance; a study from the smoothing effect of irradiance fluctuations," in *Conference Record of the IEEE Photovoltaic Specialists Conference*, 2011, pp. 1817–1821.

[223] "Automatic disconnection device between a generator and the public low-voltage grid," DIN VDE 0126-1-1, 2013.

[224] F. F. Kuo, *Network Analysis & Synthesis*, 2nd. ed. Wiley Toppan, 1966.

Publications

International Conference Publications

- M. Patsalides, D. Evagorou, G. Makrides, Z. Achillides, G. E. Georghiou, A. Stavrou, V. Efthymiou, B. Zinsser, W. Schmitt, J. H. Werner, "The effect of Solar irradiance on the power quality behaviour of grid connected photovoltaic systems", International Conference on Renewable Energy and Power Quality, 2007, pp. 1-8.
- M. Patsalides, A. Stavrou and G. E. Georghiou, "Power Quality Survey throughout the Distribution Network in the Presence of Photovoltaic Systems", Conference on Renewable Energy Sources and Energy Efficiency, 2007, pp. 1-8.
- G. Makrides, M. Patsalides, Venizelos Efthimiou, A. Stavrou, G. E. Georghiou, "Power Quality issues in light of the future uptake of Photovoltaic (PV) technology", Transmission & Distribution Europe, 2008.
- M. Patsalides, A. Stavrou, V. Efthimiou, G. E. Georghiou, "Assessing the Level of Harmonic Distortion due to PV Generation in Mini Grids", in 4th European PV-Hybrid and Mini- grid Conference, 2008, pp. 328-335.
- M. Patsalides, A. Stavrou, G. Makrides, G. E. Georghiou, "Harmonic Response of Distributed Grid Connected Photovoltaic Systems", in International Conference on Deregulated Electricity Market Issues in South-Eastern Europe, DEMSEE, 2008, pp. 1-6.
- M. Patsalides, A. Stavrou, G. Makrides, V. Efthimiou, G. E. Georghiou, "Power Quality Response of Distribution Grids with Connected Photovoltaic Systems under Different Solar Irradiation Conditions and Various Concentration Scenarios", in 6th Mediterranean, Conference and Exhibition on Power Generation, Transmission, Distribution and Energy Conversion, MEDPOWER, 2008, pp 1-6.
- A. Petousis, S. Petousis, X. Zhang, G. E. Georghiou, M. Patsalides, G. Makrides and K. Godfrey, "Electricity market modelling with photovoltaic active and reactive power generation", PP&PSC conference, 2009, pp. 1-6.
- M. Patsalides, A. Stavrou, V. Efthymiou, G. E. Georghiou, "Simulation of Power Quality behaviour of Distribution Networks in the presence of Photovoltaic Systems", 2nd International Conference on Renewable Energy Sources & Energy Efficiency, 2009, pp. 1-6.
- M. Patsalides, G.E. Georghiou, A. Stavrou and V. Efthimiou, "Assessing the power quality behaviour of high photovoltaic (PV) penetration levels inside the distribution network," 2012 3rd IEEE International Symposium on Power Electronics for Distributed Generation Systems (PEDG), 2012, pp. 709-716.
- M. Patsalides, G.E. Georghiou, A. Stavrou and V. Efthimiou, "Voltage Regulation via Photovoltaic (PV) inverters in Distribution Grids with High PV Penetration Levels," in 8th Mediterranean Conference on Power Generation, Transmission, Distribution and Energy Conversion, MEDPOWER, 2012, pp. 5–10.
- M. Patsalides, A. Stavrou, V. Efthymiou, G. E. Georghiou, "Thevenin Equivalent Circuit for the Study of High Photovoltaic Penetration in Distribution Grids", 4th IEEE PES Innovative Smart Grid Technologies Europe (ISGT Europe), 2013, pp. 1-5.
- Andreas Armenakis, M. Patsalides, V. Efthymiou, "Power Quality Measurements on Distribution Feeders with Integrated Wind Generators", 4th International Conference on Renewable Energy Sources & Energy Efficiency, Cyprus, 2013, pp. 1-6.
- M. Patsalides, G.E. Georghiou, A. Stavrou and V. Efthimiou, "New voltage regulation scheme for photovoltaic systems based on Thevenin's Theorem," IEEE International Energy Conference (ENERGYCON), vol., no., 2014, pp.132-138.
- M. Patsalides, G.E. Georghiou, A. Stavrou and V. Efthimiou, "Evaluation of Voltage Regulation Schemes for Photovoltaic Systems using a Simplified Grid Equivalent," in 9th Mediterranean Conference on Power Generation, Transmission, Distribution and Energy Conversion, MEDPOWER, 2014, pp. 1-5.

Journals

- M. Patsalides, A. Stavrou, V. Efthymiou and G.E. Georghiou, "Towards the establishment of maximum PV generation limits due to power quality constraints," International Journal of Electrical Power & Energy Systems, vol. 42, pp. 285-298, 11. 2012.
- M. Patsalides, A. Stavrou, V. Efthymiou and G.E. Georghiou, "A Simplified distribution grid model for power quality studies in the presence of photovoltaic generators", IET Renewable Power Generation, 2015.
- M. Patsalides, A. Stavrou, V. Efthymiou and G. E. Georghiou, "A Generic Transient PV System Model for use in Power Quality Studies", Renewable Energy, Pending.